On the quasi-optimal convergence of adaptive nonconforming finite element methods in three examples

D I S S E R T A T I O N

zur Erlangung des akademischen Grades

Dr. rer. nat.
im Fach Mathematik

eingereicht an der
Mathematisch-Naturwissenschaftlichen Fakultät II
der Humboldt-Universität zu Berlin

von

Dipl.-Math. Hella Andrea Rabus geb. Döring

Präsident der Humboldt-Universität zu Berlin:
Prof. Dr. Jan-Hendrik Olbertz

Dekan der Mathematisch-Naturwissenschaftlichen Fakultät II:
Prof. Dr. Elmar Kulke

Gutachter:
1. Prof. Dr. Carsten Carstensen, Humboldt-Universität zu Berlin
2. Prof. Dr. Susanne C. Brenner, Louisiana State University
3. Prof. Dr. Ronald H.W. Hoppe, Universität Augsburg

Tag der Verteidigung: 23. April 2014

Abstract

Various applications in computational fluid dynamics and solid mechanics motivate the development of reliable and efficient adaptive algorithms for nonstandard finite element methods (FEMs), such as mixed and nonconforming ones. Standard adaptive finite element algorithms consist of the iterative loop of the basic steps Solve, Estimate, Mark and Refine. To reduce the number of degrees of freedom, in adaptive algorithms not all finite element domains are refined successively, which differs from uniform refinement. Instead a selection of finite element domains is marked for refinement on each level based on some refinement indicator. Since some element domains in an automatic mesh refinement may stay relatively coarse, even the analysis of convergence and more importantly the analysis of optimality require new arguments beyond an *a priori* error analysis.

In adaptive algorithms, based on collective marking, a (total) error estimator is used as refinement indicator. For separate marking strategies, this standard scheme may be universalised. The (total) error estimator is split into a volume term and an error estimator term, which estimates the error, but possibly disregards the volume term. Since the volume term is independent of the discrete solution, if there is a poor data approximation the improvement may be realised by a possibly high degree of local mesh refinement. Otherwise, a standard level-oriented mesh refinement based on an error estimator term is performed. This observation results in a natural adaptive algorithm based on separate marking, which is analysed in this thesis.

The results of the numerical experiments displayed in this thesis provide strong evidence for the quasi-optimality of the presented adaptive algorithm based on separate marking and for all three model problems. Furthermore its flexibility (in particular the free steering parameter for data approximation) allows a sufficient data approximation in just a few number of levels of the adaptive scheme and at the same time a fast, but optimal, increase of the number of degrees of freedom.

This thesis adapts standard arguments for optimal convergence to adaptive algorithms based on separate marking with a possibly high degree of local mesh refinement, and proves quasi-optimality following a general methodology for three model problems, i.e., the Poisson model problem, the pure displacement problem in linear elasticity and the Stokes equations. The numerical experiments confirm the optimal convergence rates.

Zusammenfassung

Eine Vielzahl von Anwendungen in der numerischen Simulation der Strömungsdynamik und der Festkörpermechanik begründen die Entwicklung von zuverlässigen und effizienten Algorithmen für nicht-standard Methoden der Finite-Elemente-Methode (FEM). Dazu gehören z.B. gemischte und nicht-konforme FEM. Adaptive Algorithmen finiter Elemente bestehen aus aufeinanderfolgenden Durchläufen der Schritte Solve, Estimate, Mark und Refine. Um Freiheitsgrade zu sparen, wird in jedem Durchlauf – im Gegensatz zur uniformen Verfeinerung – auf Basis eines Verfeinerungsindikators lediglich ein Teil der Gebiete für die spätere Verfeinerung markiert. Einige Gebiete bleiben daher möglicherweise verhältnismäßig grob. Die Analyse der Konvergenz und vor allem die der Optimalität benötigt daher über die *a priori* Fehleranalyse hinausgehende Argumente.

Etablierte adaptive Algorithmen beruhen auf *collective marking*, das heißt die zu verfeinernden Gebiete werden auf Basis eines Gesamtfehlerschätzers markiert. Bei adaptiven Algorithmen mit *separate marking* wird das obige Schema verallgemeinert. Der Gesamtfehlerschätzer wird in einen Volumenterm und in einen Fehlerschätzerterm, der diesen Volumenterm möglicherweise vernachlässigt, aufgespalten. Da der Volumenterm unabhängig von der diskreten Lösung ist, kann einer schlechten Datenapproximation durch eine lokal tiefe Verfeinerung begegnet werden. Andernfalls, das heißt bei hinreichender Datenapproximation wird das Gitter bezüglich des neuen Fehlerschätzerterms wie üblich level-orientiert verfeinert.

Die numerischen Experimente dieser Arbeit liefern deutliche Indizien der quasi-optimalen Konvergenz für den in dieser Arbeit untersuchten natürlichen Ansatz eines adaptivem Algorithmus, der auf *separate marking* beruht. Der Parameter, der die Verbesserung der Datenapproximation sicherstellt, ist frei wählbar. Dadurch ist es erstmals möglich, eine ausreichende und gleichzeitig optimale Approximation der Daten innerhalb weniger Durchläufe zu erzwingen. Die Freiheitsgrade steigen zwar schnell – aber auch optimal – an.

Diese Arbeit ermöglicht es, Standardargumente auch für die Konvergenzanalyse von Algorithmen mit *separate marking* zu verwenden. Dadurch gelingt es Quasi-Optimalität des vorgestellten Algorithmus gemäß einer generellen Vorgehensweise für die drei Beispiele, dem Poisson Modellproblem, dem reinen Verschiebungsproblem der linearen Elastizität und dem Stokes Problem, zu zeigen. Numerische Experimente bestätigen die optimalen Konvergenzraten.

Contents

1 Introduction

> The asymptotic description of the algorithmic complexity is uninteresting as long as we are not forced to increase n. This need is caused by the computer technology.
>
> *(W. Hackbusch* [Hac98, page 238]*)*

1.1 Motivation

The development of computer technology in the last decades facilitates and forces advances in numerical analysis. The very transparent increase of computing power, such as storage and processing power, indeed implies the need for efficient algorithms of optimal computational complexity. "In the case of large scale computations, the development of the computer technology leads to the need of algorithms with linear complexity" [Hac98, page 237].

Finite element methods (FEMs) rely on discretisations of the domain. They start with a coarse triangulation and refine the mesh to improve the accuracy of the discrete solution. Adaptive algorithms perform successive local mesh refinements steered by refinement indicators. One of the continuing challenges in numerical analysis is the design of efficient adaptive algorithms that converge with optimal rates. Numerical experiments confirm the superiority of adaptive mesh refinement based on *a posteriori* error estimates over other refinement strategies. The analytical proof is based on the comparison of convergence rates between a theoretical sequence of optimal meshes and the sequence of triangulations generated by an adaptive algorithm.

Figure 1.1 compares the typical convergence behaviour of uniform and adaptive refinement on an L-shaped domain for the Poisson model problem. The discrete solutions are computed using the nonconforming Crouzeix–Raviart finite element method (CR-FEM). The adaptive mesh refinement is realised using Dörfler marking and varying the bulk parameter $0 < \theta_A < 1$. In all three approximated quantities (estimated error, L^2-error, and energy norm of the error), the suboptimal convergence rate of uniform mesh refinement is evident, while the adaptive algorithm with a residual-based explicit *a posteriori* error estimates yields a much better and in fact optimal rate of convergence.

Given a discrete problem, the adaptive schemes start with $\mathcal{T}_0$, a relatively coarse decomposition of the domain into triangles. Roughly, quasi-optimality in the context of FEMs means that the algorithm produces a sequence of decompositions of the domain and corresponding discrete solutions that converge with the optimal rate. Theoretically, this optimal rate can be described as follows. For any positive integer N, let $\mathbb{T}(N)$ be the set of all admissible refinements $\mathcal{T}$ from $\mathcal{T}_0$ such that the numbers of elements satisfy $|\mathcal{T}| - |\mathcal{T}_0| \leqslant N$. Suppose that the error of the discrete solutions is available for all admissible triangulations $\mathcal{T} \in \mathbb{T}(N)$, then the convergence rate of the sequence of the errors for all triangulations that minimise the error in $\mathbb{T}(N)$ is the optimal rate and is an upper bound for the convergence rate produced by any thinkable algorithm. Quasi-optimal convergence allows the error to be a multiple of the error with an arbitrary, but fixed factor. This leads to a parallel shift of the convergence behaviour in a plot with double logarithmic scaling, but no change in the convergence rate.

The computed refinement indicators are the basis for the refinement of a selection of the finite element domains for the next level. Since a sufficient approximation of the

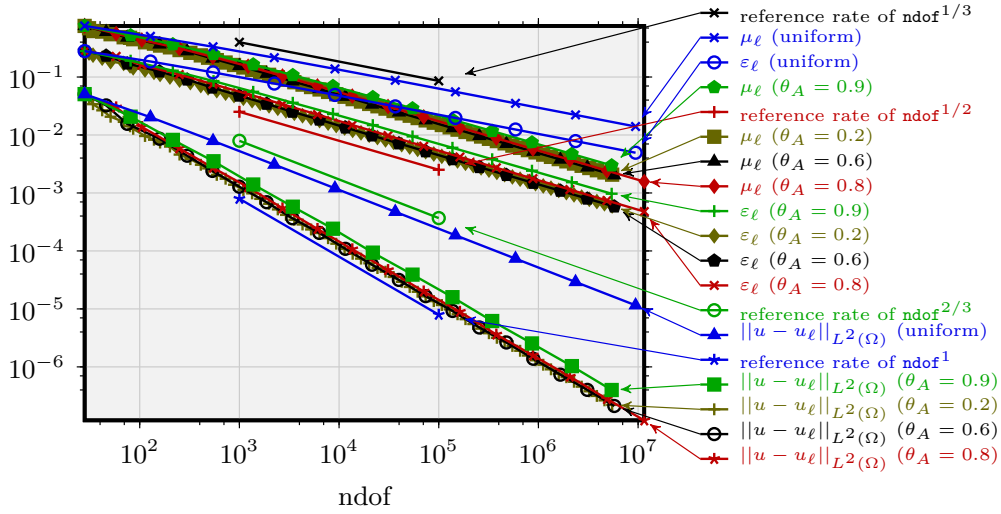

Figure 1.1: Comparison of uniform and adaptive mesh refinement (with bulk parameter $\theta_A < 1$) and CR-FEM: Convergence history of the L^2-error $\left(\|u - u_\ell\|_{L^2(\Omega)}\right)$, the energy error $\varepsilon_\ell := |||u - u_\ell|||_{\mathrm{NC}(\ell)}$ and the estimated (total) error μ_ℓ for the Poisson model problem with known exact solution $u(r, \phi) = r^{2/3} \sin(2\phi/3)$ on an L-shaped domain and $0 \equiv f \in L^2(\Omega)$.

data is necessary for convergence at all, it is a natural approach to force a simultaneous improvement of the data approximation relative to the decreasing error. In contrast to collective marking, where the refinement indicator controls both the error of the discrete solution and the approximation error of the data, separate marking distinguishes two cases and enforces refinement to improve either the discrete solution in Case (A) or the data approximation in Case (B). Since the data are available without solving the discrete problem a separate marking to improve the approximation of the data may reduce the computational complexity. In particular, this strategy may lead to a high local refinement at the beginning of the adaptive scheme, i.e., on the first levels of the adaptive algorithm.

This thesis proves that adaptive FEMs (AFEMs) that rely on separate marking can reproduce this optimal rate of convergence. Computation of finite element solutions have already verified this superiority of adaptive methods over other mesh-refinement strategies for various applications in science, engineering and industry. Nevertheless its analytical proof is an important justification for its application and implementation in various FEM software packages.

1.2 Main results

For the Poisson model problem, the pure displacement problem in linear elasticity, and the Stokes equations quasi-optimal convergence has recently been proven in [Rab10, CR12, CPR13, RC12] for the Crouzeix–Raviart FEM and collective marking. This thesis is a generalisation of the analysis in these earlier publications. Now, the results can be applied to adaptive algorithms based on separate marking. To prove optimal convergence, the sequences of triangulations and discrete solutions for the three examples generated by an AFEM algorithm based on a natural separate marking strategy (S-AFEM-AA) adapted from

[CR11] and first presented in [CR08] for mixed FEMs, are analysed.

The principal contribution of this thesis is the general mathematical methodology, which guarantees quasi-optimal convergence of S-AFEM-AA for the Poisson model problem, the pure displacement problem in linear elasticity, and the Stokes equations; see Chapters 4–6. The main theorem of each of these chapters gives the quasi-optimal convergence of the algorithm S-AFEM-AA for solving the respective model problem using adaptive Crouzeix–Raviart FEM with sufficiently small parameters θ_A (i.e., $0 < \theta_A < \theta_0 \leqslant 1$) and κ (i.e., $0 < \kappa_1 < \kappa < \kappa_2$), with bounds explicitly stated in the proofs of contraction and optimal convergence of the respective chapters. For linear elasticity (Chapter 5), the analysis is robust with respect to the Lamé parameter λ, in particular C_{opt}, θ_0, κ_1 and κ_2 are independent of λ. Depending on the specific problem either collective or separate marking may be superior. The analysis and numerical experiments in this thesis show that separate marking is a very flexible tool for designing quasi-optimal convergent adaptive algorithms for nonconforming FEM (NC-FEM). In particular the number of levels of the adaptive scheme in the pre-asymptotic range can be reduced significantly, which in general reduces the computational effort of the algorithm. This advantage is very visible when the right-hand side $f \in L^2(\Omega)$ has a very small compact support as in Section 7.2.

1.3 Mathematical methodology

The proof of quasi-optimality for the three applications in Chapters 4–6 follows a general methodology. Figure 1.2 illustrates the interplay of various key arguments in the proofs. Basic ingredients of the analysis that are independent of the three problems for the Crouzeix–Raviart nonconforming FEM (CR-FEM) are *(i)* the discrete Poincaré inequality of Lemma 3.2.11, *(ii)* reduction of the volume term $\|h_\ell f\|_{L^2(\Omega)}$ in (3.7), *(iii)* properties of the refinement method, e.g., overlay control Lemma 3.2.5, overhead of Closure Lemma 3.2.3, and Theorem 3.6.3 on key arguments of quasi-optimality, *(iv)* optimal complexity of data approximation using the approximation algorithm AA of [BDdV04] in Lemma 3.3.3.

Particular results that have to be analysed for each of the considered problems separately are *(v)* efficiency and reliability of the error estimator η_ℓ up to the volume term $\|h_\ell f\|_{L^2(\Omega)}$, *(vi)* estimator reduction of η_ℓ in Case (A) and (B) of the adaptive algorithm; see Section 3.4 for details on the separate marking in the two different cases, *(vii)* quasi-orthogonality, which replaces the Galerkin orthogonality in the nonconforming setting, *(viii)* discrete Helmholtz decomposition, and *(ix)* discrete reliability based on a discrete Helmholtz decomposition and a discrete Poincaré inequality. Using reliability, estimator reduction and quasi-orthogonality the convergence (i.e., reduction of the total error on each level ℓ) is proven. Utilising the properties of the Dörfler marking, overlay control and overhead of Closure this eventually leads to optimal convergence rates of the adaptive algorithm.

1.4 Historical review and state of the art

Since the pioneering work of Dörfler [Dör96] and Stevenson [Ste07], the question of convergence and optimality in the context of AFEMs for conforming FEMs has been introduced for Poisson-type problems [CKNS08, MNS02, BDdV04]. The extension to nonstandard FEMs, such as mixed or nonconforming FEMs, was then established [BMS10, CR11, CHX09, MZS10, Rab10, CH06a, HSX12, CD98] based on quasi-orthogonality as

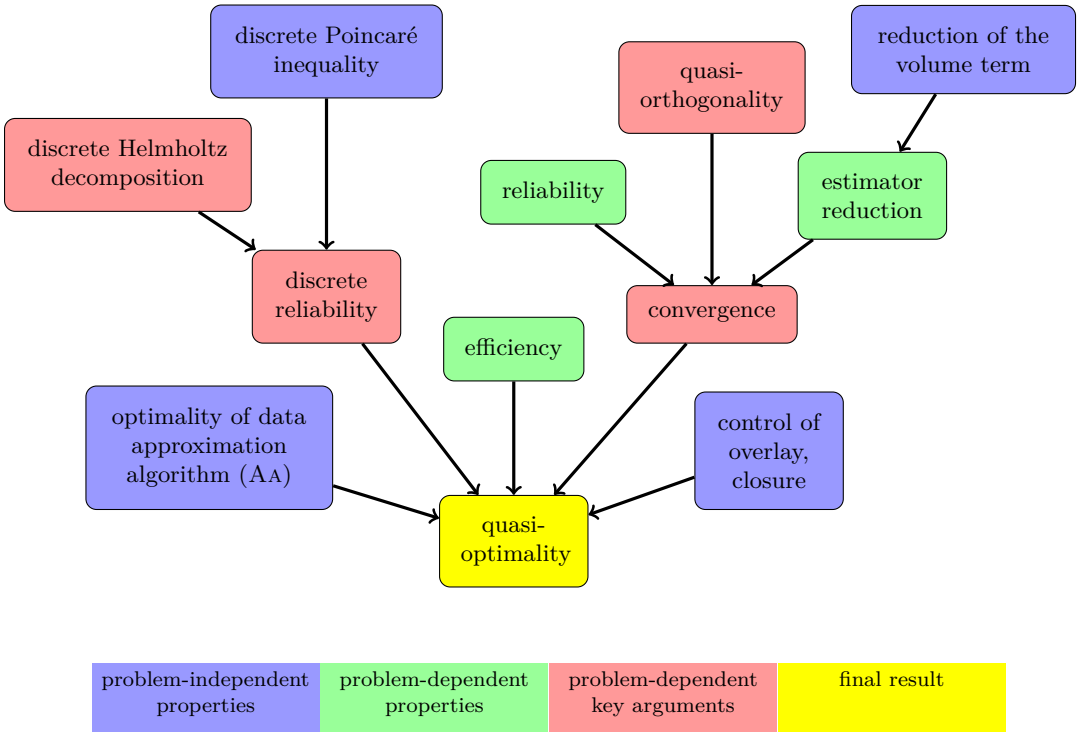

Figure 1.2: Scheme of the mathematical methodology for the proof of quasi-optimality in the three examples.

a key tool, which was introduced and established by Carstensen and Hoppe [CH06a]. Helmholtz decompositions were used already in [MZS10, Rab10] to analyse adaptive NC-FEMs for the Poisson problem, in [CR12] for linear elasticity and in [CPR13] for the Stokes problem.

There are results for quasi-optimal convergence in the sense of Stevenson [Ste07] for adaptive schemes based on collective marking (C-AFEM) [CR12, Rab10, CPR13], on separate marking strategies (S-AFEM) [CR11, BMS10, BM08], and strategies where oscillations are reduced separately by some pre-processing algorithm [BM08, CHX09].

The first convergence and optimality result for an adaptive CR-FEM for the Stokes equations was included in the technical report [HX08] and later for a S-AFEM in [BM11]. However, the lack of a discrete Helmholtz decomposition in these publications led to difficulties in proving discrete reliability for nested meshes with $k \geqslant 1$ levels of refinement and with constants independent of this k. Quasi-optimality of an adaptive algorithm based on collective marking in [CPR13] follows from the quasi-orthogonality and a novel discrete Helmholtz decomposition of piecewise constant deviatoric matrices and circumvents the incorrect analysis of [HX08, BM11].

The contraction property for adaptive NC-FEMs of [CH06a] involves volume contributions $\|h_\ell f\|_{L^2(\Omega)}$. As a first approach, optimal convergence of an adaptive NC-FEM based on separate marking is obtained in [BMS10] by two alternative bulk criteria for the Cases (A) and (B). Following the idea of [CH06a] with one refinement indicator combining the volume term and the edge terms, [Rab10, CR12, CPR13] prove quasi-optimality for a

collective marking strategy, and convergence is achieved in terms of the total error ξ_ℓ. This total error is defined by the weighted term

$$\xi_\ell^2 := \eta_\ell^2 + \alpha_f \|h_\ell f\|_{L^2(\Omega)}^2 + \alpha_\varepsilon \varepsilon_\ell^2$$

of the edge-based error estimator η_ℓ, the volume term $\|h_\ell f\|_{L^2(\Omega)}$, and the energy error ε_ℓ with proper weights α_f and α_ε.

In contrast to the widely used collective marking, the separate marking strategies split the estimated error into the volume term $\|h_\ell f\|_{L^2(\Omega)}$ and the error estimator η_ℓ. If the data approximation is sufficient compared to the size of the error estimator, Case (A) applies a standard Dörfler marking with respect to η_ℓ. However, if the error caused by the data $f \in L^2(\Omega)$ is large compared to η_ℓ, Case (B) applies and the approximation of the data is improved using some special marking and refinement instructions. One possibility is called S-AFEM-DM, which applies the Dörfler marking for the volume term in this second case [Ste07, BMS10, BM08]. A more promising option is called S-AFEM-AA, which was first introduced in [CR11] for mixed FEM. It uses the approximation algorithm (AA) (i.e., the thresholding second algorithm (TSA) plus some completion of [BDdV04, BdV04]) to give an appropriate data approximation in Case (B). Algorithm S-AFEM-AA is analysed in this thesis for NC-FEM and the three examples, namely the Poisson model problem, the pure displacement problem in linear elasticity and the Stokes equations.

1.5 Structure of this thesis

The remaining chapters are organised as follows. Chapter 2 introduces notation, definitions and preliminaries. The AFEM based on the separate marking strategy analysed in this thesis and its theoretical preliminaries are introduced in Chapter 3. The general mathematical methodology for proving quasi-optimal convergence of an adaptive FEM algorithm based on separate marking is exemplified for each of the three model problems: the Poisson model problem in Chapter 4, the pure displacement problem in linear elasticity in Chapter 5 and the Stokes problem in Chapter 6. Each of the Chapters 4–6 starts with introductory remarks and preliminary results. These lead to convergence and quasi-optimality for the presented adaptive algorithm S-AFEM-AA based on separate marking for the CR-FEM and applied to the three examples. Numerical experiments that underline the quasi-optimal convergence and enhance possible advantages of separate marking strategies are presented in Chapter 7.

Appendix A gives an overview of the MATLAB software used for the numerical experiments of this thesis. Parts of the software are unchanged and taken from the software package AFEM [CN09]. Some functions are implemented from scratch or adapted to the new situation of separate marking. The publications listed in Appendix B provide the basis for the analysis presented in Chapters 4–6. The papers are reprinted as originally published. Appendix B.1 includes [CR11], which introduced S-AFEM-AA for mixed FEM and the Poisson model problem. The subsequent Appendices B.2–B.4 include [Rab10, CR12, CPR13], which analyse C-AFEM for the three examples of this thesis: the Poisson model problem, the pure displacement problem in linear elasticity and the Stokes equations for NC-FEM.

1.6 Outlook

This thesis clarifies a mathematical methodology for proving quasi-optimal convergence for s-afem and is based on quasi-orthogonality and a discrete Helmholtz decomposition. This opens the door to an understanding of quasi-optimality for further finite element spaces such as the nonconforming Kouhia–Stenberg finite element methods and nonlinear problems such as the Navier–Stokes equations.

A flux-error analysis in $\mathrm{H}(\mathrm{div}, \Omega)$ for mixed or least-squares fem [CP] leads to volume contributions that do not have an extra mesh-size factor h_ℓ. The generalisation of the analysis of this thesis to this application indicates that the separate marking strategies with TSA in Case (B) may be the only possible mesh-refinement algorithm with guaranteed optimal convergence.

Throughout this thesis, the right-hand side function f is considered to be an L^2-function for simplicity. Separate marking, however, may also be applied to volume terms in H^{-1}, with an appropriate substitution of the TSA algorithm.

Acknowledgements One of the joys in finishing a thesis is to thank all the people who contributed to it in some way. First of all, I would like express my gratitude to my supervisor Prof. Carsten Carstensen. Any time I was struggling, he gave me the hint for how to handle the problem. When I took a family break, he saved my place in the working group, and finally – he never stopped prompting me to finish. Prof. Carstensen encouraged me to change the focus of my research to adaptive finite element methods.

Many people helped me to focus back on my thesis after the birth of my son. Their manifest support, made this thesis possible and I cannot thank them enough for their encouragement. There are younger, established and former colleagues on the one hand and friends on the other, who proofread the thesis and were available for any (software, private or research) questions. Special thank goes to my family for their sustained moral support and versatile help.

Last, but not least, during my last few years of working on the thesis at Humboldt-Universität, I was co-funded by the DFG research centre Matheon and the DFG research group 797.

2 Preliminaries

The finite element approximation of the solution of a partial differential equation relies on a discretisation of the domain Ω, e.g., into triangles, a finite dimensional function space based on finite elements for the discretised domain, and a discrete weak formulation of the problem.

This chapter introduces the point of departure. The functional analytical setting and notation are described in Section 2.1, the three model problems in Section 2.2, and the discretisation and the finite element setting in Sections 2.3 and 2.4.

The following is a collection of definitions and results from the standard FEMs literature, such as [Bra01, BS08].

2.1 Functional analytical setting

Throughout this thesis the standard notation for Lebesgue and Sobolev spaces and their norms is employed as introduced in this section. This introduction is inspired by [Bra01]. Essential descriptions are displayed in tables. The fundamental notation is summarised in Table 2.1.

For the definitions in this section, let Ω be an open subset of $\mathbb{R}^n$ with a piecewise smooth boundary. Based on the function space $L^2(\Omega)$ and the concept of weak derivatives, the Sobolev spaces $W^{m,p}(\Omega)$ and the Hilbert spaces $H^m(\Omega)$ and $H_0^m(\Omega)$ are introduced. Concise descriptions of these function spaces are displayed in Table 2.2. Further notation for vectors and matrices, and differential operators, can be found in Tables 2.3 and 2.4.

The Lebesgue spaces $L^p(\Omega)$ for $1 \leqslant p < \infty$ are defined as

$$L^p(\Omega) := \left\{ v : \Omega \to \mathbb{R} \,\middle|\, \|v\|_{L^p(\Omega)} < \infty \right\} \quad \text{with}$$
$$\|v\|_{L^p(\Omega)} := \left(\int_\Omega |v|^p \,\mathrm{dx} \right)^{1/p} \quad \text{for any } v \in L^p(\Omega).$$

For $p = 2$, $L^2(\Omega)$ is a Hilbert space with the L^2-norm $\|\cdot\|_{L^2(\Omega)}^2$ based on the scalar product

$$(u, v)_{L^2(\Omega)} := \int_\Omega uv \,\mathrm{dx} \quad \text{for any } u, v \in L^2(\Omega).$$

Definition 2.1.1 (Weak derivative)**.** *For a multi-index α a function $u \in L^p(\Omega)$ is α-weakly differentiable, if there exists a weak derivative $v = \partial^\alpha u \in L^p(\Omega)$ with*

$$\int_\Omega \varphi v \,\mathrm{dx} = (-1)^{|\alpha|} \int_\Omega u \partial^\alpha \varphi \,\mathrm{dx} \quad \textit{for all } \varphi \in C_0^\infty(\Omega).$$

$\mathbb{N}$	$:= \{1, 2, \ldots\}$, set of natural numbers
$\mathbb{N}_0$	$:= \mathbb{N} \cup \{0\}$
$\mathbb{R}, \mathbb{R}^n, \mathbb{R}^{m\times n}$	vector spaces of real numbers, vectors, and matrices for $m, n \in \mathbb{N}$
$u\vert_E$	restriction of the function u to the set E
Ω	open set in $\mathbb{R}^n$
Γ	$= \partial\Omega$, boundary of Ω
Γ_D	$\subseteq \Gamma$, Dirichlet boundary of Ω
$\vert\cdot\vert$	if the context is clear without ambiguity, $\vert\cdot\vert$ denotes the absolute value, the length of a vector (e.g., for some edge E), the area of a domain $\omega \subseteq \Omega$ (e.g., for some triangle T), or the cardinal number of a finite set (e.g., of edges, elements)
δ_{jk}	Kronecker's delta, i.e., $\delta_{jk} = 1$ if $j = k$ and $\delta_{jk} = 0$ if $j \neq k$
f_ω	$:= \fint_\omega f(x)\,\mathrm{dx} := \vert\omega\vert^{-1} \int_\omega f(x)\,\mathrm{dx}$, integral mean of f on $\omega \subseteq \Omega$
$\mathrm{osc}^2(f, \omega)$	$:= \vert\omega\vert \, \Vert f - f_\omega\Vert^2_{L^2(\omega)}$

Table 2.1: Basic notation.

Note that $C^\infty(\Omega)$ denotes the space of infinitely differentiable functions and $C_0^\infty(\Omega)$ the subspace of functions vanishing outside a compact subset of Ω.

Definition 2.1.2 (Sobolev spaces)**.** *For $m \in \mathbb{N}_0$ the space of functions with weak derivatives $\partial^\alpha u \in L^p(\Omega)$ for the multi-index α with $\vert\alpha\vert \leqslant m$ is the Sobolev space $W^{m,p}(\Omega)$ defined as*

$$W^{m,p}(\Omega) := \left\{ v \in L^p(\Omega) \,\middle|\, \|v\|_{W^{m,p}} < \infty \right\}, \qquad \text{with}$$
$$\|u\|_{W^{m,p}} := \left(\sum_{|\alpha|\leqslant m} \|\partial^\alpha u\|^p_{L^p(\Omega)} \right)^{1/p}.$$

For $p = 2$, $H^m(\Omega) := W^{m,2}(\Omega)$ is a Hilbert space. Its scalar product, associated norms and semi-norms are defined as follows.

$$H^m(\Omega) := W^{m,2}(\Omega) := \left\{ v \in L^2(\Omega) \,\middle|\, |v|_{H^m} < \infty \right\},$$
$$(u, v)_{H^m} := \sum_{|\alpha|\leqslant m} (\partial^\alpha u, \partial^\alpha v)_{L^2(\Omega)},$$
$$\|u\|_{H^m} := \sqrt{(u, u)_{H^m}},$$
$$|u|_{H^m} := \sqrt{\sum_{|\alpha|=m} \|\partial^\alpha u\|^2_{L^2(\Omega)}}.$$

Corresponding to the definition of $C^\infty(\Omega)$ and $C_0^\infty(\Omega)$, for the Hilbert spaces $H^m(\Omega)$, let $H_0^m(\Omega)$ denote the completion of $C_0^\infty(\Omega)$ with respect to the norm $\|\cdot\|_{H^m(\Omega)}$.

Since $L^2(\Omega)$ is the essential function space used in this thesis, for the ease of presentation

$L^p(\Omega; X)$	Lebesgue space with values in X $(0 \leqslant p < \infty)$
$L^2(\Omega)$	abbreviates the spaces $L^2(\Omega;\mathbb{R})$, $L^2(\Omega;\mathbb{R}^n)$, $L^2(\Omega;\mathbb{R}^{n\times n})$ $(n \in \mathbb{N})$
$L^2_0(\Omega)$	$:= \left\{v \in L^2(\Omega) \mid \fint_\Omega v \,\mathrm{dx} = 0\right\}$
$H^m(\Omega)$	Hilbert space $(m \in \mathbb{N}_0)$
$H^m_0(\Omega)$	completion of $C^\infty_0(\Omega)$ w.r.t. the Sobolev norm $\|\cdot\|_{H^m(\Omega)}$ $(m \in \mathbb{N}_0)$
$\mathrm{H}(\mathrm{div}, \Omega)$	$:= \left\{\tau \in L^2(\Omega, \mathbb{R}^n) \mid \mathrm{div}\,\tau \in L^2(\Omega)\right\}$ $(n \in \mathbb{N})$
$X^\star$	dual space of X
$\perp$	orthogonality in Hilbert spaces
$\|\cdot\|_X$	norm in the normed space X
$\|\cdot\|_{H^m(\Omega)}$	semi-norm in $H^m(\Omega)$ $(m \in \mathbb{N}_0)$, for the meaning of $\|\cdot\|$ see Table 2.1
$H^{-1}(\Omega)$	$:= \left(H^1_0(\Omega)\right)^\star$, dual space of $H^1_0(\Omega)$
$C^k(\Omega)$	set of k-times differentiable functions
$C^k_0(\Omega)$	subspace of $C^k(\Omega)$ of functions with compact support in Ω, $k \in \mathbb{N}_0$
$C^\infty(\Omega)$	set of infinitely differentiable functions
$C^\infty_0(\Omega)$	subspace of C^∞ with compact support in Ω

Table 2.2: Notation for function spaces.

most of the subsequent remarks are restricted to this case only.

The definitions of the Lebesgue and Hilbert spaces lead to the following inclusions:

$$\begin{array}{ccccccccc} L^2(\Omega) & = & H^0(\Omega) & \supset & H^1(\Omega) & \supset & H^2(\Omega) & \supset & \cdots \\ & & \| & & \cup & & \cup & & \\ & & H^0_0(\Omega) & \supset & H^1_0(\Omega) & \supset & H^2_0(\Omega) & \supset & \cdots \end{array}$$

The remainder of this Section 2.1 is a collection of basic results, which are frequently used in this thesis and are extracted from [Bra01, BS08].

Lemma 2.1.3 (Young's inequality)**.** *For nonnegative $a, b \in \mathbb{R}$ and $1 < p, q < \infty$, $1/p + 1/q = 1$ the following inequality holds*

$$ab \leqslant \frac{a^p}{p} + \frac{b^q}{q}.$$

If $p = q = 2$ and for any $\gamma > 0$ the following inequality holds

$$ab \leqslant \frac{a^2}{2\gamma} + \frac{\gamma b^2}{2}.$$

Lemma 2.1.4 (Hölder's inequality)**.** *Let $1 \leqslant p, q \leqslant \infty$, $1/p + 1/q = 1$. For $u \in L^p(\Omega)$ and $v \in L^q(\Omega)$ the following inequality holds*

$$\|uv\|_{L^1(\Omega)} \leqslant \|u\|_{L^p(\Omega)} \|v\|_{L^q(\Omega)}.$$

a_{ij}	entry of the matrix A in the i-th row and j-th column
A^T	transpose of the matrix A
$A : B$	scalar product of matrices $A, B \in \mathbb{R}^{m\times n}$
I_n	$n \times n$, unit matrix
$\operatorname{tr}(A)$	$:= A : I_n$, trace of $A \in \mathbb{R}^{n\times n}$
$\operatorname{dev}(A)$	$:= A - \frac{1}{n}\operatorname{tr}(A) I_n$, deviatoric part of $A \in \mathbb{R}^{n\times n}$
$\operatorname{sym}(A)$	$:= \frac{1}{2}\left(A + A^T\right)$, symmetric part of $A \in \mathbb{R}^{n\times n}$

Table 2.3: Notation for vectors and matrices.

∇f	$:= (\partial f/\partial x_1, \dots, \partial f/\partial x_n)$, gradient of f as a column vector
$\mathrm{D}\, v$	$:= (\nabla v_1; \dots; \nabla v_n)$, gradient of v as a matrix
$\operatorname{div} v$	$:= \sum_{j=1}^n \frac{\partial v_j}{\partial x_j}$
$\operatorname{curl} v$	$:= \frac{\partial v_2}{\partial x_1} - \frac{\partial v_1}{\partial x_2}$ (for $n = 2$)
$\operatorname{Curl} f$	$:= \left(\frac{\partial f}{\partial x_2}, -\frac{\partial f}{\partial x_1}\right)$ (for $n = 2$)
Δv	$:= \sum_{j=1}^n \partial^2 v/\partial x_j^2$, Laplace operator of v

Table 2.4: Notation for differential operators for some $f : \mathbb{R}^n \to \mathbb{R}$ and $v = (v_1, \dots, v_n)$, $v : \mathbb{R}^n \to \mathbb{R}^n$, and $x = (x_1, \dots, x_n) \in \mathbb{R}^n$.

If $p = q = 2$ the Hölder inequality is called Cauchy-Schwarz inequality.

Here, and throughout, let $\Omega \subset \mathbb{R}^n$ be a bounded Lipschitz domain and $\nu(x)$ be the outer unit normal vector at almost any point $x \in \partial\Omega$.

Lemma 2.1.5 (Integration by parts)**.** *Let $u, v \in H^1(\Omega)$, then, the integration by parts formula holds*

$$\int_\Omega u \frac{\partial v}{\partial x_j}\,\mathrm{dx} + \int_\Omega v \frac{\partial u}{\partial x_j}\,\mathrm{dx} = \int_{\partial\Omega} vu\nu_j\,\mathrm{ds} \quad \text{for } j = 1, 2, \dots, n.$$

The symbols $\lesssim$ and $\approx$ indicate that the respective (in-)equality holds up to some multiplicative constant independent of the mesh; see Table 2.6 for the precise definition.

Lemma 2.1.6 (Poincaré's inequality)**.** *Any $1 \leqslant p \leqslant \infty$ and $f \in W^{1,p}(\Omega)$ satisfies*

$$\left\| f - \fint_\Omega f\,\mathrm{dx} \right\|_{L^p(\Omega)} \lesssim \|\mathrm{D}\, f\|_{L^p(\Omega)}.$$

Lemma 2.1.7 (Friedrichs' inequality, [Bra01])**.** *Let $\Gamma_D = \partial\Omega$, then any $f \in H_0^1(\Omega)$ satisfies*

$$\|f\|_{L^2(\Omega)} \lesssim \|\mathrm{D}\, f\|_{L^2(\Omega)}.$$

Lemma 2.1.8 (Trace inequality, [BS08, Theorem 1.6.6]). *Let $v \in H^1(\Omega)$, then*

$$\|v\|_{L^2(\partial\Omega)} \lesssim \|v\|_{L^2(\Omega)}^{1/2} \|v\|_{H^1(\Omega)}^{1/2}.$$

Lemma 2.1.9 (Gauss's divergence theorem). *Any $v \in \mathrm{H}(\mathrm{div}, \Omega)$ satisfies*

$$\int_\Omega \mathrm{div}\, v \,\mathrm{dx} = \int_{\partial\Omega} v \cdot \nu \,\mathrm{ds}.$$

Lemma 2.1.10 (Trace-dev-div Lemma, [BF91, CR12]). *Any $\tau \in L^2(\Omega; \mathbb{R}^{2\times 2})$ with $\int_\Omega \mathrm{tr}(\tau)\,\mathrm{dx} = 0$ satisfies*

$$\|\tau\|_{L^2(\Omega)}^2 \lesssim \|\mathrm{dev}\,\tau\|_{L^2(\Omega)}^2 + \|\mathrm{div}\,\tau\|_{H^{-1}(\Omega)}^2.$$

Proof. [BF91, Proposition 3.1 in Section IV.3] contains this result for a symmetric τ, but the proof applies verbatim to this lemma. This was already observed in [CR12, Lemma 3.4]. □

2.2 Model problems

In this thesis adaptive algorithms based on separate marking are designed and analysed to solve the following three problems with optimal rates. Each is considered on the polygonal, simply connected domain $\Omega \subset \mathbb{R}^2$ with pure Dirichlet boundary $\Gamma_D = \partial\Omega$.

2.2.1 Poisson problem

For given $f \in L^2(\Omega)$ the Poisson model problem with unknown solution u is

$$\Delta u = -f \quad \text{in } \Omega, \qquad u = 0 \quad \text{on } \partial\Omega. \tag{2.1}$$

The corresponding weak formulation, based on a bilinear form a is: Seek $u \in H_0^1(\Omega)$ such that for all $v \in H_0^1(\Omega)$ the following holds

$$a(u, v) := \int_\Omega \nabla u \cdot \nabla v \,\mathrm{dx} = \int_\Omega f v \,\mathrm{dx}. \tag{2.2}$$

Existence and uniqueness are guaranteed via Riesz's representation theorem. The analysis of the convergence of the adaptive algorithm are presented in Chapter 4.

2.2.2 Pure displacement problem in linear elasticity

Let $f \in L^2(\Omega; \mathbb{R}^2)$ be the body force. In terms of linear elasticity the pure displacement Navier–Lamé equations read

$$-\mu\Delta u - (\lambda + \mu)\,\nabla\,\mathrm{div}\, u = f \quad \text{in } \Omega \qquad \text{and} \qquad u = 0 \quad \text{on } \partial\Omega. \tag{2.3}$$

Let $\operatorname{sym} \mathrm{D}\, u = \left(\mathrm{D}\, u + \mathrm{D}\, u^T\right)/2$ be the symmetric gradient. Here and throughout Chapter 5, the generalised Hooke's law with the two positive Lamé parameters λ and μ is modelled by

$$\mathbb{C}A = 2\mu A + \lambda \operatorname{tr}(A)\, I_2 \quad \text{for all } A \in \mathbb{R}^{2\times 2}$$

and (2.3) can be rewritten as

$$-\operatorname{div}(\mathbb{C} \operatorname{sym} \mathrm{D}\, u) = f \quad \text{in } \Omega.$$

See [BS08, Bra01] for details on the model.

Further and frequently used parameters are the Poisson ratio ν and the elasticity modulus E, which satisfy the following relations for λ and ν

$$\nu = \frac{\lambda}{2(\lambda+\mu)}, \qquad E = \frac{\mu(3\lambda+2\mu)}{\lambda+\mu},$$

with positive λ, μ and E, and $0 < \nu < 1/2$.

The pure Dirichlet problem is equivalent to the nonsymmetric version [BS08] with the weak formulation based on

$$\begin{aligned} a(u,v) &:= \int_\Omega \mathrm{D}\, u : \mathbb{C}\, \mathrm{D}\, v \,\mathrm{dx} \equiv \mu \int_\Omega \mathrm{D}\, u : \mathrm{D}\, v \,\mathrm{dx} + (\lambda+\mu) \int_\Omega (\operatorname{div} u)(\operatorname{div} v)\,\mathrm{dx}, \\ F(v) &:= \int_\Omega v \cdot f \,\mathrm{dx} \quad \text{for } u, v \in V := H_0^1(\Omega;\mathbb{R}^2). \end{aligned}$$

For a solution $u \in V$ of

$$a(u,v) = F(v) \quad \text{for all } v \in V \tag{2.4}$$

the stress is given via $\sigma := \mathbb{C}\, \mathrm{D}\, u$. For a discussion on existence and uniqueness of the solution $u \in V$ see for example [BS08, Bra01].

However, the general boundary conditions in linear elasticity are not completely properly modelled with the nonsymmetric gradients here, and the symmetric Green strains have to be involved. The nonconforming finite element method for that more general boundary value problem requires a modification [KS95] or stabilisation [Han10, HL01] and is left for future research.

The analysis of the convergence of the adaptive algorithm are presented in Chapter 5.

For the Navier–Lamé equations the locking phenomenon, which indicates that the problem is bad conditioned [Bra01], plays a crucial role in computational mathematics. For a nearly incompressible material (i.e., $\lambda \to \infty$ or $\nu \to 1/2$) (2.4) implies $\operatorname{div} u = 0$. Therefore, to get $a(u - v_h, u - v_h)$ small for $v_h \in V_h$ in some discrete space V_h, $\|\operatorname{div} v_h\|_{L^2(\Omega)}$ needs to be small. That is why a discrete space V_h with $\{v_h \in V_h \,|\operatorname{div} v_h = 0\} = \{0\}$ will lead to a small $|v_h|_{H^1(\Omega)}$ and therefore to a poor approximation of u; see [BS08].

Numerical experiments are presented in Section 7.4, where the locking phenomenon that occurs in the incompressible limit (as $\lambda \to \infty$) is additionally addressed and the outcomes from conforming and nonconforming FEMs are compared.

$\mathcal{T}_\ell$	the set of all triangles in a triangulation of the domain Ω
$\mathcal{E}_\ell$	set of all edges
$\mathcal{E}_\ell(\Omega)$	set of interior edges
$\mathcal{E}_\ell(\partial\Omega)$	set of boundary edges
$\mathcal{E}(T)$	set of edges of the triangle T
$\mathcal{E}_\ell(z)$	set of edges that share the node $z \in \mathcal{N}_\ell$
$\mathcal{N}_\ell$	set of all nodes in the triangulation $\mathcal{T}_\ell$
$\mathcal{N}_\ell(E)$	set of nodes that belong to the edge E in the triangulation $\mathcal{T}_\ell$
$\mathcal{K}_\ell$	$:= \Omega \cap \mathcal{N}_\ell$, set of free nodes (interior nodes)
E, T	an edge, a triangle in $\mathcal{T}_\ell$
$E(T)$	refinement edge of the triangle T; see Remark 2.3.2
$E(\mathcal{M}_\ell)$	$:= \bigcup_{T\in\mathcal{M}_\ell} E(T)$ set of refinement edges of the set of elements $\mathcal{M}_\ell \subseteq \mathcal{T}_\ell$
$\mathrm{mid}(E)$	midpoint of the edge E

Table 2.5: Notation of sets for a triangulation $\mathcal{T}_\ell$.

2.2.3 The Stokes equations

The two-dimensional motion of a viscous incompressible fluid in $\Omega \subset \mathbb{R}^2$ can be modelled by a velocity field $u : \Omega \to \mathbb{R}^2$ and a pressure distribution $p : \Omega \to \mathbb{R}$, which satisfy the Stokes equations under the standard no-slip boundary condition:

$$-\Delta u + \nabla p = f \quad \text{and } \operatorname{div} u = 0 \quad \text{in } \Omega, \qquad u = 0 \quad \text{on } \partial\Omega \tag{2.5}$$

for a given force density $f \in L^2(\Omega;\mathbb{R}^2)$. Let

$$a(u,v) := \int_\Omega \mathrm{D}\, u : \mathrm{D}\, v \,\mathrm{dx}, \quad b(u,q) := -\int_\Omega q \operatorname{div} u \,\mathrm{dx}, \quad F(v) := \int_\Omega v \cdot f \,\mathrm{dx}$$

for $u, v \in V := H_0^1(\Omega;\mathbb{R}^2)$ and $q \in Q := L_0^2(\Omega)$. The weak formulation of (2.5) seeks a pair $(u,p) \in V \times Q$ that satisfies the mixed variational problem:

$$\begin{aligned} a(u,v) + b(v,p) &= F(v) && \text{for all } v \in V, \\ b(u,q) &= 0 && \text{for all } q \in Q. \end{aligned} \tag{2.6}$$

For a discussion of the existence and uniqueness of the solution see [Bra01] and the references therein.

2.3 Discretisation of the domain

The approximation of an exact solution of a partial differential equation relies on a discretisation of the domain Ω, e.g., into triangles, as introduced in this section. A finite dimensional function space based on the discretised domain (Section 2.4) and the discrete formulation of the problem are given in the subsequent Chapters 4–6. This section clarifies the notation and definition of regular triangulations of the domain Ω.

η_ℓ, μ_ℓ	error estimator or refinement indicator, depending on the specific problem
$\operatorname{osc}_\ell^2$	$:= \operatorname{osc}^2(f, \mathcal{T}_\ell) := \sum_{T\in\mathcal{T}_\ell} \operatorname{osc}^2(f,T)$ with $\operatorname{osc}^2(f,T)$ as defined in Table 2.1
h_E	$:= \lvert E\rvert$
h_T	$:= \lvert T\rvert^{1/2}$, for the meaning of $\lvert\cdot\rvert$ see Table 2.1
h_ℓ	piecewise constant mesh-size function with $h_\ell\lvert_T := h_T$
$\lVert f\rVert_{\mathcal{M}}^2$	$:= \lVert f\rVert_{L^2(\bigcup\mathcal{M})}^2$, for $\mathcal{M}\subseteq\mathcal{T}_\ell$ and $f\in L^2(\Omega)$
$H^1(\mathcal{T}_\ell)$	$:= \{v\in L^2(\Omega) \,\vert\, \forall T\in\mathcal{T}_\ell\ v\lvert_T \in H^1(T)\}$
$\lvert v\rvert_{H^1(\mathcal{T}_\ell)}$	broken H^1 norm with piecewise gradients for $v\in H^1(\mathcal{T}_\ell)$; see Table 2.8
$e(T)$	error functional as input for Algorithm 3.17 (AA)
$\tilde{e}(T)$	modified error functional used within Algorithm 3.17 (AA)
$[\cdot]_E$	jump across some edge $E\in\mathcal{E}_\ell$, see detailed definition on page 15
$\langle\cdot\rangle_E$	average on $E\in\mathcal{E}_\ell$, see detailed definition on page 15
$A\lesssim B$	abbreviation for $A\leqslant CB$ with a mesh-size independent generic constant $C>0$
$A\eqsim B$	abbreviation for $A\lesssim B\lesssim A$
∇_ℓ, D_ℓ	piecewise the gradient with respect to some triangulation $\mathcal{T}_\ell$
div_ℓ	piecewise divergence with respect to some triangulation $\mathcal{T}_\ell$

Table 2.6: Mesh-related symbols.

Definition 2.3.1 (Regular triangulation)**.** *Let $\Omega\subseteq\mathbb{R}^2$ be a simply connected, polygonal Lipschitz domain. A triangulation $\mathcal{T}_\ell$ of Ω into closed triangles $T\in\mathcal{T}_\ell$ is regular if* $\operatorname{int}\left(\bigcup_{T\in\mathcal{T}_\ell} T\right) = \Omega$ *and any two distinct elements T_1 and T_2 of $\mathcal{T}$ are either*

(i) disjoint or
(ii) share exactly one node or
(iii) share exactly one common edge.

Remark 2.3.2. *Moreover, for triangulations in this thesis, each element of $T\in\mathcal{T}_\ell$ is assumed to have at least one node in the interior of Ω. For any $T\in\mathcal{T}_\ell$, one edge from the set of its interior edges $\mathcal{E}(T)$ is selected and is called its refinement edge $E(T)$.*

Definition 2.3.3 (Shape regularity)**.** *A family of triangulations $\mathcal{T}_\ell$, $\ell\in\mathbb{N}_0$ is called shape regular if for each $T\in\mathcal{T}_\ell$ the in-circle of radius r_T satisfies*

$$h_T \lesssim r_T.$$

Table 2.5 summarises the essential notation for triangulations defined above, while Table 2.6 clarifies the notation of mesh-related symbols.

For any edge $E\in\mathcal{E}_\ell$, the edge patch ω_E consists of the interior of $T_+\cup T_-$ for interior edges or the interior of T_+ for boundary edges. In addition, τ_E is the unit tangential vector along $E\subset T_+$ and $\nu_E = \nu_{T_+}$ is the unit normal vector exterior to T_+ along E; see Figure 2.7 for an illustration. Let $v\in L^1(\Omega)$. For interior edges, $[v]_E := v\lvert_{T_+}\big\rvert_E - v\lvert_{T_-}\big\rvert_E$

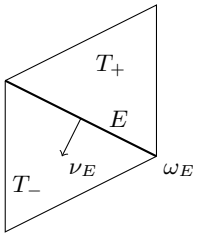

Figure 2.7: The patch ω_E of an interior edge $E \in \mathcal{E}_\ell(\Omega)$.

$P_0(\mathcal{T}_\ell)$	$:= \left\{ v_\ell \in L^2(\Omega) \middle\vert \; v_\ell\vert_T \text{ is constant for all } T \in \mathcal{T}_\ell \right\}$
$P_1(\mathcal{T}_\ell)$	$:= \left\{ v_\ell \in L^2(\Omega) \middle\vert \; v_\ell\vert_T \text{ is affine for all } T \in \mathcal{T}_\ell \right\}$
$P_1^{\mathrm{C}}(\mathcal{T}_\ell)$	$:= P_1(\mathcal{T}_\ell) \cap C(\Omega)$
$P_1^{\mathrm{NC}}(\mathcal{T}_\ell)$	$:= \{ v_\ell \in P_1(\mathcal{T}_\ell) \mid v_\ell \text{ continuous in } \operatorname{mid}(E) \text{ for } E \in \mathcal{E}_\ell \}$
$P_{1,0}^{\mathrm{NC}}(\mathcal{T}_\ell)$	$:= \{ v_\ell \in P_1^{\mathrm{NC}}(\mathcal{T}_\ell) \mid v_\ell(\operatorname{mid}(E)) = 0 \text{ for } E \subseteq \partial\Omega \}$
$\hat{P}_1(\mathcal{T}_\ell)$	$:= \left\{ v \in P_1(\mathcal{T}_\ell) \cap C\left(\bar{\Omega}\right) \middle\vert \fint_\Omega v \,\mathrm{dx} = 0 \right\}$

Table 2.8: Finite element function spaces and broken discrete function spaces.

denotes the jump of v across the edge $E = T_+ \cap T_-$ shared by the two elements $T_+, T_- \in \mathcal{T}_\ell$ and $\langle v \rangle_E := \frac{1}{2}((v|_{T_+})\big|_E + (v|_{T_-})\big|_E)$ denotes the average on E. For boundary edges $E \in \mathcal{E}_\ell(\partial\Omega)$ the jump as well as the average is the restriction to the one element T_+, namely, $\langle v \rangle_E := [v]_E := v|_{T_+}\big|_E$. As well as Ω_E, Table 3.14 includes the definition of node patches used later.

2.4 Finite element spaces

Definition 2.4.1 (Finite element, [BS08, Cia78])**.** *The triple $(T, \mathcal{P}, \mathcal{N})$ is called a finite element in the sense of Philippe G. Ciarlet, if the following properties hold*

*(i) the **element domain** $T \subseteq \mathbb{R}^n$ is a domain with piecewise smooth boundary,*
*(ii) the **space of shape functions** $\mathcal{P}$ is a finite-dimensional space of functions on T,*
*(iii) the **nodal variables** $\mathcal{N} = \{N_1, \ldots, N_m\}$ form a basis of the dual space $\mathcal{P}^\star$.*

For some finite element $(T, \mathcal{P}, \mathcal{N})$ the nodal basis $\{\phi_1, \ldots \phi_m\}$ is the basis for $\mathcal{P}$ that is dual to $\mathcal{N}$, i.e.,

$$N_j(\phi_k) = \delta_{jk} \quad \text{for } 1 \leqslant j, k \leqslant m.$$

For the linear conforming finite element, named after Courant, let $\mathcal{P} := P_1(T)$ and $\mathcal{N} = \{N_1, N_2, N_3\}$ be the nodal variables with the point evaluation $N_j(v) = v(z_j)$ in the vertices z_1, z_2, and z_3 of T.

For the linear nonconforming finite element, named after Crouzeix and Raviart, let $\mathcal{P} := P_1(T)$ and $\mathcal{N} = \{N_1, N_2, N_3\}$ be the nodal variables with the point evaluation

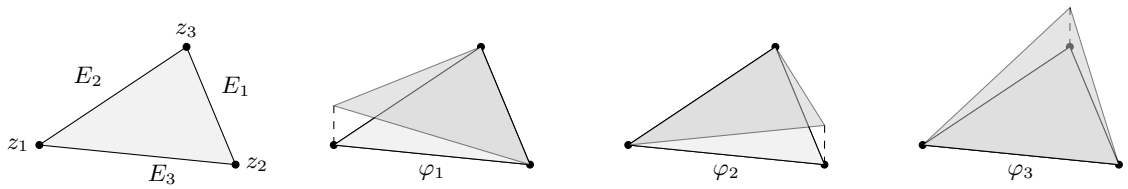

Figure 2.9: The Courant finite element (P_1) and its nodal basis functions on some triangle.

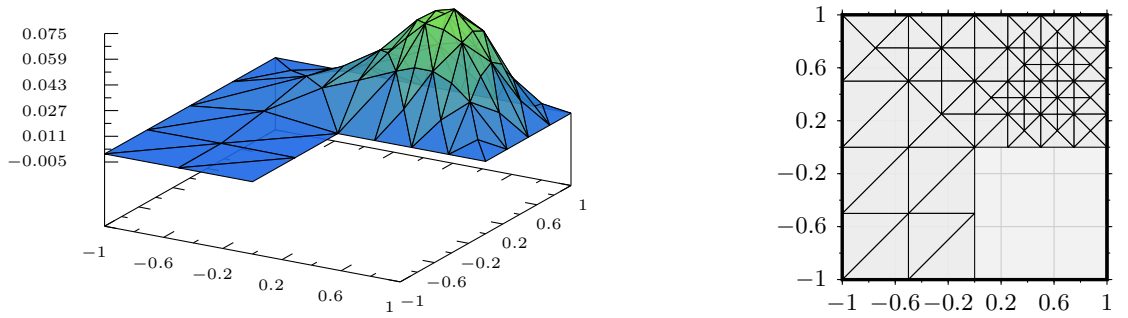

Figure 2.10: An example of a Courant finite element solution on an L-shaped domain for the benchmark problem of Section 7.3. $\epsilon = 2^{-2}$, $\nu = 0.3$ on level $\ell = 3$ with `ndof` $= 88$ computed with C-AFEM and $\theta_A = 0.6$.

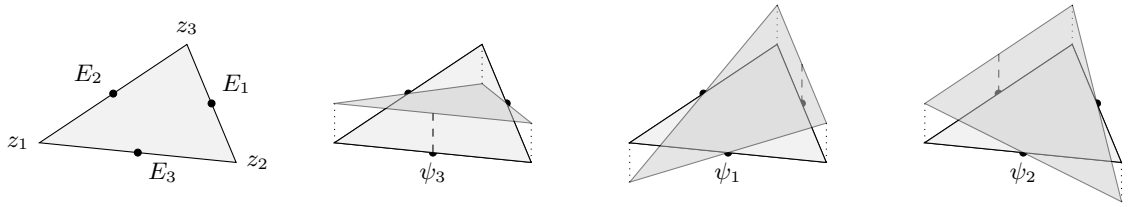

Figure 2.11: The Crouzeix–Raviart finite element (P_1^{NC}) and its edge basis functions on some triangle.

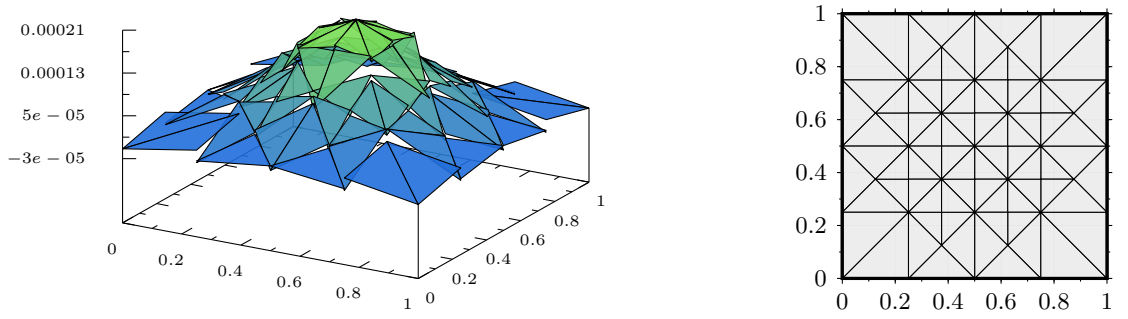

Figure 2.12: An example of a Crouzeix–Raviart finite element solution on a unit square for the benchmark problem of Section 7.3. $\epsilon = 2^{-6}$, $\nu = 0.3$ on level $\ell = 5$ with `ndof` $= 112$ computed with S-AFEM-AA and $\theta_A = 0.2$, $\rho_B = 0.625$, $\kappa = 0.1$.

$N_j(v) = v(\mathrm{mid}(E_j))$ in the midpoints of the edges E_1, E_2, and E_3 of T. Then, the dual basis is $\psi_{E_j} = 1 - 2\phi_j$.

This thesis analyses adaptive FEM algorithms based on the Crouzeix–Raviart finite element space. The definitions of specific discrete conforming and nonconforming spaces used in this thesis are shown in Table 2.8.

Definition 2.4.2 (Standard interpolant)**.** *For a finite element $(T, \mathcal{P}, \mathcal{N})$, let $\{\phi_1, \ldots, \phi_m\} \subseteq \mathcal{P}$ be the basis for $\mathcal{P}$ that is dual to $\mathcal{N}$. The local interpolant of a function v defined for all $N_j \in \mathcal{N}$ $(1 \leqslant j \leqslant m)$ is given by*

$$\mathcal{I}_T v := \sum_{j=1}^{m} N_j(v)\phi_j.$$

Let $\mathcal{T}$ be a triangulation of the domain Ω. Assume that there exists a finite element triple $(T, \mathcal{P}_T, \mathcal{N}_T)$ for all $T \in \mathcal{T}$. The global interpolant of a sufficiently smooth function $f \in C^k(\bar{\Omega})$ is defined by

$$\mathcal{I}_{\mathcal{T}} f|_T = \mathcal{I}_T f \quad \text{for all } T \in \mathcal{T}.$$

Definition 2.4.3 (Standard nonconforming interpolant)**.** *Let $v \in H^1(\mathcal{T})$ be the nonconforming interpolant $\mathcal{I}_{\mathcal{T}}^{\mathrm{NC}} : H^1(\mathcal{T}) \to P_{1,0}^{\mathrm{NC}}(\mathcal{T})$ defined by*

$$(\mathcal{I}_{\mathcal{T}}^{\mathrm{NC}} v)(\mathrm{mid}(E)) := \fint_E v \,\mathrm{ds} \qquad \text{for all } E \in \mathcal{E}\,.$$

3 Adaptive algorithms

Consider a discrete problem characterised by some bilinear form a_ℓ and linear form F written as: seek $u_\ell \in V_\ell$ such that $a_\ell(u_\ell, v_\ell) = F(v_\ell)$ for all $v_\ell \in V_\ell$. The standard scheme for AFEMs (in particular those that rely on collective marking) consists of the iterative loop of the basic steps

$$\text{Solve} \to \text{Estimate} \to \text{Mark} \to \text{Refine}.$$

The algorithm starts with a coarse initial triangulation $\mathcal{T}_0$ of Ω. On each level $\ell \in \mathbb{N}_0$ a regular triangulation $\mathcal{T}_\ell$ of Ω is available and the discrete solution $u_\ell \in V_\ell$ of the discrete problem is computed and the error is estimated. This error estimator (or other refinement indicators) lead to a set of finite element domains, which are selected for refinement and yields a regular triangulation $\mathcal{T}_{\ell+1}$ for the next level. This algorithm automatically refines the mesh for regions with singularities of the solution or poor data approximation, e.g., when there are large values on the right-hand side $f \in L^2(\Omega)$.

Section 3.1 reviews different marking strategies, such as collective and separate marking, and then introduces the refinement of triangulations using the Newest Vertex Bisection (NVB). The representation of NVB refinements by binary trees and some properties of nested triangulations are considered in Section 3.2. An algorithm that realises optimal data approximation is introduced in Section 3.3. Section 3.4 includes a detailed description of the steps of the algorithm S-AFEM-AA based on separate marking. This algorithm is analysed in this thesis. Section 3.5 deals with the optimal combination of two independently refined meshes, which is a crucial step for proving the quasi-optimality of S-AFEM-AA. The last section of this chapter presents a neat collection of fundamental results and preliminaries for the analysis of quasi-optimal convergence. This general methodology is required in Chapters 4–6.

The majority of the following definitions and results were established to analyse AFEMs based on collective marking strategies (C-AFEM) and can be found in the standard literature for FEMs [Bra01, BS08] and for adaptive FEMs, e.g., [Bra01, BDdV04, Car04, Ste08, Car97, CH06b, CH06a, Dör96, BS08]. As explicitly stated, some of the presented results can be found in recently published papers [CR11, CR12, Rab10, KPP12, CKNS08]. In particular the last section, i.e., Section 3.6 of this chapter, includes a derivation of the key arguments extracted from [CR11, Theorem 5.8], which reduces the proof of quasi-optimality in each considered example to the verification of fundamental properties.

This chapter prepares a general methodology, such that the results achieved for AFEMs based on collective marking can be applied to adaptive algorithms based on separate marking as well.

Input: Initial coarse triangulation $\mathcal{T}_0$, $0 < \theta_A < \theta_0 \leqslant 1$.
for $\ell = 0, 1, \ldots$ **do**
SOLVE the discrete problem on $\mathcal{T}_\ell$ and in V_ℓ.
ESTIMATE the error, i.e., evaluate the refinement indicator μ_ℓ^2.
MARK a quasi-minimal subset $\mathcal{M}_\ell \subseteq \mathcal{E}_\ell \cup \mathcal{T}_\ell$ of elements and edges satisfying the bulk criterion, i.e.,

$$\theta_A \mu_\ell^2 \leqslant \mu_\ell^2(\mathcal{M}_\ell) \tag{3.1}$$

and $|\mathcal{M}_\ell| \approx \min\left\{|\mathcal{M}| \,\middle|\, \theta_A \mu_\ell^2 \leqslant \mu_\ell^2(\mathcal{M}),\ \mathcal{M} \subseteq \mathcal{E}_\ell \cup \mathcal{T}_\ell\right\}$.
REFINE all edges in the CLOSURE $\mathcal{C}\ell\,(\mathcal{M}_\ell^{\mathrm{E}})$

$$\text{with } \{E(T) \in \mathcal{E}_\ell \,|\, T \in \mathcal{T}_\ell \text{ and } \mathcal{E}(T) \cap \mathcal{C}\ell\,(\mathcal{M}_\ell^{\mathrm{E}}) \neq \varnothing\} \subseteq \mathcal{C}\ell\,(\mathcal{M}_\ell^{\mathrm{E}})$$

to generate a new regular triangulation $\mathcal{T}_{\ell+1}$.
Output: Sequence of triangulations $(\mathcal{T}_k)_{0\leqslant k}$ and discrete solutions $(u_k^{\mathrm{NC}})_{0\leqslant k}$.

Algorithm 3.1: Overview of the adaptive finite element algorithm, C-AFEM, which is based on collective marking and is used to solve the discretised model problems (i.e., Poisson model problem, pure displacement problem in linear elasticity and the Stokes problem). C-AFEM is analysed in [Rab10, CR12, CPR13].

κ	parameter that steers the switching between Cases (A) and B in S-AFEM-AA and S-AFEM-DM
θ_A	bulk parameter for the Dörfler marking in Case (A) of S-AFEM or bulk parameter for the Dörfler marking of C-AFEM
θ_B	bulk parameter for the Dörfler marking in Case (B)
ρ_B	reduction factor for the volume term $\|h_\ell f\|_{L^2(\Omega)}$ in Case (B)
$\mathcal{M}_\ell$	set of edges and elements that have been marked for refinement
$\mathcal{C}\ell(\mathcal{M}_\ell)$	set of edges and triangles that will be refined (CLOSURE applied to $\mathcal{M}_\ell$; see (3.3))
$\mu_\ell^2(\mathcal{M}_\ell)$	$:= \sum_{E\in\mathcal{M}_\ell} \mu_\ell^2(E)$ for $\mathcal{M}_\ell \subseteq \mathcal{E}_\ell$, problem-specific edge-based refinement indicator for C-AFEM
μ_ℓ^2	$:= \mu_\ell^2(\mathcal{E}_\ell)$ problem-specific edge-based refinement indicator for C-AFEM
$\eta_\ell^2(\mathcal{M}_\ell)$	$:= \sum_{E\in\mathcal{M}_\ell} \eta_\ell^2(E)$ for $\mathcal{M}_\ell \subseteq \mathcal{E}_\ell$, problem-specific edge-based refinement indicator for S-AFEM
η_ℓ^2	$:= \eta_\ell^2(\mathcal{E}_\ell)$
$\mathcal{M}_\ell^{\mathrm{E}}$	$:= (\mathcal{M}_\ell \cap \mathcal{E}_\ell) \cup E(\mathcal{M}_\ell \cap \mathcal{T}_\ell)$, the union of the set of marked edges and the set of refinement edges $E(\mathcal{M}_\ell \cap \mathcal{T}_\ell)$ (see Remark 2.3.2) of the set of marked elements

Table 3.2: Notation on adaptive algorithms.

Input: Initial coarse triangulation $\mathcal{T}_0$, $0 < \theta_A < \theta_0 \leqslant 1$, $0 < \theta_B < 1$, $0 < \kappa_1 < \kappa < \kappa_2$.
for $\ell = 0, 1, \ldots$ **do**
  SOLVE the discrete problem on $\mathcal{T}_\ell$ and in V_ℓ.
  ESTIMATE the error, i.e., evaluate the refinement indicators η_ℓ^2 and $\|h_\ell f\|^2_{L^2(\Omega)}$.
  if $\|h_\ell f\|^2_{L^2(\Omega)} \leqslant \kappa \eta_\ell^2$ **then**
    MARK a quasi-minimal subset $\mathcal{M}_\ell \subseteq \mathcal{E}_\ell \cup \mathcal{T}_\ell$ of elements and edges satisfying the bulk criterion, i.e.,

$$\theta_A \eta_\ell^2 \leqslant \eta_\ell^2(\mathcal{M}_\ell)$$

    and $|\mathcal{M}_\ell| \approx \min\left\{|\mathcal{M}| \,\middle|\, \theta_A \eta_\ell^2 \leqslant \eta_\ell^2(\mathcal{M}),\ \mathcal{M} \subseteq \mathcal{E}_\ell \cup \mathcal{T}_\ell\right\}$.
  else
    MARK a quasi-minimal subset $\mathcal{M}_\ell \subseteq \mathcal{T}_\ell$ of elements satisfying the bulk criterion, i.e.,

$$\theta_B \|h_\ell f\|^2_{L^2(\Omega)} \leqslant \|h_\ell f\|^2_{\mathcal{M}_\ell}$$

    and $|\mathcal{M}_\ell| \approx \min\left\{|\mathcal{M}| \,\middle|\, \theta_B \|h_\ell f\|^2_{L^2(\Omega)} \leqslant \|h_\ell f\|^2_{\mathcal{M}},\ \mathcal{M} \subseteq \mathcal{T}_\ell\right\}$.
  REFINE all edges in the CLOSURE $\mathcal{C}\ell(\mathcal{M}_\ell^{\mathrm{E}})$ with $\{E(T) \in \mathcal{E}_\ell \,|\, T \in \mathcal{T}_\ell \text{ and } \mathcal{E}(T) \cap \mathcal{C}\ell(\mathcal{M}_\ell^{\mathrm{E}}) \neq \varnothing\} \subseteq \mathcal{C}\ell(\mathcal{M}_\ell^{\mathrm{E}})$ to generate a new regular triangulation $\mathcal{T}_{\ell+1}$.
Output: Sequence of triangulations $(\mathcal{T}_k)_{0 \leqslant k}$, and discrete solutions $(u_k^{\mathrm{NC}})_{0 \leqslant k}$.

Algorithm 3.3: Overview of an adaptive finite element algorithm, S-AFEM-DM, based on separate marking **(b)** as shown on page 22 and is used to solve the discretised model problems (i.e., Poisson model problem, pure displacement problem in linear elasticity and the Stokes problem).

3.1 Marking strategies for adaptive finite element methods

The refinement in an adaptive scheme is steered by refinement indicators (such as error estimators or data approximation terms). Due to the reliability of the estimator, the convergence of the sequence of discrete solutions is guaranteed only for small values of the volume term $\|h_\ell f\|_{L^2(\Omega)}$.

Apart from an *a priori* mesh generation, where some algorithm (e.g., Algorithm 3.17 (AA) of [BDdV04] or some adaptive scheme based on the Dörfler marking) is applied to generate an initial triangulation $\mathcal{T}_0$ with $\|h_0 f\|_{L^2(\Omega)} \leqslant \mathrm{Tol}$; there are two principal approaches for simultaneous data approximation. Both collective marking and separate marking realise a simultaneous reduction of $\|h_\ell f\|_{L^2(\Omega)}$ as well as η_ℓ and therefore fit the general concept of AFEM algorithms.

Collective marking implies that the total error is estimated and thus the volume term is reduced within the standard AFEM loop; see Algorithm 3.1 for the general scheme. In separate marking strategies a special routine is applied for the reduction of the volume term, which does not fit completely into the standard AFEM loop with the steps SOLVE, ESTIMATE, MARK and REFINE. Different approaches to guarantee approximation of the

Input: Initial coarse triangulation $\mathcal{T}_0$, $0 < \theta_A < \theta_0 \leqslant 1$, $0 < \rho_B < 1$, $0 < \kappa_1 < \kappa < \kappa_2$.
for $\ell = 0, 1, \ldots$ **do**
SOLVE the discrete problem on $\mathcal{T}_\ell$ and in V_ℓ.
ESTIMATE the error, i.e., evaluate the refinement indicators η_ℓ^2 and $\|h_\ell f\|^2_{L^2(\Omega)}$.
if $\|h_\ell f\|^2_{L^2(\Omega)} \leqslant \kappa \eta_\ell^2$ **then**
MARK a quasi-minimal subset $\mathcal{M}_\ell \subseteq \mathcal{E}_\ell \cup \mathcal{T}_\ell$ of elements and edges satisfying the bulk criterion, i.e.,

$$\theta_A \eta_\ell^2 \leqslant \eta_\ell^2(\mathcal{M}_\ell) \tag{3.2}$$

and $|\mathcal{M}_\ell| \approx \min\left\{|\mathcal{M}| \,\middle|\, \theta_A \eta_\ell^2 \leqslant \eta_\ell^2(\mathcal{M}), \mathcal{M} \subseteq \mathcal{E}_\ell \cup \mathcal{T}_\ell\right\}$.
REFINE all edges in the CLOSURE $\mathcal{C}\ell(\mathcal{M}_\ell^{\mathrm{E}})$with $\{E(T) \in \mathcal{E}_\ell \,|\, T \in \mathcal{T}_\ell \text{ and } \mathcal{E}(T) \cap \mathcal{C}\ell(\mathcal{M}_\ell^{\mathrm{E}}) \neq \varnothing\} \subseteq \mathcal{C}\ell(\mathcal{M}_\ell^{\mathrm{E}})$ to generate a new regular triangulation $\mathcal{T}_{\ell+1}$.
else
MARK elements for refinement, i.e., apply Algorithm 3.17 (AA) (i.e., TSA plus completion) of [BDdV04], to compute an optimal $\mathcal{T}$ with
$\mathrm{Tol} := \rho_B \|h_\ell f\|^2_{L^2(\Omega)}$ and
$\|h_{\mathcal{T}} f\|^2_{L^2(\Omega)} \leqslant \mathrm{Tol}$ and $|\mathcal{T}| - |\mathcal{T}_0| \lesssim \mathrm{Tol}^{-1/(2s)}$.
REFINE $\mathcal{T}_\ell$ to generate a regular triangulation $\mathcal{T}_{\ell+1}$ by computing the overlay $\mathcal{T}_{\ell+1} := \mathcal{T}_\ell \oplus \mathcal{T}$, cf. e.g, Algorithm 3.18.
Output: Sequence of triangulations $(\mathcal{T}_k)_{0 \leqslant k}$ and discrete solutions $(u_k^{\mathrm{NC}})_{0 \leqslant k}$.

Algorithm 3.4: Overview of an adaptive finite element algorithm, S-AFEM-AA, based on separate marking **(c)** and is used to solve the discretised model problems (i.e., Poisson model problem, pure displacement problem in linear elasticity and the Stokes problem). S-AFEM-AA is analysed in this thesis.

data in separate ways have been investigated, e.g.,

- **(a)** inner loop for oscillations [Ste07],
- **(b)** switch cases and use a separate bulk criterion for oscillations, as in e.g., [BM11, BM08]; see Algorithm 3.3 for the general scheme,
- **(c)** switch cases and use AA for oscillations (i.e., APPROX by [BDdV04]) and compute the overlay of meshes [CR11]; see Algorithm 3.4 and Section 3.4 for details.

Although any variant of the presented adaptive schemes were proven to give quasi-optimal convergence for at least one application (i.e., for a combination of a selected problem, a FEM and a corresponding refinement indicator), there may be huge differences in the computational effort.

Both variants **(a)** and **(b)** may lead to several iterations of the adaptive algorithm to improve data approximation. Although data approximation is independent of the discrete solution, in **(a)** and **(b)** the discrete system has to be solved repeatedly. This is avoided in **(c)** by generating an optimal triangulation $\mathcal{T}$ via AA and computing the overlay $\mathcal{T} \oplus \mathcal{T}_\ell =: \mathcal{T}_{\ell+1}$ as introduced in [CR11]. If the volume term is taken into account instead of oscillations, similar algorithms are possible. Strategy **(c)** has been analysed

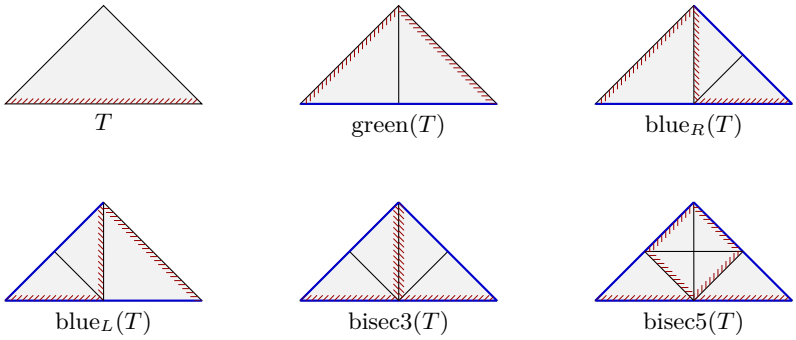

Figure 3.5: Possible refinements of a triangle T in one level using NVB.
Depending on the number of marked edges (in blue) one of the refinements is selected. If all three edges are marked, either bisec3(T) or bisec5(T) can be applied. The refinement edges for the next level of the refined triangles are highlighted in red and ruled.

in [CR11] for the Poisson model problem and lowest-order Raviart–Thomas mixed FEM. Carstensen and Park investigated a least-squares FEM [CP]. However, further applications and analysis of this potentially more effective strategy have not yet been reported.

This thesis is a first approach for showing quasi-optimal convergence for a nonconforming adaptive scheme based on separate marking and **(c)** for the three model problems. Numerical experiments verify these results. The applied separate marking strategy is based on a combination of an *a posteriori* error estimator η_ℓ and the control of the volume term $\|h_\ell f\|_{L^2(\Omega)}$ computed in step ESTIMATE and specialised steps MARK and REFINE, which are dependent on the ratio of η_ℓ and $\|h_\ell f\|_{L^2(\Omega)}$. The adaptive finite element algorithm is described in Section 3.4 and depicted in Algorithm 3.4.

3.2 Refined triangulations

This section clarifies, which refinements of the initial triangulation are admissible in the analysis of this thesis and gives their properties.

3.2.1 Admissible triangulations

To refine a triangulation, based on a set of marked elements or edges, a set of refinement rules is applied. The analysis of this thesis is based on the properties of the Newest-Vertex-Bisection (NVB). Possible NVB refinements of a triangle $T \in \mathcal{T}_\ell$ in one level of refinement are depicted in Figure 3.5 and depend on the set of edges that have to be refined; see Section 3.4 for details on the step REFINE of the adaptive algorithm.

Definition 3.2.1 (Admissible triangulations)**.** *Let $\mathcal{T}_\ell$ be a regular triangulation of Ω. A regular refinement $\mathcal{T}_{\ell+k}$ of $\mathcal{T}_\ell$ is called admissible if $\mathcal{T}_{\ell+k}$ can be generated by applying – possibly several successive levels of – NVB plus some* CLOSURE *algorithm to avoid hanging nodes and to sustain the shape regularity of the sequence $\mathcal{T}_\ell$.*

Remark 3.2.2 (CLOSURE)**.** *There are several strategies for refining a mesh by NVB with respect to a set of marked edges $\mathcal{M}_\ell$ and to ensure that the refined triangulation is*

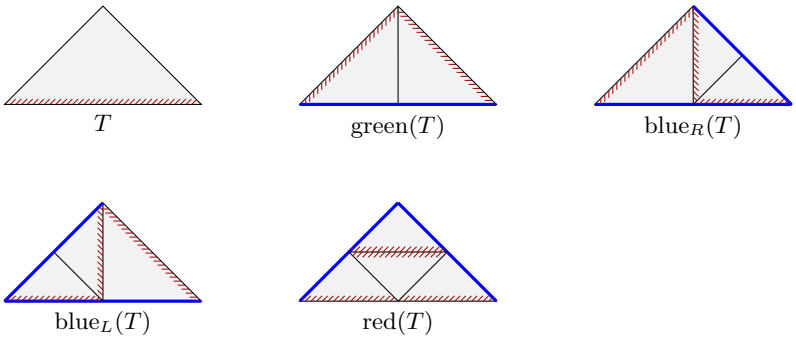

Figure 3.6: Refinements of a triangle T in one level using RGB. Refinements that rely on RGB are not feasible in this thesis.
Depending on the number of marked edges (in blue) one of the refinements is selected. If all three edges are marked, either bisec3(T) or bisec5(T) can be applied. The refinement edges for the next level of the refined triangles are highlighted in red and ruled.

admissible. One way is first to run some CLOSURE *algorithm to compute the smallest superset* $\mathcal{C}\ell(\mathcal{M}_\ell)$ *of* $\mathcal{M}_\ell$ *that satisfies*

$$\{E(T) \in \mathcal{E}_\ell \mid T \in \mathcal{T}_\ell \text{ and } \mathcal{E}(T) \cap \mathcal{C}\ell(\mathcal{M}_\ell) \neq \emptyset\} \subseteq \mathcal{C}\ell(\mathcal{M}_\ell). \tag{3.3}$$

Thereafter, refine each triangle according to Figure 3.5 and apply the indicated definition of the refinement edges.

To prove quasi-optimal complexity the overhead of CLOSURE in step REFINE has to be bounded. The following lemma is recapitulated from [Rab10] and is a straightforward extension of the result for the overhead of CLOSURE [BDdV04, Ste08, Car04, KPP12, CR11] for quasi-minimal sets in step MARK as allowed in the algorithms of this thesis. For the readers' convenience its proof is repeated here.

Lemma 3.2.3 (Overhead of CLOSURE, [Rab10])**.** *Let* $\mathcal{T}_\ell$ *be an admissible triangulation refined from* $\mathcal{T}_0$ *and* $\mathcal{M}_j \subseteq \mathcal{E}_j \cup \mathcal{T}_j$ *the set of marked elements and edges in step* MARK *and on level* $0 \leqslant j < \ell$*. Then, there exists some positive generic constant* $C_{\mathcal{C}\ell}$*, depending on* $\mathcal{T}_0$ *only, such that the overhead of* CLOSURE *is bounded as follows*

$$|\mathcal{T}_\ell| - |\mathcal{T}_0| \leqslant C_{\mathcal{C}\ell} \sum_{j=0}^{\ell-1} |\mathcal{M}_j|\,. \tag{3.4}$$

Different assumptions on the initial mesh has been established in the literature [BDdV04, Car04, Ste08]. However, in [KPP12] the estimate (3.4) has been proven without any condition on the distribution of refinement edges in $\mathcal{T}_0$. Moreover any possible refinement strategy that is a combination of iterative NVB refinement (see Figure 3.5) and red refinement, in particular the so-called RGB refinement (red-green-blue as in Figure 3.6) would be applicable. However, the restriction to NVB refinements in this thesis is essential for controlling the overhead of the overlay triangulation in step REFINE of S-AFEM-AA in Case (B), cf. Lemma 3.2.5 below. That is why RGB refinements are not feasible in this thesis.

Proof of Lemma 3.2.3 replicated from [Rab10, Lemma 2.3]. Let $\mathcal{M}_\ell^\star \subseteq \mathcal{E}_\ell \cup \mathcal{T}_\ell$ be the minimal set fulfilling the bulk criterion

$$\theta_A \eta_\ell^2 \leqslant \eta_\ell^2 (\mathcal{M}_\ell^\star)$$

in the level-oriented Case (A), $\mathcal{M}_\ell^\star$ is equivalent – with respect to the result of REFINE– to the set of marked edges

$$\begin{aligned} \mathcal{M}_\ell^{E\star} &:= \{E \in \mathcal{E}_\ell \,|\, E \in \mathcal{M}_\ell^\star \text{ or } E = E(T) \text{ with } T \in \mathcal{M}_\ell^\star\} \\ &= (\mathcal{M}_\ell^\star \cap \mathcal{E}_\ell) \cup E(\mathcal{M}_\ell^\star \cap \mathcal{T}_\ell). \end{aligned}$$

Recall that $\mathcal{M}_\ell^\star$ is quasi-minimal in the sense that

$$|\mathcal{M}_\ell^\star| \approx \min\left\{|\mathcal{M}| \,\middle|\, \theta_A \eta_\ell^2 \leqslant \eta_\ell^2(\mathcal{M}),\, \mathcal{M} \subseteq \mathcal{E}_\ell \cup \mathcal{T}_\ell\right\}.$$

Hence, (3.4) is a direct consequence of the known upper bound of CLOSURE [BDdV04, Ste08, Car04, KPP12, CR11] and the quasi-minimality, i.e.,

$$|\mathcal{T}_\ell| - |\mathcal{T}_0| \lesssim \sum_{j=0}^{\ell-1} \left|\mathcal{M}_j^{E\star}\right| \approx \sum_{j=0}^{\ell-1} \left|\mathcal{M}_j^\star\right| \approx \sum_{j=0}^{\ell-1} |\mathcal{M}_j|. \qquad \square$$

The estimate (3.4) is usually employed in Case (A), but holds in Case (B) in the sense that

$$|\mathcal{T}_\ell| - |\mathcal{T}_0| \leqslant C_{\mathcal{C}\ell} \sum_{j=0}^{\ell-1} \sum_{k=0}^{K(j)} \left|\mathcal{M}_j^{(k)}\right|, \tag{3.5}$$

where $\mathcal{M}_j^{(0)}, \dots, \mathcal{M}_j^{K(j)}$ is the output of Algorithm 3.18 in Case (B), and where $\mathcal{M}_j^{(0)} := \mathcal{M}_j$ and $K(j) := 0$ in Case (A).

3.2.2 Binary trees and forests representing refined triangulations

This subsection briefly introduces the concepts of *trees* and *forests* to clarify the notion of overlays, and the embedding of the independently refined triangulation into the iterative loop of standard level-oriented adaptive algorithms. A more detailed introduction, using a different notation, can be found in [BdV04, BDdV04].

A *rooted tree* is a graph where one *vertex* is designated to be the *root* and any two vertices are connected by exactly one path. If two vertices are connected by an edge, the vertex closer to the root is called the *parent*, the other its *child*. A vertex with at least one child is called an *interior vertex* and otherwise a *leaf*. A disjoint union of rooted trees is called a *forest*. The *master tree* is an infinite, complete binary tree. The disjoint union of master trees is called *master forest*.

Any possible NVB refinement $\mathcal{T}_\ell$ of $\mathcal{T}_0$ is represented by one forest $\mathcal{F}_\ell$, and the refinement of each triangle T of the initial triangulation $\mathcal{T}_0$ corresponds to one tree with root T in $\mathcal{F}_\ell$. The vertices in $\mathcal{F}_\ell$ are triangles in $\mathcal{T}_k$, $k = 0, \dots, \ell$. Each vertex in $\mathcal{F}_\ell$ has either two children or none and all but the root in $\mathcal{T}_0$ have an ancestor. The leaves $\mathcal{L}(\mathcal{F}_\ell)$ of all trees

$\mathcal{F}_\star$	infinite master forest, representing all admissible refinements from $\mathcal{T}_0$ by NVB (without any restrictions on regularity, i.e., hanging nodes)
$\mathcal{F}_\ell$	forest representing the refined triangulation $\mathcal{T}_\ell$ from $\mathcal{T}_0$
$\mathcal{L}(\mathcal{F}_\ell)$	set of leaves of the forest $\mathcal{F}_\ell$, in general: $\mathcal{T}_\ell := \mathcal{L}(\mathcal{F}_\ell)$
$\mathcal{V}(\mathcal{F}_\ell)$	set of interior vertices of $\mathcal{F}_\ell$
$\mathcal{F}_a \cup \mathcal{F}_b$	union of two forests, representing the overlay of the corresponding triangulations, i.e., $\mathcal{T}_a \oplus \mathcal{T}_b$
$\oplus$	coarsest common refinement of two triangulations; overlay triangulation

Table 3.7: Notation for forests.

in the forest $\mathcal{F}_\ell$ are the triangles in $\mathcal{T}_\ell$, i.e., they do not have any children. The set of interior vertices is denoted by $\mathcal{V}(\mathcal{F}_\ell)$.

A *sub-forest* $\mathcal{F}_\ell \subset \mathcal{F}_\star$ needs to satisfy the following conditions:

- If a triangle T is a vertex in $\mathcal{F}_\ell$, its siblings need to be a vertex in $\mathcal{F}_\ell$ as well.
- If a triangle T is a vertex, but not a root vertex in $\mathcal{F}_\ell \backslash \mathcal{T}_0$, its parent needs to be a vertex in $\mathcal{F}_\ell$.

A sub-forest $\mathcal{F}_\ell \subset \mathcal{F}_\star$ is a *proper* sub-forest, if each root vertex of any tree in $\mathcal{F}_\star$ is in $\mathcal{F}_\ell$, i.e., $\mathcal{F}_0 \subset \mathcal{F}_\ell$.

The forest $\mathcal{F}_\ell$ representing a NVB refinement of $\mathcal{T}_0$ is a finite proper sub-forest of the infinite master forest $\mathcal{F}_\star$. This implies that the refinement history of any triangle $T \in \mathcal{T}_0$ is included in $\mathcal{F}_\ell$.

The corresponding triangulation, i.e., the elements in that triangulation, is denoted by $\mathcal{T}_\ell := \mathcal{L}(\mathcal{F}_\ell)$. Table 3.7 summarises the essential notation for forests and the corresponding triangulations. Figure 3.8 shows the binary trees for all possible refinements of a triangle T using NVB up to *bisec5*.

In steps Mark and Refine of standard adaptive finite element algorithms a refined triangulation is computed by marking a set of edges, followed by Closure (see Remark 3.2.2) and NVB. For ease of presentation this standard version is called Case (A).

A different strategy overlays the current triangulation $\mathcal{T}_\ell$ with an admissible triangulation $\mathcal{T}$ represented by a forest $\mathcal{F}$. Note that $\mathcal{T}$ is in general independent of $\mathcal{T}_\ell$ and is refined from $\mathcal{T}_0$ by a possibly unbounded number of refinement levels using NVB. This nonstandard refinement strategy is called Case (B). The definition and the key estimate for the overlay of triangulations is given below. Then, on each level ℓ, a triangulation $\mathcal{T}_\ell$ and its forest $\mathcal{F}_\ell$ are available.

Definition 3.2.4 (Overlay of two refinements of $\mathcal{T}_0$)**.** *Given two admissible triangulations $\mathcal{T}_\ell$ and $\mathcal{T}$, both refined from $\mathcal{T}_0$, let $\mathcal{F}_\ell$ and $\mathcal{F}$ denote their forests. The coarsest common refinement $\mathcal{T}_\ell \oplus \mathcal{T}$ is called the overlay. It is defined by its forest, which is the union $\mathcal{F}_\ell \cup \mathcal{F}$ of the forests of $\mathcal{T}_\ell$ and $\mathcal{T}$.*

See Figure 3.9 for an example for the overlay of triangulations defined above.

The number of elements of the overlaid triangulation is bounded as stated in the following lemma.

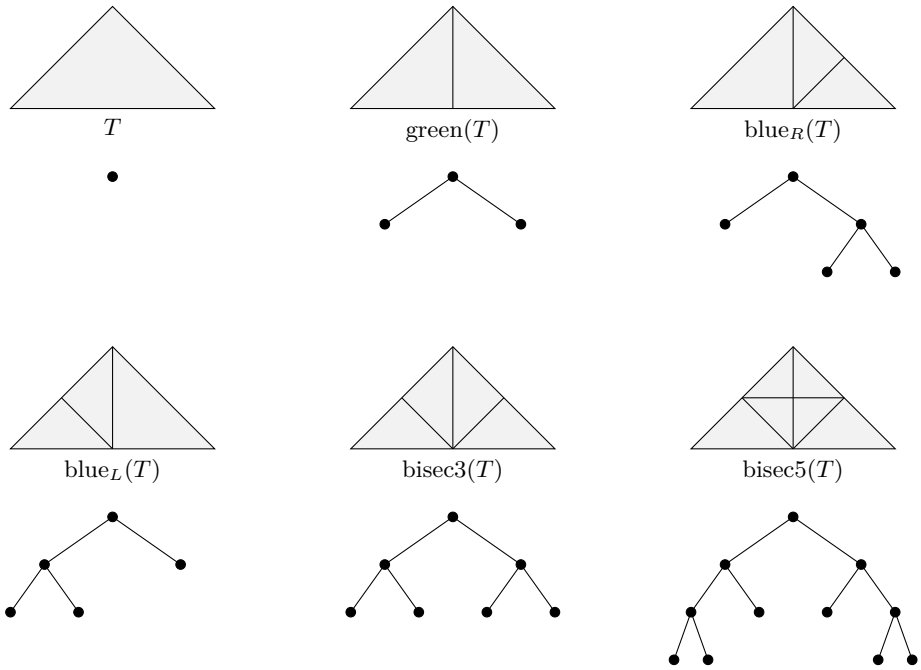

Figure 3.8: Binary trees representing the different possibilities for the NVB refinements of a triangle.

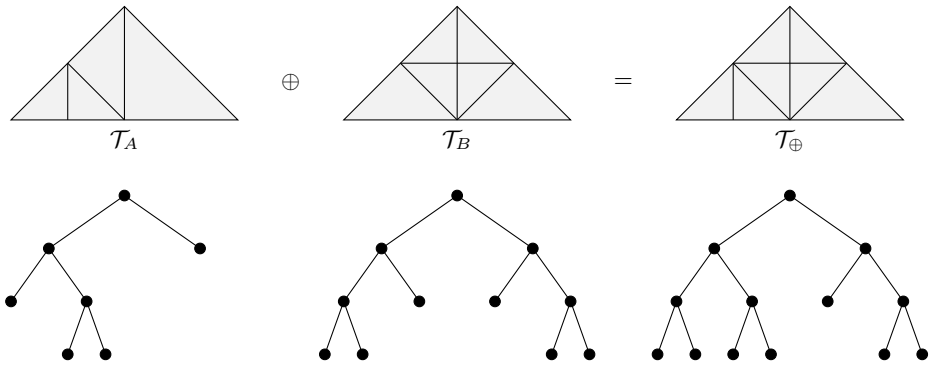

Figure 3.9: Example for the overlay of two NVB refinements of a single triangle represented by their binary trees.

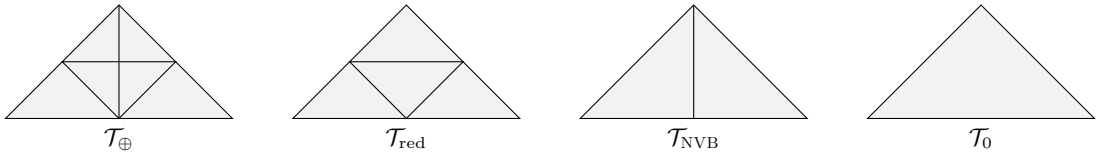

Figure 3.10: Counterexample: Overhead of the overlay of two triangulations refined using the RGB refinement shown in Figure 3.6.

$\mathcal{T}_{\ell\setminus\ell+k} \subseteq \mathcal{T}_\ell$	refined triangles from level ℓ to $\ell+k$
$\mathcal{E}_{\ell\setminus\ell+k} \subseteq \mathcal{E}_\ell$	refined edges from level ℓ to $\ell+k$
$\mathcal{T}_\ell \cap \mathcal{T}_{\ell+k}$	elements that have not been refined from level ℓ to $\ell+k$
$\mathcal{E}_\ell \cap \mathcal{E}_{\ell+k}$	edges that have not been refined from level ℓ to $\ell+k$

Table 3.11: Set notation for nested triangulations $\mathcal{T}_\ell$ and $\mathcal{T}_{\ell+k}$.

Lemma 3.2.5 (Overhead of overlay, [CKNS08])**.** *The overlay $\mathcal{T}_\ell \oplus \mathcal{T}$ of two admissible $\mathcal{T}_\ell$ and $\mathcal{T}$, both refined from $\mathcal{T}_0$, is regular and the numbers of elements satisfy*

$$|\mathcal{T}_\ell \oplus \mathcal{T}| - |\mathcal{T}_\ell| \leqslant |\mathcal{T}| - |\mathcal{T}_0|\,. \tag{3.6}$$

Figure 3.10 shows an example where the overlay of two triangulations refined from $\mathcal{T}_0$ by NVB and red refinement is computed. In this example the overhead of the overlay violates (3.6) due to the red refinement.

3.2.3 Properties of nested triangulations

Here, and in the following, let $\mathcal{T}_\ell$ and $\mathcal{T}_{\ell+k}$ be nested, admissible triangulations and $\mathcal{T}_{\ell+k}$ is a refinement of $\mathcal{T}_\ell$ in $k \in \mathbb{N}$ levels of refinements. Then, the sets of all refined elements or edges are denoted by $\mathcal{T}_{\ell\setminus\ell+k} := \mathcal{T}_\ell \setminus \mathcal{T}_{\ell+k}$ or $\mathcal{E}_{\ell\setminus\ell+k} := \mathcal{E}_\ell \setminus \mathcal{E}_{\ell+k}$, respectively; see Table 3.11.

Standard arguments show that the volume term for $f \in L^2(\Omega)$ satisfies

$$\|h_{\ell+1} f\|^2_{L^2(\Omega)} \leqslant \|h_\ell f\|^2_{L^2(\Omega)} - \frac{1}{2}\,\|h_\ell f\|^2_{\mathcal{T}_{\ell\setminus\ell+1}} = \frac{1}{2}\,\|h_\ell f\|^2_{\mathcal{T}_{\ell\setminus\ell+1}} + \|h_\ell f\|^2_{\mathcal{T}_\ell \cap \mathcal{T}_{\ell+1}}\,. \tag{3.7}$$

Furthermore, the number of elements and edges satisfy the following inequality.

Lemma 3.2.6. *The numbers of elements and edges of $\mathcal{T}_\ell$ and $\mathcal{T}_{\ell+k}$ satisfy*

$$\big|\mathcal{E}_{\ell\setminus\ell+k}\big| \leqslant 2\big(\,|\mathcal{T}_{\ell+k}| - |\mathcal{T}_\ell|\,\big). \tag{3.8}$$

[CR11] has a proof for a weaker estimate with the factor 3 on the right-hand side. The proof of Lemma 3.2.6 below improves this factor using a more detailed inspection of the assignment of one proper neighbour $K_E \in \mathcal{T}_\ell$ of E by the mapping Ψ using similar arguments as in [CR11].

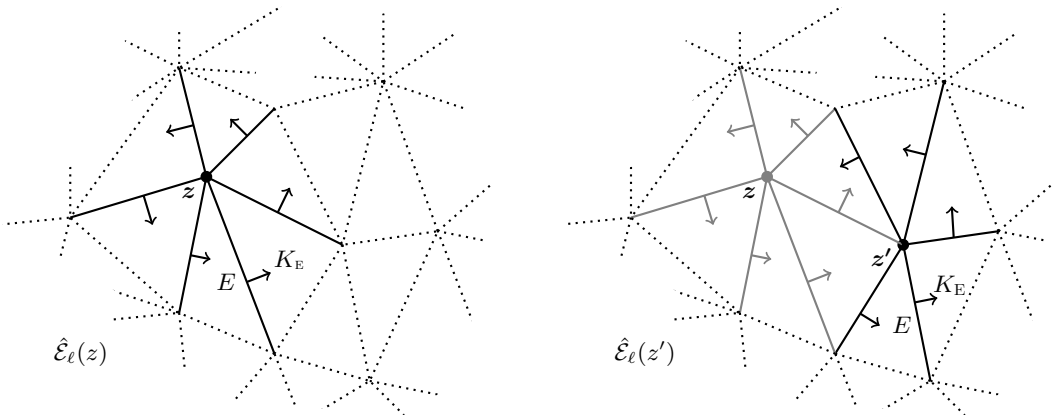

Figure 3.12: The arrows represents one possible mapping $E \mapsto K_E$ as described in Remark 3.2.7 with $\hat{\mathcal{E}}_\ell(z) \subseteq \omega_z$ for two selected situations.

Input: $\hat{\mathcal{K}}_\ell := \mathcal{K}_\ell$, $\hat{\mathcal{E}}_\ell^{(0)} := \mathcal{E}_\ell$.
while $\hat{\mathcal{K}}_\ell \neq \varnothing$ **do**
  Choose $z \in \hat{\mathcal{K}}_\ell$, define the set of edges ending at z

$$\hat{\mathcal{E}}_\ell(z) := \left\{E \in \hat{\mathcal{E}}_\ell \mid E \cap z = \{z\}\right\}$$

  and define $\Psi(E)|_{\hat{\mathcal{E}}_\ell(z)}$ such that each edge $E \in \hat{\mathcal{E}}_\ell(z)$ is assigned to exactly one element $K_E \in \omega_z$. E.g., define $\Psi(E) = K_E$ counterclockwise, as depicted in Figure 3.12.
  Let

$$\hat{\mathcal{K}}_\ell := \hat{\mathcal{K}}_\ell \setminus \{z\}, \quad \hat{\mathcal{E}}_\ell := \hat{\mathcal{E}}_\ell \setminus \hat{\mathcal{E}}_\ell(z).$$

for *each* $E \in \mathcal{E}_\ell(\partial\Omega)$ **do**
  Define $\Psi(E) := T_+$ with $E \subseteq T_+$.
Output: A mapping $\Psi : \mathcal{E}_\ell \to \mathcal{T}_\ell$, $E \to K_E$.

Algorithm 3.13: Algorithm that realises the mapping $\Psi : \mathcal{E}_\ell \to \mathcal{T}_\ell$ of Remark 3.2.7 and which is used in the proof of Lemma 3.2.6.

Remark 3.2.7. *Given any edge $E \in \mathcal{E}_\ell$, there exists exactly one or two neighbours T_+ or $T_\pm$ in $\mathcal{T}_\ell$ with $E \subseteq \partial T_+ \cap \partial\Omega$ or $E = \partial T_+ \cap \partial T_-$; see Figure 2.7. Let $\Psi : \mathcal{E}_\ell \to \mathcal{T}_\ell$, be a mapping, such that $E \mapsto K_E$. Ψ aims to select one of the elements $T_\pm$ and denotes the chosen one as K_E, such that the case*

$$K_{E_1} = K_{E_2} = K_{E_3} \quad \text{with } \mathcal{E}_\ell(T) = \{E_1, E_2, E_3\}$$

is excluded. Figure 3.12 is an example of a mapping.

In other words, for all $K \in \mathcal{T}_\ell$ there is at least one edge E of K with $K_E \neq K$. For an admissible triangulation $\mathcal{T}_\ell$ this selection is always possible. One possibility is realised by Algorithm 3.13.

Proof of Lemma 3.2.6. Let the mapping $\Psi : \mathcal{E}_\ell \to \mathcal{T}_\ell$, $E \to K_E$ of Remark 3.2.7 be defined by Algorithm 3.13. It remains to prove that the defined Ψ fulfils

$$\forall T \in \mathcal{T}_\ell \quad \exists E_1, E_2 \in \mathcal{E}_\ell(T) \quad \Psi(E_1) \neq \Psi(E_2). \tag{3.9}$$

After any iteration of the 1st loop of Algorithm 3.13 for any $T \in \mathcal{T}_\ell$ the mapping Ψ is defined for none of the edges in $\mathcal{E}_\ell(T)$, if none of its three nodes has been selected so far in a previous iteration of that loop; exactly two of the edges in $\mathcal{E}_\ell(T)$, if one of the three nodes has been selected; or for all three edges in $\mathcal{E}_\ell(T)$, if at least two nodes have been selected so far.

In the second and third cases, the two edges E_1, E_2 of T for which Ψ has been defined, satisfy $\Psi(E_1) \neq \Psi(E_2)$. Hence, for the remaining edge the definition of Ψ is irrelevant for T to satisfy (3.9).

Once this has been done for all interior nodes, all remaining edges $E \in \mathcal{E}_\ell(\partial\Omega)$ belong to the boundary of Ω. Since each triangle is assumed to include an interior node, Ψ is defined for at least two edges E_1, E_2 with $\Psi(E_1) \neq \Psi(E_2)$. Thus the choice of Ψ for boundary edges is not relevant for the validity of (3.9). For the remaining boundary edge E_3, Ψ can be chosen appropriately $\Psi(E_3) = T_+$.

For each $E \in \mathcal{E}_{\ell\setminus\ell+k}$ there is a refinement of the neighbourhood $\bar\omega_E^\ell := T_+ \cup T_-$ of E and each neighbouring $K_E \in \{T_+, T_-\} \subset \mathcal{T}_\ell$ with $E \subseteq \partial K_E$ is, at least, bisected in the refinements from $\mathcal{T}_\ell$ to $\mathcal{T}_{\ell+k}$. Let

$$\chi_j(K) := \left|\left\{T \in \mathcal{T}_j \mid T \subseteq \bar\omega_E^\ell, \Psi(E) = K\right\}\right| \quad \text{for } K \in \mathcal{T}_\ell \text{ and } j = \ell, \ell+1, \dots;$$

$$m_E := \begin{cases} 1/2 & \text{if } E \text{ is interior, } E \in \mathcal{E}_{\ell\setminus\ell+k}, \\ 1 & \text{if } E \subseteq \partial\Omega,\ E \in \mathcal{E}_{\ell\setminus\ell+k}, \\ 0 & \text{otherwise.} \end{cases}$$

Hence, $1 \leqslant m_E(\chi_{\ell+k}(K_E) - \chi_\ell(K_E))$ for $E \in \mathcal{E}_{\ell\setminus\ell+k}$. Applying the definition of χ_j from above, the mapping Ψ leads to the improved estimate (3.8) with

$$\begin{aligned} \left|\mathcal{E}_{\ell\setminus\ell+k}\right| &\leqslant \sum_{\substack{E\in\mathcal{E}_{\ell\setminus\ell+k} \\ \Psi(E)=K}} m_E\left(\chi_{\ell+k}(K) - \chi_\ell(K)\right) \\ &\leqslant \sum_{T\in\mathcal{T}_\ell} \sum_{\substack{E\in\mathcal{E}_{\ell\setminus\ell+k} \\ \Psi(E)=T}} m_E\left(\chi_{\ell+k}(T) - \chi_\ell(T)\right) \leqslant 2\left(|\mathcal{T}_{\ell+k}| - |\mathcal{T}_\ell|\right). \end{aligned}$$ □

Remark 3.2.8. *If $v_{\ell+k}^{\mathrm{NC}} \in \mathcal{T}_{\ell+k}$, then the nonconforming interpolation operator $v_\ell^{\mathrm{NC}} := \mathcal{I}_\ell^{\mathrm{NC}} v_{\ell+k}^{\mathrm{NC}} \in P_{1,0}^{\mathrm{NC}}(\mathcal{T}_\ell)$ is uniquely defined by*

$$⨍_E v_\ell^{\mathrm{NC}}\,\mathrm{ds} = ⨍_E v_{\ell+k}^{\mathrm{NC}}\,\mathrm{ds} \quad \textit{for all } E \in \mathcal{E}_\ell. \tag{3.10}$$

Definition 3.2.9 (Conforming Scott–Zhang interpolation operator [SZ90])**.** *The averaging technique of Scott and Zhang [SZ90] allows the definition of an interpolation operator $\mathcal{I}_\ell^{\mathrm{SZ}} : H_0^1(\Omega) \to P_1^{\mathrm{C}}(\mathcal{T}_\ell)$, which is a projector, i.e., $\mathcal{I}_\ell^{\mathrm{SZ}}(v_\ell) = v_\ell$ for all $v_\ell \in P_1^{\mathrm{C}}(\mathcal{T}_\ell)$.*

ω_E, ω_E^ℓ	$:= \operatorname{int} \bigcup_{\substack{T\in\mathcal{T}_\ell \\ E\cap T=E}} T,$	edge patch
Ω_E, Ω_E^ℓ	$:= \operatorname{int} \bigcup_{\substack{T\in\mathcal{T}_\ell \\ E\cap T\neq\varnothing}} T,$	enlarged edge patch
ω_z, ω_z^ℓ	$:= \operatorname{int} \bigcup_{\substack{T\in\mathcal{T}_\ell \\ z\cap T=\{z\}}} T,$	node patch

Table 3.14: Notation for patches w.r.t. some node z or edge E of $\mathcal{T}_\ell$. The patches are visualised in Figure 3.15. The level ℓ in the superscript is omitted if it is clear from the context without ambiguity.

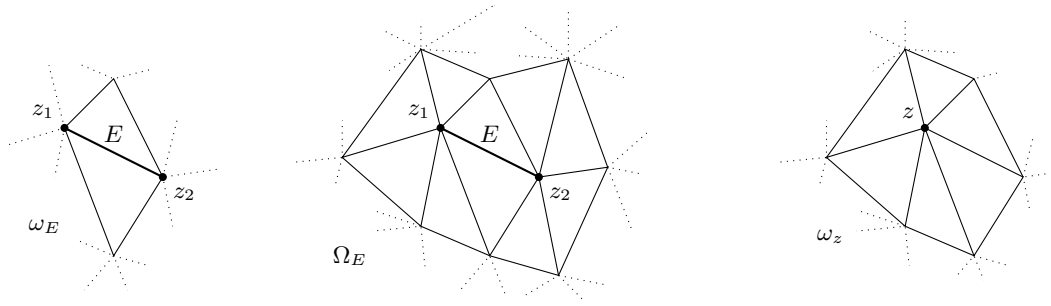

Figure 3.15: The edge and node patches ω_E, Ω_E, and ω_z for an edge E or a node z, respectively, of a triangulation $\mathcal{T}_\ell$.

Let $k \in \mathbb{N}$ and $\mathcal{T}_{\ell+k}$ be some NVB refinement of $\mathcal{T}_\ell$. In this thesis, the interpolation operator $\mathcal{I}_\ell^{\mathrm{SZ}}$ is restricted to $P_1^{\mathrm{C}}(\mathcal{T}_{\ell+k})$. For any node $z \in \mathcal{N}_\ell$ – whenever possible – an edge $E \in \mathcal{E}_\ell(z) \cap \mathcal{E}_{\ell+k}$ is chosen, such that on any $E \in \mathcal{E}_\ell$ that has not been refined, i.e., for any $E \in \mathcal{E}_\ell \cap \mathcal{E}_{\ell+k}$, the interpolant will satisfy $v_{\ell+k}^{\mathrm{C}}\big|_E = \mathcal{I}_\ell^{\mathrm{SZ}}(v_{\ell+k}^{\mathrm{C}})\big|_E$. This property implies

$$\big\|v_{\ell+k}^{\mathrm{C}} - \mathcal{I}_\ell^{\mathrm{SZ}}(v_{\ell+k}^{\mathrm{C}})\big\|_{L^2(E)} = 0 \quad \text{for } E \in \mathcal{E}_\ell \cap \mathcal{E}_{\ell+k}.$$

If $\mathcal{E}_\ell(z) \cap \mathcal{E}_{\ell+k} = \varnothing$ the selection of $E \in \mathcal{E}_\ell(z)$ is arbitrary.

Lemma 3.2.10 ([SZ90])**.** *Let Ω_E be the enlarged edge patch for $E \in \mathcal{E}_\ell$ as depicted in Figure 3.15. The construction of $\mathcal{I}_\ell^{\mathrm{SZ}}(v_{\ell+k}^{\mathrm{C}})$ leads to the following approximation property*

$$h_E^{1/2} \big\|v_{\ell+k}^{\mathrm{C}} - \mathcal{I}_\ell^{\mathrm{SZ}}(v_{\ell+k}^{\mathrm{C}})\big\|_{L^2(E)} \leqslant |v_{\ell+k}^{\mathrm{C}}|_{H^1(\Omega_E)} \quad \textit{for } E \in \mathcal{E}_{\ell\setminus\ell+k}.$$

The finite overlap of patches Ω_E in $\mathcal{T}_\ell$ verifies

$$\sum_{E\in\mathcal{E}_{\ell\setminus\ell+k}} |v_{\ell+k}^{\mathrm{C}}|_{H^1(\Omega_E)} \lesssim |v_{\ell+k}^{\mathrm{C}}|_{H^1(\Omega)}.$$

The remainder of this section proves a discrete Poincaré inequality for the nonconforming Crouzeix–Raviart FEM.

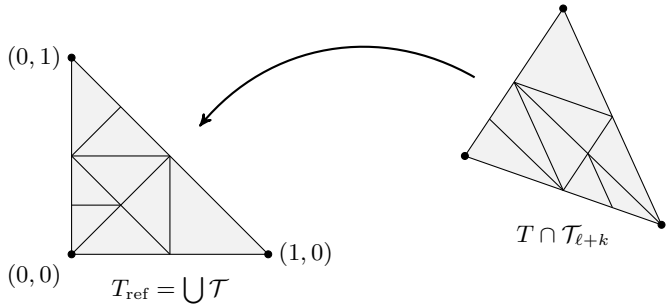

Figure 3.16: Reference triangle T_{ref} with $\mathcal{T}$ used in the proof of Lemma 3.2.11.

Lemma 3.2.11 (Discrete Poincaré inequality, [Rab10, Lemma 4.1])**.** *Let $\alpha^{\mathrm{NC}}_{\ell+k} \in P^{\mathrm{NC}}_{1,0}(\mathcal{T}_{\ell+k})$, and $\alpha^{\mathrm{NC}}_{\ell} \in P^{\mathrm{NC}}_{1,0}(\mathcal{T}_{\ell})$ with integral means satisfying $⨍_E \alpha^{\mathrm{NC}}_{\ell+k} \,\mathrm{d}s = ⨍_E \alpha^{\mathrm{NC}}_{\ell} \,\mathrm{d}s$ for any $E \in \mathcal{E}_\ell$. Then, for any $T \in \mathcal{T}_\ell$ the following discrete Poincaré inequality holds*

$$\big\|\alpha^{\mathrm{NC}}_{\ell+k} - \alpha^{\mathrm{NC}}_{\ell}\big\|_{L^2(T)} \lesssim h_T \big\|\nabla_{\ell+k}\alpha^{\mathrm{NC}}_{\ell+k}\big\|_{L^2(T)}\,.$$

Proof replicated from [Rab10, Lemma 4.1]. Let $T \in \mathcal{T}_\ell$, and $\alpha^{\mathrm{NC}}_T := ⨍_T u^{\mathrm{NC}} \,\mathrm{d}x$ be piecewise constant on $\mathcal{T}_\ell$ with $u^{\mathrm{NC}} := \alpha^{\mathrm{NC}}_{\ell+k} - \alpha^{\mathrm{NC}}_{\ell} \in P^{\mathrm{NC}}_1(\mathcal{T}_{\ell+k})$. Then, the affine transformation of $T \in \mathcal{T}_\ell$ on T_{ref} yields functions defined on T_{ref}, each marked by $\hat{\cdot}$ (i.e., $\hat{\alpha}^{\mathrm{NC}}_{\ell+k}$, $\hat{\alpha}^{\mathrm{NC}}_{\ell}$, $\hat{u}^{\mathrm{NC}}$, $\hat{\alpha}^{\mathrm{NC}}_T$).

Since $⨍_T (u^{\mathrm{NC}} - \alpha^{\mathrm{NC}}_T) \,\mathrm{d}x$ vanishes, a result by S. Brenner [BS08, Theorem 10.6.16, page 302] applies and yields

$$\|\hat{u}^{\mathrm{NC}} - \hat{\alpha}^{\mathrm{NC}}_T\|_{L^2(T_{\mathrm{ref}})} \lesssim \|\nabla_{\ell+k}\hat{u}^{\mathrm{NC}}\|_{L^2(T_{\mathrm{ref}})}\,. \tag{3.11}$$

Let $\mathcal{T}$ be the refinement of T_{ref} corresponding to the refinement of $T \in \mathcal{T}_\ell$ in $\mathcal{T}_{\ell+k}$ as depicted in Figure 3.16. Thus, $\|\hat{\alpha}^{\mathrm{NC}}_T\|_{L^2(T_{\mathrm{ref}})} \lesssim \|\nabla_{\ell+k}\hat{u}^{\mathrm{NC}}\|_{L^2(T_{\mathrm{ref}})}$ can be proven by means of Hölder's inequality, namely

$$\begin{aligned}
\|\hat{\alpha}^{\mathrm{NC}}_T\|_{L^2(T_{\mathrm{ref}})} &= \left|\sqrt{2}\int_{T_{\mathrm{ref}}} \hat{u}^{\mathrm{NC}} \,\mathrm{d}x\right| \approx \left|\int_{T_{\mathrm{ref}}} \hat{u}^{\mathrm{NC}} \operatorname{div} x \,\mathrm{d}x\right| \\
&\leqslant \left|\sum_{K\in\mathcal{T}} \left(-\int_K \nabla_{\ell+k}\hat{u}^{\mathrm{NC}} \cdot x \,\mathrm{d}x + \int_{\partial K} \hat{u}^{\mathrm{NC}}\, x\nu_K \,\mathrm{d}s\right)\right| \\
&\lesssim \|\nabla_{\ell+k}\hat{u}^{\mathrm{NC}}\|_{L^2(T_{\mathrm{ref}})} + \sum_{E\in\mathcal{E}(\mathcal{T})} \int_E [\hat{u}^{\mathrm{NC}}]_E \, x\cdot\nu_E \,\mathrm{d}s \\
&\lesssim \|\nabla_{\ell+k}\hat{u}^{\mathrm{NC}}\|_{L^2(T_{\mathrm{ref}})} + \sum_{E\in\mathcal{E}(\mathcal{T})} \int_E [\hat{u}^{\mathrm{NC}}]_E \, (x - x^\star_E)\cdot\nu_E \,\mathrm{d}s
\end{aligned}$$

with $x^\star_E$ chosen fixed for each edge E, such that $(x - x^\star_E) \perp \nu_E$ for all $x \in E$. Next the

equivalence $\int_{T_{\mathrm{ref}}} \nabla_\ell \hat{\alpha}_\ell^{\mathrm{NC}} \,\mathrm{dx} = \int_{T_{\mathrm{ref}}} \nabla_{\ell+k} \hat{\alpha}_{\ell+k}^{\mathrm{NC}} \,\mathrm{dx}$ is proven,

$$\begin{aligned}
\int_{T_{\mathrm{ref}}} \nabla_\ell \hat{\alpha}_\ell^{\mathrm{NC}} \,\mathrm{dx} &= \int_{\partial\, T_{\mathrm{ref}}} \hat{\alpha}_\ell^{\mathrm{NC}} \cdot \nu_{T_{\mathrm{ref}}} \,\mathrm{ds} = \sum_{E \in \mathcal{E}(T_{\mathrm{ref}})} \int_E \hat{\alpha}_\ell^{\mathrm{NC}} \cdot \nu_E \,\mathrm{ds} \\
&= \sum_{E \in \mathcal{E}(T_{\mathrm{ref}})} \int_E \hat{\alpha}_{\ell+k}^{\mathrm{NC}} \cdot \nu_E \,\mathrm{ds} \\
&= \int_{T_{\mathrm{ref}}} \nabla_{\ell+k} \hat{\alpha}_{\ell+k}^{\mathrm{NC}} \,\mathrm{dx} - \int_{\bigcup \mathcal{E}(\mathcal{T}) \cap \mathrm{int}(T_{\mathrm{ref}})} \left[\hat{\alpha}_{\ell+k}^{\mathrm{NC}} \cdot \nu_E\right] \mathrm{ds} \\
&= \int_{T_{\mathrm{ref}}} \nabla_{\ell+k} \hat{\alpha}_{\ell+k}^{\mathrm{NC}} \,\mathrm{dx}\,.
\end{aligned}$$

The application of this equality proves $\|\nabla_{\ell+k} \hat{u}^{\mathrm{NC}}\|^2_{L^2(T_{\mathrm{ref}})} \lesssim \left\|\nabla_{\ell+k} \hat{\alpha}_{\ell+k}^{\mathrm{NC}}\right\|^2_{L^2(T_{\mathrm{ref}})}$, i.e.,

$$\begin{aligned}
\|\nabla_{\ell+k} \hat{u}^{\mathrm{NC}}\|^2_{L^2(T_{\mathrm{ref}})} &= \int_{T_{\mathrm{ref}}} \left(\nabla_{\ell+k} \hat{\alpha}_{\ell+k}^{\mathrm{NC}} - \nabla_\ell \hat{\alpha}_\ell^{\mathrm{NC}}\right) \left(\nabla_{\ell+k} \hat{\alpha}_{\ell+k}^{\mathrm{NC}} - \nabla_\ell \hat{\alpha}_\ell^{\mathrm{NC}}\right) \mathrm{dx} \\
&= \int_{T_{\mathrm{ref}}} \left(\nabla_{\ell+k} \hat{\alpha}_{\ell+k}^{\mathrm{NC}} - \nabla_{\ell+k} \hat{\alpha}_\ell^{\mathrm{NC}}\right) \nabla_{\ell+k} \hat{\alpha}_{\ell+k}^{\mathrm{NC}} \,\mathrm{dx} \\
&= \|\nabla_{\ell+k} \hat{\alpha}_{\ell+k}^{\mathrm{NC}}\|^2_{L^2(T_{\mathrm{ref}})} - \nabla_\ell \hat{\alpha}_\ell^{\mathrm{NC}} \int_{T_{\mathrm{ref}}} \nabla_{\ell+k} \hat{\alpha}_{\ell+k}^{\mathrm{NC}} \,\mathrm{dx} \\
&\lesssim \|\nabla_{\ell+k} \hat{\alpha}_{\ell+k}^{\mathrm{NC}}\|^2_{L^2(T_{\mathrm{ref}})} - \int_{T_{\mathrm{ref}}} \nabla_\ell \hat{\alpha}_\ell^{\mathrm{NC}} \,\mathrm{dx} \int_{T_{\mathrm{ref}}} \nabla_{\ell+k} \hat{\alpha}_{\ell+k}^{\mathrm{NC}} \,\mathrm{dx} \\
&\lesssim \|\nabla_{\ell+k} \hat{\alpha}_{\ell+k}^{\mathrm{NC}}\|^2_{L^2(T_{\mathrm{ref}})}\,.
\end{aligned}$$

Finally, taking the previous estimates into consideration verifies

$$\begin{aligned}
\|\hat{\alpha}_{\ell+k}^{\mathrm{NC}} - \hat{\alpha}_\ell^{\mathrm{NC}}\|_{L^2(T_{\mathrm{ref}})} &\leqslant \|\hat{u}^{\mathrm{NC}} - \hat{\alpha}_T^{\mathrm{NC}}\|_{L^2(T_{\mathrm{ref}})} + \|\hat{\alpha}_T^{\mathrm{NC}}\|_{L^2(T_{\mathrm{ref}})} \lesssim \|\nabla_{\ell+k} \hat{u}^{\mathrm{NC}}\|_{L^2(T_{\mathrm{ref}})} \\
&\lesssim \|\nabla_{\ell+k} \hat{\alpha}_{\ell+k}^{\mathrm{NC}}\|_{L^2(T_{\mathrm{ref}})}\,.
\end{aligned}$$

A careful transformation back from T_{ref} to $T \in \mathcal{T}_\ell$ yields the factor h_T in the assertion. □

3.3 Optimal approximation of the data

This section focuses on the optimal approximation of the data $f \in L^2(\Omega)$ in steps MARK and REFINE, which leads to an optimal reduction of the volume term by computing the overlay $\mathcal{T}_\ell \oplus \mathcal{T}$. The approximation algorithm (AA), Algorithm 3.17 of [BDdV04, Section 4.3], applies the thresholding second algorithm (TSA) plus completion and is one possible realisation. Any algorithm that enforces reduction of the volume term with optimal complexity and successive refinements of Figure 3.5 is applicable. The goal is to keep the number of levels, for which the discrete problem has to be solved, small.

The algorithm is feasible in the sense that the decision in MARK is solely based on computed quantities and simultaneously reduces η_ℓ and $\|h_\ell f\|_{L^2(\Omega)}$. This avoids the computation of an initial triangulation $\mathcal{T}_0$, which approximates the data up to a given fixed tolerance as in [CHX09].

Recall the notation for forests and trees from Section 3.2.2. Further notation is adopted from [BDdV04, BdV04] and is used to develop an algorithm that generates an optimal triangulation that resolves the right-hand side $f \in L^2(\Omega)$ up to a given threshold.

Consider an error functional $e(T)$, e.g., $e(T) := \|h_T f\|^2_{L^2(T)}$, which is available and nonnegative for any vertex $T \in \mathcal{F}_\star$. Then for any proper sub-forest $\mathcal{F}_\ell$ and its corresponding triangulation $\mathcal{T}_\ell := \mathcal{L}(\mathcal{F}_\ell)$ the global error measure is given by

$$e(\mathcal{T}_\ell) := \sum_{T \in \mathcal{T}_\ell} e(T).$$

For some arbitrary integer $N > 0$, the minimising triangulation $\mathcal{T}_{\min}$ and its forest $\mathcal{F}_{\min} \subset \mathcal{F}_\star$ are denoted by

$$e(\mathcal{T}_{\min}) := \min_{\substack{\mathcal{F} \subset \mathcal{F}_\star, \\ |\mathcal{L}(\mathcal{F})| - |\mathcal{T}_0| \leqslant N}} e(\mathcal{F}).$$

However, it is unreasonable to demand that any adaptive algorithm generates $\mathcal{T}_{\min}$ exactly. To reduce e optimally, e should show the same asymptotic behaviour for the output triangulation $\mathcal{T}_\ell$ as for $\mathcal{T}_{\min}$ [BDdV04]. This optimality is proven in Lemma 3.6.5 for error functionals e that fulfil at least one of the following properties [BdV04]:

(a) *Refinement property* If T is a vertex in $\mathcal{F}_\star$ and T_1, T_2 are its children, the following estimate holds

$$e(T_1) + e(T_2) \leqslant e(T). \tag{3.12}$$

(b) *Sub-additivity* For each T in $\mathcal{F}_\star$ and each finite sub-tree $\mathcal{F}_T \subset \mathcal{F}_\star$ with root node T and leaves $\mathcal{L}(\mathcal{F}_T)$, there exists a positive generic constant C_{sa} such that

$$\sum_{\hat{T} \in \mathcal{L}(\mathcal{F}_T)} e(\hat{T}) \leqslant C_{\mathrm{sa}} e(T). \tag{3.13}$$

As in [BdV04, BDdV04], based on the functional e, a modified error functional $\tilde{e}$ is defined, which is the refinement indicator in the TSA of AA (cf. Algorithm 3.17). Initially, set

$$\tilde{e}(T) := e(T)$$

for all root nodes of $T \in \mathcal{F}_0 \subset \mathcal{F}_\star$. Assuming that $\tilde{e}(T)$ is already defined for some $T \in \mathcal{F}_\star$, then the definition for its children $T_j \in \mathcal{F}_\star$, $j = 1, 2$ is

$$\tilde{e}(T_j) := \frac{\tilde{e}(T)\,(e(T_1) + e(T_2))}{e(T) + \tilde{e}(T)}.$$

This definition implies that $\tilde{e}$ is constant for any two siblings in $\mathcal{F}_\star$.

Remark 3.3.1. *Let* $\mathrm{Tol} > 0$ *be the error tolerance in Algorithm 3.17 (*AA*). Note that the computation of* $\tilde{e}(T_j)$ *in algorithm* AA *is well defined as long as* $\tilde{e}(T) > 0$*. The error*

Input: Initial coarse triangulation $\mathcal{T}_0$, error tolerance $\mathrm{Tol} > 0$, error functional e satisfying (3.13).
Compute $e(T) = \tilde{e}(T)$ for all $T \in \mathcal{T}_0$ and $e(\mathcal{T}_0) = \sum_{T\in\mathcal{T}_0} e(T)$.
Set $\bar{\mathcal{T}} = \mathcal{T}_0$.
while $e(\bar{\mathcal{T}}) > \mathrm{Tol}$ **do**
  Compute $\tilde{e}_{\max} := \max_{T\in\bar{\mathcal{T}}} \tilde{e}(T)$.
  MARK the triangles in $\mathcal{M} := \{T \in \bar{\mathcal{T}} \mid \tilde{e}(T) = \tilde{e}_{\max}\}$.
  REFINE all elements in $\mathcal{M}$ by *green* of NVB of Figure 3.5 to get a new $\bar{\mathcal{T}}$.
Apply **completion** on $\bar{\mathcal{T}}$ to get an admissible refinement $\mathcal{T}_{\mathrm{Tol}}$ of $\mathcal{T}_0$.
Output: $\mathcal{T}_{\mathrm{Tol}}$.

Algorithm 3.17: Approximation algorithm (AA): TSA followed by completion as described in [BdV04, BDdV04].

functional $\tilde{e}(T_j)$ needs to be evaluated only if

$$\tilde{e}(T) = \tilde{e}_{\max} := \max_{T\in\mathcal{T}} \tilde{e}(T).$$

Furthermore, $\tilde{e}_{\max} > 0$ as long as $e(\mathcal{T}) > \mathrm{Tol} > 0$ in algorithm AA. Thus, a computation of $\tilde{e}(T_j)$ will not be invoked if $\tilde{e}(T) = 0$.

Remark 3.3.2. *For AA of [BdV04, BDdV04] described in Algorithm 3.17 the functional e needs to satisfy (3.13). However, if $e(T) := \|h_T f\|^2_{L^2(T)}$, $e(T)$ actually satisfies the stricter condition (3.12).*

The subsequent lemma forms the basis for optimality of Algorithm 3.17 (i.e., AA) in Lemma 3.6.5.

Lemma 3.3.3 ([BDdV04, Lemma 4.2])**.** *Given an input mesh $\mathcal{T}_0$ and an error tolerance $\mathrm{Tol} > 0$, the output triangulation $\mathcal{T}_{\mathrm{Tol}}$ of Algorithm 3.17 satisfies*

$$e(\mathcal{T}_{\mathrm{Tol}}) \leqslant \mathrm{Tol}\,.$$

In addition, there are absolute constants $C_{1,\star}$ and $C_{2,\star}$ such that whenever $\mathcal{T}_\star$ is a refinement of $\mathcal{T}_0$ that satisfies $e(\mathcal{T}_\star) \leqslant C_{1,\star}\,\mathrm{Tol}$, then the number of marked elements $\sum_{k=0}^{K} \left|\mathcal{M}^{(k)}\right|$ (e.g., the output of Algorithm 3.18 on page 38 for input triangulations $\mathcal{T}_0$, $\mathcal{T}_{\mathrm{Tol}}$) satisfies

$$\sum_{k=0}^{K} \left|\mathcal{M}^{(k)}\right| \leqslant C_{2,\star}\left(|\mathcal{T}_\star| - |\mathcal{T}_0|\right).$$

3.4 S-AFEM-AA – a natural adaptive algorithm in detail

Given parameters $0 < \theta_A, \rho_B < 1$, and $0 < \kappa$, the algorithm S-AFEM-AA distinguishes Cases (A) for $\|h_\ell f\|^2_{L^2(\Omega)} \leqslant \kappa\eta^2_\ell$ and (B) for $\kappa\eta^2_\ell < \|h_\ell f\|^2_{L^2(\Omega)}$. In Case (A), when the volume term is small compared to the estimated error, edge-oriented Dörfler marking is

applied, while in Case (B) we make use of an optimal approximation algorithm AA (see Section 3.3) to reduce $\|h_\ell f\|_{L^2(\Omega)}$.

Quasi-optimality is proven for $0 < \theta_A < \theta_0$ and $\kappa \in (\kappa_1, \kappa_2)$ with constants $0 < \theta_0 \leqslant 1$ and $0 < \kappa_1 < \kappa_2$ for each of the three examples in Chapters 4–6.

Remark 3.4.1. *The introduction of $\theta_0 \leqslant 1$ and $\kappa_1 \in (0, \kappa_2)$ in Algorithm 3.4 clarifies that to ensure optimal convergence the parameters of the adaptive algorithm, as well as the parameters in the definition of ξ_ℓ, are independent of κ and θ_A as long as $\kappa \in (\kappa_1, \kappa_2)$ and $\theta_A \in (0, \theta_0)$. More precisely there exist parameters α, β, κ_2 and $\kappa_1 \in (0, \kappa_2)$ such that for all $\kappa \in (\kappa_1, \kappa_2)$ and $\theta_A \in (0, \theta_0)$ the output of* S-AFEM-AA *shows optimal convergence rates as proven in the respective Theorems 4.4.1, 5.4.1 and 6.4.1.*

Solve

The discrete problem is solved exactly in the lowest-order Crouzeix–Raviart finite element space for the triangulation $\mathcal{T}_\ell$ of level ℓ as introduced in Section 2.4. MATLAB implementations and documentation for SOLVE are provided in [BC05, CN09].

Estimate

For the set of all edges $\mathcal{E}_\ell$ in the triangulation $\mathcal{T}_\ell$ the problem-dependent error estimator based on edges is denoted by

$$\eta_\ell := \eta_\ell(\mathcal{E}_\ell) \qquad \text{with} \qquad \eta_\ell^2(\mathcal{M}_\ell) := \sum_{E \in \mathcal{M}_\ell} \eta_\ell^2(E) \quad \text{for } \mathcal{M}_\ell \subseteq \mathcal{E}_\ell.$$

The local contributions $\eta_\ell(E)$ depend on the specific problem, such that the error estimator η_ℓ and the volume term $\|h_\ell f\|_{L^2(\Omega)}$ allows reliable and efficient error control on the given triangulation $\mathcal{T}_\ell$. Details are given in the problem-specific Chapters 4–6.

Thus, η_ℓ and $\|h_\ell f\|_{L^2(\Omega)}$ are computed in step ESTIMATE.

Mark and Refine

The marking and refinement of S-AFEM-AA distinguish two Cases (A) and (B) depending on some global parameter $\kappa > 0$ and the quantities $\|h_\ell f\|_{L^2(\Omega)}$ and η_ℓ, which are available on each level. The two alternatives are described below.

3.4.1 Case (A) for $\|h_\ell f\|_{L^2(\Omega)}^2 \leqslant \kappa \eta_\ell^2$

The estimated error η_ℓ is reduced for Case (A) as follows. A nonempty set $\mathcal{M}_\ell \subseteq \mathcal{E}_\ell$ is specified in step MARK and used in REFINE to compute a shape-regular $\mathcal{T}_{\ell+1}$ using the Newest Vertex Bisection (NVB) and completion from [BdV04, BDdV04, BC04, Ste08] or CLOSURE from [Car04, KPP12] with respect to $\mathcal{M}_\ell$. The step CLOSURE ensures regularity of $\mathcal{T}_{\ell+1}$ and its overhead is bounded; see Lemma 3.2.3. The Dörfler marking applied in Case (A) results in a level-oriented refinement of $\mathcal{T}_\ell$ as in standard adaptive schemes.

MARK: In practice one possibility is first to sort the set of all edges $\mathcal{E}_\ell$ in $(E_1, \dots, E_N)$ with $\eta_{E_1} \leqslant \cdots \leqslant \eta_{E_N}$. Second, compute a set $\mathcal{M}_\ell := \{E_N, \dots, E_{N-k}\}$ of minimal

cardinality $|\mathcal{M}_\ell| = k+1$ with

$$\theta_A \eta_\ell^2 \leqslant \eta_\ell^2(\mathcal{M}_\ell). \tag{3.14}$$

In fact, for the analysis it is sufficient to compute a set $\mathcal{M}_\ell$ of quasi-minimal cardinality, i.e.,

$$|\mathcal{M}_\ell| \approx \min\left\{|\mathcal{M}| \,\middle|\, \theta_A \eta_\ell^2 \leqslant \eta_\ell^2(\mathcal{M}),\, \mathcal{M} \subseteq \mathcal{E}_\ell \cup \mathcal{T}_\ell\right\}. \tag{3.15}$$

Thus the computation of $\mathcal{M}_\ell$ can be modified if appropriate.

Refine: The refined triangulation $\mathcal{T}_{\ell+1} := \textsc{Refine}(\mathcal{T}_\ell, \mathcal{C}\ell(\mathcal{M}_\ell))$ from $\mathcal{T}_\ell$ is uniquely defined so that just the edges in $\mathcal{C}\ell(\mathcal{M}_\ell)$ are bisected. $\mathcal{C}\ell(\mathcal{M}_\ell)$ is the minimal subset of $\mathcal{E}_\ell$ that includes $\mathcal{M}_\ell$ and is closed in the sense of (3.3). A possible choice of refinement rules are *green*, *blue*, and *bisec3* as depicted in Figure 3.5. *Red* refinement is not possible, since the upper bound for the overhead of the overlay is necessary in the upcoming analysis (see Figure 3.10 and Lemma 3.2.5) of quasi-optimality.

Remark 3.4.2. *The result of* Refine *is the smallest shape-regular refinement $\mathcal{T}_{\ell+1}$ of $\mathcal{T}_\ell$ without hanging nodes using NVB, where at least the edges in $\mathcal{M}_\ell$ are refined [BC04]. All admissible refinements of a triangle $T \in \mathcal{T}_\ell$ are depicted in Figure 3.5 and they depend on the set of its edges $\mathcal{E}(T)$ that have to be refined. The refinement edge $E(K)$ of each new triangle $K \subseteq T$ is highlighted in red in Figure 3.5. If all edges $\mathcal{E}(T)$ have to be refined either bisec3(T) or bisec5(T) can be applied.*

3.4.2 Case (B) for $\|h_\ell f\|^2_{L^2(\Omega)} > \kappa \eta_\ell^2$

For Case (B) the volume term is reduced using an algorithm that approximates the data optimally. The output triangulation $\mathcal{T}$ is an admissible refinement of $\mathcal{T}_0$ in a possibly unbounded number of levels and it is overlaid with $\mathcal{T}_\ell$, which results in the triangulation for the next level.

Mark: Given $f, \mathcal{T}_0, \mathcal{T}_\ell, 0 < \rho_B < 1$, set $\mathrm{Tol} := \rho_B \|h_\ell f\|^2_{L^2(\Omega)}$ and run the approximation algorithm aa (Algorithm 3.17 and Section 3.3), which is tsa plus completion from [BDdV04, BdV04]. This results in a regular and optimal triangulation $\mathcal{T}$ of nearly minimal cardinality $|\mathcal{T}|$ such that

$$\|h_\mathcal{T} f\|^2_{L^2(\Omega)} \leqslant \mathrm{Tol} \qquad \text{and} \qquad |\mathcal{T}| - |\mathcal{T}_0| \lesssim \mathrm{Tol}^{-1/(2s)}. \tag{3.16}$$

Refine: The regular overlay triangulation $\mathcal{T}_{\ell+1} := \mathcal{T} \oplus \mathcal{T}_\ell$ can be computed using the corresponding forests in Section 3.2.2. It satisfies

$$\|h_{\ell+1} f\|^2_{L^2(\Omega)} \leqslant \mathrm{Tol}.$$

By the definition for Tol in each level of Case (B) and the prescribed application of aa, the volume term with $0 < \rho_B < 1$ is reduced according to

$$\|h_{\ell+1} f\|^2_{L^2(\Omega)} \leqslant \rho_B \|h_\ell f\|^2_{L^2(\Omega)}.$$

The refinement in Case (B) is *not* level oriented in the sense that one element domain K of $\mathcal{T}_\ell$ may contain a seemingly uncontrolled number of refined element domains in

Input: $\mathcal{T}_\ell$ and an admissible refinement $\mathcal{T}_{\ell+m}$ of $\mathcal{T}_\ell$.
Set $\mathcal{T}_\ell^{(0)} := \mathcal{T}_\ell$, $\mathcal{E}_\ell^{(0)} := \mathcal{E}_\ell$.
for $k = 0, 1, \dots$ **do**
  Set $\mathcal{M}_\ell^{(k)} := \big\{E(T) \in \mathcal{E}_\ell^{(k)} \mid T \in \mathcal{T}_\ell^{(k)} \backslash \mathcal{T}_{\ell+1}\big\}$
  REFINE $\mathcal{T}_\ell^{(k)}$ with respect to the set of marked elements and edges $\mathcal{M}_\ell^{(k)}$ by NVB, i.e.,

$$\mathcal{T}_\ell^{(k+1)} := \text{REFINE}\big(\mathcal{T}_\ell^{(k)}, \mathcal{M}_\ell^{(k)}\big). \tag{3.18}$$

  If $\mathcal{T}_\ell^{(k+1)} \subsetneqq \mathcal{T}_{\ell+m}$, update k, else stop with $K(\ell) := k$.
Output: A sequence of refinement edges $\big(\mathcal{M}_\ell^{(k)}\big)_{k=0,\dots,K(\ell)}$.

Algorithm 3.18: Algorithm to compute the sets of marked edges $\mathcal{M}_\ell^{(k)}$ for successive refinements of $\mathcal{T}_\ell$ to generate $\mathcal{T}_{\ell+m}$ as used in Theorem 3.5.1.

$\{T \in \mathcal{T}_{\ell+1} \mid T \subseteq K\} \subseteq \mathcal{T}_{\ell+1}$. The control requires the investigations of [CR11], the subsequent Section 3.5, and the overlay control of Lemma 3.2.5. The application of algorithm AA of [BDdV04, BdV04] is one possible example, indeed the analysis applies for any algorithm that computes an admissible refinement $\mathcal{T}$ of $\mathcal{T}_0$ with (3.16).

3.5 Combination of two independently refined meshes

This section analyses the embedding of some triangulation $\mathcal{T}$ refined from $\mathcal{T}_0$ in a possibly unbounded number of refinement levels into the standard level-oriented overall adaptive mesh refinement. Algorithm 3.18, cf. [CR11, Algorithm 3.2], provides a finite sequence of sets of successively marked refinement edges $\big(\mathcal{M}_\ell^{(k)}\big)_k$. This sequence realises a finite number of successive refinements

$$\mathcal{T}_{\ell+m} := \mathcal{T}_\ell \oplus \mathcal{T} = \text{REFINE}\Big(\mathcal{T}_\ell, \big(\mathcal{M}_\ell^{(k)}\big)_{k=0,\dots,K(\ell)}\Big), \tag{3.17}$$

where in each step k each triangulation is refined as shown in Figure 3.5, with respect to the set of marked edges $\mathcal{M}_\ell^{(k)}$.

Algorithm 3.18 is for theoretical purposes only and it allows a common refinement control in S-AFEM-AA for both Cases (A) and (B). Algorithm 3.18 has already been described in [CR11]. The benefit of the artificially marked edges $\mathcal{M}_\ell^{(0)}, \dots, \mathcal{M}_\ell^{(K(\ell))}$ in Case (B) is that the refinement of (3.18) is level oriented such that each triangle in $\mathcal{T}_\ell^{(k)}$ is refined as shown in Figure 3.5 to obtain $\mathcal{T}_\ell^{(k+1)}$.

Theorem 3.5.1 ([CR11, Theorem 3.3])**.** *Consider regular triangulations $\mathcal{T}_\ell$ and $\mathcal{T}$, both refined from $\mathcal{T}_0$ by NVB. For input triangulations $\mathcal{T}_\ell$ and $\mathcal{T}_\ell \oplus \mathcal{T}$, Algorithm 3.18 stops after a finite number of $K(\ell) \geqslant 0$ steps with*

$$\mathcal{T}_\ell^{(K(\ell)+1)} = \mathcal{T}_\ell \oplus \mathcal{T}$$

and outputs a finite sequence of sets with $\big(\mathcal{M}_\ell^{(k)}\big)_{k=0,\dots,K(\ell)}$

$$\sum_{k=0}^{K(\ell)} \big|\mathcal{M}_\ell^{(k)}\big| \leqslant |\mathcal{T}| - |\mathcal{T}_0|\,,$$

that realise the successive refinements of (3.17).

Proof replicated from [CR11]. Let $\mathcal{F}$, $\mathcal{F}_\ell$, $\mathcal{F}_\ell^{(k)}$ and $\mathcal{F}_{\ell+1} = \mathcal{F}_\ell \cup \mathcal{F}$ denote the forests associated with the triangulations $\mathcal{T}$, $\mathcal{T}_\ell$, $\mathcal{T}_\ell^{(k)}$, and $\mathcal{T}_{\ell+1} := \mathcal{T}_\ell \oplus \mathcal{T}$, respectively. By induction, one observes that NVB leads to a nested sequence

$$\mathcal{F}_\ell = \mathcal{F}_\ell^{(0)} \subsetneqq \mathcal{F}_\ell^{(1)} \subsetneqq \cdots \subsetneqq \mathcal{F}_\ell^{(K(\ell))} \subsetneqq \mathcal{F}_\ell^{(K(\ell)+1)} = \mathcal{F}_{\ell+1}.$$

In fact, $\mathcal{T}_\ell^{(k)} \backslash \mathcal{T}_{\ell+1}$ denotes the triangles and $\mathcal{M}_\ell^{(k)}$ the marked edges to be refined in step k. Since $\mathcal{F}_{\ell+1} \backslash \mathcal{F}_\ell$ is finite, Algorithm 3.18 terminates after $K(\ell)$ steps with $\mathcal{F}_\ell^{(K(\ell)+1)} = \mathcal{F}_{\ell+1}$.

For each $E \in \mathcal{M}_\ell^{(k)}$ with $0 \leqslant k \leqslant K(\ell)$, at least one element in $\mathcal{T}_\ell^{(k)}$ is refined into at least two new elements in $\mathcal{T}_\ell^{(k+1)}$. Furthermore, if E is an interior edge, at least two elements in $\mathcal{T}_\ell^{(k)}$ are bisected to at least four new elements in $\mathcal{T}_\ell^{(k+1)}$. Therefore it follows that

$$\big|\mathcal{M}_\ell^{(k)}\big| \leqslant \big|\mathcal{T}_\ell^{(k+1)}\big| - \big|\mathcal{T}_\ell^{(k)}\big|. \tag{3.19}$$

Recall that $\mathcal{T}_\ell^{(0)} = \mathcal{T}_\ell$, $\mathcal{T}_\ell^{(K(\ell)+1)} = \mathcal{T}_{\ell+1} = \mathcal{T}_\ell \oplus \mathcal{T}$ and apply Lemma 3.2.5 and (3.19) to deduce

$$\sum_{k=0}^{K(\ell)} \big|\mathcal{M}_\ell^{(k)}\big| \leqslant |\mathcal{T}_\ell \oplus \mathcal{T}| - |\mathcal{T}_\ell| \leqslant |\mathcal{T}| - |\mathcal{T}_0|\,. \qquad \square$$

3.6 Optimal convergence of AFEM

The main result of this thesis is the proof of optimal convergence of the adaptive finite element algorithm S-AFEM-AA as introduced in Section 3.4 (cf. [CR11] for mixed FEM) for all three examples.

Let $\xi_\ell^2 := \eta_\ell^2 + \alpha_\varepsilon \varepsilon_\ell^2 + \alpha_f \|h_\ell f\|_{L^2(\Omega)}^2$ be the total error, with the energy error ε_ℓ, the edge-based error estimator η_ℓ and the volume term $\|h_\ell f\|_{L^2(\Omega)}$.

Consider particular positive parameters α_ε, α_f, $\kappa \in (\kappa_1, \kappa_2)$, and $\theta_A \in (0, \theta_0)$, $\rho_B < 1$ for algorithm S-AFEM-AA. Let (u, f) in some approximation class $\mathcal{A}_s$ (Section 3.6.1) for $s > 0$. The analysis of this thesis implies optimal convergence for the outcome of S-AFEM-AA with respect to $\mathcal{A}_s$ up to a multiplicative generic constant, i.e.,

$$|\mathcal{T}_\ell| - |\mathcal{T}_0| \lesssim \Big(\varepsilon_\ell^2 + \|h_\ell f\|_{L^2(\Omega)}^2\Big)^{-1/(2s)} \approx \xi_\ell^{-1/s}.$$

The proofs of quasi optimality for each of the three examples, are based on problem-independent properties: the overlay control of meshes of Theorem 3.5.1 and the optimal approximation of the data. Furthermore problem-dependent properties are required,

i.e, the estimator reduction and the contraction property of the total error ξ_ℓ, which are adapted for each of the three problems. The proofs follow a general mathematical methodology, which applies the key arguments of Section 3.6.2.

3.6.1 Approximation classes

The optimal convergence of s-afem-aa is investigated in the spirit of Stevenson [Ste07]. Given $s > 0$, the approximation class $\mathcal{A}_s$ depends on the specific model problem, i.e., on the energy norm $\varepsilon(\mathcal{T}) = \|\!|u - u_{\mathcal{T}}^{\mathrm{NC}}|\!\|_{\mathcal{T}}$ of the error of the discrete solution via

$$\mathcal{A}_s := \big\{(u,f) \mid \|(u,f)\|_{\mathcal{A}_s} < \infty\big\} \quad \text{and} \tag{3.20}$$
$$\|(u,f)\|_{\mathcal{A}_s}^2 := \sup_{N\in\mathbb{N}} \left(N^s \inf_{|\mathcal{T}|-|\mathcal{T}_0|\leqslant N} \left(\varepsilon_{\mathcal{T}}^2 + \|h_{\mathcal{T}} f\|_{L^2(\Omega)}^2\right)^{1/2}\right).$$

In the infimum, $\mathcal{T}$ runs through all admissible triangulations (i.e., regular and NVB-generated refinements $\mathcal{T}$ of $\mathcal{T}_0$; see Figure 3.5 and Definition 3.2.1) with the number of element domains $|\mathcal{T}| - |\mathcal{T}_0| \leqslant N$ and the exact energy error $\varepsilon(\mathcal{T})$.

Thus $(u,f) \in \mathcal{A}_s$ (cf. [Ste07, p. 255, Remark 5.1, p. 263, l. 17]) if and only if for all $\epsilon > 0$ there exists an admissible triangulation $\mathcal{T}_\epsilon$ refined from $\mathcal{T}_0$ such that the cr solution satisfies

$$\varepsilon^2(\mathcal{T}_\epsilon) + \|h_\epsilon f\|_{L^2(\Omega)}^2 \leqslant \epsilon^2 \quad \text{and} \quad |\mathcal{T}_\epsilon| - |\mathcal{T}_0| \lesssim \epsilon^{-1/s} \|(u,f)\|_{\mathcal{A}_s}^{1/s}.$$

There are problem-specific investigations (see (4.13) of Lemma 4.4.2, (5.21) of Lemma 5.4.2, and (6.14) of Lemma 6.4.2) that prove that there is equivalence of ξ_ℓ^2 with $\varepsilon_\ell^2 + \|h_\ell f\|_{L^2(\Omega)}^2$, i.e.,

$$\varepsilon_\ell^2 + \|h_\ell f\|_{L^2(\Omega)}^2 \approx \eta_\ell^2 + \|h_\ell f\|_{L^2(\Omega)}^2 + \varepsilon_\ell^2 \approx \xi_\ell^2 \tag{3.21}$$

with constants depending on α_f and α_ε, as well as on the problem-specific relations for efficiency and reliability.

Remark 3.6.1 ([CPR13, Remark 2.2])**.** *For the Poisson model problem, [CPS11] shows that in the definition of the approximation class*

$$\bar{\mathcal{A}}_s := \big\{(u,p,f) \in H_0^1(\Omega;\mathbb{R}^2) \times L_0^2(\Omega) \times L^2(\Omega;\mathbb{R}^2) \,\big|\, |(u,p,f)|_{\bar{\mathcal{A}}_s} < \infty\big\}$$

with $s > 0$ and $|(u,p,f)|_{\bar{\mathcal{A}}_s}$ defined by

$$\sup_{N\in\mathbb{N}} \Big(N^s \inf_{|\mathcal{T}|-|\mathcal{T}_0|\leqslant N} \big(\|\!|u - u_{\mathcal{T}}^{\mathrm{NC}}|\!\|_{\mathrm{NC}(\mathcal{T})}^2 + \|p - p_{\mathcal{T}}^{\mathrm{NC}}\|_{L^2(\Omega)}^2 + \mathrm{osc}^2(f,\mathcal{T})\big)^{1/2}\Big)$$

the error of the Crouzeix–Raviart approximation may be replaced by the best approximation error (see also [Gud10]). Using similar techniques it can be shown that for any solution (u,p) of the pure displacement problem in linear elasticity (2.4) and (5.1) or the Stokes equations (2.6) and (6.1) with right-hand side $f \in L^2(\Omega;\mathbb{R}^2)$ the following equivalence

holds

$$|(u,p,f)|_{\bar{\mathcal{A}}_s} \approx \sup_{N\in\mathbb{N}}\Big(N^s \inf_{|\mathcal{T}|-|\mathcal{T}_0|\leqslant N}\ \inf_{(v,q)\in V(\mathcal{T})\times Q(\mathcal{T})}\big(|\!|\!|u-v|\!|\!|^2_{\mathrm{NC}(\mathcal{T})} + \|p-q\|^2_{L^2(\Omega)} + \operatorname{osc}^2(f,\mathcal{T})\big)^{1/2}\Big).$$

Hence, the approximation class $\mathcal{A}_s$ may be replaced by the standard one of [CKNS08].

The following proposition, repeated from [CPR13, Proposition 5.1], states the equivalence of approximation classes $\mathcal{A}_s$ and $\bar{\mathcal{A}}_s$ for the Stokes problem of Chapter 6, which is independent of the pressure variable p. The proof is based on [DDP95, Remark 3.2] and efficiency. It yields $|(u,p,f)|_{\bar{\mathcal{A}}_s} \approx |(u,f)|_{\mathcal{A}_s}$. Hence, it suffices to prove quasi-optimality with regard to $\mathcal{A}_s$.

Proposition 3.6.2. *Let (u,p) be the exact solution of (2.6) with right-hand side $f \in L^2(\Omega;\mathbb{R}^2)$, let $\mathcal{T}$ be some admissible triangulation that is refined from $\mathcal{T}_0$ by NVB, and let $(u_{\mathcal{T}}^{\mathrm{NC}}, p_{\mathcal{T}}^{\mathrm{NC}})$ be the corresponding discrete solution of (6.1). Then*

$$|\!|\!|u-u_{\mathcal{T}}^{\mathrm{NC}}|\!|\!|^2_{\mathrm{NC}(\mathcal{T})} + \|p-p_{\mathcal{T}}^{\mathrm{NC}}\|^2_{L^2(\Omega)} + \operatorname{osc}^2(f,\mathcal{T}) \approx |\!|\!|u-u_{\mathcal{T}}^{\mathrm{NC}}|\!|\!|^2_{\mathrm{NC}(\mathcal{T})} + \|h_{\mathcal{T}} f\|^2_{L^2(\Omega)}$$

holds with hidden constants that depend on $\mathcal{T}_0$ but not on the mesh size $h_{\mathcal{T}}$.

3.6.2 Proof of optimal convergence rates

The section contains the main results, which allow the proof of quasi-optimal convergence rates in the three examples using a general mathematical methodology. Theorem 3.6.3 and the following Lemmas 3.6.4 and 3.6.6 are a consequence of the investigations in [CR11]. Lemma 3.6.5 states optimal data approximation by AA (i.e., Algorithm 3.17), which is the key observation for Case (B).

Together with the contraction property of the total error, which is proven in Chapters 4–6 for each of the three examples, these results are the basis for the proof of quasi-optimality in Chapters 4–6.

Theorem 3.6.3 (Key ingredient for proofs of optimal convergence rates, [CR11, cf. proof of Theorem 5.8])**.** *Let* S-AFEM-AA *(Algorithm 3.4) generate a sequence of triangulations $\mathcal{T}_\ell$ and discrete solutions. Assume the following properties:*

(a) *For any level ℓ in either Case (A) or (B), there exist $K(\ell) \in \mathbb{N}$ sets of marked edges $\mathcal{M}_\ell^{(0)}, \dots, \mathcal{M}_\ell^{K(\ell)}$ such that*

$$\mathcal{T}_{\ell+1} = \textsc{Refine}\Big(\mathcal{T}_\ell, \big(\mathcal{M}_\ell^{(k)}\big)_{0\leqslant k\leqslant K(\ell)}\Big), \quad \text{and} \quad \sum_{k=0}^{K(\ell)} \big|\mathcal{M}_\ell^{(k)}\big| \lesssim \xi_\ell^{-1/s}. \tag{3.22}$$

(b) *There exists $0<\rho<1$ such that on any level ℓ contraction holds in the sense*

$$\xi_{\ell+1}^2 \leqslant \rho\,\xi_\ell^2 \tag{3.23}$$

for some – problem-specific – weighted term ξ_ℓ of the error estimator, energy error and volume term.

Then,

$$|\mathcal{T}_\ell| - |\mathcal{T}_0| \lesssim \xi_\ell^{-1/s}.$$

Proof. Given (3.22), then the overhead control of Closure of (3.5) with $C_{\mathcal{C}\ell} > 0$ shows that

$$|\mathcal{T}_\ell| - |\mathcal{T}_0| \leqslant \sum_{j=0}^{\ell-1} \big(|\mathcal{T}_{j+1}| - |\mathcal{T}_j| \big) \leqslant C_{\mathcal{C}\ell} \sum_{j=0}^{\ell-1} \sum_{k=0}^{K(j)} |\mathcal{M}_j^{(k)}| \lesssim \sum_{j=0}^{\ell-1} \xi_j^{-1/s}.$$

For each level ℓ with Case (A), set $K(\ell) := 0$ and $\mathcal{M}_\ell^{(0)} := \mathcal{M}_\ell$. This and the problem-specific contraction property (3.23) give rise to the optimal global convergence as follows

$$|\mathcal{T}_\ell| - |\mathcal{T}_0| \leqslant \xi_\ell^{-1/s} \sum_{k=1}^{\ell} \rho^{-k/(2s)} = \frac{1 - \rho^{-(\ell+1)/(2s)}}{1 - \rho^{-1/(2s)}} \xi_\ell^{-1/s} \lesssim \xi_\ell^{-1/s}. \qquad \square$$

The remainder of this section presents further results, which are used to show quasi-optimality in the three examples by just verifying the two assumptions of Theorem 3.6.3. In particular, for the refinement indicators $\|h_\ell f\|_{L^2(\Omega)}$ and η_ℓ, as defined in Chapters 4–6, and the problem-dependent error ε_ℓ there exists $0 < \rho < 1$ such that the weighted term $\xi_\ell^2 := \eta_\ell^2 + \alpha_\varepsilon \varepsilon_\ell^2 + \alpha_f \|h_\ell f\|_{L^2(\Omega)}^2$ satisfies the contraction property

$$\xi_{\ell+1}^2 \leqslant \rho \xi_\ell^2.$$

This is the second main ingredient of Theorem 3.6.3.

Recall notation for nested triangulations $\mathcal{T}_\ell$ and $\mathcal{T}_{\ell+k}$ from Table 3.11, then $\mathcal{E}_{\ell \setminus \ell+k}$ and $\mathcal{T}_{\ell \setminus \ell+k}$ are the sets of edges and triangles, respectively, that have been refined from level ℓ to $\ell + k$.

Lemma 3.6.4 (Optimality (3.22) in Case (A))**.** *Consider parameters $0 < \theta_A < 1$, $0 < \kappa$, and $0 < \rho_B < 1$ for algorithm* s-afem-aa*. Let the exact solution and the right-hand side satisfy $(u, f) \in \mathcal{A}_s$ for some $s > 0$.*

Assume there exists $0 < \tau < 1$, such that for any level $\ell \in \mathbb{N}_0$ with Case (A) the set $\mathcal{E}_{\ell \setminus \ell+\epsilon(\ell)}$ fulfils the bulk criterion (4.18), namely,

$$\theta_A \eta_\ell^2 \leqslant \eta_\ell^2(\mathcal{E}_{\ell \setminus \ell+\epsilon(\ell)}),$$

where $\epsilon(\ell) := \tau \xi_\ell$ and $\mathcal{T}_{\epsilon(\ell)}$ is the admissible triangulation refined from $\mathcal{T}_0$, which satisfies

$$\varepsilon_{\epsilon(\ell)}^2 + \left\| h_{\epsilon(\ell)} f \right\|_{L^2(\Omega)}^2 \approx \xi_{\epsilon(\ell)}^2 \leqslant \epsilon(\ell)^2, \quad \text{and} \quad \left| \mathcal{T}_{\epsilon(\ell)} \right| - |\mathcal{T}_0| \lesssim \epsilon(\ell)^{-1/s}.$$

Then, optimality in the sense of (3.22) holds for $\ell \in \mathbb{N}_0$ and Case (A).

Proof. Let $0 < \tau < 1$ and $\epsilon(\ell) := \tau \xi_\ell$. Due to $(u, f) \in \mathcal{A}_s$ and (3.20) on any level $\ell \in \mathbb{N}_0$

there exists an admissible triangulation $\mathcal{T}_{\epsilon(\ell)}$ refined from $\mathcal{T}_0$, which satisfies

$$\varepsilon_{\epsilon(\ell)}^2 + \left\|h_{\epsilon(\ell)} f\right\|_{L^2(\Omega)}^2 \approx \xi_{\epsilon(\ell)}^2 \leqslant \epsilon(\ell)^2, \quad \text{and } \left|\mathcal{T}_{\epsilon(\ell)}\right| - |\mathcal{T}_0| \lesssim \epsilon(\ell)^{-1/s}.$$

This verifies

$$\left|\mathcal{T}_{\epsilon(\ell)}\right| - |\mathcal{T}_0| \lesssim \epsilon(\ell)^{-1/s} \approx \xi_\ell^{-1/s}.$$

The number of elements of the overlay $\mathcal{T}_{\ell+\epsilon(\ell)} := \mathcal{T}_{\epsilon(\ell)} \oplus \mathcal{T}_\ell$ is bounded due to Lemma 3.2.5, and the cardinality of $\mathcal{E}_{\ell\setminus\ell+\epsilon(\ell)} \cup \mathcal{T}_{\ell\setminus\ell+\epsilon(\ell)} \subseteq \mathcal{E}_\ell \cup \mathcal{T}_\ell$ (i.e., of the set of refined edges and triangles) is bounded, see Lemma 3.2.6. Thus, the aforementioned estimate and Lemmas 3.2.5 and 3.2.6 prove

$$\left|\mathcal{E}_{\ell\setminus\ell+\epsilon(\ell)}\right| \lesssim \left|\mathcal{E}_{\ell\setminus\ell+\epsilon(\ell)} \cup \mathcal{T}_{\ell\setminus\ell+\epsilon(\ell)}\right| \lesssim \left|\mathcal{T}_{\ell+\epsilon(\ell)}\right| - |\mathcal{T}_\ell| \lesssim \xi_\ell^{-1/s}.$$

$\mathcal{M}_\ell$ and $\mathcal{E}_{\ell\setminus\ell+\epsilon(\ell)}$ fulfil the bulk criterion (4.18), and $\mathcal{M}_\ell$ was chosen with quasi-minimal cardinality that satisfies $\theta_A \eta_\ell^2 \leqslant \eta_\ell^2(\mathcal{M}_\ell)$. This observation plus the upper bound for the cardinality of $\mathcal{E}_{\ell\setminus\ell+\epsilon(\ell)}$ of Lemma 3.2.6 yields (3.22), namely

$$|\mathcal{M}_\ell| \lesssim |\mathcal{E}_{\ell\setminus\ell+\epsilon(\ell)}| \lesssim |\mathcal{T}_{\ell+\epsilon(\ell)}| - |\mathcal{T}_\ell| \lesssim \xi_\ell^{-1/s}. \qquad \square$$

Lemma 3.6.5 (Complexity estimate of Algorithm 3.17 (AA))**.** *Let $(u, f) \in \mathcal{A}_s$ from (3.20) for $s > 0$ with $u \in H_0^1(\Omega)$, $f \in L^2(\Omega)$. Given an input triangulation $\mathcal{T}_0$, a tolerance $\mathrm{Tol} > 0$ and an error functional $e(f,T) := \|h_T f\|_{L^2(T)}^2$, the output triangulation $\mathcal{T}_{\mathrm{Tol}}$ of Algorithm 3.17 AA satisfies*

$$|\mathcal{T}_{\mathrm{Tol}}| - |\mathcal{T}_0| \lesssim \mathrm{Tol}^{-1/(2s)}, \quad \|h_{\mathrm{Tol}} f\|_{L^2(\Omega)}^2 \leqslant \mathrm{Tol}\,.$$

Proof. This proof follows standard arguments for optimality similar to the proof of Lemma 3.6.4 above. [BDdV04, Lemma 4.4] uses similar arguments for the Approx algorithm presented in [BDdV04]. Let $\mathrm{Tol} > 0$ and $\epsilon^2 := C_{1,\star}/C_{\mathrm{sa}}\,\mathrm{Tol}$ with $C_{1,\star}$ and C_{sa} from Lemma 3.3.3 and (3.13). The definition of the approximation class $\mathcal{A}_s$ yields the existence of a regular refinement $\mathcal{T}_\epsilon$ of $\mathcal{T}_0$ with

$$|\mathcal{T}_\epsilon| - |\mathcal{T}_0| \lesssim \epsilon^{-1/s}, \quad \varepsilon_\epsilon^2 + \|h_\epsilon f\|_{L^2(\Omega)}^2 \lesssim \epsilon^2.$$

Let $\mathcal{T}_{\mathrm{Tol}+\epsilon} := \mathcal{T}_\epsilon \oplus \mathcal{T}_{\mathrm{Tol}}$, then due to the sub-additivity (3.13)

$$e\left(\mathcal{T}_{\mathrm{Tol}+\epsilon}\right) \leqslant C_{\mathrm{sa}}\epsilon^2 = C_{1,\star}\,\mathrm{Tol}\,.$$

Furthermore, the control of the overhead of overlay in Lemma 3.2.5 verifies

$$|\mathcal{T}_{\mathrm{Tol}+\epsilon}| - |\mathcal{T}_{\mathrm{Tol}}| \leqslant |\mathcal{T}_\epsilon| - |\mathcal{T}_0| \lesssim \epsilon^{-1/s} \approx \mathrm{Tol}^{-1/(2s)}\,.$$

Algorithm 3.17 AA generates $\mathcal{T}_{\mathrm{Tol}}$ with $\|h_{\mathrm{Tol}} f\|_{L^2(\Omega)}^2 \leqslant \mathrm{Tol}$, whereas $\mathcal{T}_{\mathrm{Tol}+\epsilon}$ satisfies $\|h_{\mathrm{Tol}+\epsilon} f\|_{L^2(\Omega)}^2 \leqslant C_{1,\star}\,\mathrm{Tol}$. Thus, Lemmas 3.2.3 and 3.3.3 plus the previous estimate

ensure the optimality of AA in the sense that

$$|\mathcal{T}_{\mathrm{Tol}}| - |\mathcal{T}_0| \lesssim \sum_{k=0}^{K} \left|\mathcal{M}^{(k)}\right| \lesssim |\mathcal{T}_{\mathrm{Tol}+\epsilon}| - |\mathcal{T}_0| \lesssim \epsilon^{-1/s} \approx \mathrm{Tol}^{-1/(2s)}\,. \qquad \square$$

Lemma 3.6.6 (Optimality (3.22) in Case (B))**.** *Given parameters $0 < \theta_A < 1$, $0 < \kappa$ and $0 < \rho_B < 1$, algorithm* S-AFEM-AA *generates a sequence of discrete solutions and triangulations $\mathcal{T}_\ell$.*

Assume that the total error $\xi_\ell^2 = \eta_\ell^2 + \alpha_f \|h_\ell f\|_{L^2(\Omega)}^2 + \alpha_\varepsilon \varepsilon_\ell^2$ on level $\ell \in \mathbb{N}_0$ with Case (B) is bounded as follows

$$\xi_\ell \lesssim \|h_\ell f\|_{L^2(\Omega)}\,, \tag{3.24}$$

then the optimality for Case (B) in the sense of (3.22) holds.

Proof. In Case (B) a triangulation $\mathcal{T}_{\mathrm{Tol}}$ refined from $\mathcal{T}_0$ is generated by AA that satisfies

$$\|h_{\mathcal{T}_{\mathrm{Tol}}} f\|_{L^2(\Omega)}^2 \leqslant \mathrm{Tol} \quad \text{with } \mathrm{Tol} := \rho_B \|h_\ell f\|_{L^2(\Omega)}^2\,.$$

For the overlay triangulation $\mathcal{T}_{\ell+1} := \mathcal{T}_{\mathrm{Tol}} \oplus \mathcal{T}_\ell$, Algorithm 3.18 provides a finite sequence $\mathcal{M}_\ell^{(0)}, \dots, \mathcal{M}_\ell^{(K(\ell))}$ of marked refinement edges such that

$$\mathcal{T}_{\mathrm{Tol}} \oplus \mathcal{T}_\ell = \textsc{Refine}\left(\mathcal{T}_\ell, \left(\mathcal{M}_\ell^{(k)}\right)_{k=0,\dots,K(\ell)}\right).$$

Theorem 3.5.1 and Lemma 3.6.5 ensure

$$\sum_{k=0}^{K(\ell)} |\mathcal{M}_\ell^{(k)}| \leqslant |\mathcal{T}_{\mathrm{Tol}}| - |\mathcal{T}_0| \lesssim \mathrm{Tol}^{-1/(2s)}\,. \tag{3.25}$$

The estimate (3.24) for Case (B) together with $\rho_B \|h_\ell f\|_{L^2(\Omega)}^2 = \mathrm{Tol}$ verifies

$$\mathrm{Tol}^{-1/(2s)} \lesssim \|h_\ell f\|_{L^2(\Omega)}^{-1/s} \lesssim \xi_\ell^{-1/s}. \tag{3.26}$$

The combination of the estimates (3.25) and (3.26) proves (3.22) in Case (B). $\square$

Note that (3.24) in Case (B) can in general be proven by reliability and $\kappa\eta_\ell^2 \leqslant \|h_\ell f\|_{L^2(\Omega)}^2$.

4 The Poisson model problem

4.1 Introduction

This chapter contains a proof of the quasi-optimal convergence of s-afem-aa based on the nonconforming Crouzeix–Raviart fem to solve the Poisson model problem (2.1) for given $f \in L^2(\Omega)$ and unknown solution u, i.e.,

$$\Delta u = -f \quad \text{in } \Omega, \quad u = 0 \quad \text{on } \partial\Omega.$$

The discrete weak formulation reads: Seek $u_\ell^{\mathrm{NC}} \in V_\ell := P_{1,0}^{\mathrm{NC}}(\mathcal{T}_\ell)$, such that for all $v_\ell^{\mathrm{NC}} \in V_\ell$

$$(\nabla_\ell u_\ell^{\mathrm{NC}}, \nabla_\ell v_\ell^{\mathrm{NC}})_{L^2(\Omega)} = (f, v_\ell^{\mathrm{NC}})_{L^2(\Omega)}\,. \tag{4.1}$$

The flux error is $\varepsilon_\ell^2 := \|p_\ell^{\mathrm{NC}} - p\|_{L^2(\Omega)}^2$ with the exact flux $p := \nabla u$ and the discrete flux $p_\ell^{\mathrm{NC}} := \nabla_\ell u_\ell^{\mathrm{NC}}$ with respect to the current triangulation $\mathcal{T}_\ell$. The bilinear form

$$a_{\mathrm{NC}(\ell)}\left(u_\ell^{\mathrm{NC}}, v_\ell^{\mathrm{NC}}\right) := (\nabla_\ell u_\ell^{\mathrm{NC}}, \nabla_\ell v_\ell^{\mathrm{NC}})_{L^2(\Omega)} \qquad \text{for } u_\ell^{\mathrm{NC}}, v_\ell^{\mathrm{NC}} \in V_\ell$$

defines the energy norm $|||\cdot|||_\ell = a_{\mathrm{NC}(\ell)}\left(\cdot,\cdot\right)^{1/2}$. Furthermore, the energy error is given by $\varepsilon_\ell := |||u - u_\ell^{\mathrm{NC}}|||_\ell$. The bilinear form $a_{\mathrm{NC}(\ell)}$ is coercive in $V := H_0^1\left(\Omega;\mathbb{R}^2\right)$ and positive definite on V_ℓ, which yields the existence of a unique solution u_ℓ^{NC} on V_ℓ.

The refinement indicator for the bulk criterion in Case (A) is defined via the edge contributions

$$\eta_\ell\left(E\right) := h_E^{1/2}\left\|[p_\ell^{\mathrm{NC}}]_E \cdot \tau_E\right\|_{L^2(E)} \qquad \text{for any } E \in \mathcal{E}_\ell. \tag{4.2}$$

As introduced in Section 2.3 on page 15, $[p_\ell^{\mathrm{NC}}]_E$ denotes the jump of the discrete flux p_ℓ^{NC} across an interior edge E, which vanishes on all boundary edges $\mathcal{E}_\ell(\partial\Omega)$. The piecewise constant jump vector allows a decomposition $|[p_\ell^{\mathrm{NC}}]_E|^2 = \left([p_\ell^{\mathrm{NC}}]_E \cdot \nu_E\right)^2 + \left([p_\ell^{\mathrm{NC}}]_E \cdot \tau_E\right)^2$.

The goal of this chapter is to prove quasi-optimality for the outcome of s-afem-aa as introduced in Algorithm 3.4 and Section 3.4. s-afem-aa is applied to solve the discrete Poisson problem (4.1) adaptively using the error estimator η_ℓ from (4.2).

The remaining part of this chapter is organised as follows. Section 4.2 recapitulates preliminaries of [Rab10] which will be used to prove the contraction property and optimal convergence of Algorithm 3.4 for the Poisson model problem in Section 4.3. The final section includes the proof of optimal convergence rates for s-afem-aa and the Poisson model problem. The numerical experiments are described in Chapter 7. For the Poisson problem the experiments in Sections 7.1 and 7.3 confirm the quasi-optimality.

4.2 Preliminaries

This section is a collection of essential estimates, such as efficiency, reliability, quasi-orthogonality and discrete reliability, which are used to prove convergence and determine optimal rates in Sections 4.3 and 4.4. In [Rab10], the adaptive Algorithm 3.1 based on the estimated total error

$$\mu_\ell^2 = \eta_\ell^2 + \|h_\ell f\|_{L^2(\Omega)}^2 \tag{4.3}$$

and collective marking is proven to generate sequences of triangulations and solutions with quasi-optimal convergence rates. Discrete reliability based on the discrete Helmholtz decomposition is recapitulated from [Rab10], while results for efficiency and reliability can be found in [BMS10, CBJ02, CH06a]. Quasi-orthogonality, as the key tool for non-conforming FEM, was introduced for the Poisson problem by Carstensen and Hoppe [CH06a, CH06b], and sharpened for mixed FEM in [BM08]. The sharpened form was employed for nonconforming methods in [HSX12] and later for the Poisson model problem in [BMS10, MZS10, Rab10] and is used in the analysis below.

Recall the notation for nested meshes as introduced in Chapter 2. Here and throughout, let $\mathcal{T}_\ell$ be a triangulation of Ω and $\mathcal{T}_{\ell+k}$ an admissible refinement of $\mathcal{T}_\ell$ in $k \geqslant 1$ levels of refinement. Let $u_\ell^{\mathrm{NC}} \in V_\ell$ and $u_{\ell+k}^{\mathrm{NC}} \in V_{\ell+k}$ denote the CR solutions of (4.1) with their discrete fluxes $p_\ell^{\mathrm{NC}} = \nabla_\ell u_\ell^{\mathrm{NC}}$ and $p_{\ell+k}^{\mathrm{NC}} = \nabla_{\ell+k} u_\ell^{\mathrm{NC}}$.

Lemma 4.2.1 (Reliability, efficiency [BMS10, CBJ02, CH06a])**.** *There exist some positive, generic constants c_{eff}, C_{rel} such that the error estimator η_ℓ satisfies efficiency and reliability*

$$c_{\mathrm{eff}}\eta_\ell^2 \leqslant \varepsilon_\ell^2 \leqslant C_{\mathrm{rel}}\left(\eta_\ell^2 + \|h_\ell f\|_{L^2(\Omega)}^2\right). \tag{4.4}$$

Lemma 4.2.2 (Quasi-orthogonality [BMS10])**.** *There exists some positive, generic constant C_{qo} such that the discrete fluxes p_ℓ^{NC} and $p_{\ell+k}^{\mathrm{NC}}$ of (4.1) satisfy quasi-orthogonality*

$$\left|\left(p - p_{\ell+k}^{\mathrm{NC}}, p_\ell^{\mathrm{NC}} - p_{\ell+k}^{\mathrm{NC}}\right)_{L^2(\Omega)}\right| \leqslant C_{\mathrm{qo}}^{1/2}\varepsilon_{\ell+k}\,\|h_\ell f\|_{\mathcal{T}_\ell\setminus\mathcal{T}_{\ell+k}},$$

as well as

$$\begin{aligned}\|p_{\ell+k}^{\mathrm{NC}} - p_\ell^{\mathrm{NC}}\|_{L^2(\Omega)}^2 &\leqslant \varepsilon_\ell^2 - \varepsilon_{\ell+k}^2 + 2C_{\mathrm{qo}}^{1/2}\,\|h_\ell f\|_{\mathcal{T}_\ell\setminus\mathcal{T}_{\ell+k}}\,\varepsilon_{\ell+k},\\ \varepsilon_\ell^2 - \varepsilon_{\ell+k}^2 &\leqslant \|p_{\ell+k}^{\mathrm{NC}} - p_\ell^{\mathrm{NC}}\|_{L^2(\Omega)}^2 + 2C_{\mathrm{qo}}^{1/2}\,\|h_\ell f\|_{\mathcal{T}_\ell\setminus\mathcal{T}_{\ell+k}}\,\varepsilon_{\ell+k}.\end{aligned}$$

Without violating quasi-orthogonality in Lemma 4.2.2 we may enlarge C_{qo} to satisfy

$$\max\{2, c_{\mathrm{eff}}\} < 8C_{\mathrm{qo}} \tag{4.5}$$

as assumed in Lemma 4.4.4 and Theorem 4.4.1.

Theorem 4.2.3 (Discrete reliability, [Rab10, Theorem 2.1])**.** *There exists some generic constant $C_{\mathrm{drel}} > 0$, such that discrete reliability holds in the sense of*

$$\|p_{\ell+k}^{\mathrm{NC}} - p_\ell^{\mathrm{NC}}\|_{L^2(\Omega)}^2 \leqslant C_{\mathrm{drel}}\left(\eta_\ell^2\left(\mathcal{E}_{\ell\setminus\ell+k}\right) + \|h_\ell f\|_{\mathcal{T}_\ell\setminus\mathcal{T}_{\ell+k}}^2\right). \tag{4.6}$$

Proof replicated from [Rab10, Theorem 2.1]. To prove (4.6) we recall the discrete Helmholtz decomposition of $\delta := p^{\mathrm{NC}}_{\ell+k} - p^{\mathrm{NC}}_{\ell}$. There exist $\alpha^{\mathrm{NC}}_{\ell+k} \in V_{\ell+k}$ and $\beta^{\mathrm{C}}_{\ell+k} \in \hat{P}_1(\mathcal{T}_{\ell+k})$ with $\hat{P}_1(\mathcal{T}_{\ell+k})$ defined in Table 2.8 such that

$$\delta := p^{\mathrm{NC}}_{\ell+k} - p^{\mathrm{NC}}_{\ell} = \nabla_{\ell+k}\alpha^{\mathrm{NC}}_{\ell+k} + \operatorname{Curl}\beta^{\mathrm{C}}_{\ell+k}.$$

To estimate $\left\|p^{\mathrm{NC}}_{\ell+k} - p^{\mathrm{NC}}_{\ell}\right\|^2_{L^2(\Omega)}$ each summand of the right-hand side of

$$\|p^{\mathrm{NC}}_{\ell+k} - p^{\mathrm{NC}}_{\ell}\|^2_{L^2(\Omega)} = \int_\Omega \delta \cdot \nabla_{\ell+k}\alpha^{\mathrm{NC}}_{\ell+k}\,\mathrm{dx} + \int_\Omega \delta \cdot \operatorname{Curl}\beta^{\mathrm{C}}_{\ell+k},$$

is bounded separately in the following. Let $\alpha^{\mathrm{NC}}_{\ell} \in P^{\mathrm{NC}}_1(\mathcal{T}_\ell)$ be defined via the integral mean of $\alpha^{\mathrm{NC}}_{\ell+k}$ for all $E \in \mathcal{E}_\ell$, namely, $⨍_E \alpha^{\mathrm{NC}}_{\ell} = ⨍_E \alpha^{\mathrm{NC}}_{\ell+k}$. Thus,

$$\begin{aligned}
\int_\Omega \delta \cdot \nabla_{\ell+k}\alpha^{\mathrm{NC}}_{\ell+k}\,\mathrm{dx} &= \left(f, \alpha^{\mathrm{NC}}_{\ell+k}\right)_{L^2(\Omega)} - \sum_{E\in\mathcal{E}_\ell}\int_E [p^{\mathrm{NC}}_{\ell}\alpha^{\mathrm{NC}}_{\ell+k}]_E \nu_E\,\mathrm{ds} \\
&= \left(f, \alpha^{\mathrm{NC}}_{\ell+k} - \alpha^{\mathrm{NC}}_{\ell}\right)_{L^2(\Omega)} - \sum_{E\in\mathcal{E}_\ell}\int_E [p^{\mathrm{NC}}_{\ell}\left(\alpha^{\mathrm{NC}}_{\ell+k} - \alpha^{\mathrm{NC}}_{\ell}\right)]_E \nu_E\,\mathrm{ds} \\
&= \sum_{T\in\mathcal{T}_\ell}\left(f, \alpha^{\mathrm{NC}}_{\ell+k} - \alpha^{\mathrm{NC}}_{\ell}\right)_{L^2(T)} \leqslant \sum_{T\in\mathcal{T}_{\ell\setminus\ell+k}} \|f\|_{L^2(T)}\left\|\alpha^{\mathrm{NC}}_{\ell+k} - \alpha^{\mathrm{NC}}_{\ell}\right\|_{L^2(T)}.
\end{aligned}$$

The discrete Poincaré inequality of Lemma 3.2.11 states

$$\left\|\alpha^{\mathrm{NC}}_{\ell+k} - \alpha^{\mathrm{NC}}_{\ell}\right\|_{L^2(T)} \lesssim h_T \left\|\nabla_{\ell+k}\alpha^{\mathrm{NC}}_{\ell+k}\right\|_{L^2(T)} \leqslant h_T \left\|p^{\mathrm{NC}}_{\ell+k} - p^{\mathrm{NC}}_{\ell}\right\|_{L^2(\Omega)},$$

which implies

$$\begin{aligned}
\int_\Omega \delta \cdot \nabla_{\ell+k}\alpha^{\mathrm{NC}}_{\ell+k}\,\mathrm{dx} &\lesssim \left\|p^{\mathrm{NC}}_{\ell+k} - p^{\mathrm{NC}}_{\ell}\right\|_{L^2(\Omega)} \sum_{T\in\mathcal{T}_{\ell\setminus\ell+k}} \|f\|_{L^2(T)}\, h_T \\
&\lesssim \left\|p^{\mathrm{NC}}_{\ell+k} - p^{\mathrm{NC}}_{\ell}\right\|_{L^2(\Omega)} \|h_\ell f\|_{\mathcal{T}_{\ell\setminus\ell+k}}.
\end{aligned}$$

To bound the second part of the Helmholtz decomposition, let $\mathcal{I}_\ell$ be the Scott–Zhang interpolator (see Definition 3.2.9) on $\mathcal{T}_\ell$ and $\beta^{\mathrm{C}}_{\ell} := \mathcal{I}_\ell\beta^{\mathrm{C}}_{\ell+k}$ with $\left\|\beta^{\mathrm{C}}_{\ell+k} - \beta^{\mathrm{C}}_{\ell}\right\|_{L^2(E)} = 0$ for $E \in \mathcal{E}_{\ell+k} \cap \mathcal{E}_\ell$. For $n = 2$ and on the patch Ω^ℓ_E (see Figure 3.15 and Table 3.14) for $E \in \mathcal{E}_{\ell\setminus\ell+k}$

$$\left\|\beta^{\mathrm{C}}_{\ell+k} - \beta^{\mathrm{C}}_{\ell}\right\|_{L^2(E)} \leqslant C h_E^{1/2} \left|\beta^{\mathrm{C}}_{\ell+k}\right|_{H^1(\Omega^\ell_E)}.$$

Thus, the L^2 orthogonalities

$$\left(p^{\mathrm{NC}}_{\ell+k}, \operatorname{Curl}\beta^{\mathrm{C}}_{\ell+k}\right)_{L^2(\Omega)} = 0 = \left(p^{\mathrm{NC}}_{\ell}, \operatorname{Curl}\beta^{\mathrm{C}}_{\ell}\right)_{L^2(\Omega)}$$

lead to

$$\begin{aligned}\int_\Omega \left(p_{\ell+k}^{\mathrm{NC}} - p_\ell^{\mathrm{NC}}\right) \cdot \operatorname{Curl} \beta_{\ell+k}^{\mathrm{C}} \,\mathrm{dx} &= -\int_\Omega p_\ell^{\mathrm{NC}} \cdot \operatorname{Curl} \beta_{\ell+k}^{\mathrm{C}} \,\mathrm{dx} = -\int_\Omega p_\ell^{\mathrm{NC}} \cdot \operatorname{Curl} \left(\beta_{\ell+k}^{\mathrm{C}} - \beta_\ell^{\mathrm{C}}\right) \mathrm{dx} \\ &= -\sum_{T\in\mathcal{T}_\ell} \int_T \operatorname{curl} p_\ell^{\mathrm{NC}} \left(\beta_{\ell+k}^{\mathrm{C}} - \beta_\ell^{\mathrm{C}}\right) \mathrm{dx} + \sum_{E\in\mathcal{E}_\ell} \int_E [p_\ell^{\mathrm{NC}}]_E \cdot \tau_E \left(\beta_{\ell+k}^{\mathrm{C}} - \beta_\ell^{\mathrm{C}}\right) \mathrm{ds} \\ &\leqslant \sum_{E\in\mathcal{E}_{\ell\setminus\ell+k}} \|[p_\ell^{\mathrm{NC}}]_E \cdot \tau_E\|_{L^2(E)} \left\|\beta_{\ell+k}^{\mathrm{C}} - \beta_\ell^{\mathrm{C}}\right\|_{L^2(E)} \\ &\lesssim \sum_{E\in\mathcal{E}_{\ell\setminus\ell+k}} \|[p_\ell^{\mathrm{NC}}]_E \cdot \tau_E\|_{L^2(E)} \, h_E^{1/2} \left|\beta_{\ell+k}^{\mathrm{C}}\right|_{H^1(\Omega_E^\ell)} \\ &\lesssim \eta_\ell\left(\mathcal{E}_{\ell\setminus\ell+k}\right) \left\|p_{\ell+k}^{\mathrm{NC}} - p_\ell^{\mathrm{NC}}\right\|_{L^2(\Omega)}.\end{aligned}$$

Taking the estimates for both parts of the Helmholtz decomposition into consideration, the assertion follows directly. □

4.3 Convergence

This section analyses the convergence behaviour of a sequence of CR solutions of (4.1) generated by S-AFEM-AA.

The proofs of estimator reduction (Lemma 4.3.1), convergence (Theorem 4.3.2) and quasi-optimal convergence (Theorem 4.4.1 in the next Section 4.4) follow a similar methodology as for S-AFEM-AA in [CR11] for the adaptive algorithm for mixed finite elements and the Poisson model problem. This is the result of the design of S-AFEM-AA with the Dörfler marking in Case (A) for the refinement indicator η_ℓ and the AA in Case (B) for approximating the right-hand side $f \in L^2(\Omega)$. While in [CR11] for mixed FEM the data approximation is controlled via oscillations, in this thesis CR-FEM and the volume term are used instead. The subsequent analysis is the first example to follow the general mathematical methodology, which is applied later to the pure displacement problem in linear elasticity and the Stokes equations.

Recall that the convergence behaviour of the sequences of triangulations and discrete solutions generated by C-AFEM (Algorithm 3.1) with the collective estimator μ_ℓ of (4.3) is analysed in [Rab10].

Lemma 4.3.1 (Estimator reduction)**.** *Let $0 < \theta_A < 1$, $0 < \rho_B < 1$, and $\kappa > 0$ be parameters for algorithm* S-AFEM-AA *used to solve (4.1). Then, for any $0 < \delta < \theta_A(2 - \theta_A)$ there exist positive generic constants C_{J}, C_δ and a reduction factor $0 < \rho_A < 1$ such that on each level $\ell \in \mathbb{N}_0$ of the algorithm* S-AFEM-AA

(a) *in **Case(A)** (i.e., if $\|h_\ell f\|_{L^2(\Omega)}^2 \leqslant \kappa\eta_\ell^2$) η_ℓ and $\|h_\ell f\|_{L^2(\Omega)}$ satisfy the reduction properties*

$$\eta_{\ell+1}^2 \leqslant \rho_A \eta_\ell^2 + C_\delta \left\|p_{\ell+1}^{\mathrm{NC}} - p_\ell^{\mathrm{NC}}\right\|_{L^2(\Omega)}^2 \qquad \text{and} \tag{4.7}$$

$$\|h_{\ell+1} f\|_{L^2(\Omega)}^2 \leqslant \|h_\ell f\|_{L^2(\Omega)}^2 - 1/2 \, \|h_\ell f\|_{\mathcal{T}_{\ell\setminus\ell+1}}^2, \tag{4.8}$$

(b) *in **Case(B)** (i.e., if $\|h_\ell f\|_{L^2(\Omega)}^2 > \kappa\eta_\ell^2$) η_ℓ and $\|h_\ell f\|_{L^2(\Omega)}$ satisfy the reduction*

properties

$$\eta_{\ell+1}^2 \leqslant (1+\delta)\,\eta_\ell^2 + C_\delta \left\|p_{\ell+1}^{\mathrm{NC}} - p_\ell^{\mathrm{NC}}\right\|_{L^2(\Omega)}^2 \qquad \textit{and} \tag{4.9}$$

$$\|h_{\ell+1} f\|_{L^2(\Omega)}^2 \leqslant \rho_B \|h_\ell f\|_{L^2(\Omega)}^2 . \tag{4.10}$$

Proof. The proof follows arguments in [Car09a, CKNS08] for the estimator reduction therein. For any edge $E \in \mathcal{E}_{\ell+1}$ and any $\delta > 0$

$$\left|[p_\ell^{\mathrm{NC}}] \cdot \tau_E\right|^2 \leqslant (1+1/\delta)\left|[p_\ell^{\mathrm{NC}} - p_{\ell+1}^{\mathrm{NC}}] \cdot \tau_E\right|^2 + (1+\delta)\left|[p_{\ell+1}^{\mathrm{NC}}] \cdot \tau_E\right|^2 .$$

Since $p_{\ell+1}^{\mathrm{NC}} - p_\ell^{\mathrm{NC}}$ is piecewise constant on $\mathcal{T}_{\ell+1}$ it follows that

$$\sum_{E\in\mathcal{E}_{\ell+1}} h_E^2 \left|[p_{\ell+1}^{\mathrm{NC}} - p_\ell^{\mathrm{NC}}] \cdot \tau_E\right|^2 \lesssim \left\|p_{\ell+1}^{\mathrm{NC}} - p_\ell^{\mathrm{NC}}\right\|_{L^2(\Omega)}^2 .$$

Thus, there exists some positive generic constant C_{J}, such that $\eta_{\ell+1}$ is bounded via

$$\begin{aligned}\eta_{\ell+1}^2 &\leqslant (1+\delta)\,\eta_\ell^2\,(\mathcal{E}_\ell \cap \mathcal{E}_{\ell+1}) + (1+\delta)/2\,\eta_\ell^2\left(\mathcal{E}_{\ell\setminus\ell+1}\right) + (1+1/\delta)\,C_{\mathrm{J}}\left\|p_{\ell+1}^{\mathrm{NC}} - p_\ell^{\mathrm{NC}}\right\|_{L^2(\Omega)}^2 \\ &\leqslant (1+\delta)\,\eta_\ell^2 - (1+\delta)/2\,\eta_\ell^2\left(\mathcal{E}_{\ell\setminus\ell+1}\right) + (1+1/\delta)\,C_{\mathrm{J}}\left\|p_{\ell+1}^{\mathrm{NC}} - p_\ell^{\mathrm{NC}}\right\|_{L^2(\Omega)}^2 .\end{aligned}$$

This is (4.9) in Case (B) for $C_\delta := C_{\mathrm{J}}\,(1+1/\delta)$. The incorporation of the bulk criterion (3.14) of Case (A) leads to

$$\begin{aligned}\eta_{\ell+1}^2 &\leqslant (1+\delta)\,(1-\theta_A/2)\,\eta_\ell^2 + C_\delta \left\|p_{\ell+1}^{\mathrm{NC}} - p_\ell^{\mathrm{NC}}\right\|_{L^2(\Omega)}^2 \\ &\leqslant \rho_A \eta_\ell^2 + C_\delta \left\|p_{\ell+1}^{\mathrm{NC}} - p_\ell^{\mathrm{NC}}\right\|_{L^2(\Omega)}^2 .\end{aligned}$$

This proves (4.7) for $\delta < \theta_A/(2-\theta_A)$ with $\rho_A := (1+\delta)\,(1-\theta_A/2) < 1$. The standard estimate (3.7) for $\|h_\ell f\|_{L^2(\Omega)}$ is (4.8) for Case (A) and holds for any two nested NVB refinements.

Given arbitrary $0 < \rho_B < 1$ from S-AFEM-AA in Case (B), $\mathrm{Tol} := \rho_B \|h_\ell f\|_{L^2(\Omega)}^2$ and the output triangulation $\mathcal{T}$ of AA, the reduction of the volume term (4.10) is guaranteed for the overlay triangulation $\mathcal{T}_{\ell+1} = \mathcal{T}_\ell \oplus \mathcal{T}$

$$\|h_{\ell+1} f\|_{L^2(\Omega)}^2 \leqslant \|h_{\mathcal{T}} f\|_{L^2(\Omega)}^2 \leqslant \rho_B \|h_\ell f\|_{L^2(\Omega)}^2 . \qquad \square$$

Theorem 4.3.2 (Convergence)**.** *Given some bulk parameter $0 < \theta_A < 1$, there exists $0 < \kappa_0$, such that for any $\kappa_1 \in (0, \kappa_0)$ and $0 < \rho_B < 1$ there exist positive α_f, α_ε and $0 < \varrho < 1$, which depend on positive generic constants C_{rel}, C_{qo} and C_δ from Lemmas 4.2.1, 4.2.2 and 4.3.1 such that for all κ with $\kappa \in (\kappa_1, \kappa_0)$ the sequence of triangulations and discrete solutions generated by* S-AFEM-AA *with its total errors $\xi_\ell := \eta_\ell^2 + \alpha_f \|h_\ell f\|_{L^2(\Omega)}^2 + \alpha_\varepsilon |\!|\!| u - u_\ell^{\mathrm{NC}} |\!|\!|_{\mathrm{NC}(\ell)}^2$ satisfies a contraction property in the sense that*

$$\xi_{\ell+1}^2 \leqslant \varrho \xi_\ell^2 \quad \textit{for all } \ell \in \mathbb{N}_0.$$

Proof. Let $0 < \theta_A < 1$ and define

$$\begin{aligned}
\delta &:= \frac{\theta_A}{2}\frac{1}{2-\theta_A}, & \rho_A &:= (1+\delta)(1-\theta_A/2) = 1-\theta_A/4,\\
\gamma &:= \frac{1}{2}\min\left\{1, \frac{1-\rho_A}{C_\delta C_{\mathrm{rel}}}\right\}, & B &:= \frac{3}{4}\min\left\{1, \frac{1-\rho_A}{C_\delta C_{\mathrm{rel}}}\right\},\\
A &:= 2\left(C_{\mathrm{qo}} C_\delta/\gamma + C_\delta C_{\mathrm{rel}} B\right), & \alpha_\varepsilon &:= (1-\gamma) C_\delta,\\
\kappa_0 &:= \frac{1-\rho_A - C_\delta C_{\mathrm{rel}} B}{A} < 1.
\end{aligned}$$

Let $\kappa_1 \in (0, \kappa_0)$, $0 < \rho_B < 1$ and define

$$D := \frac{\delta + C_\delta C_{\mathrm{rel}} B}{\kappa_1}, \qquad \alpha_f := \frac{A+D}{1-\rho_B}.$$

Contraction in Case (A) Lemma 4.3.1 shows that for any $0 < \theta_A < 1$ there exist $0 < \rho_A < 1$ and $0 < C_\delta$ such that

$$\begin{aligned}
\eta_{\ell+1}^2 &\leqslant \rho_A \eta_\ell^2 + C_\delta \left\| p_{\ell+1}^{\mathrm{NC}} - p_\ell^{\mathrm{NC}} \right\|_{L^2(\Omega)}^2,\\
\|h_{\ell+1} f\|_{L^2(\Omega)}^2 &\leqslant \|h_\ell f\|_{L^2(\Omega)}^2 - \frac{1}{2}\|h_\ell f\|_{\mathcal{T}_\ell \setminus \mathcal{T}_{\ell+1}}^2,\\
\|h_\ell f\|_{L^2(\Omega)}^2 &< \kappa \eta_\ell^2.
\end{aligned} \tag{4.11}$$

For positive B and γ, the quasi-orthogonality of Lemma 4.2.2 plus the reliability of Lemma 4.2.1 and the application of Young's inequality prove

$$\begin{aligned}
\eta_{\ell+1}^2 &\leqslant \rho_A \eta_\ell^2 + C_\delta \left\| p_{\ell+1}^{\mathrm{NC}} - p_\ell^{\mathrm{NC}} \right\|_{L^2(\Omega)}^2\\
&\leqslant \rho_A \eta_\ell^2 + C_\delta \left(\varepsilon_\ell^2 - \varepsilon_{\ell+1}^2 + 2 C_{\mathrm{qo}}^{1/2} \|h_\ell f\|_{\mathcal{T}_\ell \setminus \mathcal{T}_{\ell+1}} \varepsilon_{\ell+1} \right)\\
&\leqslant \rho_A \eta_\ell^2 + C_\delta \left(\varepsilon_\ell^2 - (1-\gamma)\varepsilon_{\ell+1}^2 + C_{\mathrm{qo}}/\gamma \|h_\ell f\|_{\mathcal{T}_\ell \setminus \mathcal{T}_{\ell+1}}^2 \right)\\
&\leqslant (\rho_A + B C_{\mathrm{rel}} C_\delta)\, \eta_\ell^2 + (1-B) C_\delta \varepsilon_\ell^2 - (1-\gamma) C_\delta \varepsilon_{\ell+1}^2\\
&\quad + C_{\mathrm{qo}}/\gamma C_\delta \|h_\ell f\|_{\mathcal{T}_\ell \setminus \mathcal{T}_{\ell+1}}^2 + B C_{\mathrm{rel}} C_\delta \|h_\ell f\|_{L^2(\Omega)}^2.
\end{aligned}$$

For any A, $\alpha_f > 0$, $\alpha_\varepsilon = (1-\gamma) C_\delta$ this, (4.8) and (4.11) yield

$$\begin{aligned}
\xi_{\ell+1}^2 &\leqslant (\rho_A + B C_{\mathrm{rel}} C_\delta + A\kappa)\, \eta_\ell^2 + (1-B) C_\delta \varepsilon_\ell^2\\
&\quad + (C_{\mathrm{qo}} C_\delta/\gamma - \alpha_f/2) \|h_\ell f\|_{\mathcal{T}_\ell \setminus \mathcal{T}_{\ell+1}}^2 + (B C_{\mathrm{rel}} C_\delta - A + \alpha_f) \|h_\ell f\|_{L^2(\Omega)}^2.
\end{aligned}$$

The choice of parameters at the beginning of this proof ensures contraction in the sense of $\xi_{\ell+1}^2 \leqslant \varrho_A \xi_\ell^2$ for $\varrho_A < 1$ and for any level $\ell \in \mathbb{N}_0$ of Case (A), namely

$$\varrho_A := \max\left\{\rho_A + B C_{\mathrm{rel}} C_\delta + A\kappa, (1-B) C_\delta/\alpha_\varepsilon, 1 - \left(C_{\mathrm{qo}} C_\delta/\gamma + B C_{\mathrm{rel}} C_\delta\right)/\alpha_f\right\} < 1.$$

Contraction in Case (B) Lemma 4.3.1 shows that for any $0 < \rho_B < 1$ there exist $0 < C_\delta$ such that

$$\eta_{\ell+1}^2 \leqslant (1+\delta)\,\eta_\ell^2 + C_\delta \left\|p_{\ell+1}^{\mathrm{NC}} - p_\ell^{\mathrm{NC}}\right\|_{L^2(\Omega)}^2,$$

and

$$\begin{aligned} \|h_{\ell+1} f\|_{L^2(\Omega)}^2 &\leqslant \rho_B \|h_\ell f\|_{L^2(\Omega)}^2, \\ \kappa \eta_\ell^2 &\leqslant \|h_\ell f\|_{L^2(\Omega)}^2. \end{aligned}$$

The quasi-orthogonality of Lemma 4.2.2 plus the reliability of Lemma 4.2.1 and the application of Young's inequality prove for $B, \gamma > 0$

$$\begin{aligned} \eta_{\ell+1}^2 &\leqslant (1+\delta)\,\eta_\ell^2 + C_\delta \left\|p_{\ell+1}^{\mathrm{NC}} - p_\ell^{\mathrm{NC}}\right\|_{L^2(\Omega)}^2 \\ &\leqslant (1+\delta)\,\eta_\ell^2 + C_\delta \left(\varepsilon_\ell^2 - \varepsilon_{\ell+1}^2 + 2C_{\mathrm{qo}}^{1/2} \|h_\ell f\|_{\mathcal{T}_\ell \setminus \ell+1} \varepsilon_{\ell+1}\right) \\ &\leqslant (1+\delta)\,\eta_\ell^2 + C_\delta \left(\varepsilon_\ell^2 - (1-\gamma)\,\varepsilon_{\ell+1}^2 + C_{\mathrm{qo}}/\gamma \|h_\ell f\|_{\mathcal{T}_\ell \setminus \ell+1}^2\right) \\ &\leqslant ((1+\delta) + BC_{\mathrm{rel}}C_\delta)\,\eta_\ell^2 + (1-B)\,C_\delta \varepsilon_\ell^2 - (1-\gamma)\,C_\delta \varepsilon_{\ell+1}^2 \\ &\quad + C_{\mathrm{qo}}/\gamma C_\delta \|h_\ell f\|_{\mathcal{T}_\ell \setminus \ell+1}^2 + BC_{\mathrm{rel}}C_\delta \|h_\ell f\|_{L^2(\Omega)}^2, \\ \xi_{\ell+1}^2 &\leqslant (1 + \delta + BC_{\mathrm{rel}}C_\delta - D\kappa)\,\eta_\ell^2 + (1-B)\,C_\delta \varepsilon_\ell^2 \\ &\quad + (C_{\mathrm{qo}}C_\delta/\gamma + BC_{\mathrm{rel}}C_\delta + D + \alpha_f \rho_B) \|h_\ell f\|_{L^2(\Omega)}^2. \end{aligned}$$

The choice of parameters at the beginning of this proof ensures contraction in the sense of $\xi_{\ell+1}^2 \leqslant \varrho_B \xi_\ell^2$ for $\varrho_B < 1$ and on any level $\ell \in \mathbb{N}_0$ of Case (B), namely

$$\begin{aligned} 0 < \varrho_B := \max\{&1 + \delta + BC_\delta C_{\mathrm{rel}} - D\kappa, (1-B)\,C_\delta/\alpha_\varepsilon, \\ &\rho_B + (C_{\mathrm{qo}}C_\delta/\gamma + C_\delta C_{\mathrm{rel}} B + D)/\alpha_f\} < 1. \end{aligned}$$

Conclusion Hence, for given θ_A, $\kappa_1 < \kappa_0$, there exist positive parameters α_f, α_ε, such that for all $\kappa \in (\kappa_1, \kappa_0)$ on any level and in any of Cases (A) or (B) the term $\xi_\ell^2 := \eta_\ell^2 + \alpha_f \|h_\ell f\|_{L^2(\Omega)}^2 + \alpha_\varepsilon \varepsilon_{\ell+1}^2$ satisfies the contraction property $\xi_{\ell+1}^2 < \varrho \xi_\ell^2$ and

$$0 < \varrho := \max\{\varrho_A, \varrho_B\} < 1. \qquad \square$$

Remark 4.3.3. *To emphasise that the parameters α_ε, α_f do not depend on $0 < \kappa$, the lower bound $\kappa_1 \in (0, \kappa_0)$ is introduced explicitly. The specific choice of parameters in the proof of Theorem 4.3.2 shows that contraction is ensured for any choice of $\kappa \in (\kappa_1, \kappa_0)$ and that the constants and parameters do not depend on κ but on the range (κ_1, κ_0). Note that in [CR11] the independence is not stressed in detail.*

4.4 Optimal convergence rates

The remaining part of this chapter proves the quasi-optimal convergence of s-afem-aa for the Poisson problem (4.1) in the spirit of Stevenson [Ste07]. See Section 3.6 for the

definition of the approximation class and for the key arguments of Theorem 3.6.3.

Theorem 4.4.1 (Optimal convergence rates)**.** *Given a coarse, regular triangulation $\mathcal{T}_0$, let c_{eff}, C_{qo}, C_{drel} be positive generic constants from Lemmas 4.2.1 and 4.2.2 and Theorem 4.2.3. Furthermore let $s > 0$ such that $(u, f) \in \mathcal{A}_s$ for the exact solution u of the Poisson model problem (4.1) with right-hand side f. Let $0 < \theta_A < \theta_0 := \min\{1, c_{\mathrm{eff}}/C_{\mathrm{drel}}\}$ be the bulk parameter for Case (A) of* S-AFEM-AA*. Consider the positive parameters $\kappa_1 \in (0, \kappa_2)$, with $\kappa_2 := \min\{\kappa_0, C_{\mathrm{drel}}(\theta_0 - \theta_A)/(C_{\mathrm{drel}} + C_{\mathrm{qo}})\}$, and α_f, α_ε and $0 < \rho < 1$ as chosen in the proof of Theorem 4.3.2.*

Then, for all $\kappa \in (\kappa_1, \kappa_2)$ the algorithm S-AFEM-AA *generates a sequence of triangulations $\mathcal{T}_\ell$ and discrete solutions u_ℓ^{NC} with discrete fluxes p_ℓ^{NC} of (4.1) with an optimal rate of convergence in the following sense*

$$|\mathcal{T}_\ell| - |\mathcal{T}_0| \lesssim \xi_\ell^{-1/s} \qquad \text{with } \xi_\ell^2 := \eta_\ell^2 + \alpha_f \|h_\ell f\|_{L^2(\Omega)}^2 + \alpha_\varepsilon \varepsilon_\ell^2.$$

The following Lemmas 4.4.2 and 4.4.4 summarise estimates that are essential for the proof of Theorem 4.4.1.

Lemma 4.4.2. *Given C_{rel}, α_ε, α_f and κ from Lemma 4.2.1 and Theorem 4.3.2, there exist positive generic constants C_{A}, C_{B} such that on any level ℓ the weighted term ξ_ℓ of the energy error ε_ℓ, the estimated error η_ℓ and the volume term $\|h_\ell f\|_{L^2(\Omega)}$ satisfy*

$$\xi_\ell^2 \leqslant \begin{cases} C_{\mathrm{A}} \eta_\ell^2 & \text{if Case (A) applies,} \\ C_{\mathrm{B}} \|h_\ell f\|_{L^2(\Omega)}^2 & \text{if Case (B) applies,} \end{cases} \qquad \text{and} \tag{4.12}$$

$$\xi_\ell^2 \approx \varepsilon_\ell^2 + \|h_\ell f\|_{L^2(\Omega)}^2. \tag{4.13}$$

Proof. The estimate (4.12) is proven using the reliability and the specific relation of the estimated error and the volume term in both Cases (A) and (B) with

$$1 + \alpha_\varepsilon C_{\mathrm{rel}} + (\alpha_\varepsilon C_{\mathrm{rel}} + \alpha_f)\,\kappa < 1 + \alpha_\varepsilon C_{\mathrm{rel}} + (\alpha_\varepsilon C_{\mathrm{rel}} + \alpha_f)\,\kappa_2 =: C_{\mathrm{A}},$$
$$\frac{1 + \alpha_\varepsilon C_{\mathrm{rel}}}{\kappa} + \alpha_\varepsilon C_{\mathrm{rel}} + \alpha_f < \frac{1 + \alpha_\varepsilon C_{\mathrm{rel}}}{\kappa_1} + \alpha_\varepsilon C_{\mathrm{rel}} + \alpha_f =: C_{\mathrm{B}}.$$

The equivalence (4.13) follows directly from the efficiency (4.4) of η_ℓ. Note that C_{A} and C_{B} depend on κ_2 or κ_1, respectively, but are independent of κ as long as $\kappa \in (\kappa_1, \kappa_2)$. □

Remark 4.4.3. *Note that $C_{\mathrm{J}} > 0$ from Lemma 4.3.1 solely depends on $\mathcal{T}_0$. The definitions of the parameters and constants in the proof of Theorem 4.3.2 verify*

$$\frac{2C_{\mathrm{qo}}}{\alpha_f} \leqslant \frac{\gamma(1-\rho_B)}{C_\delta} = \frac{\gamma(1-\gamma)(1-\rho_B)}{\alpha_\varepsilon} \leqslant \frac{1}{\alpha_\varepsilon} \leqslant \frac{2}{C_\delta} \leqslant \frac{2}{C_{\mathrm{J}}}$$

and thus

$$\frac{\alpha_\varepsilon}{\alpha_f} \leqslant \frac{1}{2C_{\mathrm{qo}}}, \qquad \frac{1}{\alpha_\varepsilon} \leqslant \frac{2}{C_{\mathrm{J}}}.$$

The following lemma is an extension of [Rab10, Lemma 3.3].

Lemma 4.4.4. *Given C_{qo} from Lemma 4.2.2, and α_ε, α_f as chosen in Theorem 4.3.2, let $\mathcal{T}_{\ell+k}$ be an admissible refinement of $\mathcal{T}_\ell$. Then, the weighted terms ξ_ℓ and $\xi_{\ell+k}$ satisfy*

$$\varepsilon_{\ell+k}^2 \leqslant 2\varepsilon_\ell^2 + 4C_{\mathrm{qo}} \|h_\ell f\|^2_{\mathcal{T}_\ell \setminus \ell+k} \tag{4.14}$$

$$\leqslant 8C_{\mathrm{qo}} \left(\varepsilon_\ell^2 + \|h_\ell f\|^2_{L^2(\Omega)} - \|h_{\ell+k} f\|^2_{L^2(\Omega)}\right). \tag{4.15}$$

Furthermore, there exists a positive generic constant C_{C} such that

$$\alpha_\varepsilon \varepsilon_{\ell+k}^2 \leqslant \xi_{\ell+k}^2 \leqslant C_{\mathrm{C}} \xi_\ell^2. \tag{4.16}$$

Proof. Quasi-orthogonality and Young's inequality lead to

$$\begin{aligned}\varepsilon_{\ell+k}^2 &\leqslant \varepsilon_\ell^2 + 2C_{\mathrm{qo}}^{1/2} \varepsilon_{\ell+k} \|h_\ell f\|_{\mathcal{T}_\ell \setminus \ell+k} - \|p^{\mathrm{NC}}_{\ell+k} - p^{\mathrm{NC}}_\ell\|^2_{L^2(\Omega)} \\ &\leqslant \varepsilon_\ell^2 + 2C_{\mathrm{qo}} \|h_\ell f\|^2_{\mathcal{T}_\ell \setminus \ell+k} + \varepsilon_{\ell+k}^2/2 - \|p^{\mathrm{NC}}_{\ell+k} - p^{\mathrm{NC}}_\ell\|^2_{L^2(\Omega)}.\end{aligned}$$

This implies (4.14). Finally, the reduction of the volume term (3.7) and the convention (4.5) (i.e., $1/4 \leqslant C_{\mathrm{qo}}$) prove (4.15) via

$$\varepsilon_{\ell+k}^2 \leqslant 2\varepsilon_\ell^2 + 8C_{\mathrm{qo}} \|h_\ell f\|^2_{L^2(\Omega)} - 8C_{\mathrm{qo}} \|h_{\ell+k} f\|^2_{L^2(\Omega)}.$$

Efficiency (4.4) and (4.14) yield (4.16),

$$\begin{aligned}\xi_{\ell+k}^2 &\leqslant \left(c_{\mathrm{eff}}^{-1} + \alpha_\varepsilon\right) \varepsilon_{\ell+k}^2 + \alpha_f \|h_{\ell+k} f\|^2_{L^2(\Omega)} \\ &\leqslant 2\left(c_{\mathrm{eff}}^{-1} + \alpha_\varepsilon\right) \varepsilon_\ell^2 + \left(4C_{\mathrm{qo}}\left(c_{\mathrm{eff}}^{-1} + \alpha_\varepsilon\right) + \alpha_f\right) \|h_\ell f\|^2_{L^2(\Omega)} \\ &\leqslant \left(\frac{2}{\alpha_\varepsilon c_{\mathrm{eff}}} + 2\right) \alpha_\varepsilon \varepsilon_\ell^2 + \left(\frac{4C_{\mathrm{qo}}}{\alpha_f c_{\mathrm{eff}}} + \frac{4C_{\mathrm{qo}}\alpha_\varepsilon}{\alpha_f} + 1\right) \alpha_f \|h_\ell f\|^2_{L^2(\Omega)} \\ &\leqslant \max\left\{\frac{2}{\alpha_\varepsilon c_{\mathrm{eff}}} + 2, \frac{4C_{\mathrm{qo}}}{\alpha_f c_{\mathrm{eff}}} + \frac{4C_{\mathrm{qo}}\alpha_\varepsilon}{\alpha_f} + 1\right\} \xi_\ell^2.\end{aligned}$$

Finally, Remark 4.4.3 yields $\xi_{\ell+k}^2 \leqslant C_{\mathrm{C}} \xi_\ell^2$ with

$$C_{\mathrm{C}} := \frac{4}{C_{\mathrm{J}} c_{\mathrm{eff}}} + 3 > 0.$$

The constant C_{C} is independent of the special choice of parameters in the algorithm S-AFEM-AA, and in particular it is independent of θ_A and κ. □

Proof of Theorem 4.4.1. To use Theorem 3.6.3 to prove quasi-optimality for S-AFEM-AA, the two assumptions (3.22) and (3.23) of Theorem 3.6.3 have to be satisfied. The contraction property of ξ_ℓ with $0 < \varrho < 1$ is proven in Theorem 4.3.2. It remains to verify the first assumption (3.22) for each of the Cases (A) and (B).

Verify (3.22) for Case (A) Due to the restrictions imposed upon c_{eff}, C_{qo}, C_{drel}, α_f,

α_ε, κ and $\theta_A < \theta_0$, there exists $\tau > 0$ such that

$$0 < \tau^2 < \min\left\{1, \frac{\alpha_\varepsilon \left(c_{\mathrm{eff}} - \kappa \left(C_{\mathrm{qo}} + C_{\mathrm{drel}}\right) - C_{\mathrm{drel}}\theta_A\right)}{2C_{\mathrm{A}}C_{\mathrm{C}}}\right\}, \tag{4.17}$$

with positive constants C_{A} and C_{C} from Lemmas 4.4.2 and 4.4.4. To apply Lemma 3.6.4, it remains to prove that $\mathcal{E}_{\ell\setminus\ell+\epsilon(\ell)}$ fulfils the bulk criterion if Case (A) applies in level ℓ, i.e.,

$$\theta_A \eta_\ell^2 \leqslant \eta_\ell^2\left(\mathcal{E}_{\ell\setminus\ell+\epsilon(\ell)}\right). \tag{4.18}$$

The restrictions on the choice of θ_A and (4.17) lead to

$$C_{\mathrm{drel}}\theta_A\eta_\ell^2 \leqslant \left(c_{\mathrm{eff}} - \kappa\left(C_{\mathrm{drel}} + C_{\mathrm{qo}}\right)\right)\eta_\ell^2 - \left(2\tau^2 C_{\mathrm{A}}C_{\mathrm{C}}/\alpha_\varepsilon\right)\eta_\ell^2.$$

The combination of (4.12)–(4.14) and (4.16) gives

$$\alpha_\varepsilon \varepsilon_{\ell+\epsilon(\ell)}^2 \leqslant C_{\mathrm{C}}\xi_{\epsilon(\ell)}^2 \leqslant C_{\mathrm{C}}\tau^2\xi_\ell^2 \leqslant C_{\mathrm{A}}C_{\mathrm{C}}\tau^2\eta_\ell^2.$$

Together with the efficiency and $\|h_\ell f\|_{L^2(\Omega)}^2 \leqslant \kappa\eta_\ell^2$ these estimates verify

$$C_{\mathrm{drel}}\theta_A\eta_\ell^2 \leqslant \varepsilon_\ell^2 - \left(C_{\mathrm{drel}} + C_{\mathrm{qo}}\right)\|h_\ell f\|_{L^2(\Omega)}^2 - 2\varepsilon_{\ell+\epsilon(\ell)}^2.$$

On the other hand Lemma 4.2.2 and Theorem 4.2.3 show that

$$\begin{aligned}\varepsilon_\ell^2 - 2\varepsilon_{\ell+\epsilon(\ell)}^2 &\leqslant \left\|p_{\ell+\epsilon(\ell)}^{\mathrm{NC}} - p_\ell^{\mathrm{NC}}\right\|_{L^2(\Omega)}^2 + C_{\mathrm{qo}}\|h_\ell f\|_{\mathcal{T}_{\ell\setminus\ell+\epsilon(\ell)}}^2 \\ &\leqslant \left(C_{\mathrm{drel}} + C_{\mathrm{qo}}\right)\|h_\ell f\|_{\mathcal{T}_{\ell\setminus\ell+\epsilon(\ell)}}^2 + C_{\mathrm{drel}}\eta_\ell^2\left(\mathcal{E}_{\ell\setminus\ell+\epsilon(\ell)}\right).\end{aligned}$$

The combination of these estimates results in (4.18), the application of Lemma 3.6.4 proves (3.22) in Case (A).

Verify (3.22) for Case (B) Lemma 3.6.6 and (4.12) prove (3.22) for Case (B).

Since α_f, $\alpha_\varepsilon > 0$ are chosen according to the contraction property of Theorem 4.3.2, the application of Theorem 3.6.3 concludes the proof. □

5 The pure displacement problem in linear elasticity

5.1 Introduction

This chapter presents the analysis of S-AFEM-AA for the Navier–Lamé equations (2.3) introduced in Section 2.2 and solved using the nonconforming Crouzeix–Raviart FEM. Finally quasi-optimal convergence of S-AFEM-AA is proven.

The arguments follow the general methodology, which has already been applied for the Poisson problem in Chapter 4. For the Navier–Lamé equations, the robustness, i.e., the existence of a parameter independent of the Lamé parameter $\lambda \to \infty$ becomes an important issue. Indeed, the convergence rates are robust with respect to the Lamé parameter $\lambda \to \infty$ in the sense that all constants in the quasi-optimal convergence rate are bounded for almost incompressible materials. So the analysis of the Stokes equations in Chapter 6 is a consequence of the investigations in the limit $\lambda \to \infty$. Let

$$a_{NC(\ell)}(u_\ell^{\mathrm{NC}}, v_\ell^{\mathrm{NC}}) := \int_\Omega \mathrm{D}_\ell\, u_\ell^{\mathrm{NC}} : \mathbb{C}\,\mathrm{D}_\ell\, v_\ell^{\mathrm{NC}}\,\mathrm{d}x \qquad \text{for } u_\ell^{\mathrm{NC}}, v_\ell^{\mathrm{NC}} \in V_\ell$$

define the discrete scalar product on $V_\ell := P_{1,0}^{\mathrm{NC}}(\mathcal{T}_\ell;\mathbb{R}^2)$ with the corresponding discrete energy norm $|\!|\!| \cdot |\!|\!|_{\mathrm{NC}(\ell)} := \big\|\mathbb{C}^{1/2}\,\mathrm{D}_\ell \cdot\big\|_{L^2(\Omega)}$ where $\mathbb{C}A = 2\mu A + \lambda\,\mathrm{tr}(A)\,I_2$ for all $A \in \mathbb{R}^{2\times 2}$. The discrete Friedrichs inequality [BS08, (10.6.14)] shows that $a_{NC(\ell)}$ is positive definite. Therefore there exists a unique discrete solution $u_\ell^{\mathrm{NC}} \in V_\ell$ with

$$a_{NC(\ell)}(u_\ell^{\mathrm{NC}}, v_\ell^{\mathrm{NC}}) \;= F(v_\ell^{\mathrm{NC}}) := (f, v_\ell^{\mathrm{NC}}) \qquad \text{for all } v_\ell^{\mathrm{NC}} \in V_\ell. \tag{5.1}$$

To solve the discrete problem (5.1) adaptively, algorithm S-AFEM-AA as depicted in Algorithm 3.4 is applied. The bulk criterion in Case (A) (3.2) is based on the contributions

$$\eta_\ell^2(E) := h_E\, \|[\partial u_\ell^{\mathrm{NC}}/\partial s]_E\|_{L^2(E)}^2\,, \tag{5.2}$$

while the volume contributions $\|h_T f\|_{L^2(T)}$ control the refinement in Case (B). Furthermore, let $u \in V = H_0^1(\Omega;\mathbb{R}^2)$ be the exact displacements with exact stress $\sigma := \mathbb{C}\,\mathrm{D}\,u$ of (2.4) with right-hand side $f \in L^2(\Omega;\mathbb{R}^2)$. Let $\sigma_\ell := \mathbb{C}\,\mathrm{D}_\ell\, u_\ell^{\mathrm{NC}}$ denote the discrete stress for the discrete solution $u_\ell^{\mathrm{NC}} \in V(\mathcal{T}_\ell)$ of (5.1) and with the energy error $\varepsilon_\ell := |\!|\!| u - u_\ell^{\mathrm{NC}} |\!|\!|_{\mathrm{NC}(\ell)}$ on $\mathcal{T}_\ell$.

The convergence rate s is optimal with respect to some approximation class $\mathcal{A}_s$ (see Section 3.6.1) and the computed triangulation $\mathcal{T}_\ell$ is optimal up to some factor $C_{\mathrm{opt}} \lesssim 1$ and hence it is called quasi-optimal.

In the proof of quasi-optimal convergence, the challenge of robustness in linear elasticity is that C_{opt} is independent of the Lamé parameter λ – in particular in the incompressible limit as the Lamé parameter $\lambda \to \infty$. Several works consider the quasi-optimal convergence of adaptive FEMs based on collective marking, e.g., [BM11, HX08, CPR13] for the Stokes equation and [CR12] for the pure displacement problem in linear elasticity.

By convention, all generic constants neither depend on the mesh size h_ℓ nor the Lamé

parameter λ, but they may depend on $\mathcal{T}_0$, the fixed coarse triangulation, and its interior angles, and they may depend on the Lamé parameter μ. As in [CR12], parts of this chapter remain valid for Lamé parameters λ and μ, which may vary in the domain Ω for different materials in a composite as long as $\|\mu + 1/\mu\|_{L^\infty(\Omega)} < \infty$. For ease of presentation, the conditions on the constants are $0 \leqslant \lambda < \infty$ and $1/4 \leqslant \mu < \infty$. Then, the generic constants as well as θ_0, κ_1, κ_2 and C_{opt} depend also on $\|\mu\|_{L^\infty(\Omega)}$, but not on λ.

This chapter has a similar structure to the previous one (Chapter 4). The *a posteriori* error estimator is analysed in Section 5.2 with the Helmholtz projection, the discrete Helmholtz decomposition, discrete reliability and quasi-orthogonality. These results have been developed in [CR12] for quasi-optimality of C-AFEM. Section 5.3 is devoted to the proof of the contraction property and its fundamental estimator reduction. Theorem 5.4.1 concludes this chapter with the proof of the main theorem for the robust optimal convergence rate.

In [CR12] the total error estimators $\mu_{A,\ell}$ and $\mu_{B,\ell}$ are introduced as follows

$$\mu_{A,\ell}^2 := \sum_{E\in\mathcal{E}_\ell} \eta_\ell^2(E) + \sum_{T\in\mathcal{T}_\ell} \|h_\ell f\|_T^2\,, \quad \mu_\ell^2 := \mu_{B,\ell}^2 := \sum_{T\in\mathcal{T}_\ell} \Big(\|h_\ell f\|_T^2 + \sum_{E\in\mathcal{E}(T)} \eta_\ell^2(E)\Big). \tag{5.3}$$

The outcome of C-AFEM based on both estimators is investigated and quasi-optimality is proven.

The outcome of the numerical experiments, including a comparison of uniform and adaptive mesh refinement (namely, S-AFEM-AA, S-AFEM-DM and C-AFEM) using nonconforming CR-FEM and conform P_1 FEM for this model problem, are presented in Section 7.4. The refinement indicator $\mu_\ell := \mu_{B,\ell}$ is applied for C-AFEM.

5.2 Preliminaries

This section replicates the main arguments and their proofs that are developed in [CR12] based on the *a posteriori* error analysis in elasticity from [Car05]. This collection is the basis of the proof of convergence in Section 5.3 and quasi-optimality in Section 5.4.

Theorem 5.2.2 gives the efficiency, reliability and discrete reliability for η_ℓ and applies the subsequent Helmholtz projection.

Definition 5.2.1 (Helmholtz projection, [CR12, Definition 3.1])**.** *The Helmholtz projection $\mathcal{H}u_\ell^{\mathrm{NC}}$ of the discrete displacement $u_\ell^{\mathrm{NC}} \in V_\ell$ with $\sigma_\ell := \mathbb{C}\,\mathrm{D}_\ell\, u_\ell^{\mathrm{NC}}$ is the minimiser*

$$\mathcal{H}u_\ell^{\mathrm{NC}} := \arg\min_{v\in V} \|\mathbb{C}\,\mathrm{D}\,v - \sigma_\ell\|_{L^2(\Omega)}\,.$$

Theorem 5.2.2 (Efficiency, reliability, discrete reliability, [CR12, Theorem 3.2])**.** *There exist positive generic constants c_{eff}, C_{rel}, C_{drel} depending on $\mathcal{T}_0$, but independent of the mesh size h_ℓ and independent of the Lamé parameter λ, such that*

$$c_{\mathrm{eff}}\eta_\ell^2 \leqslant \|\sigma - \sigma_\ell\|_{L^2(\Omega)}^2 + |u - \mathcal{H}u_\ell^{\mathrm{NC}}|_{H^1(\Omega)}^2 + \mathrm{osc}^2(f,\mathcal{T}_\ell) \leqslant C_{\mathrm{rel}}\left(\eta_\ell^2 + \|h_\ell f\|_{L^2(\Omega)}^2\right). \tag{5.4}$$

Furthermore, for the set of refined triangles $\mathcal{T}_{\ell\setminus\ell+k}$ discrete reliability holds in the sense

that

$$\|\!|u_{\ell+k}^{\mathrm{NC}} - u_\ell^{\mathrm{NC}}|\!\|_{\mathrm{NC}(\ell+k)}^2 \leqslant C_{\mathrm{drel}}^{1/2} \left(\eta_\ell\left(\mathcal{E}_{\ell\setminus\ell+k}\right) + \|h_\ell f\|_{\mathcal{T}_{\ell\setminus\ell+k}}\right) |u_{\ell+k}^{\mathrm{NC}} - u_\ell^{\mathrm{NC}}|_{H^1(\mathcal{T}_{\ell+k})}. \tag{5.5}$$

The proof of Theorem 5.2.2 is split into three parts for the efficiency, reliability and discrete reliability. The proofs of reliability and efficiency in Theorem 5.2.2 require the equivalence claim of Theorem 5.2.3 below, which relies on the standard estimate

$$2\mu|v_\ell|_{H^1(\mathcal{T}_\ell)}^2 \leqslant |\!|\!|v_\ell|\!|\!|_{\mathrm{NC}(\ell)}^2 \leqslant \frac{1}{2\mu}\,\|\mathbb{C}\,\mathrm{D}_\ell\, v_\ell\|_{L^2(\Omega)}^2\,, \quad \text{for } v_\ell \in H^1(\mathcal{T}_\ell), \tag{5.6}$$

which is frequently used in this chapter and directly derived from the definitions of $\mathbb{C}$ and $|\!|\!|\cdot|\!|\!|_{\mathrm{NC}(\ell)}$.

Theorem 5.2.3 ([CR12, Theorem 3.5])**.** *Let $\mathcal{H}$ be the Helmholtz projector of Definition 5.2.1. The following equivalence is robust in λ*

$$\|\sigma - \sigma_\ell\|_{L^2(\Omega)} + |u - \mathcal{H}u_\ell^{\mathrm{NC}}|_{H^1(\Omega)} \approx \left\|\mathbb{C}^{-1}\sigma_\ell - \mathrm{D}\,\mathcal{H}u_\ell^{\mathrm{NC}}\right\|_{L^2(\Omega)} + \|f + \operatorname{div}\sigma_\ell\|_{H^{-1}(\Omega)}\,. \tag{5.7}$$

Proof replicated from [CR12]. Let

$$L^2(\Omega;\mathbb{R}^{2\times2})/\mathbb{R} := \left\{\tau \in L^2(\Omega;\mathbb{R}^{2\times2}) \;\middle|\; \int_\Omega \operatorname{tr}(\tau)\,\mathrm{dx} = 0\right\}.$$

A direct proof of this equivalence follows from the theory of mixed formulations [BF91, Bra01] with the operator

$$\mathcal{A} : L^2(\Omega;\mathbb{R}^{2\times2})/\mathbb{R} \times H_0^1(\Omega;\mathbb{R}^2) \to \left(L^2(\Omega;\mathbb{R}^{2\times2})/\mathbb{R} \times H_0^1(\Omega;\mathbb{R}^2)\right)^\star$$

associated with the bilinear form

$$\mathcal{A}\,(\sigma,u)\,,(\tau,v) := \int_\Omega \sigma : \mathbb{C}^{-1}\tau\,\mathrm{dx} + \int_\Omega \sigma : \mathrm{D}\,v\,\mathrm{dx} + \int_\Omega \tau : \mathrm{D}\,u\,\mathrm{dx}$$

in (σ,u), $(\tau,v) \in L^2(\Omega;\mathbb{R}^{2\times2})/\mathbb{R} \times H_0^1(\Omega;\mathbb{R}^2)$. Note that $\sigma = \mathbb{C}\,\mathrm{D}\,u \in L^2(\Omega;\mathbb{R}^{2\times2})/\mathbb{R}$ is satisfied whenever $u \in V = H_0^1(\Omega;\mathbb{R}^2)$ and for all discrete stresses $\sigma_\ell = \mathbb{C}\,\mathrm{D}_\ell\, u_\ell^{\mathrm{NC}} \in L^2(\Omega;\mathbb{R}^{2\times2})/\mathbb{R}$ with $u_\ell^{\mathrm{NC}} \in V_\ell$. Indeed the pure homogeneous Dirichlet boundary conditions imply

$$\int_\Omega \operatorname{tr}(\sigma)\,\mathrm{dx} = \int_\Omega 2(\lambda+\mu)\operatorname{tr}(\mathrm{D}\,u)\,\mathrm{dx} = \int_\Omega 2(\lambda+\mu)\operatorname{div} u\,\mathrm{dx} = 0$$

and, correspondingly, $\int_\Omega \operatorname{tr}(\sigma_\ell)\,\mathrm{dx} = 0$.

To verify that $\mathcal{A}$ is an isomorphism and to compute bounds for $\mathcal{A}$ and $\mathcal{A}^{-1}$, observe that the bilinear forms

$$\int_\Omega \sigma : \mathbb{C}^{-1}\tau\,\mathrm{dx} \qquad \text{and} \qquad b(\tau,u) := \int_\Omega \tau : \mathrm{D}\,u\,\mathrm{dx}$$

are bounded independently of λ. The inf-sup constant of $b(\tau, u)$ is independent of λ as well and the associated kernel is

$$\begin{aligned} Z &:= \left\{\tau \in L^2(\Omega;\mathbb{R}^{2\times 2})/\mathbb{R} \,\middle|\, \forall v \in H^1_0(\Omega;\mathbb{R}^2),\, b(\tau, v) = 0\right\} \\ &= \left\{\tau \in \mathrm{H}(\mathrm{div},\Omega)/\mathbb{R} \,\middle|\, \mathrm{div}\,\tau = 0\right\}. \end{aligned}$$

It is important that ellipticity of the first bilinear form $\int_\Omega \sigma : \mathbb{C}^{-1}\tau \,\mathrm{dx}$ is required on Z only. Note that since $\tau := \sigma - \sigma_\ell$ satisfies $\int_\Omega \mathrm{tr}(\tau)\,\mathrm{dx} = 0$, Lemma 2.1.10 implies

$$\|\tau\|_{L^2(\Omega)} \lesssim \|\mathrm{dev}\,\tau\|_{L^2(\Omega)} + \|\mathrm{div}\,\tau\|_{H^{-1}(\Omega)} \lesssim \left\|\mathbb{C}^{-1/2}\tau\right\|_{L^2(\Omega)}. \tag{5.8}$$

Furthermore, (5.6) is $|u - u_\ell^{\mathrm{NC}}|_{H^1(\mathcal{T}_\ell)} \leqslant \varepsilon_\ell \leqslant \|\sigma - \sigma_\ell\|_{L^2(\Omega)}$ for $1/4 \leqslant \mu$. This concludes the proof of the bijectivity of $\mathcal{A}$ and $\|\mathcal{A}\| + \left\|\mathcal{A}^{-1}\right\| \lesssim 1$. The equivalence (5.7) follows from

$$\|\mathcal{A}(\sigma - \sigma_\ell, u - \mathcal{H}u_\ell^{\mathrm{NC}})\|_{L^2(\Omega)\times H^{-1}(\Omega)} \approx \|(\sigma - \sigma_\ell, u - \mathcal{H}u_\ell^{\mathrm{NC}})\|_{L^2(\Omega)\times H^1_0(\Omega)}.$$

The remaining arguments are from [Car05] and include the two arguments for the residual $\mathcal{A}(\sigma - \sigma_\ell, u - \mathcal{H}u_\ell^{\mathrm{NC}})$ in $L^2(\Omega;\mathbb{R}^{2\times 2})/\mathbb{R}$ and in $H^{-1}(\Omega;\mathbb{R}^2)$. □

Proof of reliability in Theorem 5.2.2 replicated from [CR12]. Since the residual in $H^{-1}(\Omega)$ vanishes on the conforming subspace

$$V_\ell^C := P_1(\mathcal{T}_\ell;\mathbb{R}^2) \cap C_0(\Omega;\mathbb{R}^2) \subseteq P^{\mathrm{NC}}_{1,0}(\mathcal{T}_\ell) \times P^{\mathrm{NC}}_{1,0}(\mathcal{T}_\ell) = V_\ell,$$

standard arguments in the *a posteriori* error analysis [AO00, BS01] of conforming FEMs lead to

$$\begin{aligned} \|f + \mathrm{div}\,\sigma_\ell\|_{H^{-1}(\Omega)} &:= \sup_{v\in V\setminus\{0\}} \mathrm{Res}(v)/\|v\|_{H^1(\Omega)} \\ &\lesssim \|h_\ell f\|_{L^2(\Omega)} + \sqrt{\textstyle\sum_{E\in\mathcal{E}(\Omega)} h_E \left\|[\sigma_\ell]_E \nu_E\right\|^2_{L^2(E)}}. \end{aligned}$$

Let ψ_E be the Crouzeix–Raviart edge-basis function for $E \in \mathcal{E}_\ell$, and f_α the α-th component of f ($\alpha = 1, 2$), and let $e_\alpha = (\delta_{\alpha\beta})_{\beta=1,2}$ be the α-th canonical unit vector in $\mathbb{R}^2$. A piecewise integration by parts gives

$$\begin{aligned} \int_\Omega f_\alpha \psi_E \,\mathrm{dx} = a_{\mathrm{NC}(\ell)}(u_\ell^{\mathrm{NC}}, e_\alpha\psi_E) &= \int_\Omega \sigma_\ell : \mathrm{D}_\ell(\psi_E e_\alpha)\,\mathrm{dx} \\ &= \int_E ([\sigma_\ell\nu_E]_E)\cdot e_\alpha \langle\psi_E\rangle \,\mathrm{ds} = h_E[\sigma_\ell\nu_E]_E \cdot e_\alpha. \end{aligned}$$

The resulting identity $\int_\Omega f\psi_E\,\mathrm{dx} = \int_E [\sigma_\ell\nu_E]_E\,\mathrm{ds}$ gives

$$\begin{aligned} h_E\,|[\sigma_\ell\nu_E]_E| = \left|\int_\Omega f\psi_E\,\mathrm{dx}\right| &\leqslant \|\psi_E\|_{L^2(\omega_E)}\,\|f\|_{L^2(\omega_E)} \\ &\leqslant |\omega_E|^{1/2}\,\|f\|_{L^2(\omega_E)} \approx \|h_\ell f\|_{L^2(\omega_E)}. \end{aligned}$$

Therefore, $\|h_\ell f\|_{L^2(\Omega)}$ dominates the edge jumps of the discrete stress as in [CH06a]

$$\|f + \operatorname{div} \sigma_\ell\|_{H^{-1}(\Omega)} \lesssim \|h_\ell f\|_{L^2(\Omega)}\,. \tag{5.9}$$

[CH07, Theorem 3.1] shows $\|\mathrm{D}_\ell\, u_\ell^{\mathrm{NC}} - \mathrm{D}\,\mathcal{H}u_\ell^{\mathrm{NC}}\|^2_{L^2(\Omega)} \lesssim \eta_\ell^2$. The equivalence (5.7) and the considerations above imply reliability

$$\|\sigma - \sigma_\ell\|_{L^2(\Omega)} + |u - \mathcal{H}u_\ell^{\mathrm{NC}}|_{H^1(\Omega)} \lesssim \eta_\ell + \|h_\ell f\|_{L^2(\Omega)}\,. \qquad \square$$

Proof of efficiency in Theorem 5.2.2 replicated from [CR12]. Efficiency follows from the bubble methodology of Verfürth [Ver96]. Those arguments show that for any edge $E \in \mathcal{E}_\ell$ and for all $v \in V$

$$h_E^{1/2}\, \|[\partial u_\ell^{\mathrm{NC}}/\partial s]_E\|_{L^2(E)} \lesssim \|\mathrm{D}_\ell(v - u_\ell^{\mathrm{NC}})\|_{L^2(\omega_E)}\,.$$

Furthermore, equivalence (5.7) verifies

$$\eta_\ell \lesssim \|\sigma - \sigma_\ell\|_{L^2(\Omega)} + |u - \mathcal{H}u_\ell^{\mathrm{NC}}|_{H^1(\Omega)}.$$

Further details can be found, e.g., in [BCJ02, proof of Theorem 3.2]. $\square$

The proof of the discrete reliability in Theorem 5.2.2 utilises the following orthogonal Helmholtz decomposition and the discrete Poincaré inequality of Lemma 3.2.11.

Lemma 5.2.4 (Discrete Helmholtz decomposition, [CR12, Lemma 3.6])**.** *There exist* $\alpha_{\ell+k}^{\mathrm{NC}} \in V_{\ell+k}$ *and* $\beta_{\ell+k}^{\mathrm{C}} \in C(\Omega;\mathbb{R}^2) \cap P_1(\mathcal{T}_{\ell+k};\mathbb{R}^2)$ *with* $\fint_\Omega \beta_{\ell+k}^{\mathrm{C}}\,\mathrm{dx} = 0$ *such that*

$$\mathbb{C}\,\mathrm{D}_{\ell+k}(u_\ell^{\mathrm{NC}} - u_{\ell+k}^{\mathrm{NC}}) = \mathbb{C}\,\mathrm{D}_{\ell+k}\,\alpha_{\ell+k}^{\mathrm{NC}} + \operatorname{Curl}\beta_{\ell+k}^{\mathrm{C}}.$$

Proof replicated from [CR12]. Given $u_\ell^{\mathrm{NC}} \in V_\ell$, $u_{\ell+k}^{\mathrm{NC}} \in V_{\ell+k}$ there exists some unique $\alpha_{\ell+k}^{\mathrm{NC}} \in V_{\ell+k}$ such that all $v_{\ell+k}^{\mathrm{NC}} \in V_{\ell+k}$ satisfy

$$a_{\mathrm{NC}(\ell+k)}\left(\alpha_{\ell+k}^{\mathrm{NC}}, v_{\ell+k}^{\mathrm{NC}}\right) = a_{\mathrm{NC}(\ell+k)}\left(u_\ell^{\mathrm{NC}} - u_{\ell+k}^{\mathrm{NC}}, v_{\ell+k}^{\mathrm{NC}}\right).$$

Let ψ_E be the scalar edge-basis function with average $\langle\psi_E\rangle$ equal to 1 along $E \in \mathcal{E}_{\ell+k}$ and 0 along any other $F \in \mathcal{E}_{\ell+k}\backslash\{E\}$. Then

$$B := \mathbb{C}\,\mathrm{D}_{\ell+k}(u_\ell^{\mathrm{NC}} - u_{\ell+k}^{\mathrm{NC}}) - \mathbb{C}\,\mathrm{D}_{\ell+k}\,\alpha_{\ell+k}^{\mathrm{NC}} \in P_0(\mathcal{T}_{\ell+k};\mathbb{R}^{2\times 2})$$

satisfies

$$\int_\Omega B\nabla_{\ell+k}\psi_E\,\mathrm{dx} = 0 \in \mathbb{R}^2 \quad \text{for any } E \in \mathcal{E}_{\ell+k}.$$

An element-wise integration by parts on the edge patch ω_E of E (see Table 3.14 for the definition) in $\mathcal{T}_{\ell+k}$ shows that this equals

$$\int_E [(B\nu_E)\psi_E]_E\,\mathrm{ds} + \int_{\partial\omega_E} (B\nu_{\omega_E})\psi_E\,\mathrm{ds} = [B\nu_E]\int_E \langle\psi_E\rangle\,\mathrm{ds} = [B\nu_E]h_E.$$

Since $[B\nu_E]_E = 0$ for all $E \in \mathcal{E}_{\ell+k}$, $B \in \mathrm{H}(\mathrm{div}, \Omega; \mathbb{R}^{2\times 2})$ and $\mathrm{div}\, B = 0$. Therefore, B equals some Curl and since B is piecewise constant, there exists $\beta^{\mathrm{C}}_{\ell+k} \in C(\Omega; \mathbb{R}^2) \cap P_1(\mathcal{T}_{\ell+k}; \mathbb{R}^2)$ with $\fint_\Omega \beta^{\mathrm{C}}_{\ell+k}\,\mathrm{dx} = 0$ and $B = \mathrm{Curl}\,\beta^{\mathrm{C}}_{\ell+k}$ (see [CD98, 194ff.] and [GR86, Chapter 1, Theorem 3.1]). □

Proof of the discrete reliability in Theorem 5.2.2. This is from [CR12]. Lemma 5.2.4 gives a discrete Helmholtz decomposition and leads to $\alpha^{\mathrm{NC}}_{\ell+k} \in V_{\ell+k}$ and $\beta^{\mathrm{C}}_{\ell+k} \in C(\Omega; \mathbb{R}^2) \cap P_1(\mathcal{T}_{\ell+k}; \mathbb{R}^2)$ with

$$\sigma_{\ell+k} - \sigma_\ell = \mathbb{C}\,\mathrm{D}_{\ell+k}\,\alpha^{\mathrm{NC}}_{\ell+k} + \mathrm{Curl}\,\beta^{\mathrm{C}}_{\ell+k}.$$

This implies

$$\begin{aligned}
\|\!| u^{\mathrm{NC}}_{\ell+k} - u^{\mathrm{NC}}_\ell |\!\|^2_{\mathrm{NC}(\ell+k)} &= \int_\Omega \left(\mathrm{D}_{\ell+k}\,u^{\mathrm{NC}}_{\ell+k} - \mathrm{D}_\ell\,u^{\mathrm{NC}}_\ell\right) : \mathbb{C}\,\mathrm{D}_{\ell+k}\,\alpha^{\mathrm{NC}}_{\ell+k}\,\mathrm{dx} \\
&\quad + \int_\Omega \left(\mathrm{D}_{\ell+k}\,u^{\mathrm{NC}}_{\ell+k} - \mathrm{D}_\ell\,u^{\mathrm{NC}}_\ell\right) : \mathrm{Curl}\,\beta^{\mathrm{C}}_{\ell+k}\,\mathrm{dx} \\
&= \|\!| \alpha^{\mathrm{NC}}_{\ell+k} |\!\|^2_{\mathrm{NC}(\ell+k)} + \left\| \mathbb{C}^{-1/2}\,\mathrm{Curl}\,\beta^{\mathrm{C}}_{\ell+k} \right\|^2_{L^2(\Omega)}.
\end{aligned}$$

The nonconforming interpolation $\alpha^{\mathrm{NC}}_\ell =: \mathcal{I}^{\mathrm{NC}}_\ell \alpha^{\mathrm{NC}}_{\ell+k} \in V_\ell$ of (3.10) is defined uniquely by

$$\fint_E \alpha^{\mathrm{NC}}_\ell\,\mathrm{ds} = \fint_E \alpha^{\mathrm{NC}}_{\ell+k}\,\mathrm{ds} \quad \text{for all } E \in \mathcal{E}_\ell.$$

This identity holds on either side of each $E \in \mathcal{E}_\ell$ and so

$$\int_E [(\alpha^{\mathrm{NC}}_{\ell+k} - \alpha^{\mathrm{NC}}_\ell)\mathbb{C}\,\mathrm{D}_\ell\,u^{\mathrm{NC}}_\ell]_E \cdot \nu_E\,\mathrm{ds} = 0 \quad \text{for all } E \in \mathcal{E}_\ell.$$

Moreover, $\alpha^{\mathrm{NC}}_{\ell+k} = \alpha^{\mathrm{NC}}_\ell$ on $T \in \mathcal{T}_\ell \cap \mathcal{T}_{\ell+k}$. This leads to

$$\begin{aligned}
\|\!| \alpha^{\mathrm{NC}}_{\ell+k} |\!\|^2_{\mathrm{NC}(\ell+k)} &= \int_\Omega \left(\mathrm{D}_{\ell+k}\,u^{\mathrm{NC}}_{\ell+k} - \mathrm{D}_\ell\,u^{\mathrm{NC}}_\ell\right) : \mathbb{C}\,\mathrm{D}_{\ell+k}\,\alpha^{\mathrm{NC}}_{\ell+k}\,\mathrm{dx} \\
&= \int_\Omega f \cdot \alpha^{\mathrm{NC}}_{\ell+k}\,\mathrm{dx} - \sum_{E\in\mathcal{E}_\ell} \int_E [\alpha^{\mathrm{NC}}_{\ell+k}\,\mathbb{C}\,\mathrm{D}_\ell\,u^{\mathrm{NC}}_\ell]_E \cdot \nu_E\,\mathrm{ds} \\
&= \sum_{T\in\mathcal{T}_{\ell\setminus\ell+k}} \int_T f \cdot \left(\alpha^{\mathrm{NC}}_{\ell+k} - \alpha^{\mathrm{NC}}_\ell\right)\mathrm{dx} \\
&\quad - \sum_{E\in\mathcal{E}_\ell} \int_E [\left(\alpha^{\mathrm{NC}}_{\ell+k} - \alpha^{\mathrm{NC}}_\ell\right)\,\mathbb{C}\,\mathrm{D}_\ell\,u^{\mathrm{NC}}_\ell]_E \cdot \nu_E\,\mathrm{ds} \\
&\leqslant \sum_{T\in\mathcal{T}_{\ell\setminus\ell+k}} \left(\|f\|_{L^2(T)}\,\|\alpha^{\mathrm{NC}}_{\ell+k} - \alpha^{\mathrm{NC}}_\ell\|_{L^2(T)}\right).
\end{aligned}$$

The combination of the aforementioned estimates and the discrete Poincaré inequality of

Lemma 3.2.11 results in

$$\begin{aligned}\|\!|\alpha^{\mathrm{NC}}_{\ell+k}|\!\|^2_{\mathrm{NC}(\ell+k)} &\lesssim \sum_{T\in\mathcal{T}_{\ell\setminus\ell+k}} \|f\|_{L^2(T)}\, h_T\, \|\mathrm{D}_{\ell+k}\,\alpha^{\mathrm{NC}}_{\ell+k}\|_{L^2(T)}\\ &\lesssim \|h_\ell f\|_{L^2(\mathcal{T}_{\ell\setminus\ell+k})}\, \|\mathrm{D}_{\ell+k}\,u^{\mathrm{NC}}_{\ell+k} - \mathrm{D}_\ell\,u^{\mathrm{NC}}_\ell\|_{L^2(\Omega)}\,.\end{aligned}$$

The analysis of the second term in the decomposition of $|\!|\!|u^{\mathrm{NC}}_{\ell+k} - u^{\mathrm{NC}}_\ell|\!|\!|^2_{\mathrm{NC}(\ell+k)}$ requires the Scott–Zhang [SZ90] interpolation $\beta^{\mathrm{C}}_\ell := \mathcal{I}_\ell\beta^{\mathrm{C}}_{\ell+k}$ on $\mathcal{T}_\ell$ of Definition 3.2.9. Then β^{C}_ℓ satisfies

$$\|\beta^{\mathrm{C}}_{\ell+k} - \beta^{\mathrm{C}}_\ell\|_{L^2(E)} = 0 \quad \text{for all } E\in\mathcal{E}_{\ell+k}\cap\mathcal{E}_\ell.$$

On the edge patch Ω^ℓ_E (see Table 3.14 for the definition) of $E\in\mathcal{E}_{\ell\setminus\ell+k}$, the following estimate holds

$$\|\beta^{\mathrm{C}}_{\ell+k} - \beta^{\mathrm{C}}_\ell\|_{L^2(E)} \lesssim h_E^{1/2}\,\|\beta^{\mathrm{C}}_{\ell+k}\|_{H^1(\Omega^\ell_E)}\,.$$

This leads to

$$\begin{aligned}\left\|\mathbb{C}^{-1/2}\,\mathrm{Curl}\,\beta^{\mathrm{C}}_{\ell+k}\right\|^2_{L^2(\Omega)} &= \int_\Omega \left(\mathrm{D}_{\ell+k}\,u^{\mathrm{NC}}_{\ell+k} - \mathrm{D}_\ell\,u^{\mathrm{NC}}_\ell\right) : \mathrm{Curl}\,\beta^{\mathrm{C}}_{\ell+k}\,\mathrm{dx}\\ &= \int_\Omega \left(\mathrm{D}_{\ell+k}\,u^{\mathrm{NC}}_{\ell+k} - \mathrm{D}_\ell\,u^{\mathrm{NC}}_\ell\right) : \mathrm{Curl}\left(\beta^{\mathrm{C}}_{\ell+k} - \beta^{\mathrm{C}}_\ell\right)\mathrm{dx}\\ &= -\sum_{T\in\mathcal{T}_{\ell+k}}\int_T \mathrm{curl}\left(\mathrm{D}_{\ell+k}\,u^{\mathrm{NC}}_{\ell+k} - \mathrm{D}_\ell\,u^{\mathrm{NC}}_\ell\right)\cdot\left(\beta^{\mathrm{C}}_{\ell+k} - \beta^{\mathrm{C}}_\ell\right)\mathrm{dx}\\ &\quad + \sum_{E\in\mathcal{E}_{\ell+k}}\int_E [\partial u^{\mathrm{NC}}_\ell/\partial s]_E\cdot\left(\beta^{\mathrm{C}}_{\ell+k} - \beta^{\mathrm{C}}_\ell\right)\mathrm{ds}\\ &\leqslant \sum_{E\in\mathcal{E}_{\ell\setminus\ell+k}} \|[\partial u^{\mathrm{NC}}_\ell/\partial s]_E\|_{L^2(E)}\,\|\beta^{\mathrm{C}}_{\ell+k} - \beta^{\mathrm{C}}_\ell\|_{L^2(E)}\\ &\lesssim \sum_{E\in\mathcal{E}_{\ell\setminus\ell+k}} \|[\partial u^{\mathrm{NC}}_\ell/\partial s]_E\|_{L^2(E)}\,h_E^{1/2}|\beta^{\mathrm{C}}_{\ell+k}|_{H^1(\Omega^\ell_E)}\\ &\lesssim \eta_\ell\left(\mathcal{E}_{\ell\setminus\ell+k}\right)|\beta^{\mathrm{C}}_{\ell+k}|_{H^1(\Omega)}.\end{aligned}$$

Lemma 2.1.10 proves

$$\begin{aligned}|\beta^{\mathrm{C}}_{\ell+k}|_{H^1(\Omega)} &\lesssim \|\mathrm{Curl}\,\beta^{\mathrm{C}}_{\ell+k}\|_{L^2(\Omega)}\\ &\lesssim \|\mathrm{tr}\left(\mathrm{Curl}\,\beta^{\mathrm{C}}_{\ell+k}\right)\|_{L^2(\Omega)} + \|\mathrm{div}\,\mathrm{Curl}\,\beta^{\mathrm{C}}_{\ell+k}\|_{H^{-1}(\Omega)}\\ &\leqslant \left\|\mathrm{tr}\left(\mathbb{C}^{-1/2}\,\mathrm{Curl}\,\beta^{\mathrm{C}}_{\ell+k}\right)\right\|_{L^2(\Omega)} \leqslant \left\|\mathbb{C}^{-1/2}\,\mathrm{Curl}\,\beta^{\mathrm{C}}_{\ell+k}\right\|_{L^2(\Omega)}\,.\end{aligned}$$

The combination of the previous two estimates leads to

$$\begin{aligned}\left\|\mathbb{C}^{-1/2}\,\mathrm{Curl}\,\beta^{\mathrm{C}}_{\ell+k}\right\|^2_{L^2(\Omega)} &\lesssim \eta_\ell\left(\mathcal{E}_{\ell\setminus\ell+k}\right)\left\|\mathbb{C}^{-1/2}\,\mathrm{Curl}\,\beta^{\mathrm{C}}_{\ell+k}\right\|_{L^2(\Omega)}\\ &\lesssim \eta_\ell\left(\mathcal{E}_{\ell\setminus\ell+k}\right)\|\mathrm{D}_{\ell+k}\,u^{\mathrm{NC}}_{\ell+k} - \mathrm{D}_\ell\,u^{\mathrm{NC}}_\ell\|_{L^2(\Omega)}\,.\end{aligned}$$

The combination of the above estimates concludes the proof

$$\begin{aligned}\|\!|u_{\ell+k}^{\mathrm{NC}} - u_\ell^{\mathrm{NC}}|\!\|_{\mathrm{NC}(\ell+k)}^2 &\lesssim \left(\|h_\ell f\|_{\mathcal{T}_{\ell\setminus\ell+k}} + \eta_\ell\left(\mathcal{E}_{\ell\setminus\ell+k}\right)\right)\|\mathrm{D}_{\ell+k}\, u_{\ell+k}^{\mathrm{NC}} - \mathrm{D}_\ell\, u_\ell^{\mathrm{NC}}\|_{L^2(\Omega)}\\ &\lesssim \eta_\ell\left(\mathcal{E}_{\ell\setminus\ell+k}\right)\|\mathrm{D}_{\ell+k}\, u_{\ell+k}^{\mathrm{NC}} - \mathrm{D}_\ell\, u_\ell^{\mathrm{NC}}\|_{L^2(\Omega)}\,. \qquad \square\end{aligned}$$

Lemma 5.2.5 ([CR12, Lemma 3.8])**.** *There exists some positive λ-independent constant C_{up} such that*

$$\|\sigma - \sigma_\ell\|_{L^2(\Omega)}^2 + |u - u_\ell^{\mathrm{NC}}|_{H^1(\mathcal{T}_\ell)}^2 + \mathrm{osc}^2(f,\mathcal{T}_\ell) \leqslant C_{\mathrm{up}}\left(\varepsilon_\ell^2 + \|h_\ell f\|_{L^2(\Omega)}^2\right). \tag{5.10}$$

Proof replicated from [CR12]. Observe that $\tau := \sigma - \sigma_\ell \in L^2\left(\Omega;\mathbb{R}^{2\times 2}\right)$ satisfies $\int_\Omega \mathrm{tr}(\tau)\,\mathrm{dx} = 0$ and hence Lemma 2.1.10 implies

$$\|\tau\|_{L^2(\Omega)} \lesssim \|\mathrm{dev}\,\tau\|_{L^2(\Omega)} + \|\mathrm{div}\,\tau\|_{H^{-1}(\Omega)}\,.$$

Therefore, a separate investigation of the isochoric part and the divergence part of the stress is possible. Since

$$\|\mathbb{C}A\|_{L^2(\Omega)}^2 = \|2\mu\,\mathrm{dev}\,A\|_{L^2(\Omega)}^2 + \|(\lambda+\mu)\,\mathrm{tr}(A)\|_{L^2(\Omega)}^2$$

for all $A \in \mathbb{R}^{2\times 2}$, the deviator of τ can be bounded from above with

$$\|\mathrm{dev}\,\tau\|_{L^2(\Omega)}^2 = \|2\mu\,\mathrm{dev}\left(\mathrm{D}\,u - \mathrm{D}_\ell\, u_\ell^{\mathrm{NC}}\right)\|_{L^2(\Omega)}^2 \leqslant 2\mu\varepsilon_\ell^2.$$

Furthermore, (5.9) leads to

$$\|\mathrm{div}\,\tau\|_{H^{-1}(\Omega)} = \|f + \mathrm{div}\,\sigma_\ell\|_{H^{-1}(\Omega)} \lesssim \|h_\ell f\|_{L^2(\Omega)}\,.$$

Thus,

$$\|\sigma - \sigma_\ell\|_{L^2(\Omega)}^2 \lesssim \|\mathrm{dev}\,\tau\|_{L^2(\Omega)}^2 + \|\mathrm{tr}\,\tau\|_{L^2(\Omega)}^2 \lesssim \varepsilon_\ell^2 + \|h_\ell f\|_{L^2(\Omega)}^2\,.$$

The combination with the standard estimates $|u - u_\ell^{\mathrm{NC}}|_{H^1(\mathcal{T}_\ell)}^2 \leqslant 1/(2\mu)\varepsilon_\ell^2$ of (5.6) and $\mathrm{osc}_\ell^2 \leqslant \|h_\ell f\|_{L^2(\Omega)}^2$ concludes the proof with $C_{\mathrm{up}} \lesssim \mu + 1/\mu \lesssim 1$. $\square$

The following lemma asserts quasi-orthogonality for the pure displacement problem in linear elasticity and the Crouzeix–Raviart FEM of [CR12]. The concept of quasi-orthogonality goes back to [CH06a, CH06b] for the Poisson problem and nonconforming FEM. Its sharpened form has been employed for the Poisson problem in Chapter 4 before and will be essential for the proof of quasi-optimality for the pure displacement problem in linear elasticity below.

Lemma 5.2.6 (Quasi-orthogonality, [CR12, Lemma 4.3])**.** *There exists some positive constant C_{qo}, which depends on $\mathcal{T}_0$ only, such that quasi-orthogonality holds in the sense of*

$$\left|a_{\mathrm{NC}(\ell+k)}\left(u - u_{\ell+k}^{\mathrm{NC}}, u_{\ell+k}^{\mathrm{NC}} - u_\ell^{\mathrm{NC}}\right)\right| \leqslant C_{\mathrm{qo}}^{1/2}|u - u_{\ell+k}^{\mathrm{NC}}|_{H^1(\mathcal{T}_{\ell+k})}\,\|h_\ell f\|_{\mathcal{T}_{\ell\setminus\ell+k}}\,, \tag{5.11}$$

as well as

$$\begin{aligned} 2\mu|u_{\ell+k}^{\mathrm{NC}} - u_\ell^{\mathrm{NC}}|_{H^1(\mathcal{T}_{\ell+k})}^2 &\leqslant \|\!| u_{\ell+k}^{\mathrm{NC}} - u_\ell^{\mathrm{NC}} |\!\|_{\mathrm{NC}(\ell+k)}^2 \\ &\leqslant \varepsilon_\ell^2 - \varepsilon_{\ell+k}^2 + 2C_{\mathrm{qo}}^{1/2}|u - u_{\ell+k}^{\mathrm{NC}}|_{H^1(\mathcal{T}_{\ell+k})} \|h_\ell f\|_{\mathcal{T}_\ell \setminus \ell+k} \end{aligned} \tag{5.12}$$

and

$$\varepsilon_\ell^2 - \varepsilon_{\ell+k}^2 \leqslant \|\!| u_{\ell+k}^{\mathrm{NC}} - u_\ell^{\mathrm{NC}} |\!\|_{\mathrm{NC}(\ell+k)}^2 + 2C_{\mathrm{qo}}^{1/2}|u - u_{\ell+k}^{\mathrm{NC}}|_{H^1(\mathcal{T}_{\ell+k})} \|h_\ell f\|_{\mathcal{T}_\ell \setminus \ell+k}\,. \tag{5.13}$$

Without loss of generality we will assume throughout this chapter that

$$1/2 \leqslant C_{\mathrm{qo}}. \tag{5.14}$$

Proof of Lemma 5.2.6, replicated from [CR12]. Let $\mathcal{I}_\ell^{\mathrm{NC}}$ be the nonconforming interpolation operator defined by Remark 3.2.8 and $\mathcal{I}_{\ell+k}^{\mathrm{NC}}$ denote the standard nonconforming interpolation operator of Definition 2.4.3. Since $\fint_E \mathcal{I}_{\ell+k}^{\mathrm{NC}} u \,\mathrm{ds} = \fint_E u \,\mathrm{ds}$ for all $E \in \mathcal{E}_{\ell+k}$ an integration by parts argument shows

$$\mathrm{D}_{\ell+k}\, \mathcal{I}_{\ell+k}^{\mathrm{NC}} u\big|_T = \fint_T \mathrm{D}\, u \,\mathrm{dx} \qquad \text{for } T \in \mathcal{T}_{\ell+k}.$$

The interpolation operators lead to

$$\begin{aligned} &a_{\mathrm{NC}(\ell+k)}\left(u - u_{\ell+k}^{\mathrm{NC}}, u_{\ell+k}^{\mathrm{NC}} - u_\ell^{\mathrm{NC}}\right) \\ &\quad = \int_\Omega \left(\mathrm{D}\, u - \mathrm{D}_{\ell+k}\, u_{\ell+k}^{\mathrm{NC}}\right) : \mathbb{C}\left(\mathrm{D}_{\ell+k}\left(u_{\ell+k}^{\mathrm{NC}} - u_\ell^{\mathrm{NC}}\right)\right) \mathrm{dx} \\ &\quad = \int_\Omega \mathrm{D}_{\ell+k}\left(\mathcal{I}_{\ell+k}^{\mathrm{NC}} u - u_{\ell+k}^{\mathrm{NC}}\right) : \mathbb{C}\, \mathrm{D}_{\ell+k}\, u_{\ell+k}^{\mathrm{NC}} \,\mathrm{dx} - \int_\Omega \mathrm{D}_\ell\left(\mathcal{I}_\ell^{\mathrm{NC}}\left(u - u_{\ell+k}^{\mathrm{NC}}\right)\right) : \mathbb{C}\, \mathrm{D}_\ell\, u_\ell^{\mathrm{NC}} \,\mathrm{dx}\,. \end{aligned}$$

The integral mean property for $\mathcal{I}_\ell^{\mathrm{NC}}$ proves $\mathcal{I}_\ell^{\mathrm{NC}} u = \mathcal{I}_\ell^{\mathrm{NC}} \mathcal{I}_{\ell+k}^{\mathrm{NC}} u$. Hence,

$$\begin{aligned} &a_{\mathrm{NC}(\ell+k)}\left(u - u_{\ell+k}^{\mathrm{NC}}, u_{\ell+k}^{\mathrm{NC}} - u_\ell^{\mathrm{NC}}\right) \\ &\quad = a_{\mathrm{NC}(\ell+k)}\left(u_{\ell+k}^{\mathrm{NC}}, \mathcal{I}_{\ell+k}^{\mathrm{NC}} u - u_{\ell+k}^{\mathrm{NC}}\right) - a_{\mathrm{NC}(\ell)}\left(u_\ell^{\mathrm{NC}}, \mathcal{I}_\ell^{\mathrm{NC}}\left(\mathcal{I}_{\ell+k}^{\mathrm{NC}} u - u_{\ell+k}^{\mathrm{NC}}\right)\right) \\ &\quad = \int_\Omega f\left(I_2 - \mathcal{I}_\ell^{\mathrm{NC}}\right)\left(\mathcal{I}_{\ell+k}^{\mathrm{NC}} u - u_{\ell+k}^{\mathrm{NC}}\right) \mathrm{dx}\,. \end{aligned}$$

Let $v_{\ell+k}^{\mathrm{NC}} := \mathcal{I}_{\ell+k}^{\mathrm{NC}} u - u_{\ell+k}^{\mathrm{NC}} \in V_{\ell+k}$. Since $\mathcal{I}_{\ell+k}^{\mathrm{NC}}$ sustains the integral mean on any $E \in \mathcal{E}_\ell$, Lemma 3.2.11 proves

$$\left\|v_{\ell+k}^{\mathrm{NC}} - \mathcal{I}_{\ell+k}^{\mathrm{NC}} v_{\ell+k}^{\mathrm{NC}}\right\|_{L^2(T)} \lesssim h_T \left\|\mathrm{D}_{\ell+k}\, v_{\ell+k}^{\mathrm{NC}}\right\|_{L^2(T)} \qquad \text{for all } T \in \mathcal{T}_\ell.$$

This results in

$$\left|a_{\mathrm{NC}(\ell+k)}\left(u - u_{\ell+k}^{\mathrm{NC}}, u_{\ell+k}^{\mathrm{NC}} - u_\ell^{\mathrm{NC}}\right)\right| \lesssim \sum_{T \in \mathcal{T}_{\ell \setminus \ell+k}} \|f\|_{L^2(T)}\, h_T \left\|\mathrm{D}_{\ell+k}\left(\mathcal{I}_{\ell+k}^{\mathrm{NC}} u - u_{\ell+k}^{\mathrm{NC}}\right)\right\|_{L^2(T)}.$$

Pythagoras' theorem on $T \in \mathcal{T}_\ell$ is

$$\|\mathrm{D}_{\ell+k}\,\mathcal{I}^{\mathrm{NC}}_{\ell+k}u - \mathrm{D}_{\ell+k}\,u^{\mathrm{NC}}_{\ell+k}\|^2_{L^2(T)} + \|\mathrm{D}\,u - D_{\ell+k}\mathcal{I}^{\mathrm{NC}}_{\ell+k}u\|^2_{L^2(T)} = \|\mathrm{D}\,u - \mathrm{D}_{\ell+k}\,u^{\mathrm{NC}}_{\ell+k}\|^2_{L^2(T)}\,,$$

which concludes the proof for (5.11). (5.12) and (5.13) follow directly by

$$|\!|\!|u^{\mathrm{NC}}_{\ell+k} - u^{\mathrm{NC}}_\ell|\!|\!|^2_{\mathrm{NC}(\ell+k)} = \varepsilon^2_\ell - \varepsilon^2_{\ell+k} - 2a_{\mathrm{NC}(\ell+k)}\left(u - u^{\mathrm{NC}}_{\ell+k}, u^{\mathrm{NC}}_{\ell+k} - u^{\mathrm{NC}}_\ell\right)$$

plus the standard estimate (5.6), which is $2\mu|\cdot|^2_{H^1(\mathcal{T}_{\ell+k})} \leqslant |\!|\!|\cdot|\!|\!|^2_{\mathrm{NC}(\ell+k)}$ for (5.12). □

5.3 Convergence

This section proves the convergence of a sequence of solutions and triangulations generated by s-afem-aa in solving the discrete problem (5.1).

The analysis of the quasi-optimal convergence of Section 5.4 involves error estimator reduction, quasi-orthogonality and the contraction property for the total error ξ_ℓ, which is some linear combination of the refinement indicators η_ℓ, and the volume term $\|h_\ell f\|_{L^2(\Omega)}$, plus the error in the broken energy norm $\varepsilon_\ell := |\!|\!|u - u^{\mathrm{NC}}_\ell|\!|\!|_{\mathrm{NC}(\ell)}$. The investigations are similar to the ones in [CR12] for c-afem and for the Poisson problem, and s-afem-aa in Chapter 4 and the first application of s-afem-aa in [CR11] for mixed fem.

The proof of the contraction property is based on Lemmas 5.2.6 and 5.3.1 for quasi-orthogonality and estimator reduction.

Lemma 5.3.1 (Estimator reduction)**.** *Let $0 < \theta_A < 1$, $0 < \rho_B < 1$, and $\kappa > 0$ be parameters for algorithm* s-afem-aa *used to solve (5.1). Then, for any $0 < \delta < \theta_A\,(2 - \theta_A)$ there exist positive generic constants $C_{\mathrm{J}}0$, C_δ, and a reduction factor $0 < \rho_A < 1$ such that on each level $\ell \in \mathbb{N}_0$ of algorithm* s-afem-aa

(a) *in* ***Case(A)*** *(i.e., $\|h_\ell f\|^2_{L^2(\Omega)} \leqslant \kappa\eta^2_\ell$) η_ℓ and $\|h_\ell f\|_{L^2(\Omega)}$ satisfy the reduction properties*

$$\eta^2_{\ell+1} \leqslant \rho_A\eta^2_\ell + C_\delta\,\|\mathrm{D}_{\ell+1}\,u^{\mathrm{NC}}_{\ell+1} - \mathrm{D}_\ell\,u^{\mathrm{NC}}_\ell\|^2_{L^2(\Omega)} \qquad \textit{and} \tag{5.15}$$

$$\|h_{\ell+1}f\|^2_{L^2(\Omega)} \leqslant \|h_\ell f\|^2_{L^2(\Omega)} - 1/2\,\|h_\ell f\|^2_{\mathcal{T}_{\ell\setminus\ell+1}}\,, \tag{5.16}$$

(b) *in* ***Case(B)*** *(i.e., $\|h_\ell f\|^2_{L^2(\Omega)} > \kappa\eta^2_\ell$) η_ℓ and $\|h_\ell f\|_{L^2(\Omega)}$ satisfy the reduction properties*

$$\eta^2_{\ell+1} \leqslant (1+\delta)\,\eta^2_\ell + C_\delta\,\|\mathrm{D}_{\ell+1}\,u^{\mathrm{NC}}_{\ell+1} - \mathrm{D}_\ell\,u^{\mathrm{NC}}_\ell\|^2_{L^2(\Omega)} \qquad \textit{and} \tag{5.17}$$

$$\|h_{\ell+1}f\|^2_{L^2(\Omega)} \leqslant \rho_B\,\|h_\ell f\|^2_{L^2(\Omega)}\,. \tag{5.18}$$

Proof. For any edge $E \in \mathcal{E}_{\ell+1}$ and any $\delta > 0$ the following estimate holds

$$\begin{aligned}\|[\mathrm{D}_{\ell+1}\,u^{\mathrm{NC}}_{\ell+1}]_E \cdot \tau_E\|^2_{L^2(E)} \leqslant{}& (1+1/\delta)\,\|[\mathrm{D}_{\ell+1}\,u^{\mathrm{NC}}_{\ell+1} - \mathrm{D}_\ell\,u^{\mathrm{NC}}_\ell]_E \cdot \tau_E\|^2_{L^2(E)} \\ &+ (1+\delta)\,\|[\mathrm{D}_\ell\,u^{\mathrm{NC}}_\ell]_E \cdot \tau_E\|^2_{L^2(E)}\,.\end{aligned}$$

Since $\mathrm{D}_{\ell+1}\,u^{\mathrm{NC}}_{\ell+1} - \mathrm{D}_\ell\,u^{\mathrm{NC}}_\ell$ is piecewise constant on $\mathcal{T}_{\ell+1}$, there exists some positive generic

constant C_{J} such that

$$\sum_{E\in\mathcal{E}_{\ell+1}} \left\|[\mathrm{D}_{\ell+1}\, u_{\ell+1}^{\mathrm{NC}} - \mathrm{D}_\ell\, u_\ell^{\mathrm{NC}}]_E \cdot \tau_E\right\|_{L^2(E)}^2 \leqslant C_{\mathrm{J}} \left\|\mathrm{D}_{\ell+1}\, u_{\ell+1}^{\mathrm{NC}} - \mathrm{D}_\ell\, u_\ell^{\mathrm{NC}}\right\|_{L^2(\Omega)}^2.$$

Let $\eta_\ell^2 := \sum_{E\in\mathcal{E}_\ell} h_E \left\|[\partial u_\ell^{\mathrm{NC}}/\partial s]_E\right\|_{L^2(E)}^2$, then $\eta_{\ell+1}$ is bounded as follows

$$\begin{aligned}
\eta_{\ell+1}^2 &\leqslant C_{\mathrm{J}}\,(1+1/\delta)\left\|\mathrm{D}_{\ell+1}\, u_{\ell+1}^{\mathrm{NC}} - \mathrm{D}_\ell\, u_\ell^{\mathrm{NC}}\right\|_{L^2(\Omega)}^2 + (1+\delta)\,\eta_\ell^2 \\
&\leqslant C_{\mathrm{J}}\,(1+1/\delta)\left\|\mathrm{D}_{\ell+1}\, u_{\ell+1}^{\mathrm{NC}} - \mathrm{D}_\ell\, u_\ell^{\mathrm{NC}}\right\|_{L^2(\Omega)}^2 \\
&\quad + (1+\delta)\,\eta_\ell^2\,(\mathcal{E}_{\ell+1}\cap\mathcal{E}_\ell) + (1+\delta)\,/2\eta_\ell^2\left(\mathcal{E}_{\ell\setminus\ell+1}\right) \\
&\leqslant C_{\mathrm{J}}(1+1/\delta)\left\|\mathrm{D}_{\ell+1}\, u_{\ell+1}^{\mathrm{NC}} - \mathrm{D}_\ell\, u_\ell^{\mathrm{NC}}\right\|_{L^2(\Omega)}^2 \\
&\quad + (1+\delta)\,\eta_\ell^2 - (1+\delta)\,/2\eta_\ell^2\left(\mathcal{E}_{\ell\setminus\ell+1}\right).
\end{aligned}$$

This verifies estimator reduction in Case (B), i.e., (5.17) for $C_\delta := C_{\mathrm{J}}(1+1/\delta)$. Given $\rho_A := (1+\delta)\,(1-\theta_A)$, the incorporation of the bulk criterion (3.2) of Case (A) proves the estimator reduction (5.15) for Case (A)

$$\begin{aligned}
\eta_{\ell+1}^2 &\leqslant C_\delta \left\|\mathrm{D}_{\ell+1}\, u_{\ell+1}^{\mathrm{NC}} - \mathrm{D}_\ell\, u_\ell^{\mathrm{NC}}\right\|_{L^2(\Omega)}^2 + (1+\delta)\,(1-\theta_A/2)\,\eta_\ell^2 \\
&\leqslant C_\delta \left\|\mathrm{D}_{\ell+1}\, u_{\ell+1}^{\mathrm{NC}} - \mathrm{D}_\ell\, u_\ell^{\mathrm{NC}}\right\|_{L^2(\Omega)}^2 + \rho_A\eta_\ell^2.
\end{aligned}$$

For arbitrarily nested meshes, as well as in Case (A), the volume term satisfies (3.7), which proves (5.16). In Case (B), using the definition of $\mathrm{Tol} := \rho_B \left\|h_\ell f\right\|_{L^2(\Omega)}^2$ in Algorithm 3.4, the reduction of the volume term is

$$\left\|h_{\ell+1} f\right\|_{L^2(\Omega)}^2 \leqslant \left\|h_{\mathcal{T}} f\right\|_{L^2(\Omega)}^2 \leqslant \rho_B \left\|h_\ell f\right\|_{L^2(\Omega)}^2,$$

which is (5.18). □

Theorem 5.3.2 (Contraction property)**.** *Given some bulk parameter $0<\theta_A<1$, there exists $0<\kappa_0$ such that for any $\kappa_1\in(0,\kappa_0)$ and $0<\rho_B<1$ there exist positive α_f, α_ε and $0<\varrho<1$, which depend on C_{rel}, C_δ, ρ and C_{qo} from Theorem 5.2.2 and Lemmas 5.2.6 and 5.3.1 and which are independent of the Lamé parameter λ, such that for all $\kappa\in(\kappa_1,\kappa_0)$ the sequence of triangulations and discrete solutions generated by* S-AFEM-AA *with total error $\xi_\ell := \eta_\ell^2 + \alpha_f \left\|h_\ell f\right\|_{L^2(\Omega)}^2 + \alpha_\varepsilon\varepsilon_\ell^2$, satisfies a contraction property in the sense that*

$$\xi_{\ell+1}^2 \leqslant \varrho\,\xi_\ell^2 \quad \text{for all } \ell\in\mathbb{N}_0.$$

Proof. Let $0<\theta_A<1$ and define

$$\begin{aligned}
\delta &:= \frac{\theta_A}{2}\frac{1}{2-\theta_A}, & \rho_A &:= (1+\delta)\,(1-\theta_A/2) = 1-\theta_A/4, \\
\gamma &:= \min\{\mu,\mu B\}, & B &:= \min\left\{1/2, \frac{1-\rho_A}{C_\delta C_{\mathrm{rel}}}\right\}, \\
A &:= C_{\mathrm{qo}}C_\delta/(\gamma\mu) + C_\delta C_{\mathrm{rel}}B/2\mu^2, & \alpha_\varepsilon &:= \left(1-\frac{\gamma}{2\mu}\right)\frac{C_\delta}{2\mu},
\end{aligned}$$

$$\kappa_0 := \frac{1-\rho_A - C_\delta C_{\mathrm{rel}} B/(2\mu)^2}{A}.$$

Let $0 < \kappa_1 < \kappa_0 < 1$, $0 < \rho_B < 1$ and define

$$D := \frac{\delta + C_\delta C_{\mathrm{rel}} B/(2\mu)^2}{\kappa_1}, \qquad \alpha_f := \frac{A+D}{1-\rho_B}.$$

Contraction in Case (A) Lemma 5.3.1 shows that for any $0 < \theta_A < 1$ there exist $0 < \rho_A < 1$ and $0 < C_\delta$ such that

$$\begin{aligned} \eta_{\ell+1}^2 &\leqslant \rho_A \eta_\ell^2 + C_\delta \left\| \mathrm{D}_{\ell+1} u_{\ell+1}^{\mathrm{NC}} - \mathrm{D}_\ell u_\ell^{\mathrm{NC}} \right\|_{L^2(\Omega)}^2, \\ \|h_{\ell+1} f\|_{L^2(\Omega)}^2 &\leqslant \|h_\ell f\|_{L^2(\Omega)}^2 - \frac{1}{2} \|h_\ell f\|_{\mathcal{T}_\ell \setminus \mathcal{T}_{\ell+1}}^2, \\ \|h_\ell f\|_{L^2(\Omega)}^2 &< \kappa \eta_\ell^2. \end{aligned} \tag{5.19}$$

For positive B and γ, the quasi-orthogonality of Lemma 5.2.6 plus the reliability of Theorem 5.2.2 with the standard estimate (5.6) and the application of Young's inequality prove

$$\begin{aligned} \eta_{\ell+1}^2 &\leqslant \rho_A \eta_\ell^2 + \frac{C_\delta}{2\mu} \left\| \mathrm{D}_{\ell+1} u_{\ell+1}^{\mathrm{NC}} - \mathrm{D}_\ell u_\ell^{\mathrm{NC}} \right\|_{L^2(\Omega)}^2 \\ &\leqslant \rho_A \eta_\ell^2 + \frac{C_\delta}{2\mu} \left(\varepsilon_\ell^2 - \varepsilon_{\ell+1}^2 + 2 C_{\mathrm{qo}}^{1/2} \|h_\ell f\|_{\mathcal{T}_\ell \setminus \mathcal{T}_{\ell+1}} |u - u_{\ell+1}^{\mathrm{NC}}|_{H^1(\mathcal{T}_{\ell+1})} \right) \\ &\leqslant \rho_A \eta_\ell^2 + \frac{C_\delta}{2\mu} \varepsilon_\ell^2 - \frac{C_\delta}{2\mu} \left(1 - \frac{\gamma}{2\mu} \right) \varepsilon_{\ell+1}^2 + \frac{C_\delta C_{\mathrm{qo}}}{2\gamma\mu} \|h_\ell f\|_{\mathcal{T}_\ell \setminus \mathcal{T}_{\ell+1}}^2 \\ &\leqslant \left(\rho_A + \frac{B C_{\mathrm{rel}} C_\delta}{(2\mu)^2} \right) \eta_\ell^2 + \frac{(1-B)\, C_\delta}{2\mu} \varepsilon_\ell^2 - \left(1 - \frac{\gamma}{2\mu} \right) \frac{C_\delta}{2\mu} \varepsilon_{\ell+1}^2 \\ &\quad + \frac{C_{\mathrm{qo}} C_\delta}{2\gamma\mu} \|h_\ell f\|_{\mathcal{T}_\ell \setminus \mathcal{T}_{\ell+1}}^2 + \frac{B C_{\mathrm{rel}} C_\delta}{(2\mu)^2} \|h_\ell f\|_{L^2(\Omega)}^2. \end{aligned}$$

For any A, $\alpha_f > 0$, $\alpha_\varepsilon = \left(1 - \frac{\gamma}{2\mu}\right) \frac{C_\delta}{2\mu}$ this, (5.16) and (5.19) yield

$$\begin{aligned} \xi_{\ell+1}^2 &\leqslant \left(\rho_A + \frac{B C_{\mathrm{rel}} C_\delta}{(2\mu)^2} + A\kappa \right) \eta_\ell^2 + \frac{(1-B)\, C_\delta}{2\mu} \varepsilon_\ell^2 \\ &\quad + \left(\frac{C_{\mathrm{qo}} C_\delta}{2\gamma\mu} - \frac{\alpha_f}{2} \right) \|h_\ell f\|_{\mathcal{T}_\ell \setminus \mathcal{T}_{\ell+1}}^2 + \left(\frac{B C_{\mathrm{rel}} C_\delta}{(2\mu)^2} - A + \alpha_f \right) \|h_\ell f\|_{L^2(\Omega)}^2. \end{aligned}$$

The choice of parameters at the beginning of this proof ensures contraction in the sense of $\xi_{\ell+1}^2 \leqslant \varrho_A \xi_\ell^2$ for $\varrho_A < 1$ and for any level $\ell \in \mathbb{N}_0$ of Case (A), namely

$$\varrho_A := \max \left\{ \rho_A + \frac{B C_{\mathrm{rel}} C_\delta}{(2\mu)^2} + A\kappa, \frac{(1-B)\, C_\delta}{2\mu\alpha_\varepsilon}, 1 - \frac{1}{\alpha_f} \left(\frac{C_{\mathrm{qo}} C_\delta}{2\gamma\mu} + \frac{B C_{\mathrm{rel}} C_\delta}{(2\mu)^2} \right) \right\}.$$

Contraction in Case (B) Lemma 5.3.1 shows that for any $0 < \rho_B < 1$ there exists $0 < C_\delta$

such that

$$\eta_{\ell+1}^2 \leqslant (1+\delta)\,\eta_\ell^2 + C_\delta \left\|\mathrm{D}_{\ell+1}\, u_{\ell+1}^{\mathrm{NC}} - \mathrm{D}_\ell\, u_\ell^{\mathrm{NC}}\right\|_{L^2(\Omega)}^2,$$
$$\|h_{\ell+1} f\|_{L^2(\Omega)}^2 \leqslant \rho_B \|h_\ell f\|_{L^2(\Omega)}^2, \qquad \kappa\eta_\ell^2 \leqslant \|h_\ell f\|_{L^2(\Omega)}^2.$$

The quasi-orthogonality of Lemma 5.2.6 plus reliability Theorem 5.2.2 and the application of Young's inequality prove for $B, \gamma > 0$

$$\begin{aligned}
\eta_{\ell+1}^2 &\leqslant (1+\delta)\,\eta_\ell^2 + C_\delta \left\|\mathrm{D}_{\ell+1}\, u_{\ell+1}^{\mathrm{NC}} - \mathrm{D}_\ell\, u_\ell^{\mathrm{NC}}\right\|_{L^2(\Omega)}^2 \\
&\leqslant (1+\delta)\,\eta_\ell^2 + \frac{C_\delta}{2\mu}\left(\varepsilon_\ell^2 - \varepsilon_{\ell+1}^2 + 2C_{\mathrm{qo}}^{1/2}\,\|h_\ell f\|_{\mathcal{T}_\ell\setminus\mathcal{T}_{\ell+1}}\,|u - u_{\ell+1}^{\mathrm{NC}}|_{H^1(\mathcal{T}_{\ell+1})}\right) \\
&\leqslant (1+\delta)\,\eta_\ell^2 + \frac{C_\delta}{2\mu}\varepsilon_\ell^2 - \left(1 - \frac{\gamma}{2\mu}\right)\frac{C_\delta}{2\mu}\varepsilon_{\ell+1}^2 + \frac{C_\delta C_{\mathrm{qo}}}{2\gamma\mu}\,\|h_\ell f\|_{\mathcal{T}_\ell\setminus\mathcal{T}_{\ell+1}}^2 \\
&\leqslant \left((1+\delta) + \frac{BC_{\mathrm{rel}}C_\delta}{(2\mu)^2}\right)\eta_\ell^2 + \frac{(1-B)\,C_\delta}{2\mu}\varepsilon_\ell^2 - \left(1 - \frac{\gamma}{2\mu}\right)\frac{C_\delta}{2\mu}\varepsilon_{\ell+1}^2 \\
&\quad + \frac{C_\delta C_{\mathrm{qo}}}{2\gamma\mu}\,\|h_\ell f\|_{\mathcal{T}_\ell\setminus\mathcal{T}_{\ell+1}}^2 + \frac{BC_{\mathrm{rel}}C_\delta}{(2\mu)^2}\,\|h_\ell f\|_{L^2(\Omega)}^2, \\
\xi_{\ell+1}^2 &\leqslant \left(1 + \delta + \frac{BC_{\mathrm{rel}}C_\delta}{(2\mu)^2} - D\kappa\right)\eta_\ell^2 + \frac{(1-B)\,C_\delta}{2\mu}\varepsilon_\ell^2 \\
&\quad + \left(\frac{C_{\mathrm{qo}}C_\delta}{2\gamma\mu} + \frac{BC_{\mathrm{rel}}C_\delta}{(2\mu)^2} + D + \alpha_f\rho_B\right)\|h_\ell f\|_{L^2(\Omega)}^2.
\end{aligned}$$

The choice of parameters at the beginning of this proof ensures contraction in the sense of $\xi_{\ell+1}^2 \leqslant \varrho_B\xi_\ell^2$ for $\varrho_B < 1$ and on any level $\ell \in \mathbb{N}_0$ of Case (B), namely

$$\varrho_B := \max\left\{1 + \delta + \frac{BC_\delta C_{\mathrm{rel}}}{(2\mu)^2} - D\kappa, \frac{(1-B)\,C_\delta}{2\mu\alpha_\varepsilon}, \rho_B + \frac{1}{\alpha_f}\left(\frac{C_{\mathrm{qo}}C_\delta}{2\gamma\mu} + \frac{BC_\delta C_{\mathrm{rel}}}{(2\mu)^2} + D\right)\right\}.$$

Conclusion Hence, for given θ_A, $\kappa_1 < \kappa_0$, there exist positive parameters α_f, α_ε, such that for all $\kappa \in (\kappa_1, \kappa_0)$ and on any level ℓ and any Cases (A) and (B) the term $\xi_\ell^2 := \eta_\ell^2 + \alpha_f\,\|h_\ell f\|_{L^2(\Omega)}^2 + \alpha_\varepsilon\varepsilon_{\ell+1}^2$ satisfies the contraction property $\xi_{\ell+1}^2 < \varrho\xi_\ell^2$ and

$$0 < \varrho := \max\{\varrho_A, \varrho_B\} < 1. \qquad \square$$

To emphasise that the parameters α_ε, α_f do not depend on $0 < \kappa$, the parameter $\kappa_1 \in (0, \kappa_0)$ is introduced; see Remark 4.3.3 for the Poisson problem, which is similar. The specific choice of parameters in the proof of Theorem 5.3.2 shows that contraction is ensured for any choice of $\kappa \in (\kappa_1, \kappa_0)$.

5.4 Optimal convergence rates

This final section is on the main theorem of this chapter, which asserts the quasi-optimality of s-afem-aa for the pure displacement problem in linear elasticity solved with the nonconforming cr-fem.

Theorem 5.4.1 (Optimal convergence rates)**.** *Given a coarse, regular triangulation $\mathcal{T}_0$, let c_{eff}, C_{drel}, C_{qo} be positive generic constants from Theorem 5.2.2 and Lemma 5.2.6. Furthermore, let $s > 0$ be such that $(u, f) \in \mathcal{A}_s$ for the exact solution u of the pure displacement problem in linear elasticity (2.4) with right-hand side $f \in L^2(\Omega)$. Let $0 < \theta_A < \theta_0 := \min\{1, 1/(C_\eta C_{\mathrm{drel}})\}$ be the bulk parameter for Case (A) of* S-AFEM-AA*. Consider the positive parameters $\kappa_1 \in (0, \kappa_2)$ with $\kappa_2 := \min\{\kappa_0, C_{\mathrm{drel}}(\theta_0 - \theta_A)/(1 + C_{\mathrm{drel}} + C_{\mathrm{qo}})\}$ and κ_0, α_ε, α_f, and $0 < \rho < 1$ as chosen in the proof of Theorem 5.3.2.*

Then, for all $\kappa \in (\kappa_1, \kappa_2)$ the algorithm S-AFEM-AA *generates a sequence of triangulations and discrete solutions with an optimal rate of convergence in the following sense*

$$|\mathcal{T}_\ell| - |\mathcal{T}_0| \lesssim \xi_\ell^{-1/s} \qquad \text{with } \xi_\ell^2 := \eta_\ell^2 + \alpha_f \|h_\ell f\|_{L^2(\Omega)}^2 + \alpha_\varepsilon \varepsilon_\ell^2.$$

In the proof of Theorem 5.4.1, Lemmas 5.4.2 and 5.4.4 summarise essential estimates.

Lemma 5.4.2. *Given C_{rel}, α_ε, α_f and κ from Theorems 5.2.2 and 5.3.2, there exist positive generic constants C_{A}, C_{B} such that on any level ℓ the weighted term ξ_ℓ of the energy error ε_ℓ, the estimated error η_ℓ and the volume term $\|h_\ell f\|_{L^2(\Omega)}$ satisfies*

$$\xi_\ell^2 \leqslant \begin{cases} C_{\mathrm{A}} \eta_\ell^2 & \text{if Case (A) applies,} \\ C_{\mathrm{B}} \|h_\ell f\|_{L^2(\Omega)}^2 & \text{if Case (B) applies,} \end{cases} \qquad \text{and} \tag{5.20}$$

$$\xi_\ell^2 \approx \varepsilon_\ell^2 + \|h_\ell f\|_{L^2(\Omega)}^2. \tag{5.21}$$

Proof. The estimate (5.20) is proven using the standard estimate (5.6) for the energy error and the stress error. Furthermore reliability (5.4) and the specific relation of the estimated error and the volume term in both Cases (A) and (B) verify

$$1 + \frac{\alpha_\varepsilon C_{\mathrm{rel}}}{2\mu} + \left(\frac{\alpha_\varepsilon C_{\mathrm{rel}}}{2\mu} + \alpha_f\right)\kappa < 1 + \frac{\alpha_\varepsilon C_{\mathrm{rel}}}{2\mu} + \left(\frac{\alpha_\varepsilon C_{\mathrm{rel}}}{2\mu} + \alpha_f\right)\kappa_2 =: C_{\mathrm{A}},$$
$$\frac{1}{\kappa} + \frac{\alpha_\varepsilon C_{\mathrm{rel}}}{2\kappa\mu} + \frac{\alpha_\varepsilon C_{\mathrm{rel}}}{2\mu} + \alpha_f < \frac{1}{\kappa_1} + \frac{\alpha_\varepsilon C_{\mathrm{rel}}}{2\kappa_1\mu} + \frac{\alpha_\varepsilon C_{\mathrm{rel}}}{2\mu} + \alpha_f =: C_{\mathrm{B}}.$$

The equivalence (5.21) follows directly from the efficiency (5.4) of η_ℓ. Note that C_{A}, C_{B} depend on κ_1 or κ_2 and are independent of κ as long as $\kappa \in (\kappa_1, \kappa_2)$. □

Lemma 5.4.4 below is a direct consequence of the quasi-orthogonality of Lemma 5.2.6 and the following remark.

Remark 5.4.3. *Note that $C_{\mathrm{J}} > 0$ from Lemma 5.3.1 solely depends on $\mathcal{T}_0$. The definitions of parameters and constants in the proof of Theorem 5.3.2 verify*

$$\frac{2C_{\mathrm{qo}}}{\alpha_f} \leqslant \frac{2\gamma\mu(1-\rho_B)}{C_\delta} = \frac{\gamma(1-\gamma/(2\mu))(1-\rho_B)}{\alpha_\varepsilon} \leqslant \frac{1}{\alpha_\varepsilon} \leqslant \frac{4\mu}{C_\delta} \leqslant \frac{4\mu}{C_{\mathrm{J}}}$$

and thus, the following estimates hold

$$\frac{1}{\alpha_\varepsilon} \leqslant \frac{4\mu}{C_{\mathrm{J}}}, \qquad \frac{1}{\alpha_f} \leqslant \frac{2\mu}{C_{\mathrm{J}} C_{\mathrm{qo}}}, \qquad \frac{\alpha_\varepsilon}{\alpha_f} \leqslant \frac{1}{2C_{\mathrm{qo}}}.$$

Lemma 5.4.4. *Given C_{qo} from Lemma 5.2.6, and α_ε, α_f as chosen in Theorem 5.3.2, let $\mathcal{T}_{\ell+k}$ be an admissible refinement of $\mathcal{T}_\ell$. Then, there exists a positive generic constant C_{C} such that the weighted terms ξ_ℓ and $\xi_{\ell+k}$ satisfy*

$$\varepsilon_{\ell+k}^2 \leqslant 2\varepsilon_\ell^2 + 8\mu C_{\mathrm{qo}} \|h_\ell f\|^2_{\mathcal{T}_\ell \setminus \ell+k} \tag{5.22}$$

$$\leqslant 16\mu C_{\mathrm{qo}} \left(\varepsilon_\ell^2 + \|h_\ell f\|^2_{L^2(\Omega)} - \|h_{\ell+k} f\|^2_{L^2(\Omega)}\right), \tag{5.23}$$

$$\alpha_\varepsilon \varepsilon_{\ell+k}^2 \leqslant \xi_{\ell+k}^2 \leqslant C_{\mathrm{C}} \xi_\ell^2. \tag{5.24}$$

Proof. Quasi-orthogonality and Young's inequality lead to

$$\begin{aligned}\varepsilon_{\ell+k}^2 &\leqslant \varepsilon_\ell^2 + 2C_{\mathrm{qo}}^{1/2} |u - u_{\ell+k}^{\mathrm{NC}}|_{H^1(\mathcal{T}_{\ell+k})} \|h_\ell f\|_{\mathcal{T}_\ell \setminus \ell+k} - |\!|\!| u_{\ell+k}^{\mathrm{NC}} - u_\ell^{\mathrm{NC}} |\!|\!|^2_{\mathrm{NC}(\ell+k)} \\ &\leqslant \varepsilon_\ell^2 + 4\mu C_{\mathrm{qo}} \|h_\ell f\|^2_{\mathcal{T}_\ell \setminus \ell+k} + \frac{1}{4\mu} |u - u_{\ell+k}^{\mathrm{NC}}|^2_{H^1(\mathcal{T}_{\ell+k})} - |\!|\!| u_{\ell+k}^{\mathrm{NC}} - u_\ell^{\mathrm{NC}} |\!|\!|^2_{\mathrm{NC}(\ell+k)}.\end{aligned}$$

This plus the standard estimate for the energy error (5.6) imply (5.22). Finally, the reduction of $\|h_\ell f\|_{L^2(\Omega)}$ (3.7), the conventions $1/2 \leqslant C_{\mathrm{qo}}$ of (5.14), and $1/4 \leqslant \mu$ prove (5.23)

$$\varepsilon_{\ell+k}^2 \leqslant 2\varepsilon_\ell^2 + 16\mu C_{\mathrm{qo}} \|h_\ell f\|^2_{L^2(\Omega)} - 16\mu C_{\mathrm{qo}} \|h_{\ell+k} f\|^2_{L^2(\Omega)}.$$

The efficiency of Theorem 5.2.2 plus the estimate (5.8) in the proof of Theorem 5.2.3 verify

$$\begin{aligned}c_{\mathrm{eff}} \eta_{\ell+k}^2 &\leqslant \|\sigma - \sigma_{\ell+k}\|^2_{L^2(\Omega)} + |u - \mathcal{H} u_{\ell+k}^{\mathrm{NC}}|^2_{H^1(\Omega)} + \operatorname{osc}^2(f, \mathcal{T}_{\ell+k}) \\ &\lesssim \left\|\mathbb{C}^{-1/2} (\sigma - \sigma_{\ell+k})\right\|^2_{L^2(\Omega)} + |u - u_{\ell+k}^{\mathrm{NC}}|^2_{H^1(\mathcal{T}_{\ell+k})} + \|h_{\ell+k} f\|^2_{L^2(\Omega)}.\end{aligned}$$

Together with the standard estimate (5.6) for the energy error, this estimate implies the existence of a λ-independent generic constant $C_\eta > 0$, which is independent of any parameter of Algorithm 3.4 used to solve (5.1), in particular it is independent of α_ε, α_f, θ_A, ρ_B and κ, with

$$\eta_{\ell+k}^2 \leqslant C_\eta \left(\varepsilon_{\ell+k}^2 + \|h_{\ell+k} f\|^2_{L^2(\Omega)}\right). \tag{5.25}$$

The application of (5.22) finally proves (5.24), i.e.,

$$\begin{aligned}\xi_{\ell+k}^2 &\leqslant (C_\eta + \alpha_\varepsilon)\varepsilon_{\ell+k}^2 + (C_\eta + \alpha_f) \|h_{\ell+k} f\|^2_{L^2(\Omega)} \\ &\leqslant 2(C_\eta + \alpha_\varepsilon)\varepsilon_\ell^2 + (8\mu C_{\mathrm{qo}} (C_\eta + \alpha_\varepsilon) + C_\eta + \alpha_f) \|h_\ell f\|^2_{L^2(\Omega)} \\ &\leqslant \left(\frac{2C_\eta}{\alpha_\varepsilon} + 2\right) \alpha_\varepsilon \varepsilon_\ell^2 + \left(\frac{8\mu C_{\mathrm{qo}} (C_\eta + \alpha_\varepsilon) + C_\eta}{\alpha_f} + 1\right) \alpha_f \|h_\ell f\|^2_{L^2(\Omega)} \\ &\leqslant \max\left\{\frac{2C_\eta}{\alpha_\varepsilon} + 2, \frac{8\mu C_{\mathrm{qo}} (C_\eta + \alpha_\varepsilon) + C_\eta}{\alpha_f} + 1\right\} \xi_\ell^2.\end{aligned}$$

Remark 5.4.3 yields $\xi_{\ell+k}^2 \leqslant C_{\mathrm{C}} \xi_\ell^2$ with

$$C_{\mathrm{C}} := \max\left\{\frac{8\mu C_\eta}{C_{\mathrm{J}}} + 2, \frac{16\mu^2 C_\eta}{C_{\mathrm{J}}} + 4\mu + \frac{2\mu C_\eta}{C_{\mathrm{J}} C_{\mathrm{qo}}} + 1\right\}.$$

The constant C_{C} is independent of the special choice of parameters in the algorithm S-AFEM-AA, and in particular it is independent of θ_A and κ. □

Proof of Theorem 5.4.1. To apply Theorem 3.6.3 to prove quasi-optimal convergence for S-AFEM-AA, the two assumptions (3.22) and (3.23) have to be satisfied. The contraction property of ξ_ℓ with $0 < \varrho < 1$ is proven in Theorem 5.3.2. It remains to verify the first assumption (3.22) of Theorem 3.6.3 for each of the Cases (A) and (B).

Verify (3.22) for Case (A) Due to the restrictions imposed upon c_{eff}, C_{qo}, C_{drel}, α_f, α_ε, κ and $\theta_A < \theta_0$ there exists $\tau > 0$ such that

$$0 < \tau^2 < \min\left\{1, \frac{\alpha_\varepsilon\left(1/C_\eta - \kappa\left(1 + C_{\mathrm{qo}} + C_{\mathrm{drel}}\right) - C_{\mathrm{drel}}\theta_A\right)}{2C_{\mathrm{A}}C_{\mathrm{C}}}\right\}, \tag{5.26}$$

with positive constants C_{A} and C_{C} from Lemmas 5.4.2 and 5.4.4. To apply Lemma 3.6.4, it remains to prove that if Case (A) applies in level ℓ, $\mathcal{E}_{\ell\setminus\ell+\epsilon(\ell)}$ fulfils the bulk criterion

$$\theta_A\eta_\ell^2 \leqslant \eta_\ell^2\left(\mathcal{E}_{\ell\setminus\ell+\epsilon(\ell)}\right). \tag{5.27}$$

The restrictions on the choice of θ_A and (5.26) lead to

$$C_{\mathrm{drel}}\theta_A\eta_\ell^2 \leqslant \left(1/C_\eta - \kappa\left(1 + C_{\mathrm{drel}} + C_{\mathrm{qo}}\right)\right)\eta_\ell^2 - \left(2\tau^2 C_{\mathrm{A}}C_{\mathrm{C}}/\alpha_\varepsilon\right)\eta_\ell^2.$$

The combination of (5.20)–(5.22) and (5.24) gives

$$\alpha_\varepsilon\varepsilon_{\ell+\epsilon(\ell)}^2 \leqslant C_{\mathrm{C}}\xi_{\epsilon(\ell)}^2 \leqslant C_{\mathrm{C}}\tau^2\xi_\ell^2 \leqslant C_{\mathrm{A}}C_{\mathrm{C}}\tau^2\eta_\ell^2.$$

Together with (5.25), i.e., $\eta_\ell^2/C_\eta - \|h_\ell f\|_{L^2(\Omega)}^2 \leqslant \varepsilon_\ell^2$, and $\|h_\ell f\|_{L^2(\Omega)}^2 \leqslant \kappa\eta_\ell^2$ these estimates verify

$$C_{\mathrm{drel}}\theta_A\eta_\ell^2 \leqslant \varepsilon_\ell^2 - \left(C_{\mathrm{drel}} + C_{\mathrm{qo}}\right)\|h_\ell f\|_{L^2(\Omega)}^2 - 2\varepsilon_{\ell+\epsilon(\ell)}^2.$$

On the other hand Lemma 5.2.6 and Theorem 5.2.2 and the standard estimate (5.6) show that

$$\begin{aligned}\varepsilon_\ell^2 - 2\varepsilon_{\ell+\epsilon(\ell)}^2 &\leqslant \left|\!\left|\!\left| u_{\ell+\epsilon(\ell)}^{\mathrm{NC}} - u_\ell^{\mathrm{NC}}\right|\!\right|\!\right|_{\mathrm{NC}(\ell+\epsilon(\ell))}^2 + C_{\mathrm{qo}}\|h_\ell f\|_{\mathcal{T}_{\ell\setminus\ell+\epsilon(\ell)}}^2 \\ &\leqslant \left(C_{\mathrm{drel}} + C_{\mathrm{qo}}\right)\|h_\ell f\|_{\mathcal{T}_{\ell\setminus\ell+\epsilon(\ell)}}^2 + C_{\mathrm{drel}}\eta_\ell^2\left(\mathcal{E}_{\ell\setminus\ell+\epsilon(\ell)}\right).\end{aligned}$$

The combination of the previous estimates results in (5.27), the application of Lemma 3.6.4 proves (3.22) in Case (A).

Verify (3.22) for Case (B) Lemma 3.6.6 and (5.20) prove (3.22) for Case (B).

Since α_f, $\alpha_\varepsilon > 0$ are chosen according to the contraction property of Theorem 5.3.2, the application of Theorem 3.6.3 concludes the proof. □

6 The Stokes problem

6.1 Introduction

This chapter presents the analysis of the quasi-optimal convergence of adaptive nonconforming FEM computed using S-AFEM-AA for the discrete version of the Stokes equations (2.5) with respect to the natural approximation classes of Section 3.6.

Adaptive CR-FEM is based on sequences of shape-regular triangulations $\mathcal{T}_\ell$, and the discrete spaces $V_\ell := P^{\rm NC}_{1,0}(\mathcal{T}_\ell) \times P^{\rm NC}_{1,0}(\mathcal{T}_\ell)$ and $Q_\ell := P_0(\mathcal{T}_\ell) \cap L^2_0(\Omega)$. Let

$$a_{{\rm NC}(\ell)}(u^{\rm NC}_\ell, v^{\rm NC}_\ell) := \int_\Omega {\rm D}_\ell\, u^{\rm NC}_\ell : {\rm D}_\ell\, v^{\rm NC}_\ell \,{\rm dx} \quad \text{for all } u^{\rm NC}_\ell, v^{\rm NC}_\ell \in V_\ell$$

define the discrete energy scalar product on V_ℓ and let

$$b_{{\rm NC}(\ell)}(v^{\rm NC}_\ell, q_\ell) := -\int_\Omega q_\ell\, {\rm div}_\ell\, v^{\rm NC}_\ell \,{\rm dx} \quad \text{for all } v^{\rm NC}_\ell \in V_\ell,\ q_\ell \in Q_\ell$$

be the discrete counterpart of the bounded bilinear form b.

The discrete Friedrichs inequality [BS08, (10.6.14)] shows that $a_{{\rm NC}(\ell)}$ is positive definite, and hence, induces a norm $|\!|\!| \cdot |\!|\!|_{{\rm NC}(\ell)} := \|{\rm D}_\ell \cdot\|_{L^2(\Omega)}$ on V_ℓ. Moreover, the inf-sup stability of b yields discrete inf-sup stability of $b_{{\rm NC}(\ell)}$ [CR73]. Thus, there exists a unique discrete solution $(u^{\rm NC}_\ell, p^{\rm NC}_\ell) \in V_\ell \times Q_\ell$ with

$$a_{{\rm NC}(\ell)}(u^{\rm NC}_\ell, v^{\rm NC}_\ell) + b_{{\rm NC}(\ell)}(v^{\rm NC}_\ell, p^{\rm NC}_\ell) = F(v^{\rm NC}_\ell) := (f, v^{\rm NC}_\ell) \quad \text{for all } v^{\rm NC}_\ell \in V_\ell, \tag{6.1.a}$$

$$b_{{\rm NC}(\ell)}(u^{\rm NC}_\ell, q_\ell) = 0 \quad \text{for all } q_\ell \in Q_\ell. \tag{6.1.b}$$

With the given choice $Q_\ell = P_0(\mathcal{T}_\ell) \cap L^2_0(\Omega)$, the discrete conservation of volume (6.1.b) implies ${\rm div}_\ell\, u^{\rm NC}_\ell = 0$. Denote the subspace of discrete divergence-free velocities in V_ℓ with

$$Z^{\rm NC}_\ell := Z^{\rm NC}_{\mathcal{T}_\ell} := \left\{ v^{\rm NC}_\ell \in V_\ell \;\middle|\; {\rm div}_\ell\, v^{\rm NC}_\ell = 0 \right\}.$$

Then, the solution $u^{\rm NC}_\ell \in Z^{\rm NC}_\ell$ of the discrete system (6.1) uniquely solves

$$a_{{\rm NC}(\ell)}(u^{\rm NC}_\ell, z^{\rm NC}_\ell) = F(z^{\rm NC}_\ell) \quad \text{for all } z^{\rm NC}_\ell \in Z^{\rm NC}_\ell.$$

The analysis of [CPR13] employs the algorithm C-AFEM based on the *a posteriori* error estimator of [DDP95]

$$\mu^2_\ell(T) := h^2_T \,\|f\|^2_{L^2(T)} + h_T \sum_{E \in \mathcal{E}(T)} \|[\partial u^{\rm NC}_\ell / \partial s]_E\|^2_{L^2(E)}. \tag{6.2}$$

This chapter considers the adaptive algorithm S-AFEM-AA for (6.1) based on separate marking as in Chapters 4–5 for the Poisson model problem and the pure displacement problem in linear elasticity. The edge-based error estimator of Algorithm 3.4 for S-AFEM-AA

is

$$\eta_\ell^2(E) := \|[\partial u_\ell^{\mathrm{NC}}/\partial s]_E\|_{L^2(E)}^2 . \tag{6.3}$$

The remaining part of this chapter follows the same methodology as in Chapters 4–5. Section 6.2 is a collection of preliminaries, such as the properties of the error estimator, Helmholtz decomposition, discrete reliability and quasi-orthogonality. These results were developed for adaptive algorithms based on collective marking in [CPR13]. Convergence based on estimator reduction is proven in Section 6.3. The final section proves quasi-optimal convergence for s-afem-aa and the Stokes equations.

The numerical experiments provide evidence for quasi-optimal convergence. Their results, given in Section 7.5, reveal the advantages of s-afem and in particular s-afem-aa.

6.2 Preliminaries

This section recalls efficiency, reliability and discrete reliability for the estimator η_ℓ, which are results for μ_ℓ and algorithm c-afem for the Stokes equations from [CPR13]. They are used to prove the convergence and quasi-optimal convergence of s-afem-aa for (6.1) later.

Throughout this section let (u, p) be the exact solution of (2.6) with right-hand side $f \in L^2(\Omega;\mathbb{R}^2)$, and let $(u_\ell^{\mathrm{NC}}, p_\ell^{\mathrm{NC}})$ be the discrete solution of (6.1) on a triangulation $\mathcal{T}_\ell$ refined from $\mathcal{T}_0$, while the discrete velocity $u_{\ell+k}^{\mathrm{NC}}$ and the discrete pressure $p_{\ell+k}^{\mathrm{NC}}$ solve (2.6) for the triangulation $\mathcal{T}_{\ell+k}$ refined from $\mathcal{T}_\ell$.

Theorem 6.2.1 (Efficiency, reliability, discrete reliability, [CPR13, Theorem 3.1])**.** *There exist positive constants c_{eff}, C_{rel}, C_{drel} depending on $\mathcal{T}_0$ but independent of the mesh size h_ℓ such that*

$$\begin{aligned} c_{\mathrm{eff}}\left(\eta_\ell^2 + \|h_\ell f\|_{L^2(\Omega)}^2\right) &\leqslant \|\mathrm{D}\, u - \mathrm{D}_\ell\, u_\ell^{\mathrm{NC}}\|_{L^2(\Omega)}^2 + \|p - p_\ell^{\mathrm{NC}}\|_{L^2(\Omega)}^2 + \mathrm{osc}^2(f,\mathcal{T}_\ell) \\ &\leqslant C_{\mathrm{rel}}\left(\eta_\ell^2 + \|h_\ell f\|_{L^2(\Omega)}^2\right). \end{aligned}$$

Furthermore, discrete reliability holds in the sense that

$$|||u_{\ell+k}^{\mathrm{NC}} - u_\ell^{\mathrm{NC}}|||_{\mathrm{NC}(\ell+k)} + \|p_{\ell+k}^{\mathrm{NC}} - p_\ell^{\mathrm{NC}}\|_{L^2(\Omega)} \leqslant C_{\mathrm{drel}}^{1/2}\left(\eta_\ell(\mathcal{T}_\ell\backslash\mathcal{T}_{\ell+k}) + \|h_\ell f\|_{\mathcal{T}_\ell\backslash\mathcal{T}_{\ell+k}}\right).$$

Proofs of the efficiency and the reliability of Theorem 6.2.1 are given in [DDP95]. The proof of the discrete reliability follows from an orthogonal decomposition and a discrete Poincaré inequality.

The discrete Helmholtz decomposition requires the following notation. Let $\mathbb{R}^{2\times 2}_{\mathrm{dev}}$ denote the set of trace-free 2×2 matrices and $Z_{\mathcal{T}}^{\mathrm{NC}}$ the set of discrete divergence-free Crouzeix–Raviart functions (with homogeneous Dirichlet boundary condition enforced point-wise in the midpoints of boundary edges) with respect to some regular triangulation $\mathcal{T}$. Define

$$X := \left\{v^{\mathrm{C}} \in C(\Omega;\mathbb{R}^2) \cap P_1(\mathcal{T};\mathbb{R}^2) \middle|\ \textstyle\int_\Omega v^{\mathrm{C}}\,\mathrm{dx} = 0 \text{ and } \int_\Omega \mathrm{curl}\, v^{\mathrm{C}}\,\mathrm{dx} = 0\right\}.$$

Theorem 6.2.2 (Discrete Helmholtz decomposition of piecewise constant deviatoric matrices, [CPR13, Theorem 3.2])**.** *The decomposition*

$$P_0(\mathcal{T};\mathbb{R}^{2\times 2}_{\mathrm{dev}}) = \mathrm{D}_{\mathcal{T}}\, Z^{\mathrm{NC}}_{\mathcal{T}} \oplus \operatorname{dev}\operatorname{Curl} X$$

is orthogonal in $L^2(\Omega;\mathbb{R}^{2\times 2}_{\mathrm{dev}})$.

Proof replicated from [CPR13, Theorem 3.2]. Since, for any $z^{\mathrm{NC}}_{\mathcal{T}} \in Z^{\mathrm{NC}}_{\mathcal{T}}$ and any $v^{\mathrm{C}} \in X$,

$$\int_\Omega \mathrm{D}_{\mathcal{T}}\, z^{\mathrm{NC}}_{\mathcal{T}} : \operatorname{dev}\operatorname{Curl} v^{\mathrm{C}}\,\mathrm{dx} = \int_\Omega \mathrm{D}_{\mathcal{T}}\, z^{\mathrm{NC}}_{\mathcal{T}} : \operatorname{Curl} v^{\mathrm{C}}\,\mathrm{dx} = 0,$$

the decomposition is orthogonal. Moreover, the inclusion

$$\mathrm{D}_{\mathcal{T}}\, Z^{\mathrm{NC}}_{\mathcal{T}} \oplus \operatorname{dev}\operatorname{Curl} X \subset P_0(\mathcal{T};\mathbb{R}^{2\times 2}_{\mathrm{dev}})$$

is obvious. Hence, it remains to prove that the dimensions of the two spaces coincide. Since $\dim\left(P_0(\mathcal{T};\mathbb{R}^{2\times 2}_{\mathrm{dev}})\right) = 3|\mathcal{T}|$, we have to show $\dim\left(\operatorname{dev}\operatorname{Curl} X \oplus \dim Z^{\mathrm{NC}}_{\mathcal{T}}\right) = 3|\mathcal{T}|$.

To prove injectivity of the linear operator $\operatorname{dev}\operatorname{Curl} : X \to P_0(\mathcal{T};\mathbb{R}^{2\times 2}_{\mathrm{dev}})$, let $v^{\mathrm{C}} \in X$ with $\operatorname{dev}\operatorname{Curl} v^{\mathrm{C}} = 0$. Since $\int_\Omega \operatorname{tr}\left(\operatorname{Curl} v^{\mathrm{C}}\right)\mathrm{dx} = \int_\Omega \operatorname{curl} v^{\mathrm{C}}\,\mathrm{dx} = 0$ by the definition of X, and since $\operatorname{div}\operatorname{Curl} v^{\mathrm{C}} = 0$, trace-dev-div Lemma 2.1.10 implies that $\operatorname{Curl} v^{\mathrm{C}} = 0$. Since the integral mean of v^{C} is zero, one concludes $v^{\mathrm{C}} = 0$, hence dev Curl is injective.

The injectivity of dev Curl implies

$$\dim(\operatorname{dev}\operatorname{Curl} X) = \dim X = 2|\mathcal{N}| - 3.$$

Since Ω is simply connected, $Z^{\mathrm{NC}}_{\mathcal{T}}$ is spanned by the $|\mathcal{N}(\Omega)| + |\mathcal{E}(\Omega)|$ basis functions given in [Bra01, Chapter III, §7]. Euler's formula proves

$$\dim(\operatorname{dev}\operatorname{Curl} X \oplus \dim Z^{\mathrm{NC}}_{\mathcal{T}}) = \dim\left(\operatorname{dev}\operatorname{Curl} X\right) + \dim\left(Z^{\mathrm{NC}}_{\mathcal{T}}\right) = 3|\mathcal{T}|. \qquad \square$$

Proof of discrete reliability in Theorem 6.2.1. This is from [CPR13, Theorem 3.1]. We will only prove that

$$\left|\!\left|\!\left| u^{\mathrm{NC}}_{\ell+k} - u^{\mathrm{NC}}_{\ell} \right|\!\right|\!\right|_{\mathrm{NC}(\ell+k)} \leqslant C^{1/2}_{\mathrm{drel}} \left(\eta_\ell\left(\mathcal{T}_{\ell\setminus\ell+k}\right) + \|h_\ell f\|_{\mathcal{T}_{\ell\setminus\ell+k}}\right).$$

Since the upper bound of the pressure difference $\left\|p^{\mathrm{NC}}_{\ell+k} - p^{\mathrm{NC}}_{\ell}\right\|_{L^2(\Omega)}$ is not needed in the remaining analysis of this chapter, its proof is omitted; it can be found in [HX08, Lemma 8.1].

The discrete Helmholtz decomposition from Theorem 6.2.2 leads to $\alpha^{\mathrm{NC}}_{\ell+k} \in Z^{\mathrm{NC}}_{\ell+k}$ and $\beta^{\mathrm{C}}_{\ell+k} \in C(\Omega;\mathbb{R}^2) \cap P_1(\mathcal{T}_{\ell+k};\mathbb{R}^2)$ with

$$\int_\Omega \beta^{\mathrm{C}}_{\ell+k}\,\mathrm{dx} = 0, \quad \int_\Omega \operatorname{curl}\beta^{\mathrm{C}}_{\ell+k}\,\mathrm{dx} = 0, \quad \text{and}$$
$$\mathrm{D}_{\ell+k}\, u^{\mathrm{NC}}_{\ell+k} - \mathrm{D}_\ell\, u^{\mathrm{NC}}_{\ell} = \mathrm{D}_{\ell+k}\,\alpha^{\mathrm{NC}}_{\ell+k} + \operatorname{dev}\operatorname{Curl}\beta^{\mathrm{C}}_{\ell+k}.$$

This implies

$$\|\!|u^{\mathrm{NC}}_{\ell+k} - u^{\mathrm{NC}}_{\ell}|\!\|^2_{\mathrm{NC}(\ell+k)} = |\!|\!|\alpha^{\mathrm{NC}}_{\ell+k}|\!|\!|^2_{\mathrm{NC}(\ell+k)} + \left\|\operatorname{dev}\operatorname{Curl}\beta^{\mathrm{C}}_{\ell+k}\right\|^2_{L^2(\Omega)}. \tag{6.4}$$

The nonconforming interpolation $\alpha^{\mathrm{NC}}_{\ell} =: \mathcal{I}^{\mathrm{NC}}_{\ell}\alpha^{\mathrm{NC}}_{\ell+k} \in V_\ell$ of (3.10) is defined uniquely by

$$⨍_E \alpha^{\mathrm{NC}}_{\ell}\,\mathrm{ds} = ⨍_E \alpha^{\mathrm{NC}}_{\ell+k}\,\mathrm{ds} \quad \text{for all } E \in \mathcal{E}_\ell.$$

In fact, since $\alpha^{\mathrm{NC}}_{\ell+k} \in Z^{\mathrm{NC}}_{\ell+k}$, we have $\alpha^{\mathrm{NC}}_{\ell} \in Z^{\mathrm{NC}}_{\ell}$. The identity (3.10) holds for both sides of any $E \in \mathcal{E}_\ell$ and so

$$\int_E \left[\left(\alpha^{\mathrm{NC}}_{\ell+k} - \alpha^{\mathrm{NC}}_{\ell}\right)\mathrm{D}_\ell\, u^{\mathrm{NC}}_{\ell}\right]_E \cdot \nu_E\,\mathrm{ds} = 0 \quad \text{for all } E \in \mathcal{E}_\ell.$$

Moreover, $\alpha^{\mathrm{NC}}_{\ell+k} = \alpha^{\mathrm{NC}}_{\ell}$ on $T \in \mathcal{T}_\ell \cap \mathcal{T}_{\ell+k}$. This leads to

$$\begin{aligned}
|\!|\!|\alpha^{\mathrm{NC}}_{\ell+k}|\!|\!|^2_{\mathrm{NC}(\ell+k)} &= \int_\Omega \left(\mathrm{D}_{\ell+k}\, u^{\mathrm{NC}}_{\ell+k} - \mathrm{D}_\ell\, u^{\mathrm{NC}}_{\ell}\right) : \mathrm{D}_{\ell+k}\,\alpha^{\mathrm{NC}}_{\ell+k}\,\mathrm{dx} \\
&= \int_\Omega f \cdot \alpha^{\mathrm{NC}}_{\ell+k}\,\mathrm{dx} - \sum_{E\in\mathcal{E}_\ell}\int_E [\alpha^{\mathrm{NC}}_{\ell+k}\,\mathrm{D}_\ell\, u^{\mathrm{NC}}_{\ell}]_E \cdot \nu_E\,\mathrm{ds} \\
&= \sum_{T\in\mathcal{T}_{\ell\setminus\ell+k}}\int_T f\cdot\left(\alpha^{\mathrm{NC}}_{\ell+k} - \alpha^{\mathrm{NC}}_{\ell}\right)\mathrm{dx} \\
&\quad - \sum_{E\in\mathcal{E}_\ell}\int_E \left[\left(\alpha^{\mathrm{NC}}_{\ell+k} - \alpha^{\mathrm{NC}}_{\ell}\right)\mathrm{D}_\ell\, u^{\mathrm{NC}}_{\ell}\right]_E \cdot \nu_E\,\mathrm{ds} \\
&\leqslant \sum_{T\in\mathcal{T}_{\ell\setminus\ell+k}} \left(\|f\|_{L^2(T)}\left\|\alpha^{\mathrm{NC}}_{\ell+k} - \alpha^{\mathrm{NC}}_{\ell}\right\|_{L^2(T)}\right).
\end{aligned}$$

The combination of the above estimates and the discrete Poincaré inequality of Lemma 3.2.11 results in

$$|\!|\!|\alpha^{\mathrm{NC}}_{\ell+k}|\!|\!|_{\mathrm{NC}(\ell+k)} \lesssim \|h_\ell f\|_{L^2(\mathcal{T}_{\ell\setminus\ell+k})}. \tag{6.5}$$

An analysis of the second term on the right-hand side of (6.4) requires the Scott–Zhang [SZ90] interpolation $\beta^{\mathrm{C}}_{\ell} := \mathcal{I}_\ell\beta^{\mathrm{C}}_{\ell+k}$ on $\mathcal{T}_\ell$ of Definition 3.2.9. Then $\beta^{\mathrm{C}}_{\ell}$ satisfies

$$\left\|\beta^{\mathrm{C}}_{\ell+k} - \beta^{\mathrm{C}}_{\ell}\right\|_{L^2(E)} = 0 \quad \text{for all } E \in \mathcal{E}_{\ell+k} \cap \mathcal{E}_\ell.$$

On the edge patch Ω^ℓ_E (see Table 3.14 for the definition) for $E \in \mathcal{E}_{\ell\setminus\ell+k}$

$$\left\|\beta^{\mathrm{C}}_{\ell+k} - \beta^{\mathrm{C}}_{\ell}\right\|_{L^2(E)} \lesssim h_E^{1/2}\left\|\beta^{\mathrm{C}}_{\ell+k}\right\|_{H^1(\Omega^\ell_E)}.$$

Since $\int_\Omega \left(\mathrm{D}_{\ell+k}\, u^{\mathrm{NC}}_{\ell+k} - \mathrm{D}_\ell\, u^{\mathrm{NC}}_{\ell}\right) : \operatorname{Curl}\beta^{\mathrm{C}}_{\ell}\,\mathrm{dx} = 0$, this leads to

$$\left\|\operatorname{dev}\operatorname{Curl}\beta^{\mathrm{C}}_{\ell+k}\right\|^2_{L^2(\Omega)} = \int_\Omega \left(\mathrm{D}_{\ell+k}\, u^{\mathrm{NC}}_{\ell+k} - \mathrm{D}_\ell\, u^{\mathrm{NC}}_{\ell}\right) : \operatorname{dev}\operatorname{Curl}\beta^{\mathrm{C}}_{\ell+k}\,\mathrm{dx}$$

$$
\begin{aligned}
&= \int_\Omega \left(\mathrm{D}_{\ell+k}\, u^{\mathrm{NC}}_{\ell+k} - \mathrm{D}_\ell\, u^{\mathrm{NC}}_\ell\right) : \mathrm{Curl}\left(\beta^{\mathrm{C}}_{\ell+k} - \beta^{\mathrm{C}}_\ell\right) \mathrm{dx} \\
&= -\sum_{T\in\mathcal{T}_{\ell+k}} \int_T \mathrm{curl}\left(\mathrm{D}_{\ell+k}\, u^{\mathrm{NC}}_{\ell+k} - \mathrm{D}_\ell\, u^{\mathrm{NC}}_\ell\right) \cdot \left(\beta^{\mathrm{C}}_{\ell+k} - \beta^{\mathrm{C}}_\ell\right) \mathrm{dx} \\
&\quad + \sum_{E\in\mathcal{E}_{\ell+k}} \int_E [\partial u^{\mathrm{NC}}_\ell/\partial s]_E \cdot \left(\beta^{\mathrm{C}}_{\ell+k} - \beta^{\mathrm{C}}_\ell\right) \mathrm{ds} \\
&\leqslant \sum_{E\in\mathcal{E}_{\ell\setminus\ell+k}} \|[\partial u^{\mathrm{NC}}_\ell/\partial s]_E\|_{L^2(E)} \left\|\beta^{\mathrm{C}}_{\ell+k} - \beta^{\mathrm{C}}_\ell\right\|_{L^2(E)} \\
&\lesssim \sum_{E\in\mathcal{E}_{\ell\setminus\ell+k}} h_E^{1/2} \|[\partial u^{\mathrm{NC}}_\ell/\partial s]_E\|_{L^2(E)} \left\|\beta^{\mathrm{C}}_{\ell+k}\right\|_{H^1(\Omega^\ell_E)} \\
&\lesssim \eta_\ell\left(\mathcal{T}_{\ell\setminus\ell+k}\right) \left\|\mathrm{D}\,\beta^{\mathrm{C}}_{\ell+k}\right\|_{L^2(\Omega)}.
\end{aligned}
$$

Since $\left\|\mathrm{D}\,\beta^{\mathrm{C}}_{\ell+k}\right\|_{L^2(\Omega)} \lesssim \left\|\mathrm{dev}\,\mathrm{Curl}\,\beta^{\mathrm{C}}_{\ell+k}\right\|_{L^2(\Omega)}$ this proves

$$
\left\|\mathrm{dev}\,\mathrm{Curl}\,\beta^{\mathrm{C}}_{\ell+k}\right\|_{L^2(\Omega)} \lesssim \eta_\ell\left(\mathcal{T}_{\ell\setminus\ell+k}\right). \tag{6.6}
$$

The combination of (6.4)–(6.6) concludes the proof. □

The following lemma asserts quasi-orthogonality for the Stokes problem with Crouzeix–Raviart FEM as in [CPR13] and for the pure displacement problem in elasticity in [CR12]. The result will be essential in the proof of quasi-optimality below. Quasi-orthogonality for the Poisson model problem was introduced in [CH06a, CH06b] and sharpened for a mixed FEM [BM08]. Its sharpened form has already been employed for the Poisson model problem in Chapters 4 and 5 and will be essential for the proof of quasi-optimality for the Stokes equations.

Lemma 6.2.3 (Quasi-orthogonality, [CPR13, Lemma 4.3])**.** *There exists some positive generic constant C_{qo} such that quasi-orthogonality holds in the sense of*

$$
\left|a_{\mathrm{NC}(\ell+k)}\left(u - u^{\mathrm{NC}}_{\ell+k}, u^{\mathrm{NC}}_{\ell+k} - u^{\mathrm{NC}}_\ell\right)\right| \leqslant C_{\mathrm{qo}}^{1/2} |\!|\!| u - u^{\mathrm{NC}}_{\ell+k} |\!|\!|_{\mathrm{NC}(\ell+k)} \|h_\ell f\|_{\mathcal{T}_{\ell\setminus\ell+k}}.
$$

Without loss of generality we will assume throughout this chapter that

$$
1/2 \leqslant C_{\mathrm{qo}}. \tag{6.7}
$$

Proof replicated from [CPR13, Lemma 4.3]. Let $\mathcal{I}^{\mathrm{NC}}_\ell$ be the nonconforming interpolation operator as in (3.10) and $\mathcal{I}^{\mathrm{NC}}_{\ell+k}$ denote the standard nonconforming interpolation operator of Definition 2.4.3. Since $⨍_E \mathcal{I}^{\mathrm{NC}}_{\ell+k} u\,\mathrm{ds} = ⨍_E u\,\mathrm{ds}$ for all $E \in \mathcal{E}_{\ell+k}$, an integration by parts argument shows

$$
\mathrm{D}_{\ell+k}\,\mathcal{I}^{\mathrm{NC}}_{\ell+k} u\big|_T = ⨍_T \mathrm{D}\,u\,\mathrm{dx} \qquad \text{for } T \in \mathcal{T}_{\ell+k}.
$$

The definition of the interpolation operators lead to

$$\begin{aligned} a_{\mathrm{NC}(\ell+k)}&\left(u-u_{\ell+k}^{\mathrm{NC}},u_{\ell+k}^{\mathrm{NC}}-u_{\ell}^{\mathrm{NC}}\right)\\ &=\int_{\Omega}\left(\mathrm{D}\,u-\mathrm{D}_{\ell+k}\,u_{\ell+k}^{\mathrm{NC}}\right):\mathrm{D}_{\ell+k}\left(u_{\ell+k}^{\mathrm{NC}}-u_{\ell}^{\mathrm{NC}}\right)\mathrm{dx}\\ &=\int_{\Omega}\mathrm{D}_{\ell+k}\left(\mathcal{I}_{\ell+k}^{\mathrm{NC}}u-u_{\ell+k}^{\mathrm{NC}}\right):\mathrm{D}_{\ell+k}\,u_{\ell+k}^{\mathrm{NC}}\,\mathrm{dx}\\ &\quad-\int_{\Omega}\mathrm{D}_{\ell}\left(\mathcal{I}_{\ell}^{\mathrm{NC}}\left(u-u_{\ell+k}^{\mathrm{NC}}\right)\right):\mathrm{D}_{\ell}\,u_{\ell}^{\mathrm{NC}}\,\mathrm{dx}\,. \end{aligned}$$

The integral mean property of $\mathcal{I}_{\ell}^{\mathrm{NC}}$ proves

$$\mathcal{I}_{\ell}^{\mathrm{NC}}u=\mathcal{I}_{\ell}^{\mathrm{NC}}\mathcal{I}_{\ell+k}^{\mathrm{NC}}u\ \text{ and }\ \mathrm{div}_{\ell}\,\mathcal{I}_{\ell}^{\mathrm{NC}}u=\mathrm{div}_{\ell+k}\,\mathcal{I}_{\ell+k}^{\mathrm{NC}}u=0.$$

Hence, with $v_{\ell+k}:=\mathcal{I}_{\ell+k}^{\mathrm{NC}}u-u_{\ell+k}^{\mathrm{NC}}\in V_{\ell+k}$,

$$\begin{aligned} a_{\mathrm{NC}(\ell+k)}&\left(u-u_{\ell+k}^{\mathrm{NC}},u_{\ell+k}^{\mathrm{NC}}-u_{\ell}^{\mathrm{NC}}\right)\\ &=a_{\mathrm{NC}(\ell+k)}\left(u_{\ell+k}^{\mathrm{NC}},\mathcal{I}_{\ell+k}^{\mathrm{NC}}u-u_{\ell+k}^{\mathrm{NC}}\right)-a_{\mathrm{NC}(\ell)}\left(u_{\ell}^{\mathrm{NC}},\mathcal{I}_{\ell}^{\mathrm{NC}}\left(\mathcal{I}_{\ell+k}^{\mathrm{NC}}u-u_{\ell+k}^{\mathrm{NC}}\right)\right)\\ &=F\left(v_{\ell+k}-\mathcal{I}_{\ell+k}^{\mathrm{NC}}v_{\ell+k}\right). \end{aligned}$$

Since $\mathcal{I}_{\ell+k}^{\mathrm{NC}}$ sustains the integral mean on any $E\in\mathcal{E}_{\ell}$, Lemma 3.2.11 proves

$$\left\|v_{\ell+k}-\mathcal{I}_{\ell+k}^{\mathrm{NC}}v_{\ell+k}\right\|_{L^2(T)}\lesssim h_T\left\|\mathrm{D}_{\ell+k}\,v_{\ell+k}\right\|_{L^2(T)}\qquad\text{for all } T\in\mathcal{T}_{\ell}.$$

This concludes the proof,

$$\begin{aligned} &\left|a_{\mathrm{NC}(\ell+k)}\left(u-u_{\ell+k}^{\mathrm{NC}},u_{\ell+k}^{\mathrm{NC}}-u_{\ell}^{\mathrm{NC}}\right)\right|\\ &\quad\lesssim\sum_{T\in\mathcal{T}_{\ell}\setminus\ell+k}\|f\|_{L^2(T)}\,h_T\left\|\mathrm{D}_{\ell+k}\left(\mathcal{I}_{\ell+k}^{\mathrm{NC}}u-u_{\ell+k}^{\mathrm{NC}}\right)\right\|_{L^2(T)}\\ &\quad\lesssim\|h_{\ell}f\|_{\mathcal{T}_{\ell}\setminus\ell+k}\left|\!\left|\!\left|u-u_{\ell+k}^{\mathrm{NC}}\right|\!\right|\!\right|_{\mathrm{NC}(\ell+k)}. \end{aligned}$$

□

6.3 Convergence

This section is devoted to the proof of convergence of the sequences of discrete solutions and triangulations generated by s-afem-aa. The analysis of convergence of the adaptive algorithm based on collective marking (i.e., c-afem for the Stokes equations) can be found in [CPR13].

The analysis of quasi-optimal convergence of Section 6.4 involves error estimator reduction, quasi-orthogonality and the contraction property for a linear combination ξ_{ℓ} of the jumps η_{ℓ}, the volume term $\|h_{\ell}f\|_{L^2(\Omega)}$, and the error in the broken energy norm $\varepsilon_{\ell}:=\left|\!\left|\!\left|u-u_{\ell}^{\mathrm{NC}}\right|\!\right|\!\right|_{\mathrm{NC}(\ell)}$. A similar linear combination including the pressure error is used in [HX08, Theorem 4.4].

The proof of the contraction property is based on the Lemmas 6.2.3 and 6.3.2 on quasi-orthogonality and the estimator reduction. It follows similar arguments as for the Poisson model problem and the pure displacement problem in linear elasticity of Sections 4.3

and 5.3 and for the Poisson model problem and mixed FEM in [CR11].

Theorem 6.3.1 (Contraction property)**.** *Given some bulk parameter $0 < \theta_A < 1$, there exists $0 < \kappa_0$ such that for any $\kappa_1 \in (0, \kappa_0)$ and $0 < \rho_B < 1$ there exist positive α_f, α_ε and $0 < \varrho < 1$, which depend on C_{rel}, C_δ, ρ and C_{qo} from Theorem 6.2.1, and Lemmas 6.2.3 and 6.3.2, such that for all $\kappa \in (\kappa_1, \kappa_0)$ the sequence of triangulations and discrete solutions generated by* S-AFEM-AA *with its total errors $\xi_\ell := \eta_\ell^2 + \alpha_f \|h_\ell f\|^2_{L^2(\Omega)} + \alpha_\varepsilon |\!|\!| u - u_\ell^{\mathrm{NC}} |\!|\!|^2_{\mathrm{NC}(\ell)}$ satisfies a contraction property in the sense that*

$$\xi_{\ell+1}^2 \leqslant \varrho\, \xi_\ell^2 \quad \text{for all } \ell \in \mathbb{N}_0.$$

Lemma 6.3.2 (Estimator reduction)**.** *Let $0 < \theta_A < 1$, $0 < \rho_B < 1$, and $\kappa > 0$ be parameters for algorithm* S-AFEM-AA *to solve the discrete Stokes problem (6.1). Then, for any $0 < \delta < \theta_A(2 - \theta_A)$ there exist positive generic constants C_{J}, C_δ, and a reduction factor$0 < \rho_A$ such that on each level $\ell \in \mathbb{N}_0$ of algorithm* S-AFEM-AA

(a) *in **Case(A)** (i.e., $\|h_\ell f\|^2_{L^2(\Omega)} \leqslant \kappa \eta_\ell^2$) η_ℓ and $\|h_\ell f\|_{L^2(\Omega)}$ satisfy the reduction properties*

$$\eta_{\ell+1}^2 \leqslant \rho_A \eta_\ell^2 + C_\delta \left\| \mathrm{D}_{\ell+1} u_{\ell+1}^{\mathrm{NC}} - \mathrm{D}_\ell u_\ell^{\mathrm{NC}} \right\|^2_{L^2(\Omega)} \quad \text{and} \tag{6.8}$$

$$\|h_{\ell+1} f\|^2_{L^2(\Omega)} \leqslant \|h_\ell f\|^2_{L^2(\Omega)} - 1/2 \, \|h_\ell f\|^2_{\mathcal{T}_\ell \setminus \ell+1}, \tag{6.9}$$

(b) *in **Case(B)** (i.e., $\|h_\ell f\|^2_{L^2(\Omega)} > \kappa \eta_\ell^2$) η_ℓ and $\|h_\ell f\|_{L^2(\Omega)}$ satisfy the reduction properties*

$$\eta_{\ell+1}^2 \leqslant (1 + \delta)\, \eta_\ell^2 + C_\delta \left\| \mathrm{D}_{\ell+1} u_{\ell+1}^{\mathrm{NC}} - \mathrm{D}_\ell u_\ell^{\mathrm{NC}} \right\|^2_{L^2(\Omega)} \quad \text{and} \tag{6.10}$$

$$\|h_{\ell+1} f\|^2_{L^2(\Omega)} \leqslant \rho_B \, \|h_\ell f\|^2_{L^2(\Omega)}. \tag{6.11}$$

Proof. The proof works verbatim as the one for Lemma 5.3.1 and is therefore omitted. □

Proof of Theorem 6.3.1. Let $0 < \theta_A < 1$ and define

$$\delta := \frac{\theta_A}{2} \frac{1}{2 - \theta_A}, \qquad \rho_A := (1 + \delta)\,(1 - \theta_A/2) = 1 - \theta_A/4,$$

$$\gamma := \min \frac{1}{2} \left\{ 1, \frac{1 - \rho_A}{C_\delta C_{\mathrm{rel}}} \right\}, \qquad B := \min \frac{3}{4} \left\{ 1, \frac{1 - \rho_A}{C_\delta C_{\mathrm{rel}}} \right\},$$

$$A := 2\,(C_{\mathrm{qo}} C_\delta / \gamma + C_\delta C_{\mathrm{rel}} B), \qquad \alpha_\varepsilon := (1 - \gamma)\, C_\delta,$$

$$\kappa_0 := \frac{1 - \rho_A - C_\delta C_{\mathrm{rel}} B}{A}.$$

Let $0 < \kappa_1 < \kappa_0 < 1$, $0 < \rho_B < 1$ and define

$$D := \frac{\delta + C_\delta C_{\mathrm{rel}} B}{\kappa_1}, \qquad \alpha_f := \frac{A + D}{1 - \rho_B}.$$

Contraction in Case (A) Lemma 6.3.2 shows that for any $0 < \theta_A < 1$ there exist $0 < \rho_A < 1$ and $0 < C_\delta$ such that

$$\begin{aligned} \eta_{\ell+1}^2 &\leqslant \rho_A \eta_\ell^2 + C_\delta \left\| \mathrm{D}_{\ell+1} u_{\ell+1}^{\mathrm{NC}} - \mathrm{D}_\ell u_\ell^{\mathrm{NC}} \right\|_{L^2(\Omega)}^2, \\ \|h_{\ell+1} f\|_{L^2(\Omega)}^2 &\leqslant \|h_\ell f\|_{L^2(\Omega)}^2 - \frac{1}{2} \|h_\ell f\|_{\mathcal{T}_\ell \setminus \mathcal{T}_{\ell+1}}^2, \\ \|h_\ell f\|_{L^2(\Omega)}^2 &< \kappa \eta_\ell^2. \end{aligned} \tag{6.12}$$

For positive B, and γ quasi-orthogonality of Lemma 6.2.3 plus reliability of Theorem 6.2.1 and the application of Young's inequality prove

$$\begin{aligned} \eta_{\ell+1}^2 &\leqslant \rho_A \eta_\ell^2 + C_\delta \left\| \mathrm{D}_{\ell+1} u_{\ell+1}^{\mathrm{NC}} - \mathrm{D}_\ell u_\ell^{\mathrm{NC}} \right\|_{L^2(\Omega)}^2 \\ &\leqslant \rho_A \eta_\ell^2 + C_\delta \left(\varepsilon_\ell^2 - \varepsilon_{\ell+1}^2 + 2C_{\mathrm{qo}}^{1/2} \|h_\ell f\|_{\mathcal{T}_\ell \setminus \mathcal{T}_{\ell+1}} |u - u_{\ell+1}^{\mathrm{NC}}|_{H^1(\mathcal{T}_{\ell+1})} \right) \\ &\leqslant \rho_A \eta_\ell^2 + C_\delta \varepsilon_\ell^2 + C_\delta (\gamma - 1) \varepsilon_{\ell+1}^2 + \frac{C_\delta C_{\mathrm{qo}}}{\gamma} \|h_\ell f\|_{\mathcal{T}_\ell \setminus \mathcal{T}_{\ell+1}}^2 \\ &\leqslant (\rho_A + B C_{\mathrm{rel}} C_\delta) \eta_\ell^2 + (1 - B) C_\delta \varepsilon_\ell^2 + (\gamma - 1) C_\delta \varepsilon_{\ell+1}^2 \\ &\quad + \frac{C_{\mathrm{qo}} C_\delta}{\gamma} \|h_\ell f\|_{\mathcal{T}_\ell \setminus \mathcal{T}_{\ell+1}}^2 + B C_{\mathrm{rel}} C_\delta \|h_\ell f\|_{L^2(\Omega)}^2. \end{aligned}$$

For any A, $\alpha_f > 0$, $\alpha_\varepsilon = (1 - \gamma) C_\delta$ and $\rho_A = (1 + \delta)(1 - \theta_A/2)$ the previous estimate plus (6.9) and (6.12) yield

$$\begin{aligned} \xi_{\ell+1}^2 &\leqslant (\rho_A + B C_{\mathrm{rel}} C_\delta + A\kappa) \eta_\ell^2 + (1 - B) C_\delta \varepsilon_\ell^2 \\ &\quad + \left(\frac{C_{\mathrm{qo}} C_\delta}{\gamma} - \frac{\alpha_f}{2} \right) \|h_\ell f\|_{\mathcal{T}_\ell \setminus \mathcal{T}_{\ell+1}}^2 + (B C_{\mathrm{rel}} C_\delta - A + \alpha_f) \|h_\ell f\|_{L^2(\Omega)}^2. \end{aligned}$$

The choice of parameters at the beginning of this proof ensures contraction in the sense of $\xi_{\ell+1}^2 \leqslant \varrho_A \xi_\ell^2$ for $\varrho_A < 1$ and for any level $\ell \in \mathbb{N}_0$ of Case (A), namely

$$\varrho_A := \max \left\{ \rho_A + B C_{\mathrm{rel}} C_\delta + A\kappa, \frac{C_\delta (1 - B)}{\alpha_\varepsilon}, 1 - \frac{1}{\alpha_f} \left(\frac{C_{\mathrm{qo}} C_\delta}{\gamma} + B C_{\mathrm{rel}} C_\delta \right) \right\} < 1.$$

Contraction in Case (B) Lemma 6.3.2 shows that for any $0 < \rho_B < 1$ there exist $0 < C_\delta$ such that

$$\begin{aligned} \eta_{\ell+1}^2 &\leqslant (1 + \delta) \eta_\ell^2 + C_\delta \left\| \mathrm{D}_{\ell+1} u_{\ell+1}^{\mathrm{NC}} - \mathrm{D}_\ell u_\ell^{\mathrm{NC}} \right\|_{L^2(\Omega)}^2, \\ \|h_{\ell+1} f\|_{L^2(\Omega)}^2 &\leqslant \rho_B \|h_\ell f\|_{L^2(\Omega)}^2, \\ \kappa \eta_\ell^2 &\leqslant \|h_\ell f\|_{L^2(\Omega)}^2. \end{aligned}$$

Quasi-orthogonality of Lemma 6.2.3 plus reliability Theorem 6.2.1 and the application of Young's inequality prove for $B, \gamma > 0$

$$\begin{aligned} \eta_{\ell+1}^2 &\leqslant (1 + \delta) \eta_\ell^2 + C_\delta \left\| \mathrm{D}_{\ell+1} u_{\ell+1}^{\mathrm{NC}} - \mathrm{D}_\ell u_\ell^{\mathrm{NC}} \right\|_{L^2(\Omega)}^2 \\ &\leqslant (1 + \delta) \eta_\ell^2 + C_\delta \left(\varepsilon_\ell^2 - \varepsilon_{\ell+1}^2 + 2C_{\mathrm{qo}}^{1/2} \|h_\ell f\|_{\mathcal{T}_\ell \setminus \mathcal{T}_{\ell+1}} |u - u_{\ell+1}^{\mathrm{NC}}|_{H^1(\mathcal{T}_{\ell+1})} \right) \end{aligned}$$

$$
\begin{aligned}
&\leqslant (1+\delta)\,\eta_\ell^2 + C_\delta\varepsilon_\ell^2 + (\gamma-1)\,C_\delta\varepsilon_{\ell+1}^2 + C_\delta C_{\mathrm{qo}}/\gamma\,\|h_\ell f\|^2_{\mathcal{T}_\ell\setminus\mathcal{T}_{\ell+1}}\\
&\leqslant ((1+\delta) + BC_{\mathrm{rel}}C_\delta)\,\eta_\ell^2 + (1-B)\,C_\delta\varepsilon_\ell^2 - (\gamma-1)\,C_\delta\varepsilon_{\ell+1}^2\\
&\quad + C_\delta C_{\mathrm{qo}}/\gamma\,\|h_\ell f\|^2_{\mathcal{T}_\ell\setminus\mathcal{T}_{\ell+1}} + BC_{\mathrm{rel}}C_\delta\,\|h_\ell f\|^2_{L^2(\Omega)}\,,\\
\xi_{\ell+1}^2 &\leqslant (1+\delta+BC_{\mathrm{rel}}C_\delta - D\kappa)\,\eta_\ell^2 + (1-B)\,C_\delta\varepsilon_\ell^2\\
&\quad + (C_{\mathrm{qo}}C_\delta/\gamma + BC_{\mathrm{rel}}C_\delta + D + \alpha_f\rho_B)\,\|h_\ell f\|^2_{L^2(\Omega)}\,.
\end{aligned}
$$

The choice of parameters at the beginning of this proof ensures contraction in the sense of $\xi_{\ell+1}^2 \leqslant \varrho_B\xi_\ell^2$ for $\varrho_B < 1$ and on any level $\ell \in \mathbb{N}_0$ of Case (B), namely

$$
\begin{aligned}
0 < \varrho_B := \max\{&1+\delta+C_\delta C_{\mathrm{rel}}B - D\kappa, C_\delta\,(1-B)\,/\alpha_\varepsilon,\\
&\rho_B + (C_{\mathrm{qo}}C_\delta/\gamma + BC_\delta C_{\mathrm{rel}} + D)\,/\alpha_f\} < 1.
\end{aligned}
$$

Conclusion Hence, for given $0 < \theta_A < 1$, $0 < \kappa_1 < \kappa_0$, there exist positive parameters α_f, α_ε, such that for all $\kappa \in (\kappa_1, \kappa_0)$ and on any level ℓ with Case (A) or (B) the total error $\xi_\ell^2 := \eta_\ell^2 + \alpha_f\,\|h_\ell f\|^2_{L^2(\Omega)} + \alpha_\varepsilon\varepsilon_\ell^2$ satisfies the contraction property $\xi_{\ell+1}^2 < \varrho\xi_\ell^2$ and

$$
0 < \varrho := \max\{\varrho_A, \varrho_B\} < 1. \qquad \square
$$

To emphasise that the parameters α_ε, α_f do not depend on $0 < \kappa$, the parameter $\kappa_1 \in (0, \kappa_0)$ is introduced, see Remark 4.3.3 for the Poisson model problem. The specific choice of parameters in the proof of Theorem 6.3.1 shows that contraction is ensured for any choice of $\kappa \in (\kappa_1, \kappa_0)$.

6.4 Optimal convergence rates

This section proves the quasi-optimality of s-afem-aa when applied to the Stokes problem (6.1). The proof is based on the contraction property (Theorem 6.3.1), discrete reliability (Theorem 6.2.1), and quasi-orthogonality (Lemma 6.2.3) from the previous Sections 6.2–6.3.

Theorem 6.4.1 (Optimal convergence)**.** *Given a coarse, regular triangulation $\mathcal{T}_0$, let c_{eff}, C_{qo}, C_{drel} be positive generic constants from Theorem 6.2.1 and Lemma 6.2.3. Furthermore, let $s > 0$ be such that $(u, f) \in \mathcal{A}_s$ for the exact velocity u of the Stokes equations (2.6) with right-hand side $f \in L^2(\Omega)$. Let $0 < \theta_A < \theta_0 := \min\{1, 1/(C_\eta C_{\mathrm{drel}})\}$ be the bulk parameter for Case (A) of* s-afem *AA. Consider the positive parameters $\kappa_1 \in (0, \kappa_2)$ with $\kappa_2 := \min\{\kappa_0, C_{\mathrm{drel}}\,(\theta_0 - \theta_A)\,/\,(1 + C_{\mathrm{drel}} + C_{\mathrm{qo}})\}$ and κ_0, α_f, α_ε and $0 < \rho < 1$ as chosen in the proof of Theorem 6.3.1.*

Then, for all $\kappa \in (\kappa_1, \kappa_0)$ the algorithm s-afem-aa *generates a sequence of triangulations $\mathcal{T}_\ell$ and discrete solutions $(u_\ell^{\mathrm{NC}}, p_\ell^{\mathrm{NC}})$ of (6.1) with optimal rate of convergence in the following sense*

$$
|\mathcal{T}_\ell| - |\mathcal{T}_0| \lesssim \xi_\ell^{-1/s} \qquad \text{with } \xi_\ell^2 := \eta_\ell^2 + \alpha_f\,\|h_\ell f\|^2_{L^2(\Omega)} + \alpha_\varepsilon\varepsilon_\ell^2.
$$

In the proof of Theorem 6.4.1, Lemmas 6.4.2 and 6.4.4 and Remark 6.4.3 summarise essential estimates.

Lemma 6.4.2. *Given C_{rel}, α_ε, α_f and κ from Theorems 6.2.1 and 6.3.1, there exist generic positive constants C_{A}, C_{B} such that the weighted term ξ_ℓ for triangulation $\mathcal{T}_\ell$ of the energy error ε_ℓ, the estimated error η_ℓ and the volume term $\|h_\ell f\|_{L^2(\Omega)}$ satisfy*

$$\xi_\ell^2 \leqslant \begin{cases} C_{\mathrm{A}}\eta_\ell^2 & \text{if Case (A) applies,} \\ C_{\mathrm{B}}\,\|h_\ell f\|_{L^2(\Omega)}^2 & \text{if Case (B) applies,} \quad \text{and} \end{cases} \tag{6.13}$$

$$\xi_\ell^2 \approx \varepsilon_\ell^2 + \|h_\ell f\|_{L^2(\Omega)}^2 . \tag{6.14}$$

Proof. (6.13) is proven using reliability and the specific relation of the estimated error and the volume term in both Cases (A) and (B) with

$$1 + \alpha_\varepsilon C_{\mathrm{rel}} + (\alpha_\varepsilon C_{\mathrm{rel}} + \alpha_f)\,\kappa < 1 + \alpha_\varepsilon C_{\mathrm{rel}} + (\alpha_\varepsilon C_{\mathrm{rel}} + \alpha_f)\,\kappa_2 =: C_{\mathrm{A}},$$
$$\frac{1 + \alpha_\varepsilon C_{\mathrm{rel}}}{\kappa} + \alpha_\varepsilon C_{\mathrm{rel}} + \alpha_f < \frac{1 + \alpha_\varepsilon C_{\mathrm{rel}}}{\kappa_1} + \alpha_\varepsilon C_{\mathrm{rel}} + \alpha_f =: C_{\mathrm{B}}.$$

(6.14) follows directly from the efficiency of Theorem 6.2.1 of η_ℓ and the estimate

$$\|p - p_\ell^{\mathrm{NC}}\|_{L^2(\Omega)} \lesssim |\!|\!| u - u_\ell^{\mathrm{NC}} |\!|\!|_{\mathrm{NC}(\ell)} + \|h_\ell f\|_{L^2(\Omega)}$$

of [DDP95, Remark 3.2]. Note, C_{A}, C_{B} depend on κ_1 or κ_2 but are independent of κ as long as $\kappa \in (\kappa_1, \kappa_2)$. □

Remark 6.4.3. *Note that $C_{\mathrm{J}} > 0$ from Lemma 6.3.2 solely depends on $\mathcal{T}_0$. The definitions of parameters and constants in the proof of Theorem 6.3.1 verify*

$$\frac{2C_{\mathrm{qo}}}{\alpha_f} \leqslant \frac{\gamma\,(1-\rho_B)}{C_\delta} = \frac{\gamma\,(1-\gamma)\,(1-\rho_B)}{\alpha_\varepsilon} \leqslant \frac{1}{\alpha_\varepsilon} \leqslant \frac{2}{C_\delta} \leqslant \frac{2}{C_{\mathrm{J}}}$$

and thus

$$\frac{1}{\alpha_\varepsilon} \leqslant \frac{2}{C_{\mathrm{J}}}, \qquad\qquad \frac{\alpha_\varepsilon}{\alpha_f} \leqslant \frac{1}{2C_{\mathrm{qo}}}.$$

Lemma 6.4.4. *Given C_{qo} from Lemma 6.2.3, and α_ε, α_f as chosen in Theorem 6.3.1, let $\mathcal{T}_{\ell+k}$ be an admissible refinement of $\mathcal{T}_\ell$. Then, there exists a positive generic constant C_{C} such that the weighted terms ξ_ℓ and $\xi_{\ell+k}$ satisfy*

$$\varepsilon_{\ell+k}^2 \leqslant 2\varepsilon_\ell^2 + 4C_{\mathrm{qo}}\,\|h_\ell f\|_{\mathcal{T}_\ell \setminus \ell+k}^2 \tag{6.15}$$

$$\leqslant 8C_{\mathrm{qo}}\left(\varepsilon_\ell^2 + \|h_\ell f\|_{L^2(\Omega)}^2 - \|h_{\ell+k} f\|_{L^2(\Omega)}^2\right), \tag{6.16}$$

$$\alpha_\varepsilon \varepsilon_{\ell+k}^2 \leqslant \xi_{\ell+k}^2 \leqslant C_{\mathrm{C}}\xi_\ell^2. \tag{6.17}$$

Proof. Quasi-orthogonality and Young's inequality lead to

$$\begin{aligned} \varepsilon_{\ell+k}^2 &\leqslant \varepsilon_\ell^2 + 2C_{\mathrm{qo}}^{1/2}\varepsilon_{\ell+k}\,\|h_\ell f\|_{\mathcal{T}_\ell \setminus \ell+k} - \left\|p_{\ell+k}^{\mathrm{NC}} - p_\ell^{\mathrm{NC}}\right\|_{L^2(\Omega)}^2 \\ &\leqslant \varepsilon_\ell^2 + 2C_{\mathrm{qo}}\,\|h_\ell f\|_{\mathcal{T}_\ell \setminus \ell+k}^2 + \varepsilon_{\ell+k}^2/2 - \left\|p_{\ell+k}^{\mathrm{NC}} - p_\ell^{\mathrm{NC}}\right\|_{L^2(\Omega)}^2 . \end{aligned}$$

This implies (6.15). Finally, the reduction of the volume term (3.7) and the convention $1/4 \leqslant C_{\mathrm{qo}}$ of (6.7) prove (6.16) via

$$\varepsilon_{\ell+k}^2 \leqslant 2\varepsilon_\ell^2 + 8C_{\mathrm{qo}} \|h_\ell f\|_{L^2(\Omega)}^2 - 8C_{\mathrm{qo}} \|h_{\ell+k} f\|_{L^2(\Omega)}^2 .$$

The efficiency of Theorem 6.2.1 and the equivalence of Proposition 3.6.2 verify

$$\begin{aligned} c_{\mathrm{eff}} \eta_{\ell+k}^2 &\leqslant \varepsilon_{\ell+k}^2 + \|p - p_{\ell+k}^{\mathrm{NC}}\|_{L^2(\Omega)}^2 + \operatorname{osc}^2(f, \mathcal{T}_{\ell+k}) \\ &\approx \varepsilon_{\ell+k}^2 + \|h_{\ell+k} f\|_{L^2(\Omega)}^2 . \end{aligned}$$

This implies the existence of a positive generic constant C_η with

$$\eta_{\ell+k}^2 \leqslant C_\eta \left(\varepsilon_{\ell+k}^2 + \|h_{\ell+k} f\|_{L^2(\Omega)}^2 \right). \tag{6.18}$$

The application of (6.15) finally proves (6.17), i.e.,

$$\begin{aligned} \xi_{\ell+k}^2 &\leqslant (C_\eta + \alpha_\varepsilon)\, \varepsilon_{\ell+k}^2 + (C_\eta + \alpha_f) \|h_{\ell+k} f\|_{L^2(\Omega)}^2 \\ &\leqslant 2\,(C_\eta + \alpha_\varepsilon)\, \varepsilon_\ell^2 + (4C_{\mathrm{qo}}\,(C_\eta + \alpha_\varepsilon) + C_\eta + \alpha_f) \|h_\ell f\|_{L^2(\Omega)}^2 \\ &\leqslant \left(\frac{2C_\eta}{\alpha_\varepsilon} + 2 \right) \alpha_\varepsilon \varepsilon_\ell^2 + \left(\frac{4C_{\mathrm{qo}}\,(C_\eta + \alpha_\varepsilon) + C_\eta}{\alpha_f} + 1 \right) \alpha_f \|h_\ell f\|_{L^2(\Omega)}^2 \\ &\leqslant \max\left\{ \frac{2C_\eta}{\alpha_\varepsilon} + 2, \frac{4C_{\mathrm{qo}}\,(C_\eta + \alpha_\varepsilon) + C_\eta}{\alpha_f} + 1 \right\} \xi_\ell^2 . \end{aligned}$$

Finally, Remark 6.4.3 yields $\xi_{\ell+k}^2 \leqslant C_{\mathrm{C}} \xi_\ell^2$ with

$$C_{\mathrm{C}} := \frac{4C_\eta}{C_{\mathrm{J}}} + \frac{C_\eta}{C_{\mathrm{J}} C_{\mathrm{qo}}} + 3.$$

The constant C_{C} is independent of the special choice of parameters in the algorithm s-afem-aa, and in particular it is independent of θ_A and κ. □

Proof of Theorem 6.4.1. To apply Theorem 3.6.3 to prove quasi-optimal convergence for s-afem-aa, the two assumptions (3.22) and (3.23) have to be satisfied. The contraction property of ξ_ℓ with $0 < \varrho < 1$ is proven in Theorem 6.3.1 for s-afem-aa. It remains to verify the first assumption (3.22) of Theorem 3.6.3 for each of the Cases (A) and (B).

Verify (3.22) for Case (A) Due to the restrictions imposed upon c_{eff}, C_{qo}, C_{drel}, α_f, α_ε, κ and $0 < \theta_A < \theta_0$ there exists $\tau > 0$ such that

$$0 < \tau^2 < \min\left\{ 1, \frac{\alpha_\varepsilon\,(1/C_\eta - \kappa\,(1 + C_{\mathrm{drel}} + C_{\mathrm{qo}}) - C_{\mathrm{drel}}\theta_A)}{2C_{\mathrm{A}} C_{\mathrm{C}}} \right\}, \tag{6.19}$$

with positive constants C_{A} and C_{C} from Lemmas 6.4.2 and 6.4.4. To apply Lemma 3.6.4, it remains to prove that if Case (A) applies in level ℓ, $\mathcal{E}_{\ell \setminus \ell+\epsilon(\ell)}$ fulfils the bulk criterion

$$\theta_A \eta_\ell^2 \leqslant \eta_\ell^2(\mathcal{E}_{\ell \setminus \ell+\epsilon(\ell)}). \tag{6.20}$$

The restrictions on the choice of θ_A and (6.19) lead to

$$C_{\mathrm{drel}}\theta_A\eta_\ell^2 \leqslant (1/C_\eta - \kappa\,(1 + C_{\mathrm{drel}} + C_{\mathrm{qo}}))\,\eta_\ell^2 - \left(2\tau^2 C_{\mathrm{A}} C_{\mathrm{C}}/\alpha_\varepsilon\right)\eta_\ell^2.$$

The combination of (6.13)–(6.15) and (6.17) gives

$$\alpha_\varepsilon \varepsilon^2_{\ell+\epsilon(\ell)} \leqslant C_{\mathrm{C}}\xi^2_{\epsilon(\ell)} \leqslant C_{\mathrm{C}}\tau^2\xi_\ell^2 \leqslant C_{\mathrm{A}}C_{\mathrm{C}}\tau^2\eta_\ell^2.$$

Together with (6.18), i.e., $\eta_\ell^2/C_\eta - \|h_\ell f\|^2_{L^2(\Omega)} \leqslant \varepsilon_\ell^2$ and $\|h_\ell f\|^2_{L^2(\Omega)} \leqslant \kappa\eta_\ell^2$ these estimates verify

$$C_{\mathrm{drel}}\theta_A\eta_\ell^2 \leqslant \varepsilon_\ell^2 - (C_{\mathrm{drel}} + C_{\mathrm{qo}})\,\|h_\ell f\|^2_{L^2(\Omega)} - 2\varepsilon^2_{\ell+\epsilon(\ell)}.$$

On the other hand Lemma 6.2.3 and Theorem 6.2.1 show that

$$\begin{aligned}\varepsilon_\ell^2 - 2\varepsilon^2_{\ell+\epsilon(\ell)} &\leqslant \left\|p^{\mathrm{NC}}_{\ell+\epsilon(\ell)} - p^{\mathrm{NC}}_\ell\right\|^2_{L^2(\Omega)} + C_{\mathrm{qo}}\,\|h_\ell f\|^2_{\mathcal{T}_{\ell\setminus\ell+\epsilon(\ell)}}\\ &\leqslant (C_{\mathrm{drel}} + C_{\mathrm{qo}})\,\|h_\ell f\|^2_{\mathcal{T}_{\ell\setminus\ell+\epsilon(\ell)}} + C_{\mathrm{drel}}\eta_\ell^2\left(\mathcal{E}_{\ell\setminus\ell+\epsilon(\ell)}\right).\end{aligned}$$

The combination of the previous estimates results in (6.20), the application of Lemma 3.6.4 proves (3.22) in Case (A).

Verify (3.22) for Case (B) Lemma 3.6.6 and (6.13) prove (3.22) for Case (B).

Since α_f, $\alpha_\varepsilon > 0$ are chosen according to the contraction property of Theorem 6.3.1, the application of Theorem 3.6.3 concludes the proof. □

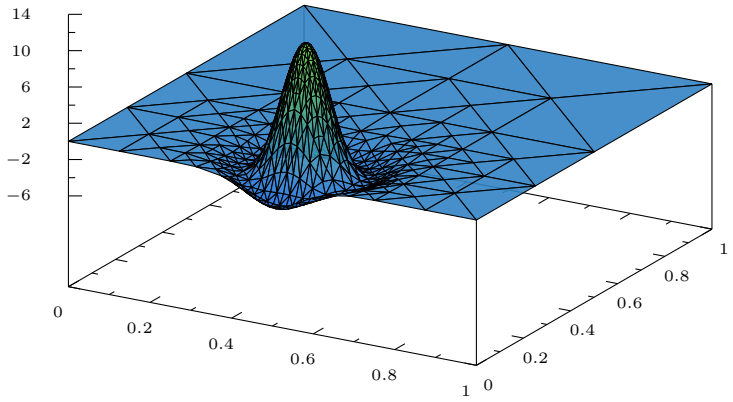

Figure 7.1: Visualisation of the right-hand side function $f \in L^2(\Omega)$ in Section 7.1. The triangulation $\mathcal{T}_4$ of S-AFEM-AA with the parameters of Figure 7.2 is plotted on the graph to highlight the 3D shape of the function.

7 Numerical experiments

This chapter discusses the numerical experiments for the three model problems: the Poisson model problem, the pure displacement problem in linear elasticity and the Stokes problem. The results were computed using the three adaptive Algorithms 3.1, 3.3 and 3.4. The convergence behaviours as well as the demand for computational resources are compared. The quasi-optimal convergence of S-AFEM-AA for all three model problems as analysed in Chapters 4–6 is verified numerically. The flexibility of the adaptive algorithms, in particular of S-AFEM-AA, allows a reduction in the number of levels of the pre-asymptotic range, which is apparent in the convergence graphs.

Graphs of the numerical experiments are shown for each model problem. There are detailed explanations for how to read the figures (especially the legend) for the first benchmark problem in Section 7.1. These explanations also serve as a reference for the figures in Sections 7.3–7.5.

7.1 A first benchmark problem for the Poisson model problem with known exact solution

This section presents the numerical results of the three adaptive algorithms: C-AFEM, S-AFEM-AA and S-AFEM-DM for the Poisson model problem and a given exact solution. The differences in functionality are revealed.

The experiments show that the discrete solutions of each of the three algorithms converge with an optimal rate. The known exact solution is used to investigate the energy error. This benchmark is motivated by the numerical computations in [BM08, LW] for the Poisson

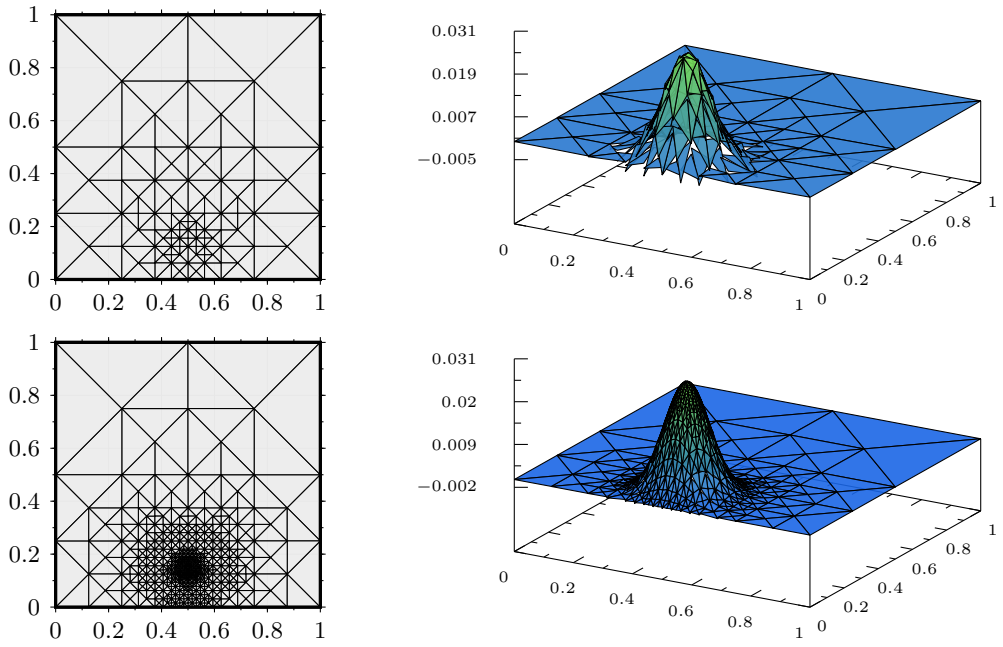

Figure 7.2: Triangulation and corresponding discrete CR solution computed with S-AFEM-AA: $\theta_A = 0.2$, $\rho_B = 0.1$, $\kappa = 0.1$ on levels $\ell = 3$ (top, `ndof` $= 244$) and $\ell = 4$ (bottom, `ndof` $= 1522$) for the benchmark problem of Section 7.1. This is abbreviated as follows $\ell = 3, 4$ with `ndof` $= 244, 1522$.

model problem and reads

$$\Delta u + f = 0 \quad \text{in } \Omega := (0,1)^2 \qquad \text{and} \qquad u = 0 \quad \text{on } \partial\Omega.$$

The data $f \in L^2(\Omega)$ and $u_D \equiv 0$ are given through the exact solution

$$u(x) := x_1(1-x_1)x_2(1-x_2)\exp(-100\,|x-(1/2,1/2)|) \quad \text{for } x = (x_1, x_2) \in \Omega.$$

The initial uniform mesh $\mathcal{T}_0$ consists of eight congruent, right isosceles triangles aligned to the principal diagonal as displayed in Figure 7.3.

Figure 7.1 visualises the right-hand side function $f \in L^2(\Omega)$, while Figure 7.2 shows the nonconforming solutions u_ℓ^{NC} of the problem and the corresponding triangulations computed by S-AFEM-AA and parameter values $\theta_A = 0.2$, $\rho_B = 0.1$ and $\kappa = 0.1$. The figure shows the result for two levels: $\ell = 3$ (top with `ndof` $= 244$) and $\ell = 4$ (bottom with `ndof` $= 1522$); in short $\ell = 3, 4$ with `ndof` $= 244, 1522$. This abbreviation is used in the following figures as well.

Besides the standard convergence plots, this chapter presents plots, which give a visual comparison of the different adaptive algorithms versus uniform mesh refinements.

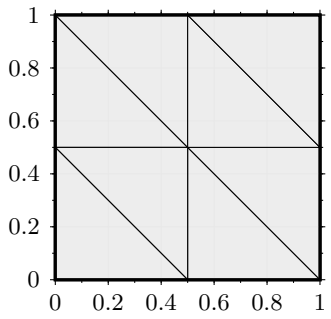

Figure 7.3: Initial triangulation for the Poisson model problem of Section 7.1.

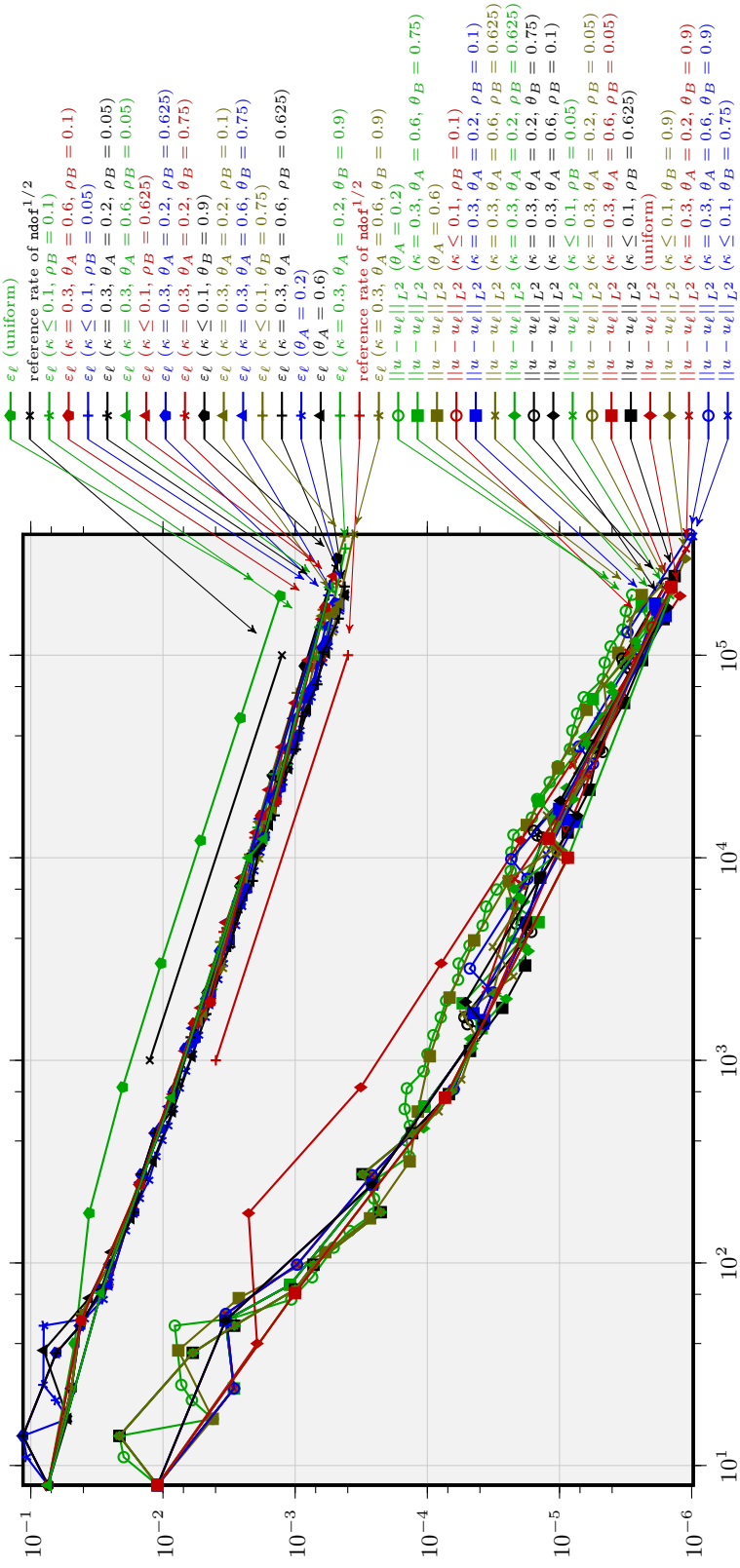

Figure 7.4: Optimal convergence of all three algorithms for the energy error ε_ℓ for the benchmark problem of Section 7.1.

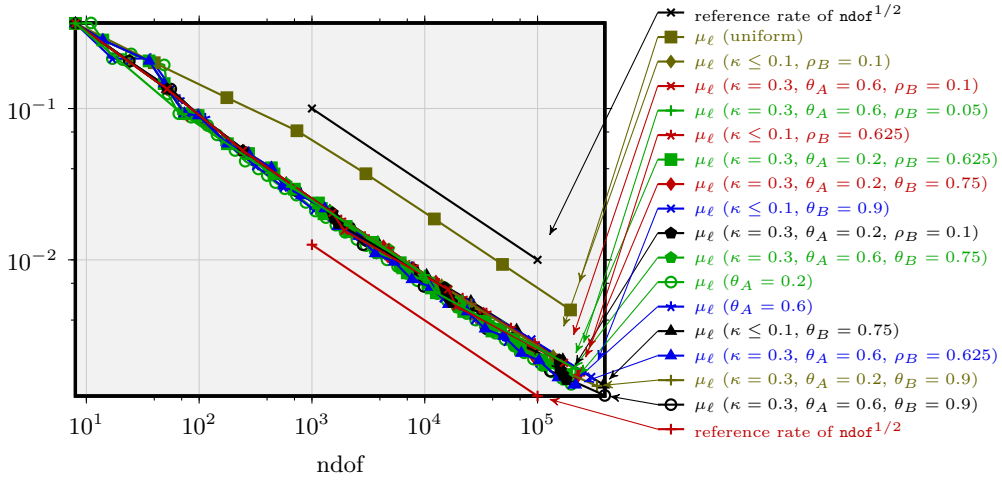

Figure 7.5: Optimal convergence of all three algorithms of the estimated error μ_ℓ for the benchmark problem of Section 7.1.

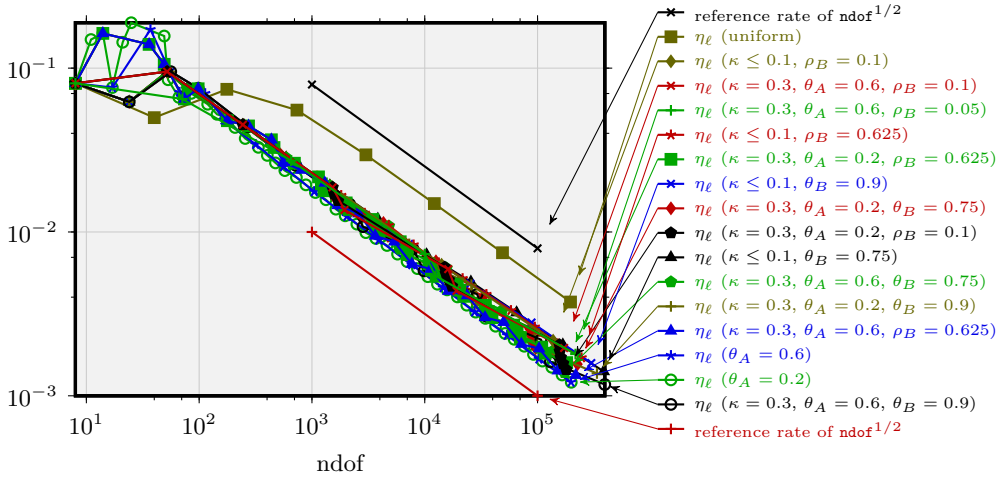

Figure 7.6: Optimal convergence of all three algorithms of the estimated error η_ℓ for the benchmark problem of Section 7.1.

As well as evaluating the numerical results of this first example, the purpose of this section is to explain how to interpret these graphs.

Convergence plots

The convergence plots show the exact errors (i.e., the L^2 error and the energy error ε_ℓ in Figure 7.4) and one of the refinement indicators (μ_ℓ, η_ℓ or $\|h_\ell f\|_{L^2(\Omega)}$ in Figures 7.5–7.7) versus the number of degrees of freedom (`ndof`) in double-logarithmic scaling. At the side of the figure, the legends give the plotted quantity and in parentheses the parameters used. The presence of κ and either θ_B or ρ_B indicates that the graph is for S-AFEM-DM or S-AFEM-AA, respectively; it is for C-AFEM if only θ_A is present. The key word "uniform" denotes uniform mesh refinements. As introduced in the previous chapters, μ_ℓ corresponds

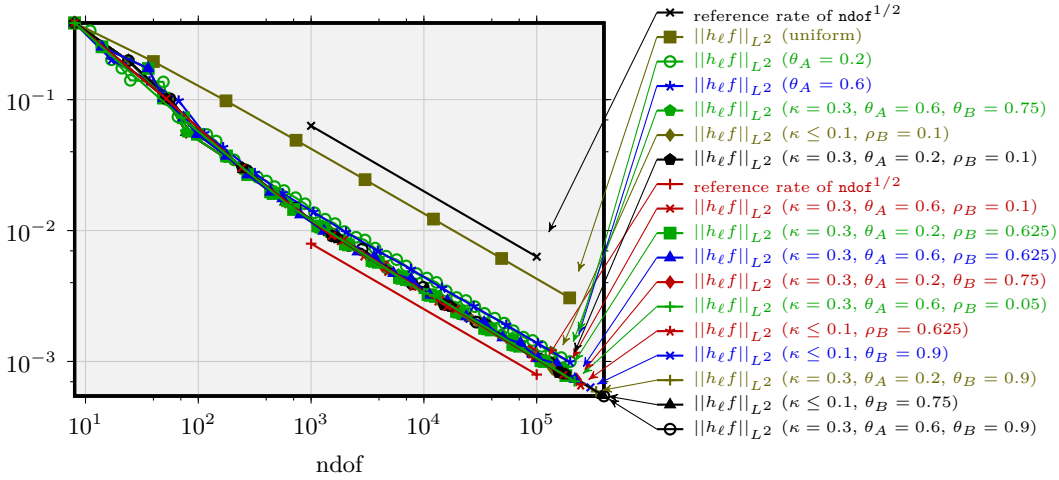

Figure 7.7: Optimal convergence of all three algorithms of the volume term $\|h_\ell f\|_{L^2(\Omega)}$ for the benchmark problem of Section 7.1.

to the collective error estimator (4.3) for the Poisson model problem ((5.3) for linear elasticity or (6.2) for the Stokes equations), which is used as refinement indicator for C-AFEM. In contrast, η_ℓ and $\|h_\ell f\|_{L^2(\Omega)}$ are the refinement indicators from (4.2) for the Poisson model problem ((5.2) for linear elasticity or (6.3) for the Stokes equations) for S-AFEM-DM and S-AFEM-AA.

Figure 7.4 displays the convergence behaviour of the L^2 error and the energy error. The empirical convergence curves of the energy error are together in the upper bundle in Figure 7.4. They exhibit the optimal convergence rate of 1/2 starting at about $\texttt{ndof} = 70$ for the adaptive algorithms C-AFEM, S-AFEM-DM and S-AFEM-AA. Uniform refinement shows the same convergence rate for the energy error with a somewhat larger constant and a larger pre-asymptotic range up to about $\texttt{ndof} = 700$.

For S-AFEM-AA and small values of ρ_B, the pre-asymptotic range even vanishes, for example for $\kappa = 0.3$, $\theta_A = 0.6$ and $\rho_B = 0.05$.

Obviously, convergence is also achieved for the L^2 norm; see the lower bundle of curves in Figure 7.4. However, the sequence of discrete solutions based on uniform mesh refinements converges faster than that for the adaptive schemes for the L^2 norm; see Figure 7.4. As stressed in [DS11], one cannot expect simultaneous optimal convergence of the energy norm and the L^2 norm of the error.

Similar behaviour is observed for the refinement indicator μ_ℓ (see Figure 7.5) including both the volume term and the jump terms (4.3), as well as for η_ℓ and $\|h_\ell f\|_{L^2(\Omega)}$ in Figures 7.6 and 7.7. All refinement indicators have an optimal convergence rate of 1/2 for the adaptive algorithms tested.

All adaptive schemes have the optimal convergence rate, even for large values of $\|h_\ell f\|_{L^2(\Omega)}$. The expected advantage of S-AFEM-AA is not fully demonstrated by this example.

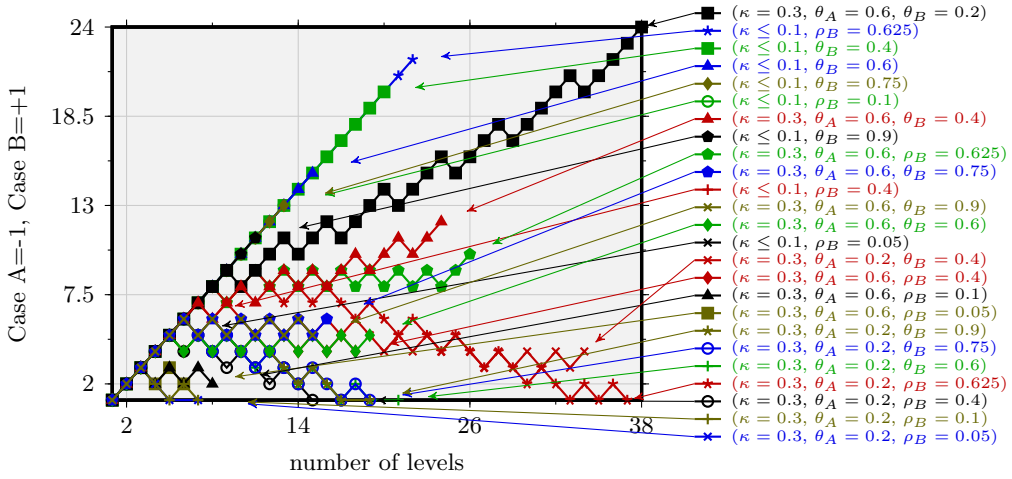

Figure 7.8: Use of Cases (A) and (B) in S-AFEM as a function of the number of levels for the benchmark problem of Section 7.1.

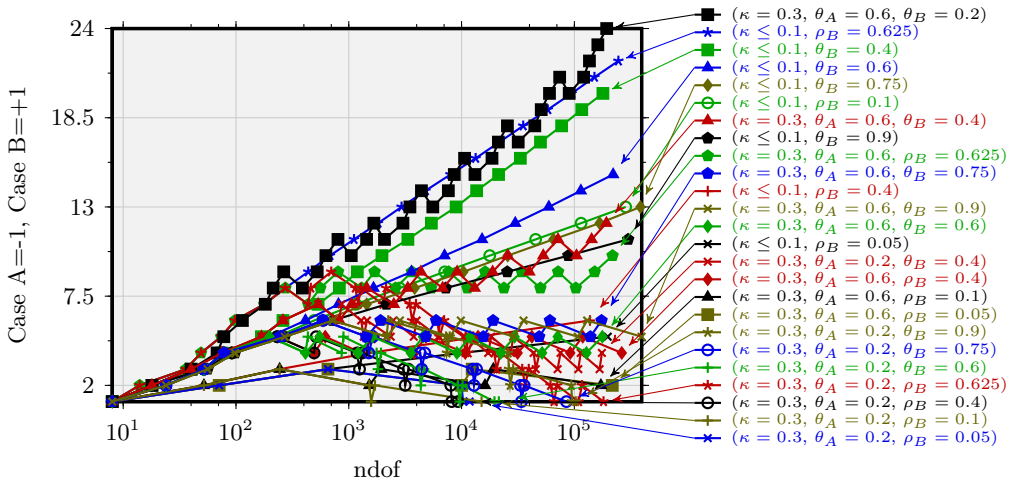

Figure 7.9: Use of Cases (A) and (B) as a function of `ndof` for the benchmark problem of Section 7.1.

Progress of separate marking

Figures 7.8 and 7.9 visualise the use of Cases (A) and (B) by the adaptive algorithms based on separate marking with respect to the application of Cases (A) and (B). On each level, the plotted value increases by 1 if Case (B) applies and decreases by 1 otherwise. For small values of κ (such as $\kappa \leqslant 0.1$), due to the high values of $\|h_\ell f\|_{L^2(\Omega)}$, none of the test scenarios ever triggers Case (B).

As observed in the analysis, the parameter $0 < \rho_B < 1$, which controls the refinement of S-AFEM-AA in Case (B), is unconstrained. Hence, small values of ρ_B are possible, which enforce a fast (i.e., in a small number of levels) but optimal increase of `ndof` to approximate the data appropriately. In S-AFEM-DM, Dörfler marking is applied in both Cases (A) and (B), therefore a similar behaviour cannot be enforced by any parameter set for S-AFEM-DM.

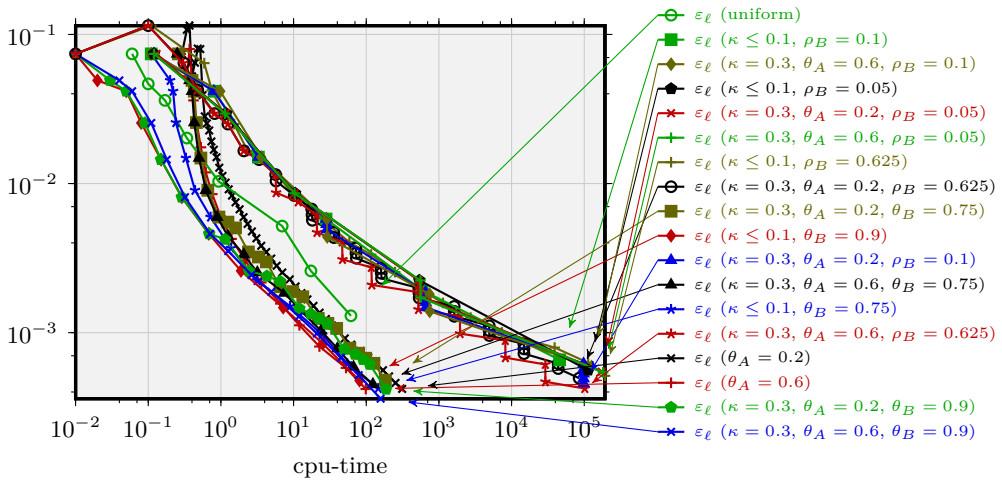

Figure 7.10: Energy error versus overall processing time for the benchmark problem of Section 7.1.

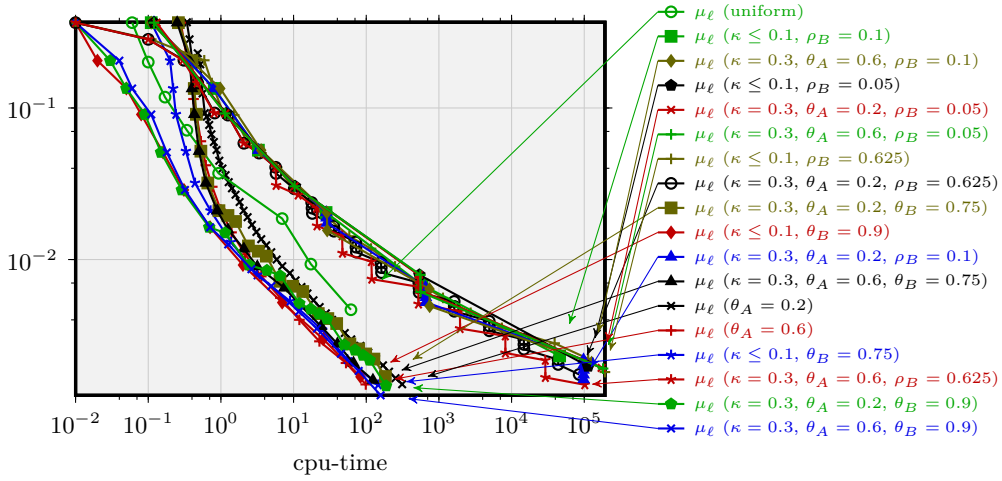

Figure 7.11: μ_ℓ versus overall processing time for the benchmark problem of Section 7.1.

The results are shown in Figures 7.8 and 7.9, where for $\rho_B \leqslant 0.1$ (and $\kappa = 0.3$) only a few levels with Case (B) are necessary before Case (A) is applied for the first time. In general, S-AFEM-AA allows for parameter sets such that only a few iterations with Case (B) are required, while S-AFEM-DM and C-AFEM are restricted to the standard level-oriented NVB refinements as depicted in Figure 3.5 for one level and therefore need more iterations to reduce $\|h_\ell f\|_{L^2(\Omega)}$ appropriately. Furthermore, large values of $\theta_A < 1$ in C-AFEM and $\theta_B < 1$ in S-AFEM-DM may require less iterations, but tend to use a suboptimal uniform refinement, which is not the case for small values of $0 < \rho_B$.

It is obvious that for small values of ρ_B (such as $\rho_B = 0.1$ or $\rho_B = 0.05$), `ndof` grows very quickly as long as Case (B) applies. As explained before, the parameters for S-AFEM-DM do not give such extreme control of the volume term due to the Dörfler marking in Case (B).

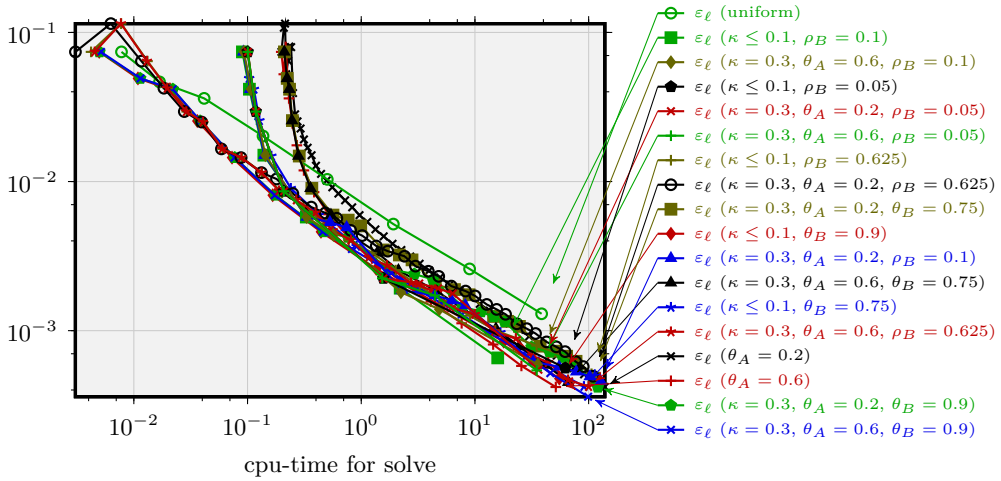

Figure 7.12: Energy error versus cumulative processing time of SOLVE for the benchmark problem of Section 7.1.

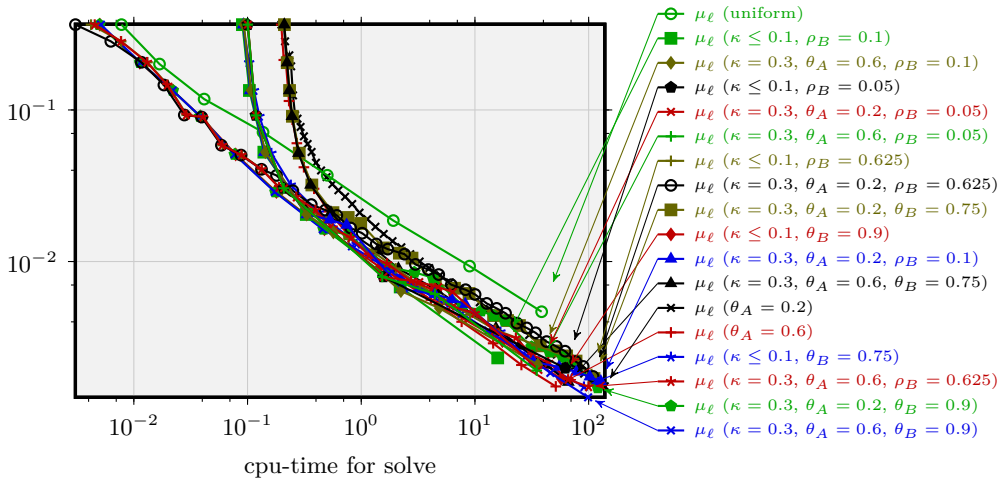

Figure 7.13: μ_ℓ versus cumulative processing time of SOLVE for the benchmark problem of Section 7.1.

Computational costs

To compare the computational costs, terms such as the exact errors and refinement indicators are plotted as a function of the overall processing time and the cumulative processing time of step SOLVE in a double-logarithmic scaling.

Figures 7.10 and 7.11 show the energy error ε_ℓ and the refinement indicator μ_ℓ as a function of the overall processing time, while Figures 7.12 and 7.13 show ε_ℓ and μ_ℓ, versus the cumulative processing time for SOLVE. Both comparisons reveal that μ_ℓ has the same qualitative behaviour as ε_ℓ. Note that ε_ℓ is in general not available (in particular for the benchmark considered below in Section 7.2).

In contrast to these CPU-time-based comparisons, Figures 7.14 and 7.15 display these terms as a function of the level ℓ. Algorithm S-AFEM-AA requires less levels (e.g., with

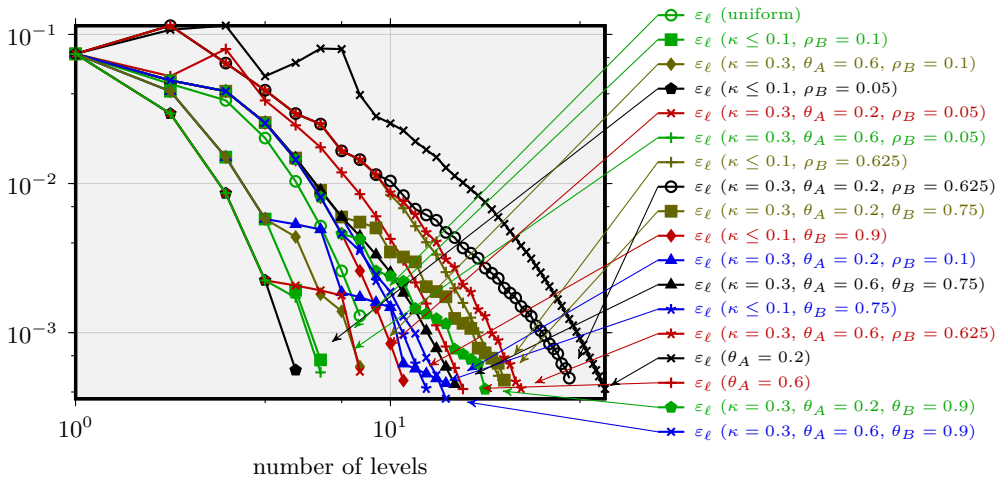

Figure 7.14: Energy error as a function of the number of levels for the benchmark problem of Section 7.1.

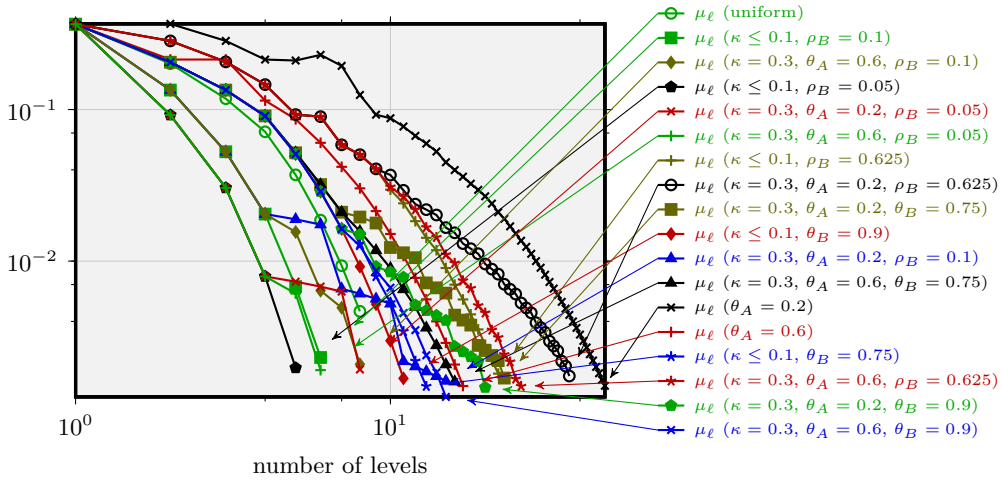

Figure 7.15: μ_ℓ as a function of the number of levels for the benchmark problem of Section 7.1.

$\rho_B = 0.1$ or $\rho_B = 0.05$ and $\kappa \leqslant 0.1$), to resolve the right-hand side $f \in L^2(\Omega)$ sufficiently. However, the computation time is not competitive compared with C-AFEM (e.g., $\theta_A = 0.6$) or S-AFEM-DM (e.g., $\theta_A = 0.2$, $\kappa = 0.3$, $\theta_B = 0.75$). Note that the coding of Algorithm 3.17 has room for improvement. The flexibility of S-AFEM-AA makes it superior to C-AFEM and S-AFEM-DM due to its lower cumulative computational costs for all SOLVE steps. Figures 7.14 and 7.15 show the potential of S-AFEM-AA to reduce computational costs compared to C-AFEM and S-AFEM-DM.

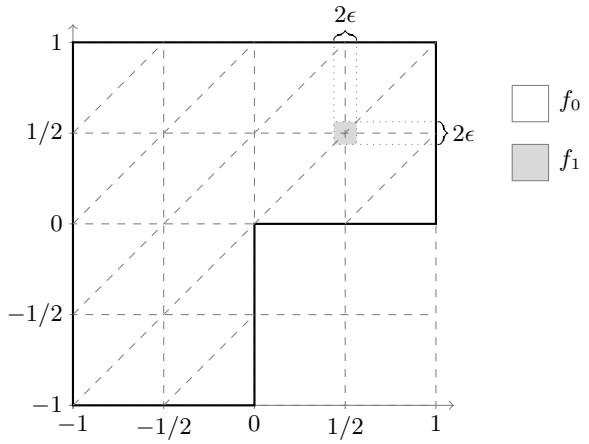

Figure 7.16: The initial triangulation of the L-shaped domain plus a visualisation of the right-hand side function $f \in L^2(\Omega)$.

7.2 General benchmark: L-shaped domain with microstructures

The following artificial benchmark is applied to all three model problems of this thesis, i.e., the Poisson model problem, the pure displacement problem in linear elasticity and the Stokes equations. The benchmark is constructed to emphasise the advantages of AFEMs based on separate marking.

The model problems are solved on an L-shaped domain with homogeneous Dirichlet boundary data and a piecewise constant right-hand side $f \in L^2(\Omega)$, which takes two values $f_0 \equiv 0$ and $f_1 \neq 0$ in Ω as depicted in Figure 7.16. The function $f \in L^2(\Omega)$ vanishes on Ω up to a small rectangular neighbourhood of $(1/2, 1/2)$, with edge length $\epsilon = 2^{-n}$, $n \geqslant 2$. This choice allows for an exact computation of the volume term and an exact integration within the solution step. The initial mesh $\mathcal{T}_0$ divides Ω into 24 congruent triangles with 28 interior edges and 5 interior nodes as shown in Figure 7.16. Note that the parameter ϵ used here denotes the edge length of the small region where $f \in L^2(\Omega)$ does not vanish and should not be confused with the ϵ used in the proof of the optimal convergence rates of Chapters 4–6.

This artificial example simulates a microstructure in a single region. As before, uniform mesh refinement as well as the three adaptive algorithms, C-AFEM, S-AFEM-DM and S-AFEM-AA, are used. The experiments show that S-AFEM-AA is superior in the sense that the size of the pre-asymptotic regime is reduced by a significant number of levels and thus the number of discrete systems that have to be solved is reduced.

By substituting numerical integration with explicit computations, the computational costs for Case (B) are reduced in certain situations, such as the present one. In this situation, the costs of Case (B) are negligible when compared to the total costs of Solve.

Indeed most applications of computational mechanics have a piecewise-constant right-hand side function $f \in L^2(\Omega)$ (as applied in this benchmark problem depicted in Figure 7.16) such that a problem-specific numerical integration is computationally cheap.

The costs of steps Mark and Refine in Cases (A) and (B) are similar if the numerical integration of $f \in L^2(\Omega)$ is not more expensive than the computation of the refinement

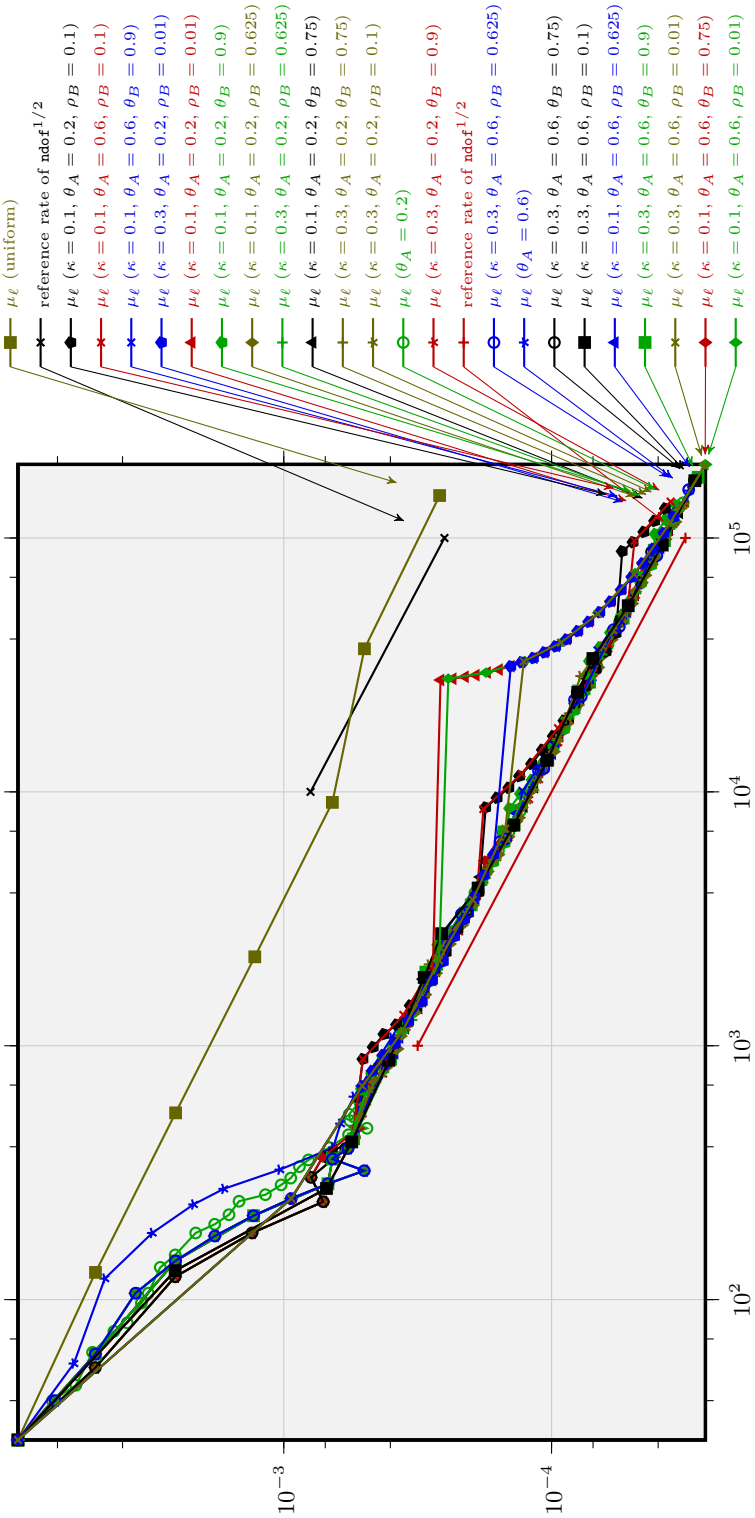

Figure 7.17: μ_ℓ versus `ndof` for the benchmark problem of Section 7.3.

indicator in Case (A) of s-afem (or the error estimator in c-afem). Thus the advantage is the avoidance of the computation time needed to solve the discrete problem. A more complicated $f \in L^2(\Omega)$ (cf. Section 7.1) may lead to high computational costs for Case (B) in s-afem-aa, especially for aa. Furthermore, it is thought the code for Algorithm 3.17 in s-afem-aa as tested can be improved with respect to the required computation time.

As shown in Figures 7.20 and 7.21, s-afem-aa is inferior to c-afem and s-afem-dm in terms of the computation time but it is competitive for the overall solution time.

7.3 The Poisson model problem for the benchmark of Section 7.2

The Poisson problem is solved for the benchmark of Section 7.2, with $f_0 \equiv 0$, $f_1 \equiv 1$ and $n = 6$.

Convergence plots

Figure 7.17 shows that the three adaptive algorithms converge at the optimal rate. The overall convergence curves of μ_ℓ for the afems are close together and converge with the same optimal convergence rate. The uniform mesh refinement has the same convergence rate; however, the fast pre-asymptotic decay of μ_ℓ for the adaptive mesh refinement yields an improved multiplicative constant for the convergence plot. In particular, the fast decay of μ_ℓ in the pre-asymptotic range for specific parameter sets of s-afem-aa (e.g., $\kappa = 0.3$, $\theta_A = 0.6$ and $\rho_B = 0.625$) shows the advantage of the adaptive algorithm analysed in this thesis. As already observed for the first problem setting of Section 7.1, the convergence behaviour of the remaining refinement indicators (η_ℓ and $\|h_\ell f\|_{L^2(\Omega)}$) is similar for the adaptive schemes and for uniform mesh refinements. The corresponding convergence plots are omitted.

Obviously, small values of ρ_B (e.g., $\rho_B = 0.01$) lead to a large increase of `ndof` in one level of the adaptive scheme without an appropriate decrease of μ_ℓ. In the convergence plots, steps occur. For $\rho = 0.1$, these steps occur for small $\kappa = 0.1$ and are significantly smaller. For moderate $\kappa = 0.3$ and $\rho_B = 0.1$ or larger values of ρ_B this behaviour can no longer be observed.

Progress of separate marking

Figures 7.18 and 7.19 show the interplay of Cases (A) and (B) for s-afem-aa and s-afem-dm. Furthermore a fast or slow increase of `ndof` per level can be seen in Figure 7.19.

The increase of `ndof` in Case (B) is restricted due to the Dörfler marking in s-afem-dm. For s-afem-aa, however, a fast increase of `ndof` and simultaneously an optimal data approximation are possible, in particular for small values of ρ_B. This behaviour is also apparent in Figures 7.18 and 7.19, where the choice of $\rho_B = 0.1$ (together with $\kappa = 0.3$) reduces the number of levels, until Case (A) is applied for the first time in $\ell = 3$.

Computational costs

Comparisons of the computational costs for this benchmark problem are shown in Figures 7.20–7.22. For the overall processing time, Figure 7.20, uniform mesh refinements are inferior to nearly all parameter sets of the three adaptive strategies. Each of the afems

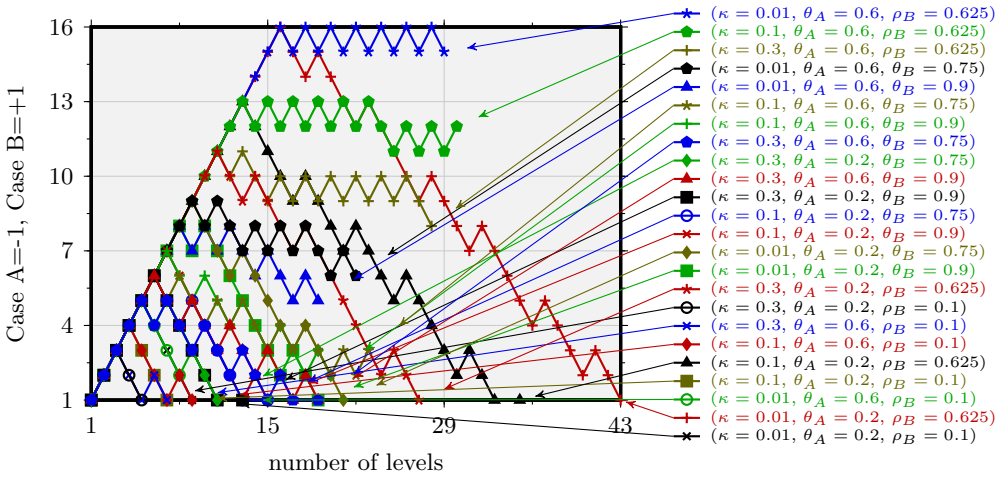

Figure 7.18: Use of Cases (A) and (B) in S-AFEM as a function of the number of levels for the benchmark problem of Section 7.3.

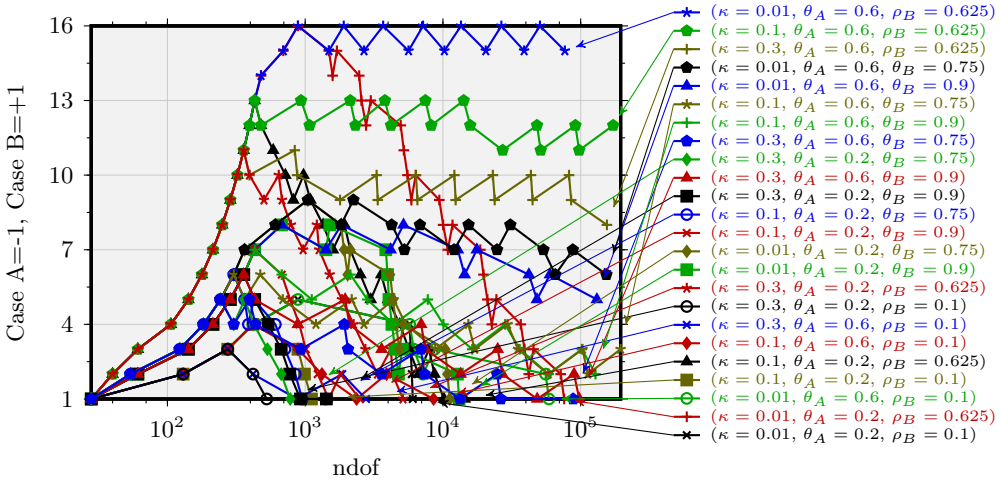

Figure 7.19: Use of Cases (A) and (B) in S-AFEM as a function of `ndof` for the benchmark problem of Section 7.3.

(C-AFEM, S-AFEM-AA and S-AFEM-DM) has a parameter set, that is among the best choices. All adaptive schemes require less processing time than uniform mesh refinements.

At the end of the pre-asymptotic range (of about 0.7 seconds of CPU time), S-AFEM-AA (with $\kappa = 0.3$, $\theta_A = 0.2$ and $\rho_B = 0.1$) and S-AFEM-DM (with $\kappa = 0.3$, $\theta_A = 0.6$ and $\theta_B = 0.9$) seem the best choices. In the mid-range (of about 3 seconds), S-AFEM-AA (with $\kappa = 0.3$, $\theta_A = 0.6$ and $\rho_B = 0.01$) and S-AFEM-DM (with $\kappa = 0.3$, $\theta_A = 0.6$ and $\theta_B = 0.9$) are best.

As expected, C-AFEM needs many more levels of refinement (and in particular CPU time) to approximate the data sufficiently. However, beyond that point C-AFEM is competitive, too.

Considering only the processing time used for step Solve (see Figure 7.21), the improvement in the pre-asymptotic range for S-AFEM and in particular S-AFEM-AA is obvious. Especially for small values of ρ_B (e.g., $\rho_B = 0.01$ and 0.1), S-AFEM-AA is better than both C-AFEM and S-AFEM-DM. For S-AFEM-AA, the choice of $\kappa = 0.3$, $\theta_A = 0.6$ and $\rho_B = 0.1$ seems to be best for μ_ℓ as a function of processing time for Solve.

These observations are confirmed by Figure 7.22, where the reduction of the number of levels is apparent. The best algorithms with respect to the reduction of μ_ℓ versus the number of levels are S-AFEM-AA with parameters $\kappa = 0.3$ or 0.1, $\theta_A = 0.6$ and $\rho_B = 0.01$, followed by S-AFEM-AA with $\rho_B = 0.1$. As uniform mesh refinements permit the highest increase of `ndof` per level on the basis of the Dörfler marking, this strategy is competitive in this situation.

Adaptive meshes

This section ends with a selection of adaptively generated meshes and the corresponding nonconforming solutions for the three adaptive algorithms and a selection of parameter values; see Figures 7.23–7.28.

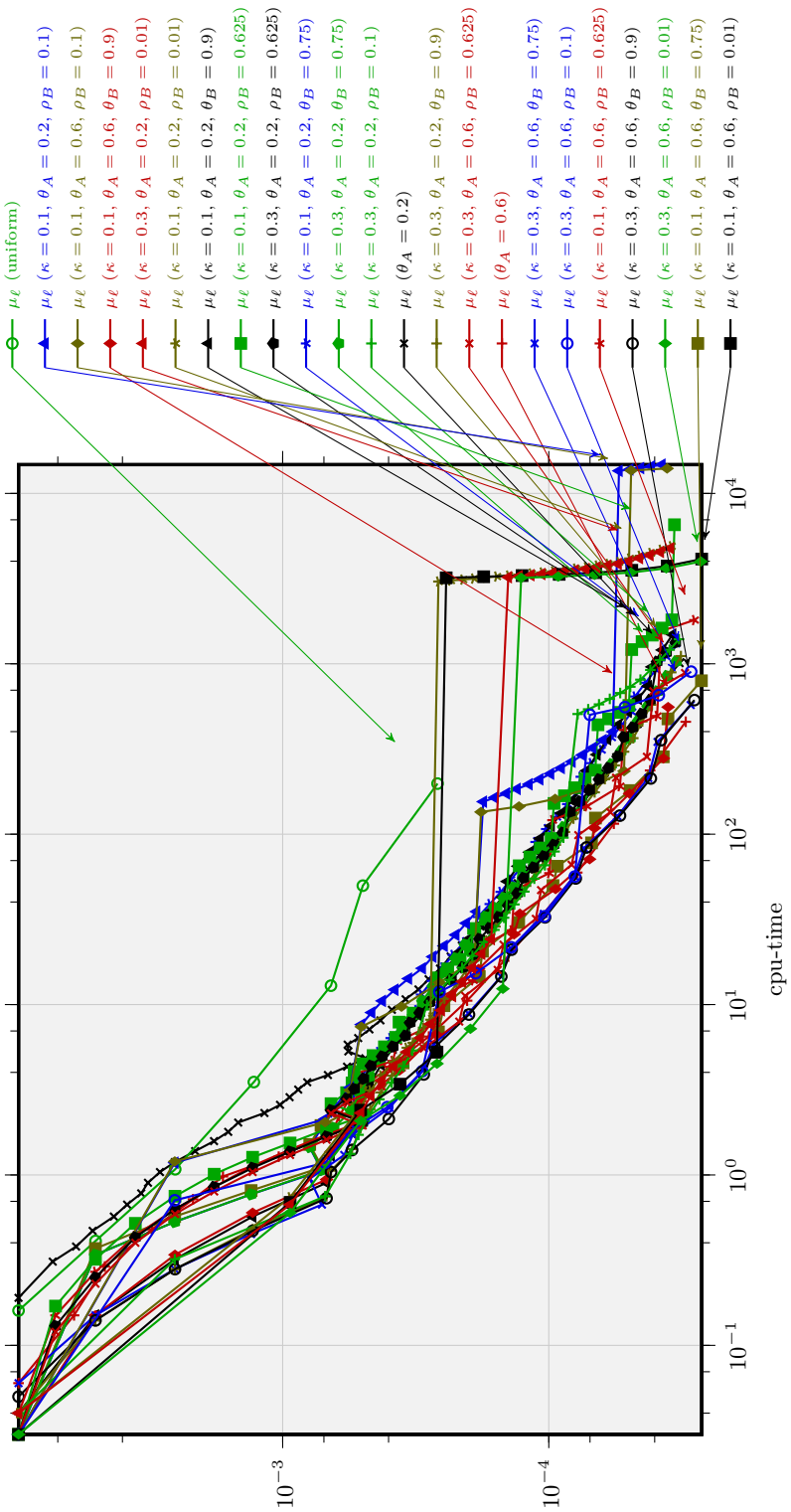

Figure 7.20: μ_ℓ versus overall processing time for the benchmark problem of Section 7.3.

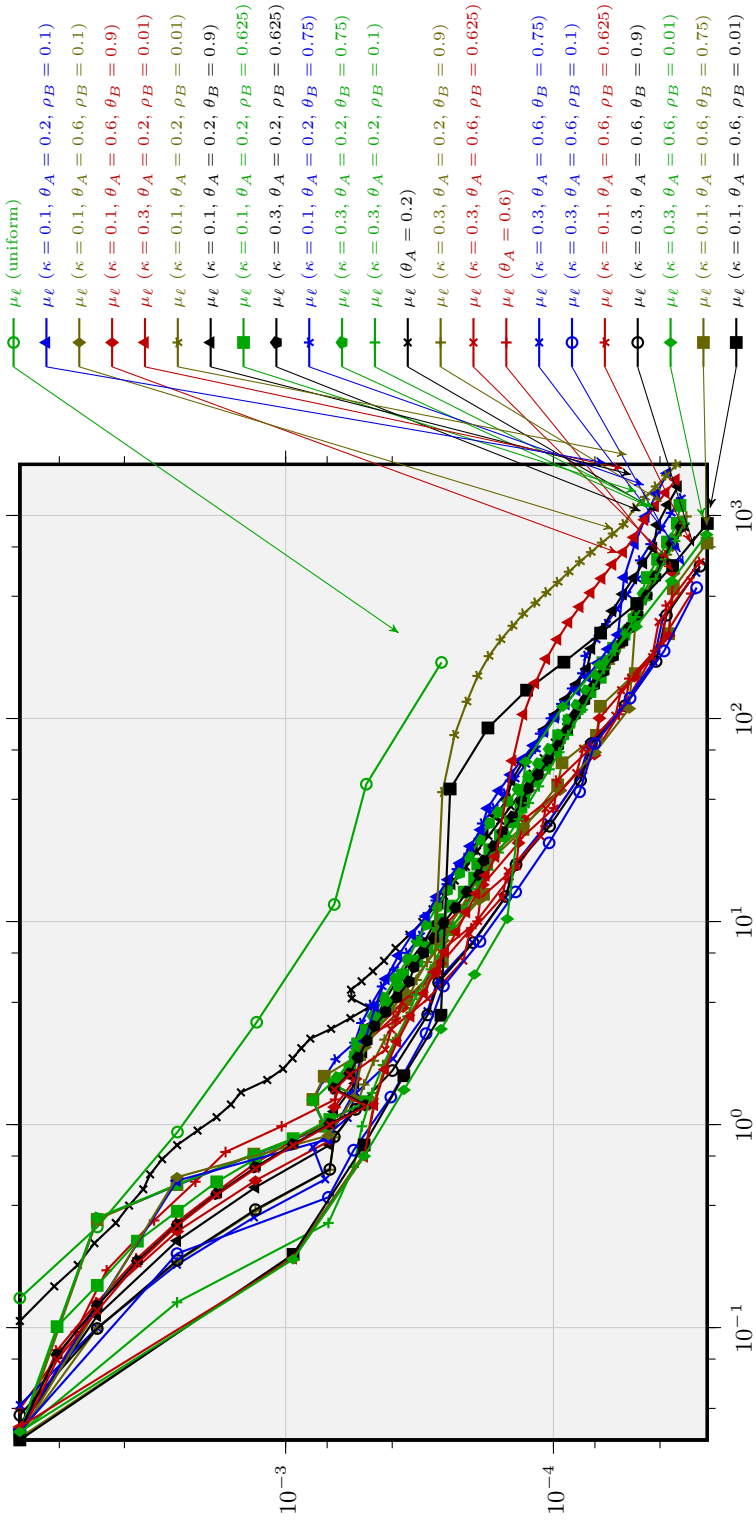

Figure 7.21: μ_ℓ versus cumulative processing time of Solve for the benchmark problem of Section 7.3.

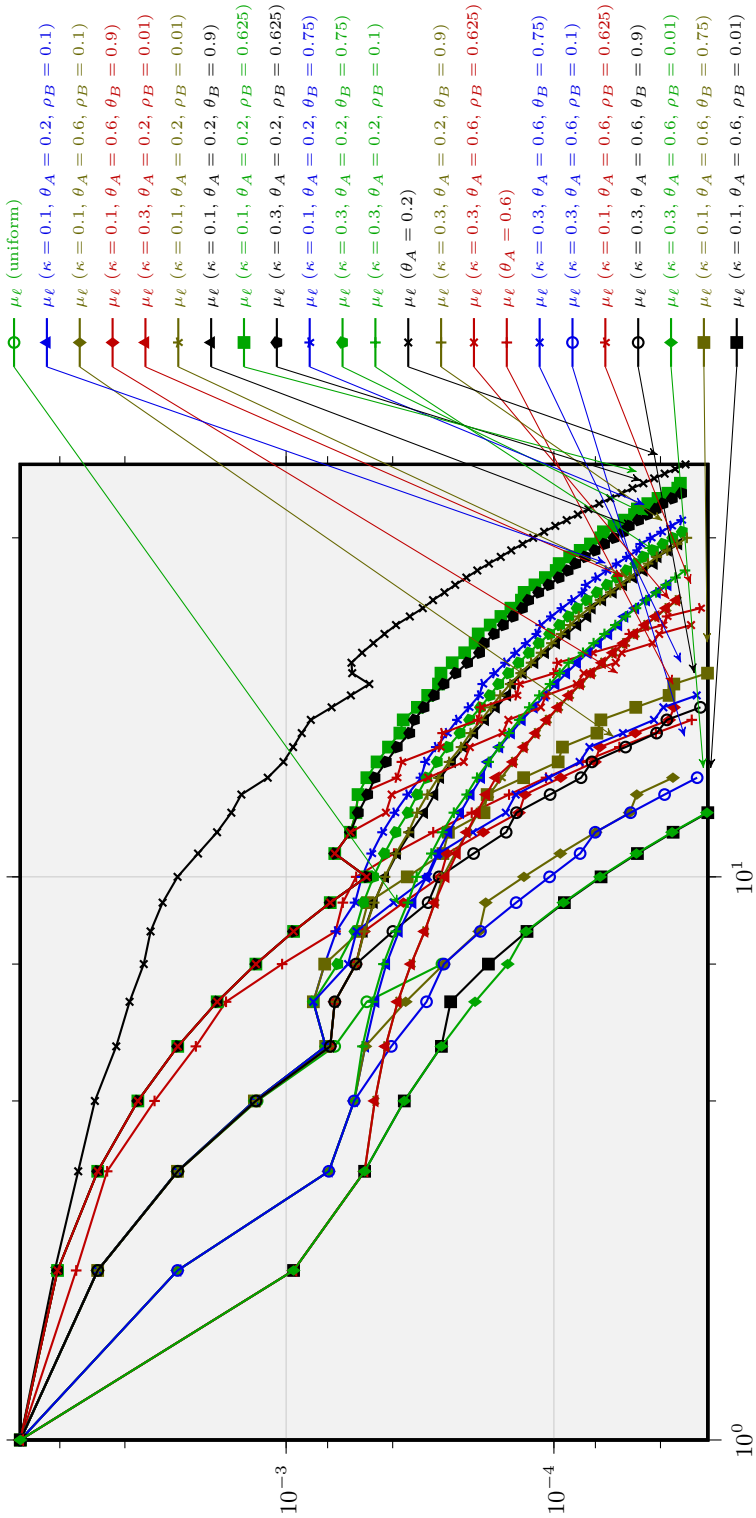

Figure 7.22: μ_ℓ versus number of levels for the benchmark problem of Section 7.3.

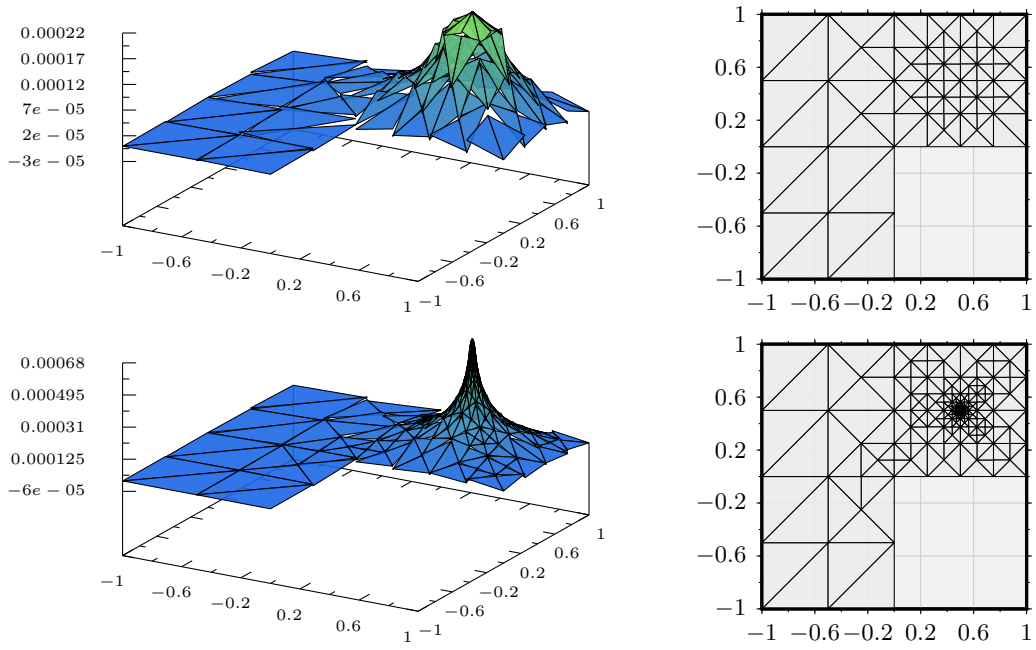

Figure 7.23: S-AFEM-AA: $\theta_A = 0.2$, $\rho_B = 0.625$ and $\kappa = 0.1$ on $\ell = 5$, 15 with `ndof` = 142, 586 for the benchmark problem of Section 7.3.

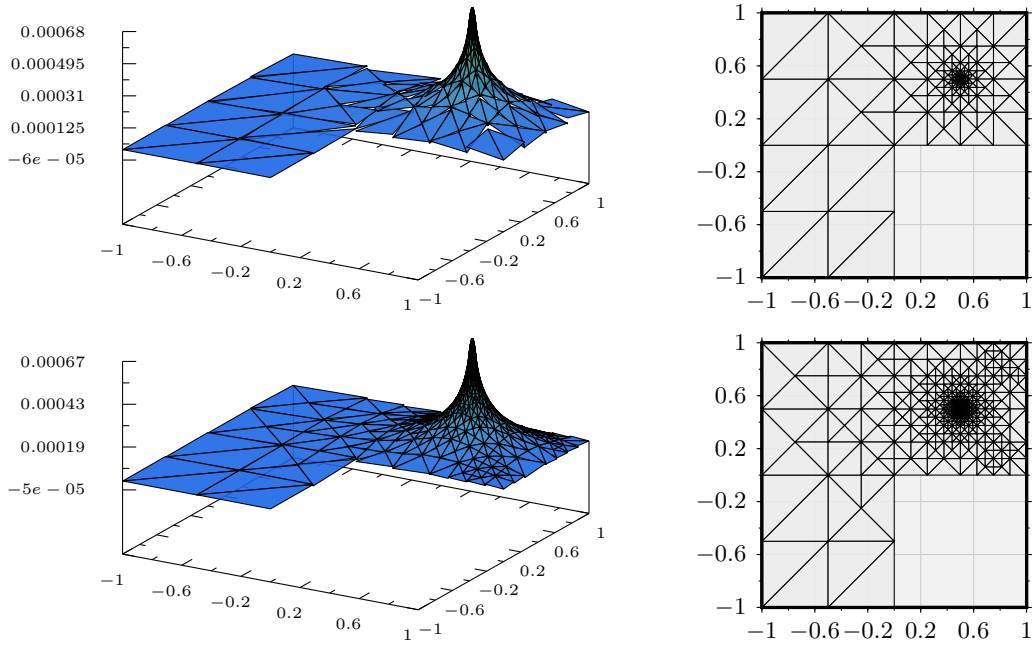

Figure 7.24: S-AFEM-AA: $\theta_A = 0.2$, $\rho_B = 0.1$ and $\kappa = 0.1$ on $\ell = 5$, 10 with `ndof` = 886, 1686 for the benchmark problem of Section 7.3.

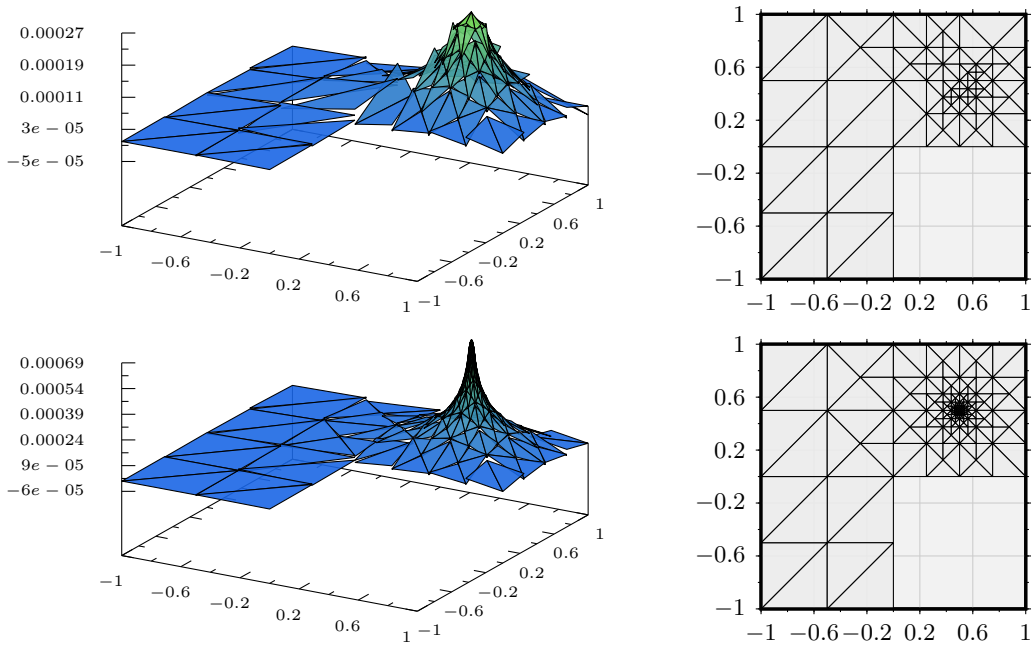

Figure 7.25: S-AFEM-DM: $\theta_A = 0.2$, $\theta_B = 0.4$ and $\kappa = 0.1$ on $\ell = 5$, 15 with `ndof` = 162, 523 for the benchmark problem of Section 7.3.

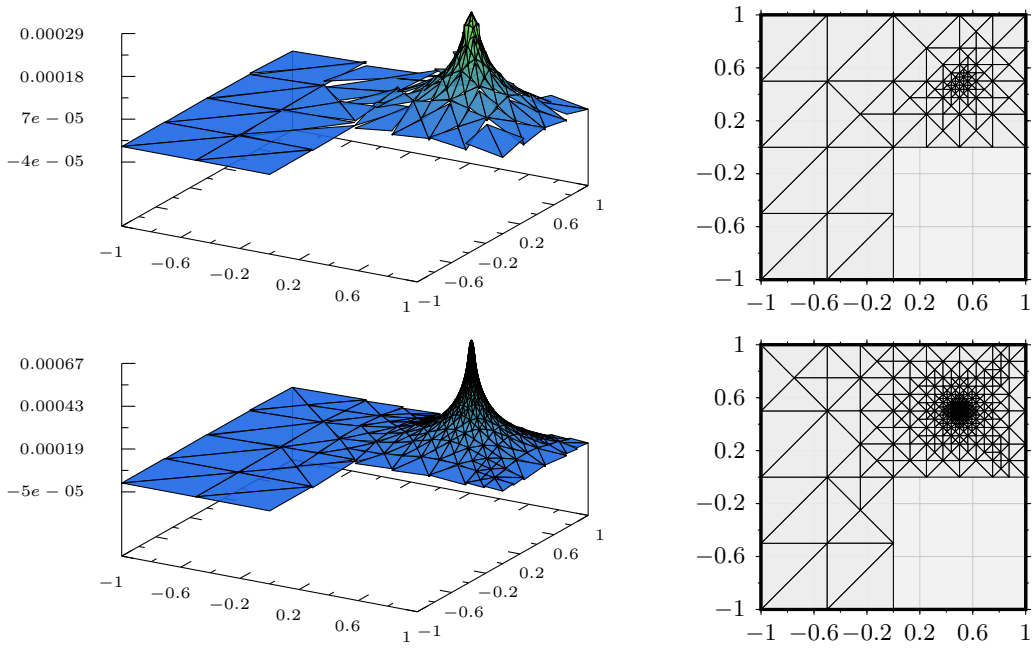

Figure 7.26: S-AFEM-DM: $\theta_A = 0.2$, $\theta_B = 0.4$ and $\kappa = 0.1$ on $\ell = 5$, 15 with `ndof` = 243, 1407 for the benchmark problem of Section 7.3.

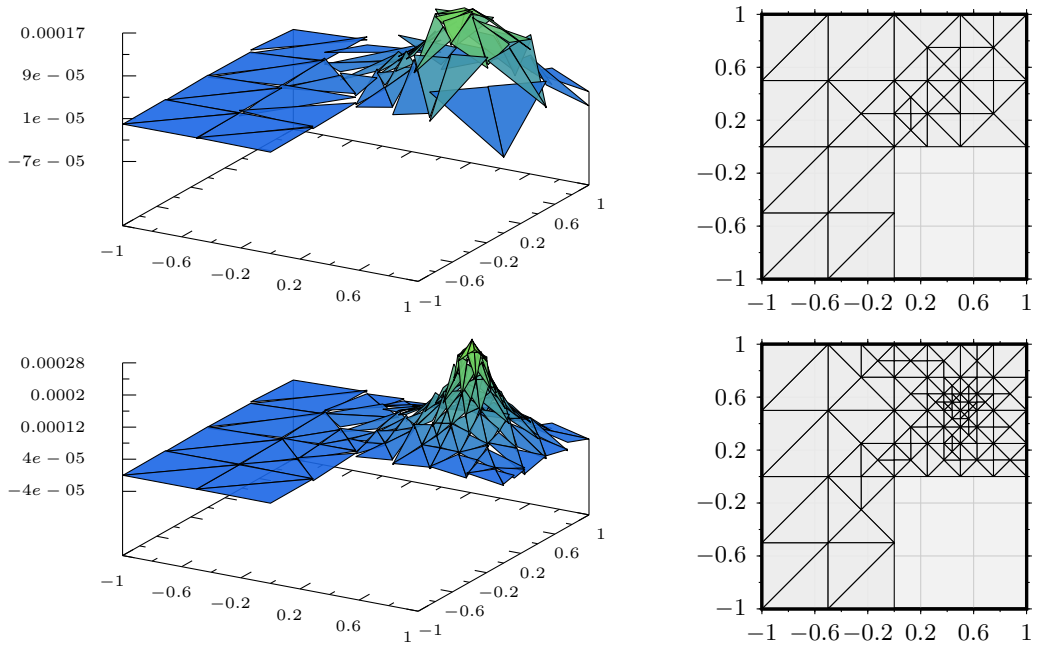

Figure 7.27: C-AFEM: $\theta_A = 0.2$ on $\ell = 5$, 12 with `ndof` = 75, 259 for the benchmark problem of Section 7.3.

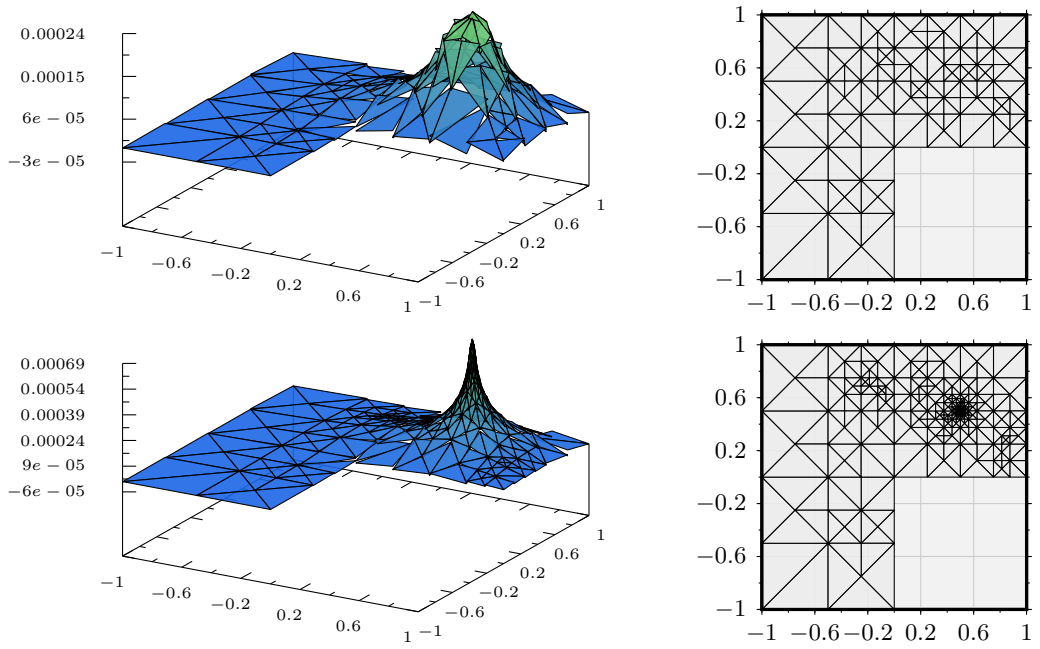

Figure 7.28: C-AFEM: $\theta_A = 0.6$ on $\ell = 5$, 10 with `ndof` = 237, 630 for the benchmark problem of Section 7.3.

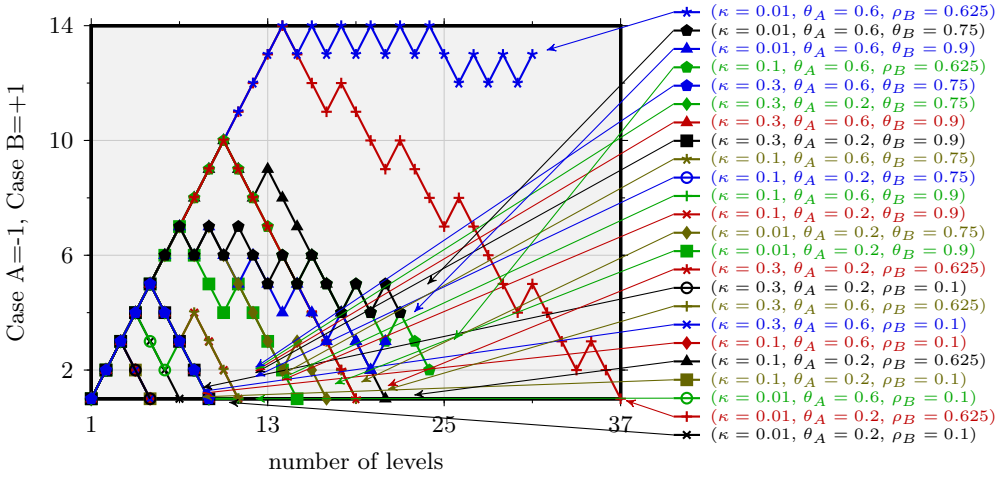

Figure 7.29: Use of Cases (A) and (B) in S-AFEM as a function of the number of levels for $\nu = 0.3$ for the benchmark problem of Section 7.4.

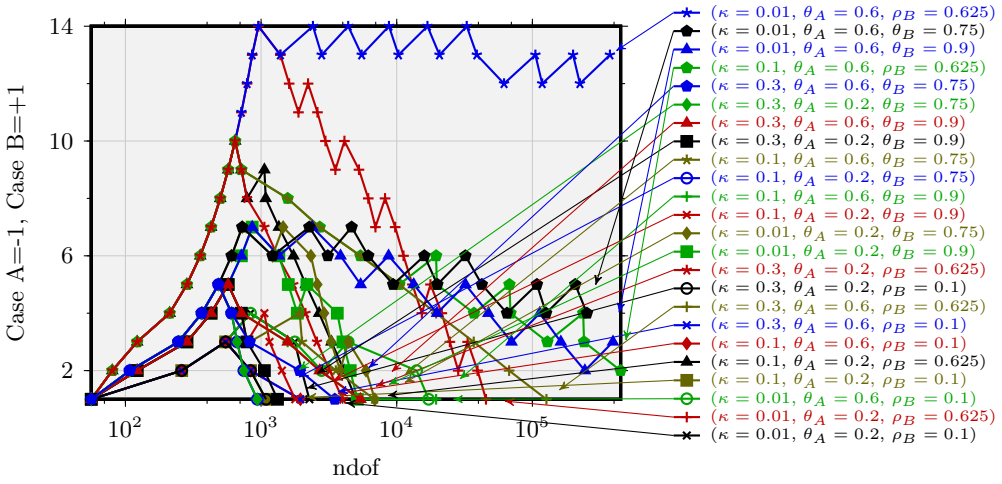

Figure 7.30: Use of Cases (A) and (B) in S-AFEM as a function of `ndof` for $\nu = 0.3$ for the benchmark problem of Section 7.4.

7.4 The pure displacement problem in linear elasticity for the benchmark of Section 7.2

The right-hand side $f \in L^2(\Omega)$ on the L-shaped domain Ω is piecewise constant as introduced in Section 7.2 with given $f_0 \equiv (0,0)$ and $f_1(x_1,x_2) \equiv (1,0)$ in the neighbourhood of $(1/2,1/2)$; see Figure 7.16. The Lamé parameters $\lambda = \nu/((1+\nu)(1-2\nu))$ and $\mu = 1/(2(1+\mu))$ are used for different values of the Poisson ratio $\nu = 0.3$ and 0.499.

The following numerical experiments provide strong empirical evidence of the superiority of nonconforming over conforming FEM and adaptive over uniform mesh refinements. Moreover, the ability of S-AFEM-AA to reduce the absolute number of levels in the pre-asymptotic regime is confirmed for selected parameter values.

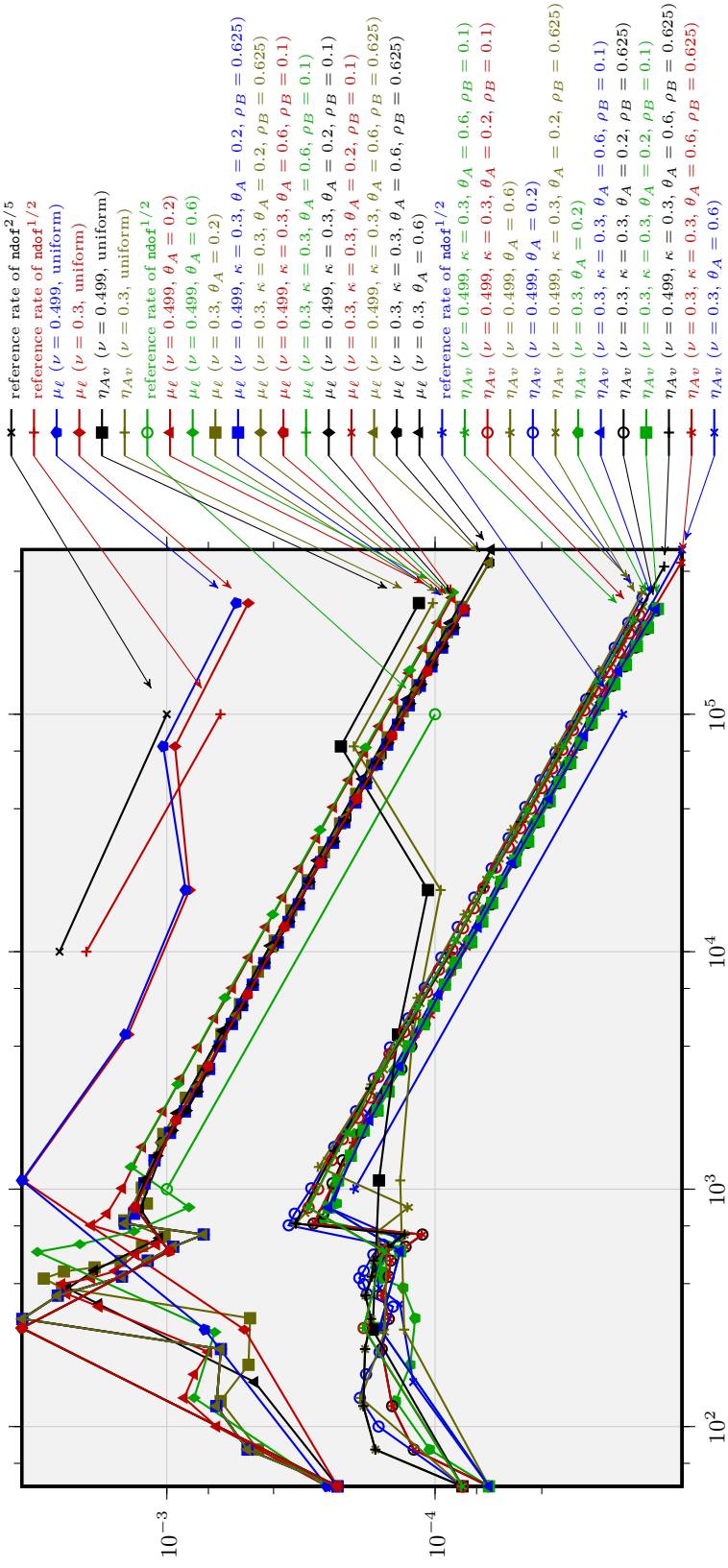

Figure 7.31: Convergence plots of μ_ℓ and η_{Av} for the benchmark problem of Section 7.4 solved with CR-FEM and S-AFEM-AA.

Convergence plots

Figures 7.31 and 7.32 show the convergence behaviour of nonconforming CR-FEM and conforming P_1 FEM for this benchmark problem and $\epsilon = 2^{-6}$. The collective error estimators μ_ℓ and η_{Av} (defined in [CF01]) are plotted as a function of `ndof` in a double-logarithmic scaling. For nonconforming CR-FEM, the convergence curves of μ_ℓ (as well as η_{Av}) for the adaptive algorithms for both values of ν are close together and have the optimal convergence rate, while uniform mesh refinements show a huge pre-asymptotic range (with `ndof` reaching up to 10^5) and an almost similar convergence rate of 1/2 with a clearly larger constant.

The locking phenomenon is observed for conforming FEM, as in [CR12]; see Section 2.2 for an explanation. This leads to a large pre-asymptotic range. The experiments show, that there is no pre-asymptotic range for $\nu = 0.3$. For a nearly incompressible material, $\nu = 0.499$, the pre-asymptotic range is significantly large (for `ndof` up to about `ndof` $= 10^3$). For uniform mesh refinements and conforming FEM, the pre-asymptotic range is again very large (with `ndof` goes up to `ndof` $= 2\,10^4$). For both values of ν, $\nu = 0.3$ and $\nu = 0.499$, lower convergence rates are observed.

Progress of separate marking

Figures 7.29 and 7.30 illustrate the flexibility of separate marking for the adaptive algorithms for $\nu = 0.3$. The behaviour for $\nu = 0.499$ is similar, therefore its corresponding plot is omitted. For S-AFEM-AA with $\rho_B = 0.1$, the number of levels with Case (B) – until Case (A) is triggered for the first time – is reduced to 2 and this leads to a very fast increase of `ndof`, along with an optimal data approximation.

Computational costs

μ_ℓ as a function of the overall processing time is similar for S-AFEM-AA and S-AFEM-DM for $\nu = 0.3$ for some parameter values; see Figure 7.33. E.g., S-AFEM-AA with $\kappa = 0.3$, $\theta_A = 0.6$ and $\rho_B = 0.1$ requires a similar amount of overall processing time as S-AFEM-DM with $\kappa = 0.3$, $\theta_A = 0.6$ and $\theta_B = 0.75$. Surprisingly C-AFEM is better than S-AFEM-AA and S-AFEM-DM for $\theta_A = 0.6$ in the mid-range. However, C-AFEM is not competitive at an early stage (w.r.t. a CPU time of about 2 seconds). Here, the advantages of S-AFEM-AA are apparent, while S-AFEM-DM performs similarly only for $\theta_B = 0.9$. In contrast, S-AFEM-AA has competitive results for various parameter settings.

Considering only the cumulative processing time of step SOLVE in Figure 7.34, the advantage of S-AFEM-AA at an early stage (of about 3 seconds of cumulative CPU time for SOLVE) is clearer; see Figure 7.33. At this stage S-AFEM-AA (with $\theta_A = 0.6$ and $\rho_B = 0.1$) performs the best. However, C-AFEM with $\theta_A = 0.6$ again performs better than both S-AFEM-AA and S-AFEM-DM in the mid-range. At a later stage, S-AFEM-AA and S-AFEM-DM perform similarly (i.e., for $\kappa = 0.3$, $\theta_A = 0.6$ and $\theta_B = 0.75$ or $\rho_B = 0.1$) – again, as before, for the overall processing time. In general both, the computational costs of the overall adaptive algorithm and the cumulative processing time of SOLVE, are higher for all adaptive schemes with $\theta_A = 0.6$ than with $\theta_A = 0.2$. This reflects the expectation that the number of levels must be reduced when a discrete system needs to be solved.

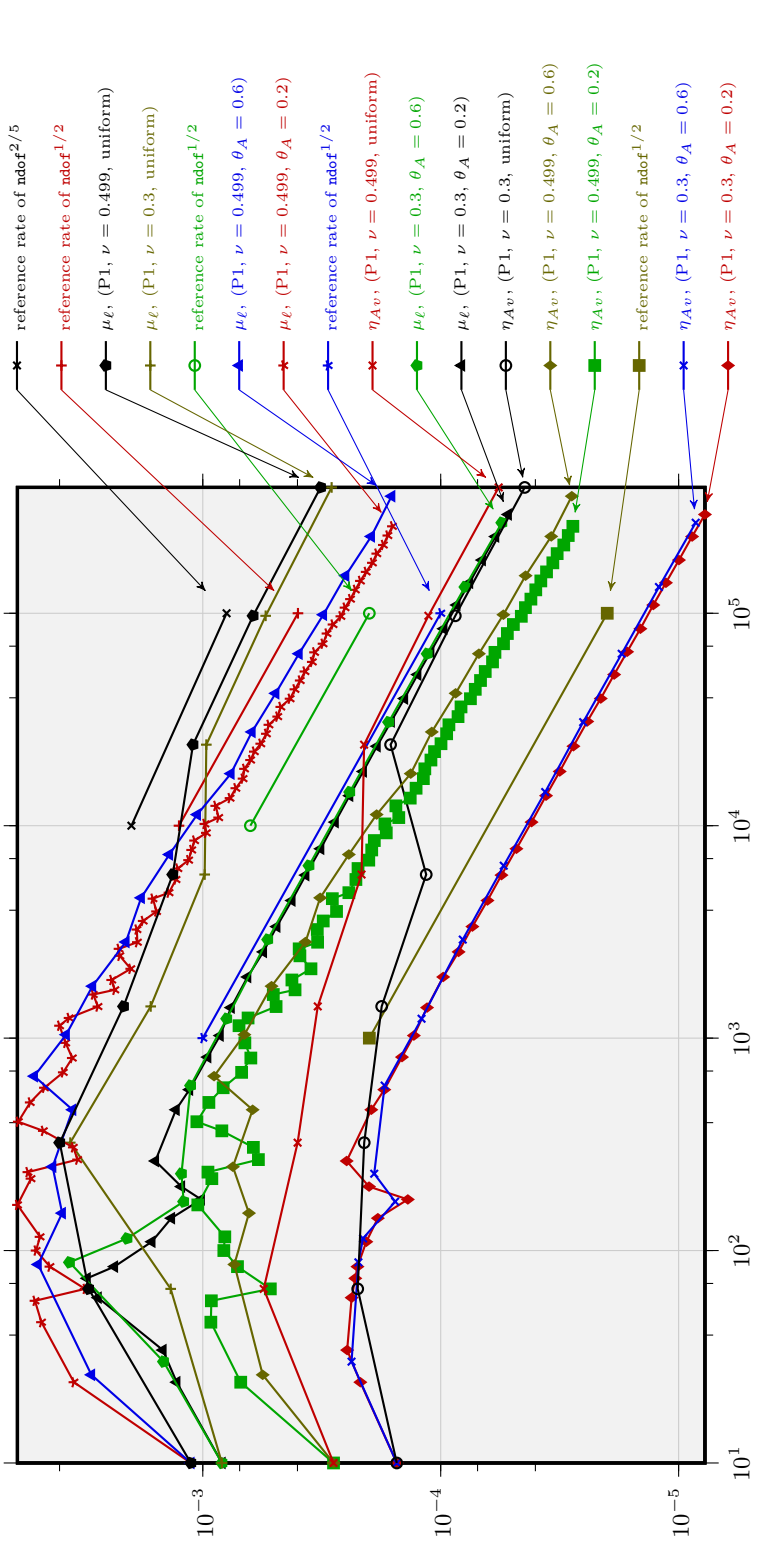

Figure 7.32: Convergence plots of μ_ℓ and η_{Av} for the benchmark problem of Section 7.4 solved with P_1 conforming FEM and C-AFEM.

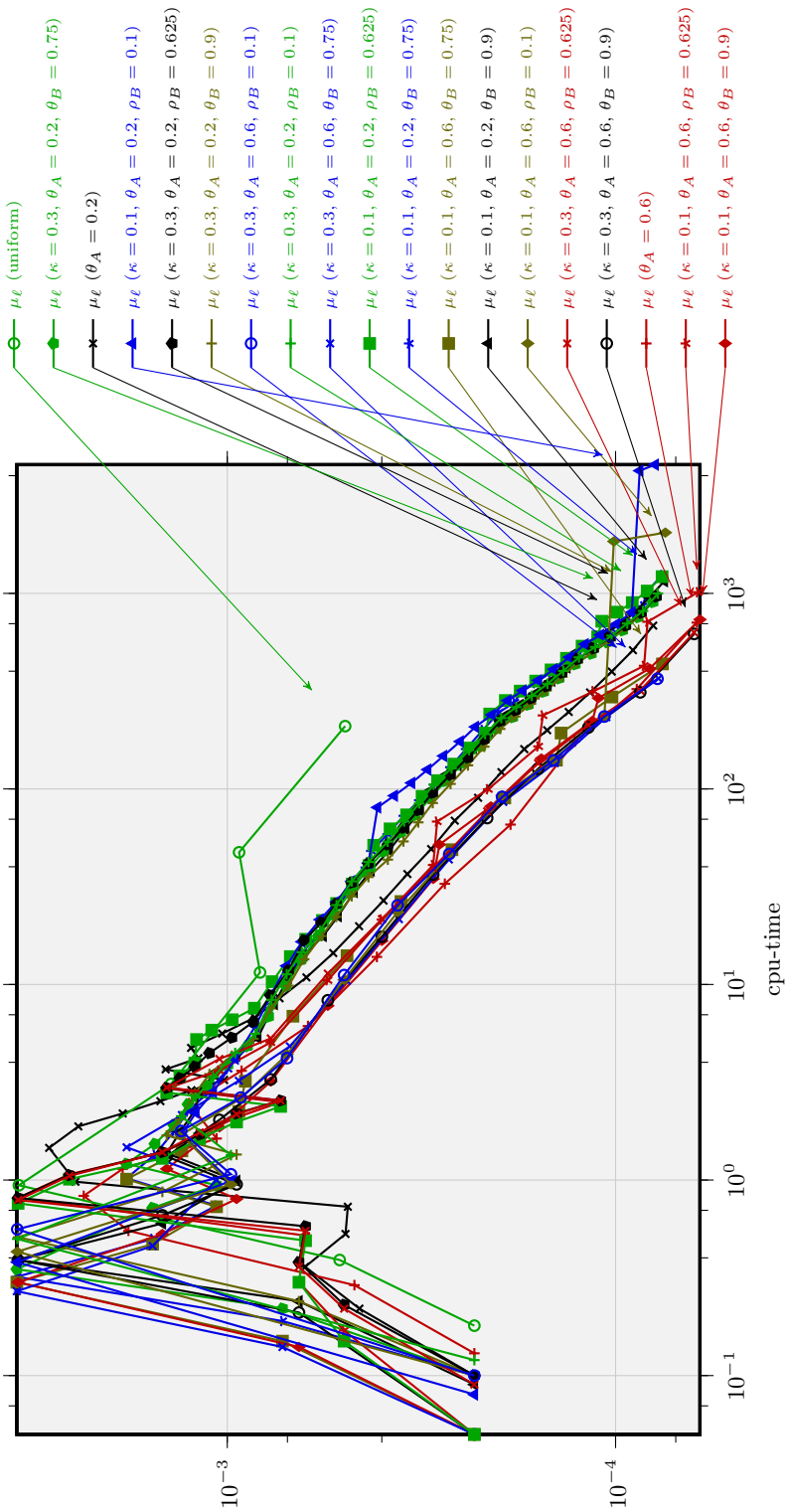

Figure 7.33: μ_ℓ versus processing time for $\nu = 0.3$ for the benchmark problem of Section 7.4.

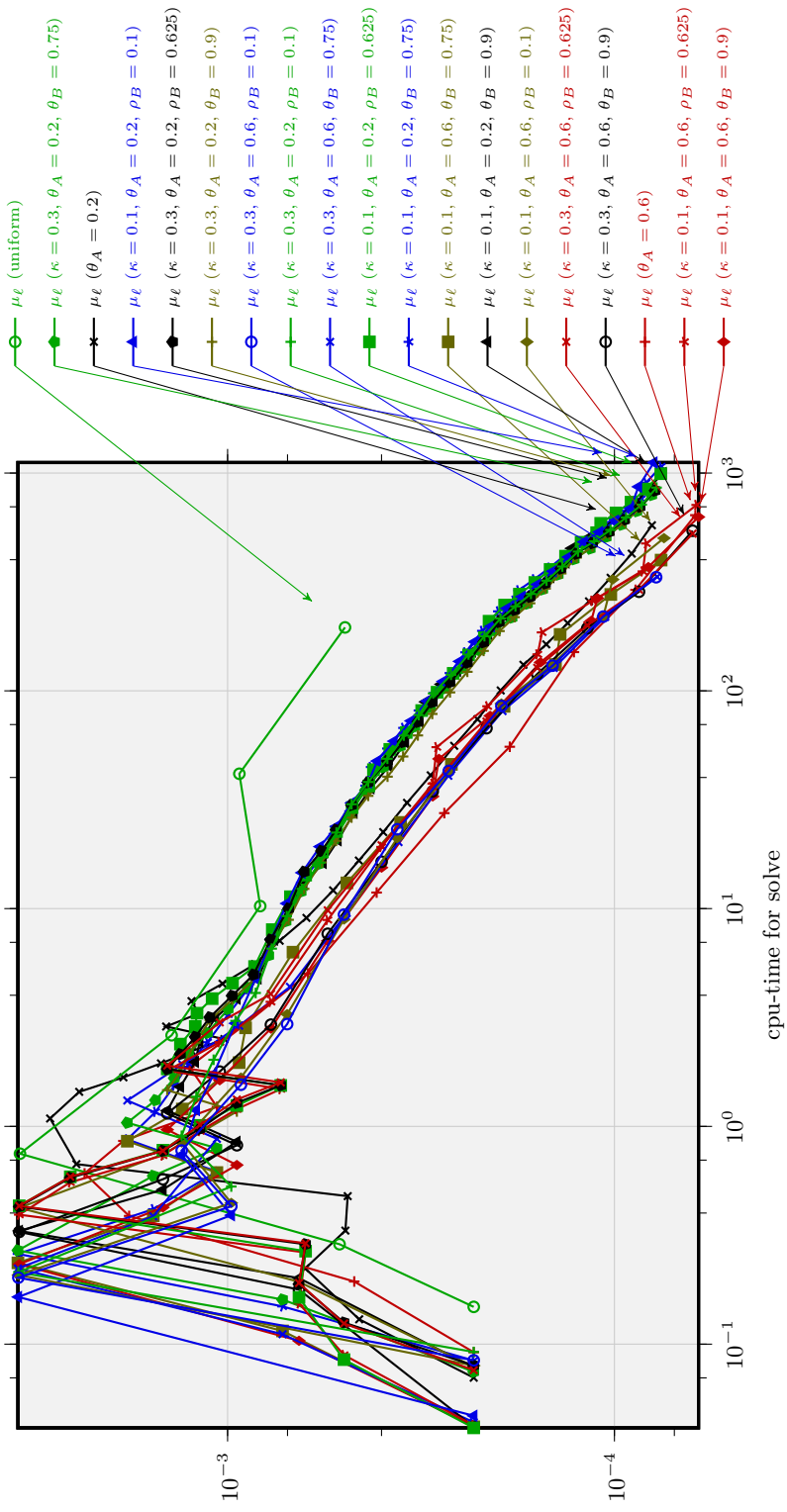

Figure 7.34: μ_ℓ versus cumulative processing time for SOLVE for $\nu = 0.3$ for the benchmark problem of Section 7.4.

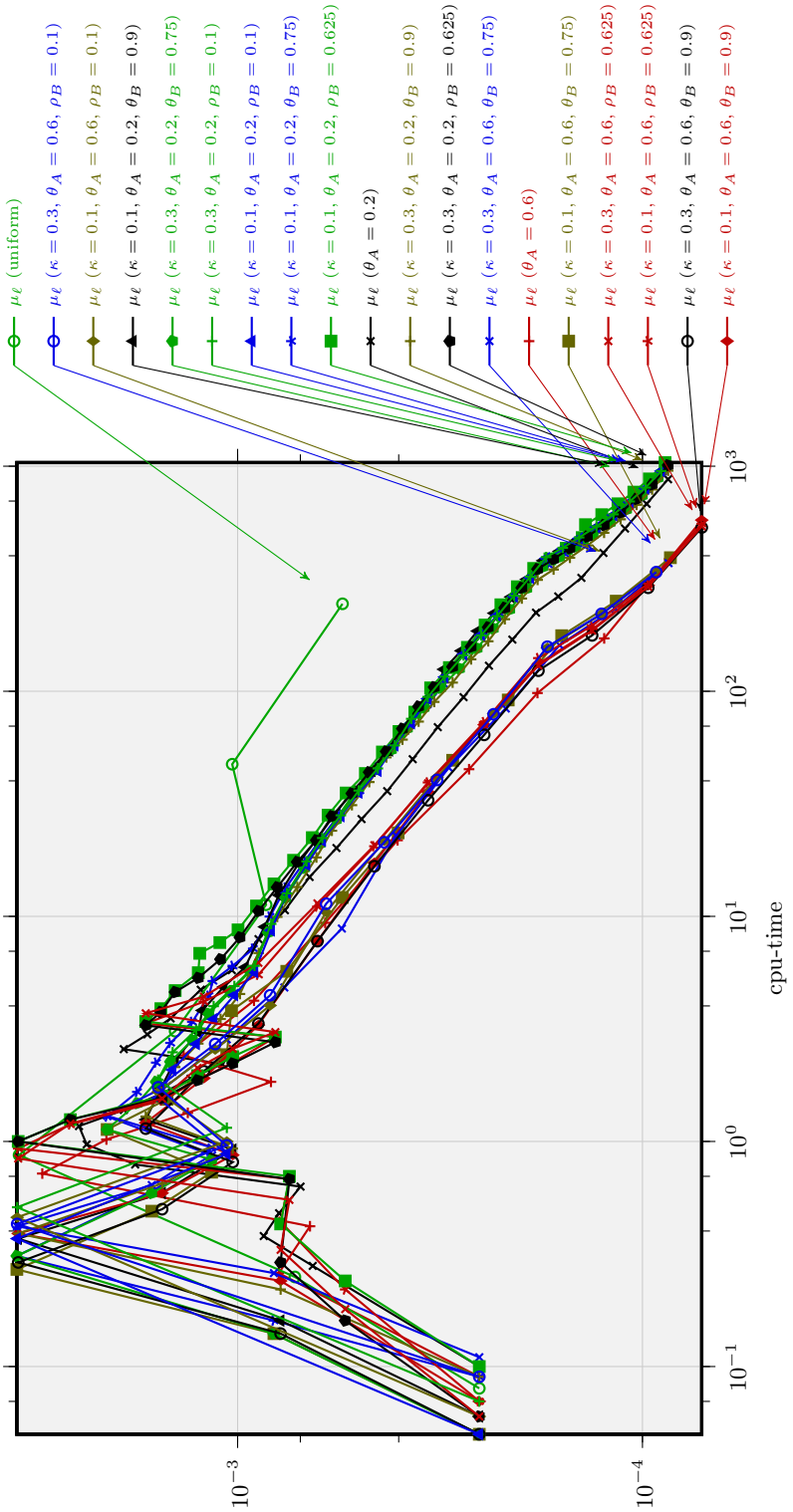

Figure 7.35: μ_ℓ versus overall processing time for $\nu = 0.499$ for the benchmark problem of Section 7.4.

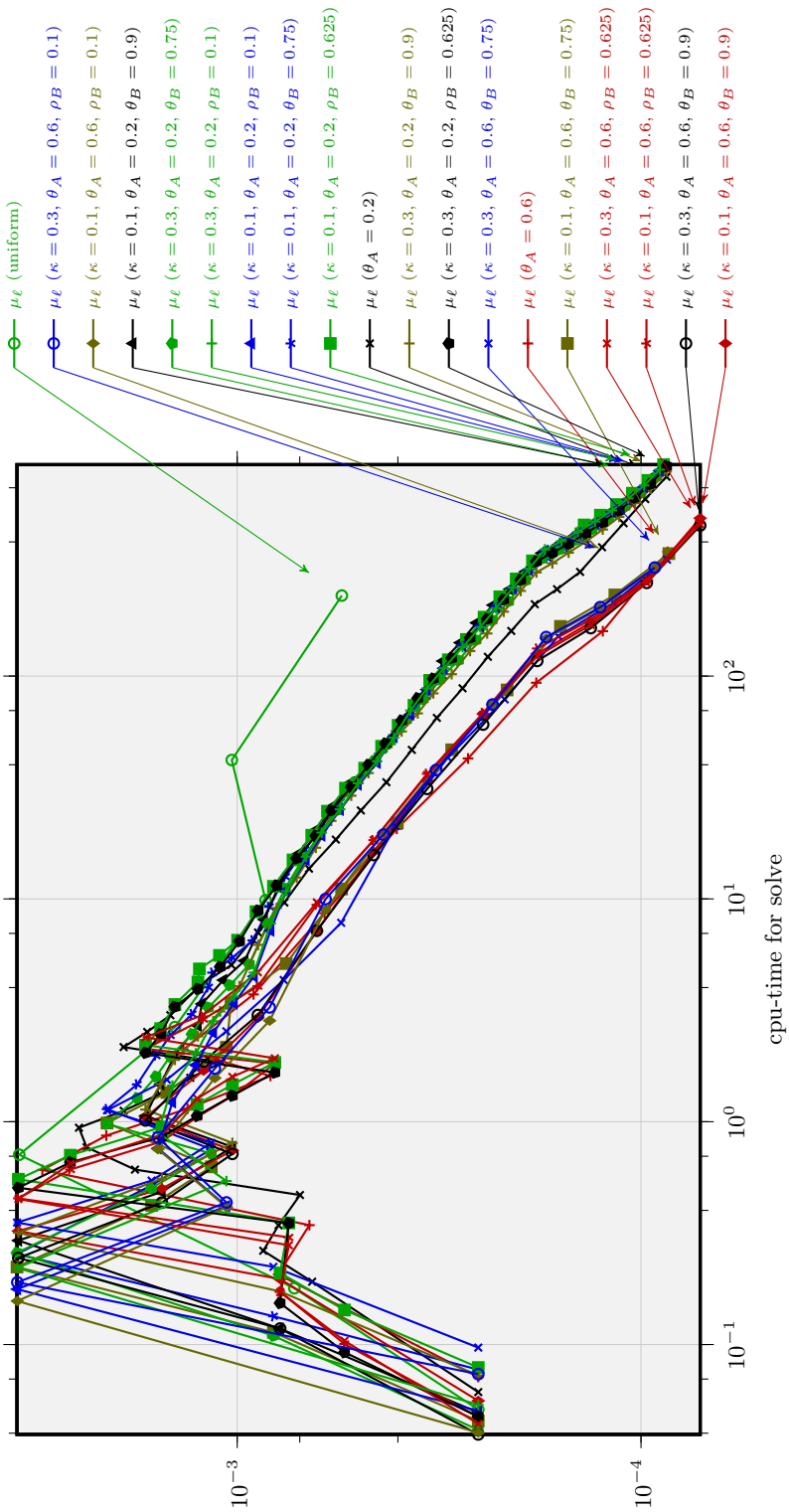

Figure 7.36: μ_ℓ versus cumulative processing time for SOLVE for $\nu = 0.499$ for the benchmark problem of Section 7.4.

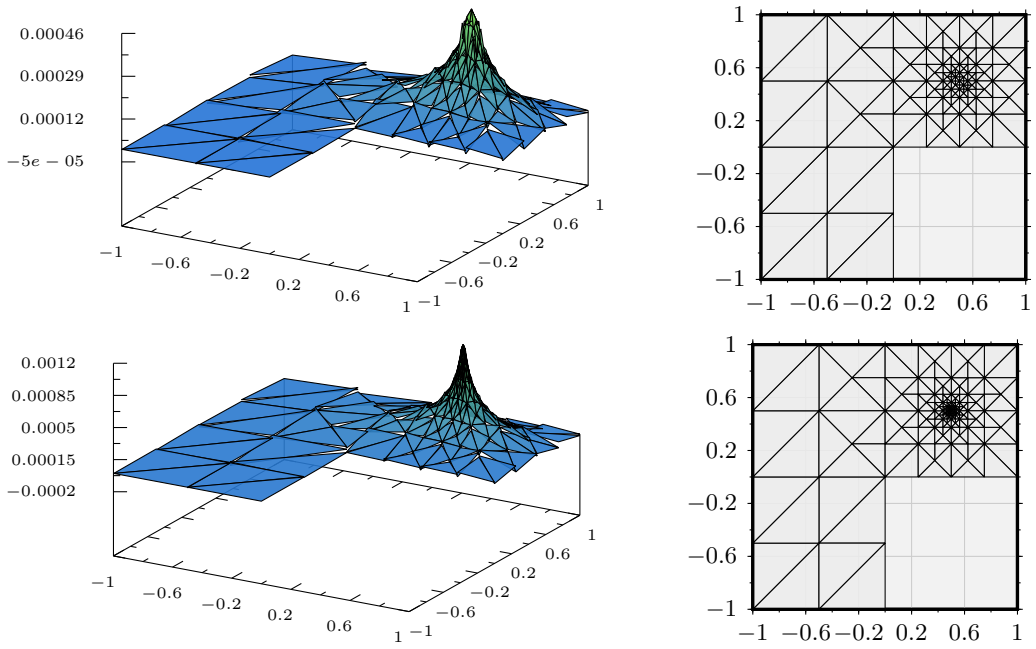

Figure 7.37: S-AFEM-AA: $\theta_A = 0.2$, $\rho_B = 0.1$ and $\kappa = 0.1$ for $\nu = 0.3$ and $\nu = 0.499$ on levels $\ell = 3$, 4 and `ndof` = 548, 836 for the benchmark problem of Section 7.4.

For a nearly incompressible material (i.e., $\nu = 0.499$), at an early stage, S-AFEM-AA performs better than C-AFEM and S-AFEM-DM as vor $\nu = 0.3$. However, at a later stage, for all adaptive schemes with $\theta_A = 0.6$, the convergence curves of μ_ℓ versus the overall processing time are close together in Figure 7.35, and also versus the cumulative processing time of step SOLVE in Figure 7.35.

Adaptive meshes

As long as only Case (B) is applied in S-AFEM (in particular for a small number of levels ℓ) the adaptive meshes do not depend on ν. Figure 7.37 shows two successive levels of S-AFEM-AA, while in Figures 7.38 and 7.39 the difficuilties of a proper approximation of the solution are apparent for conforming FEM.

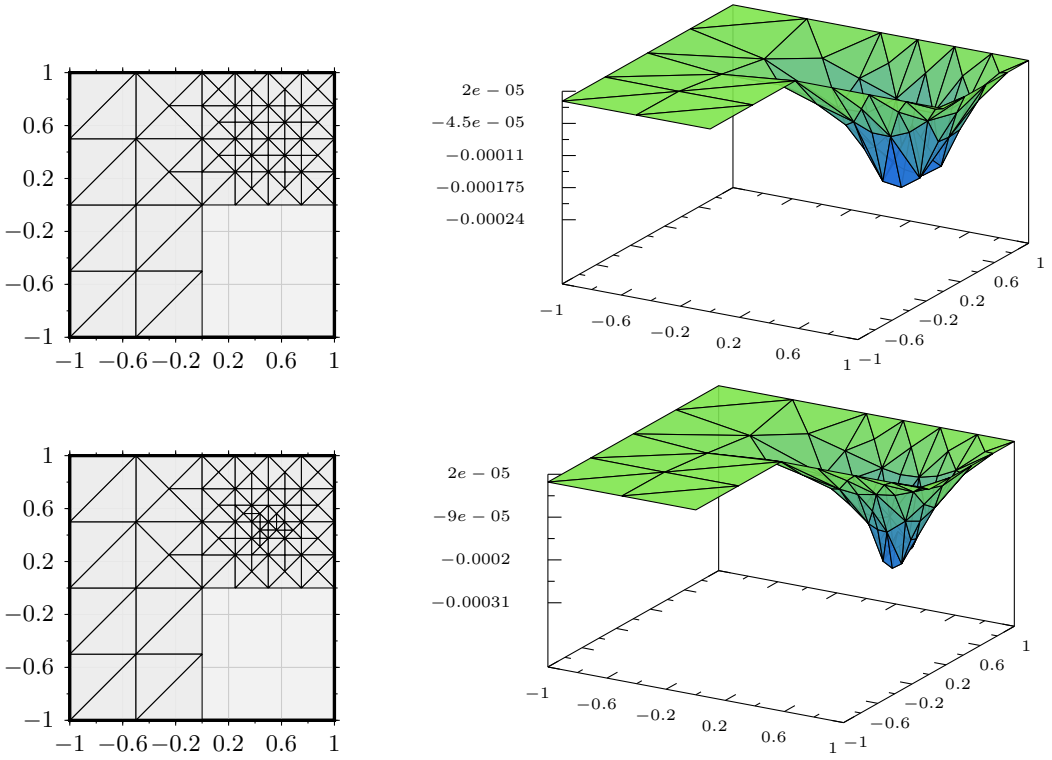

Figure 7.38: P_1 FEM with C-AFEM: $\theta_A = 0.6$ for $\nu = 0.3$ on levels $\ell = 3$, 4 and `ndof` = 88, 114 for the benchmark problem of Section 7.4.

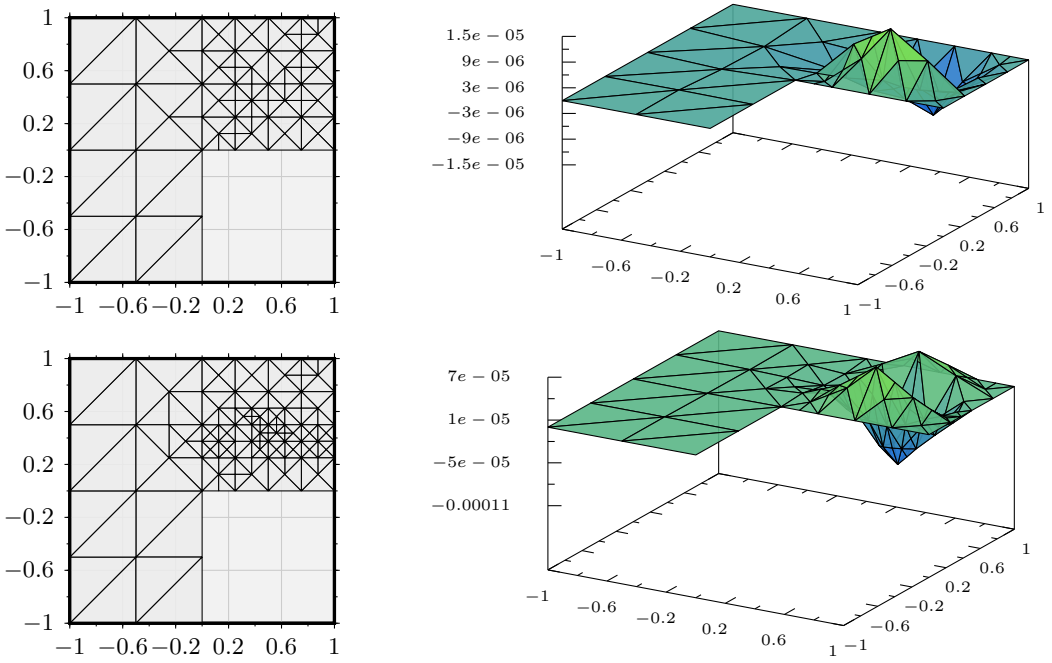

Figure 7.39: P_1 FEM with C-AFEM: $\theta_A = 0.6$ for $\nu = 0.499$ on levels $\ell = 3$, 4 and `ndof` = 86, 150 for the benchmark problem of Section 7.4.

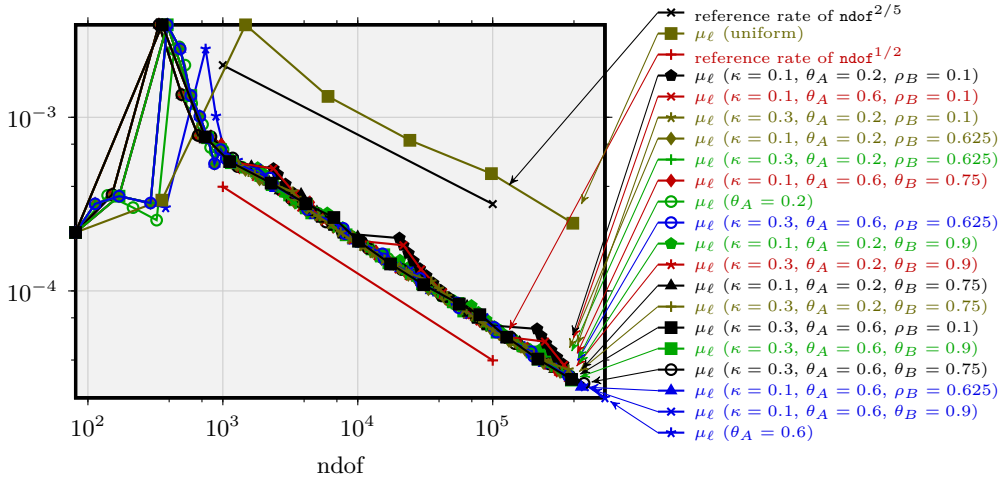

Figure 7.40: μ_ℓ versus `ndof` for the Stokes problem of Section 7.5, $\epsilon = 2^{-6}$.

7.5 The Stokes problem for the benchmark of Section 7.2

In this section, the benchmark of Section 7.2 is applied to the Stokes equations. The Stokes equations are solved on the L-shaped domain Ω and piecewise constant right-hand side $f \in L^2(\Omega)$ as described in Section 7.2 and Figure 7.16 with $f_0 \equiv (0,0)$ and $f_1(x_1,x_2) \equiv (1,0)$ in a small neighbourhood of $(1/2,1/2)$; see Figure 7.16. Two settings are considered, the standard setting with $\epsilon = 2^{-6}$ and a microstructure with $\epsilon = 2^{-10}$.

As an example, the discrete nonconforming solution u_ℓ^{NC} of the standard setting is plotted for some coarse meshes and S-AFEM-AA in Figure 7.42.

The numerical experiments confirm the analytical optimal convergence rates.

7.5.1 Standard setting, $\epsilon = 2^{-6}$

As for the Poisson model problem and the pure displacement problem in linear elasticity, the adaptive algorithms are tested using the benchmark problem with the width of the nonzero region being $\epsilon = 2^{-6}$.

Figure 7.40 shows that all adaptive schemes (C-AFEM, S-AFEM-AA and S-AFEM-DM) have the optimal convergence rate of 1/2 for the error estimator of the total error μ_ℓ. The convergence behaviour of S-AFEM-AA for small values of ρ_B (such as $\rho_B = 0.01$) has the steps that are seen for the Poisson model problem in Section 7.3 and indicate a fast increase of `ndof` without an appropriate decrease of μ_ℓ or η_{Av}.

For uniform mesh refinements, a reduced convergence rate of approximately 2/5 is observed for μ_ℓ, while for η_{Av} there is a wide pre-asymptotic range, which leads to a larger multiplicative constant. For uniform refinement, the convergence rate of 1/2 can be observed from level 5, when the right-hand side function $f \in L^2(\Omega)$ is resolved by the mesh. The number of levels in the pre-asymptotic range corresponds to the edge length of the neighbourhood $\epsilon = 2^{-6}$ of the support of f. Although μ_ℓ and η_{Av} are equivalent, the large gap between them underlines the difficulties in obtaining a sufficient approximation of the data.

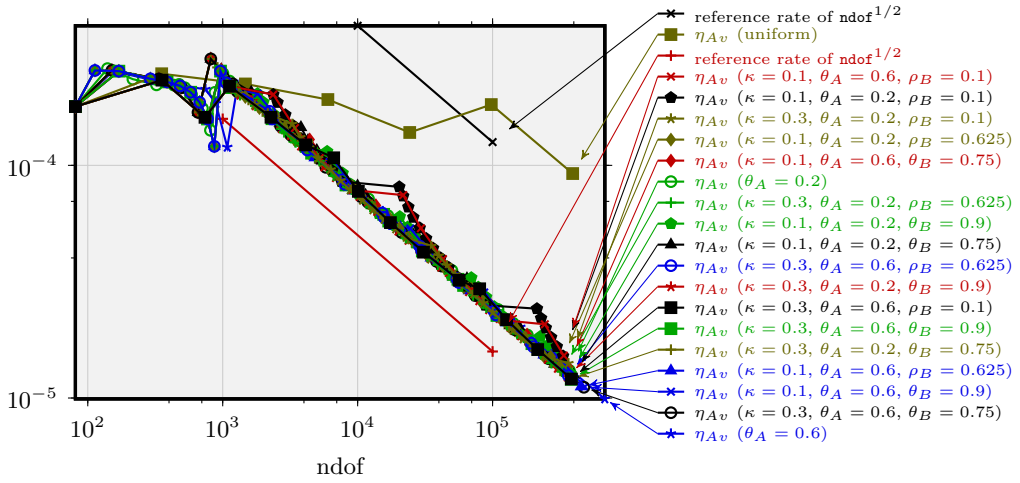

Figure 7.41: η_{Av} versus `ndof` for the Stokes problem of Section 7.5, $\epsilon = 2^{-6}$.

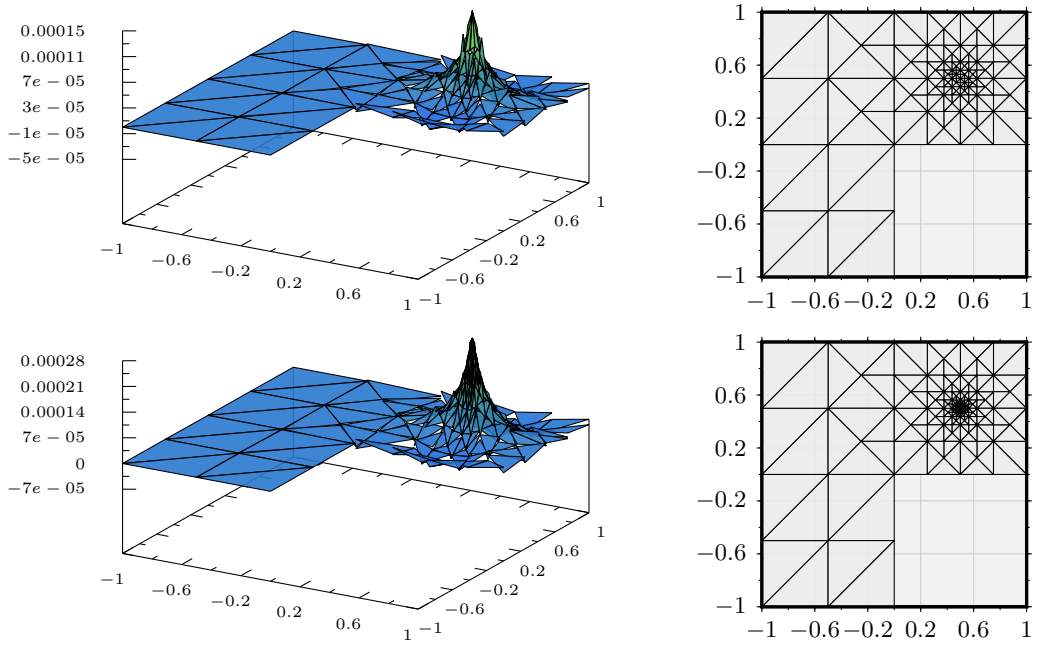

Figure 7.42: Triangulation and corresponding discrete CR solution computed with S-AFEM-AA for the Stokes problem of Section 7.5 ($\epsilon = 2^{-6}$) with $\theta_A = 0.2$, $\rho_B = 0.1$ and $\kappa = 0.1$ on levels $\ell = 2$, 4 with `ndof` = 739, 1123.

Computational costs

Figure 7.43 proves that S-AFEM-AA can reduce the number of levels in the pre-asymptotic regime. The choice of $\kappa = 0.1$ or $\kappa = 0.3$ with $\theta_A = 0.6$ and $\rho_B = 0.01$ perform best. For C-AFEM, when $\theta_A = 0.6$ obviously more iterations are necessary to reach a similar level of μ_ℓ, but it catches up later. However, the computational costs of the best set of parameter values for S-AFEM-DM ($\kappa = 0.3$, $\theta_A = 0.6$ and $\theta_B = 0.9$) are clearly higher than the computational costs of either S-AFEM-AA or C-AFEM for the aforementioned parameter values.

The comparison of the computational costs in Figures 7.46 and 7.47 for the Stokes problem shows that all adaptive schemes exhibit a similar overall behaviour although the width of the bundle of curves is relatively large. Considering the cumulative processing time of step Solve, see Figure 7.47, in the pre-asymptotic range S-AFEM-AA (with $\kappa = 0.3$, $\theta_A = 0.6$ and $\rho_B = 0.1$) performs better than S-AFEM-DM or C-AFEM. C-AFEM with $\theta_A = 0.6$ and S-AFEM-DM (with $\kappa = 0.3$, $\theta_A = 0.6$ and $\theta_B = 0.9$) seem to catch up.

Again there are steps (Figure 7.46), which reflect the high mesh refinement of S-AFEM-AA. This is induced in particular by small values of ρ_B. As predicted, these steps are not present in Figure 7.47, which shows only the CPU time for step Solve.

However, there are differences in the early, mid and late ranges, as observed before. Looking only at the CPU time needed for step Solve (Figure 7.47), at an early stage of about 1 second of CPU time, S-AFEM-AA (with $\kappa = 0.3$, $\theta_A = 0.2$ and $\rho_B = 0.1$) is significantly better than any of the other adaptive (and uniform) mesh refinements. From the mid-range on, C-AFEM (with $\theta_A = 0.6$) is the best choice. Its pre-asymptotic behaviour is clearly worse than that of S-AFEM-AA. Again, S-AFEM-AA, with $\kappa = 0.3$, $\theta_A = 0.2$ and $\rho_B = 0.1$ as before, is among the best choices and it is not worse than S-AFEM-DM.

Progress of separate marking

Figures 7.44 and 7.45 again show the flexibility of adaptive schemes that rely on separate marking. As predicted, S-AFEM-AA uses radically fewer levels (just 3) for Case (B) – until Case (A) can be applied. Due to the refinement restrictions of the Dörfler marking this is not possible for S-AFEM-DM.

7.5.2 Microstructure with a small support of $f \in L^2(\Omega)$

In the final experiments, the edge length of the support of the right-hand side function f is reduced to $\epsilon = 2^{-10}$. This simulates a microstructure. A more complicated microstructure with exact integration would be very complex to implement and therefore this has not yet been realised.

Convergence plots

Figures 7.48 and 7.49 show a larger pre-asymptotic range for $\epsilon = 2^{-10}$ compared to $\epsilon = 2^{-6}$ (Figures 7.40 and 7.41). Moreover, for uniform refinement, convergence of η_{Av} and μ_ℓ cannot be observed in the plotted range. Within eight levels of uniform refinement and a barely acceptable CPU time, convergence can only be vaguely supposed. Due to the choice of $\epsilon = 2^{-10}$, the right-hand side function $f \in L^2(\Omega)$ is resolved by the triangulation after

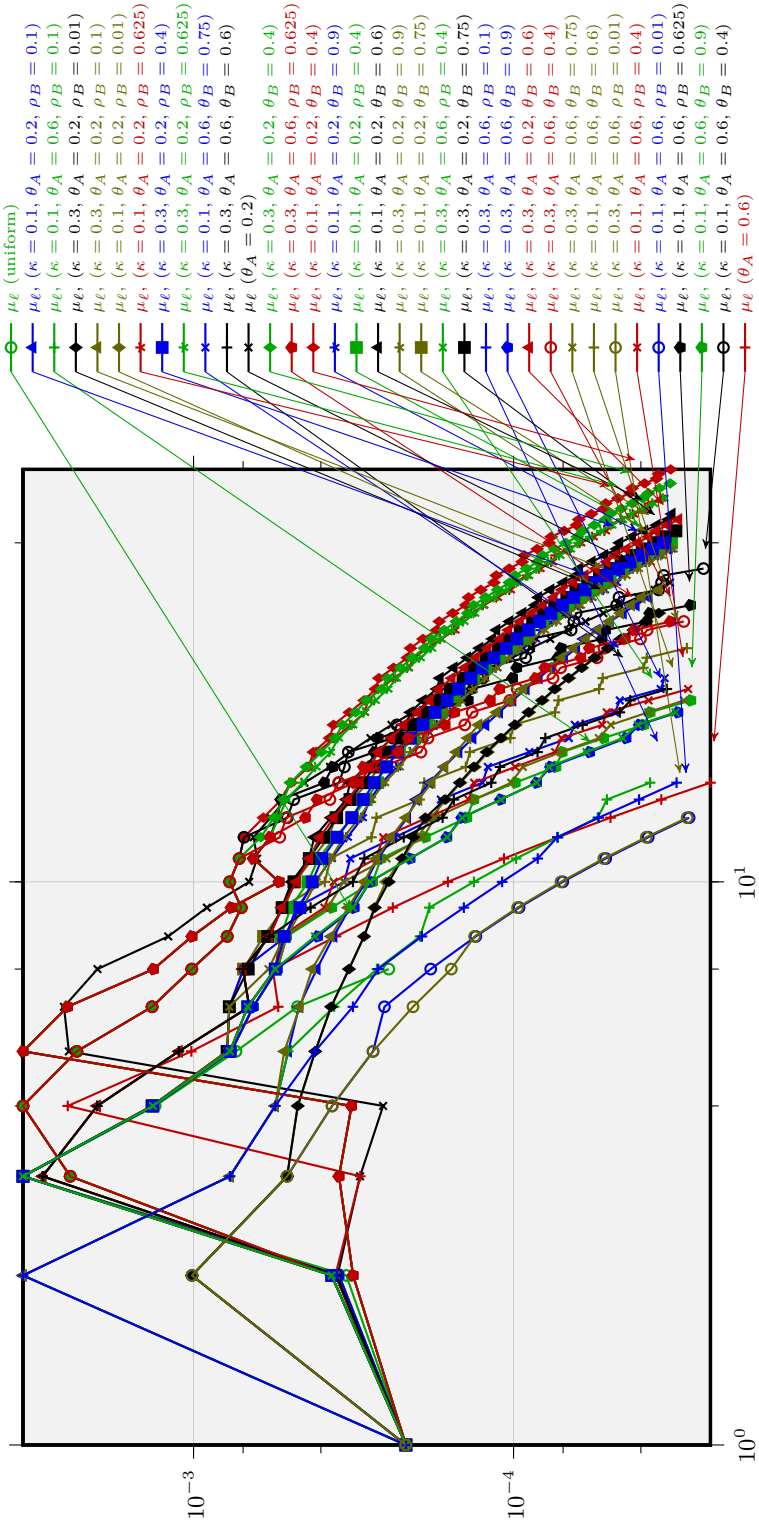

Figure 7.43: μ_ℓ versus number of levels for the Stokes problem of Section 7.5, $\epsilon = 2^{-6}$.

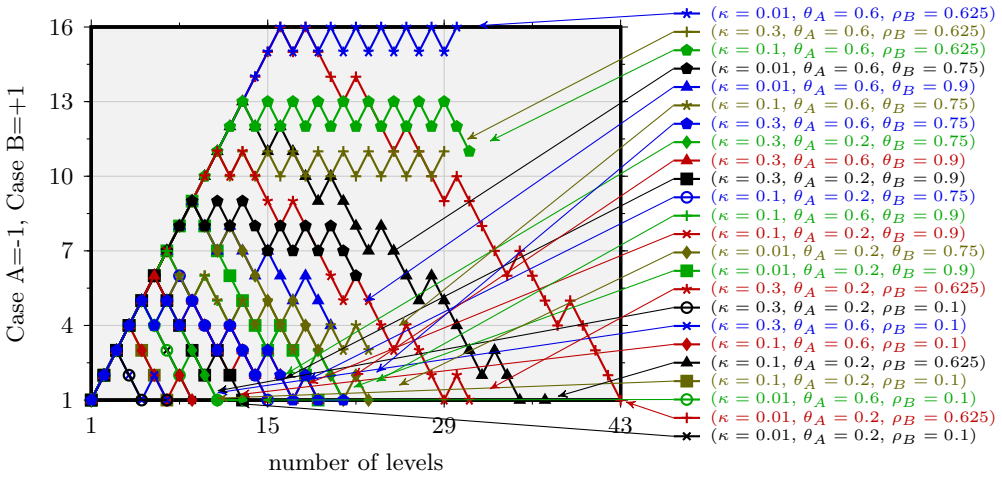

Figure 7.44: Use of Cases (A) and (B) in S-AFEM as a function of the number of levels for the Stokes problem of Section 7.5, $\epsilon = 2^{-6}$.

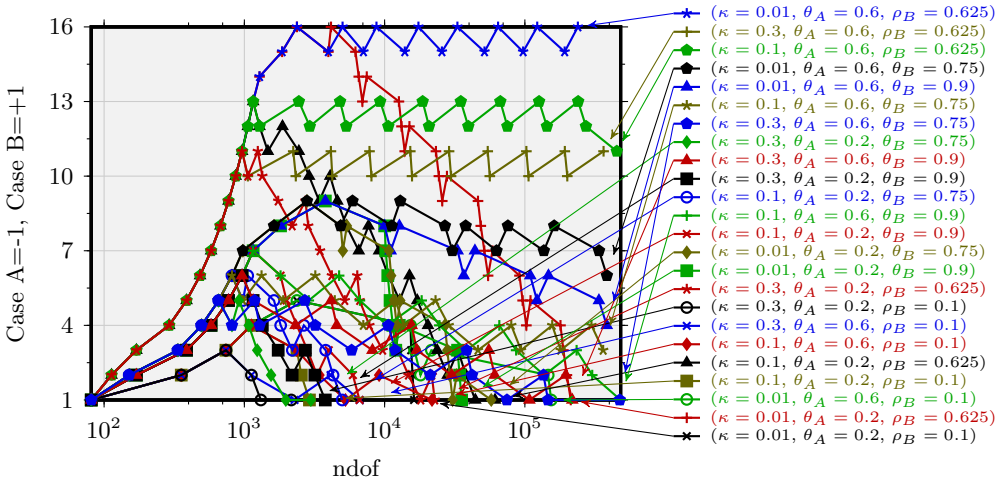

Figure 7.45: Use of Cases (A) and (B) in S-AFEM as a function of `ndof` for the Stokes problem of Section 7.5, $\epsilon = 2^{-6}$.

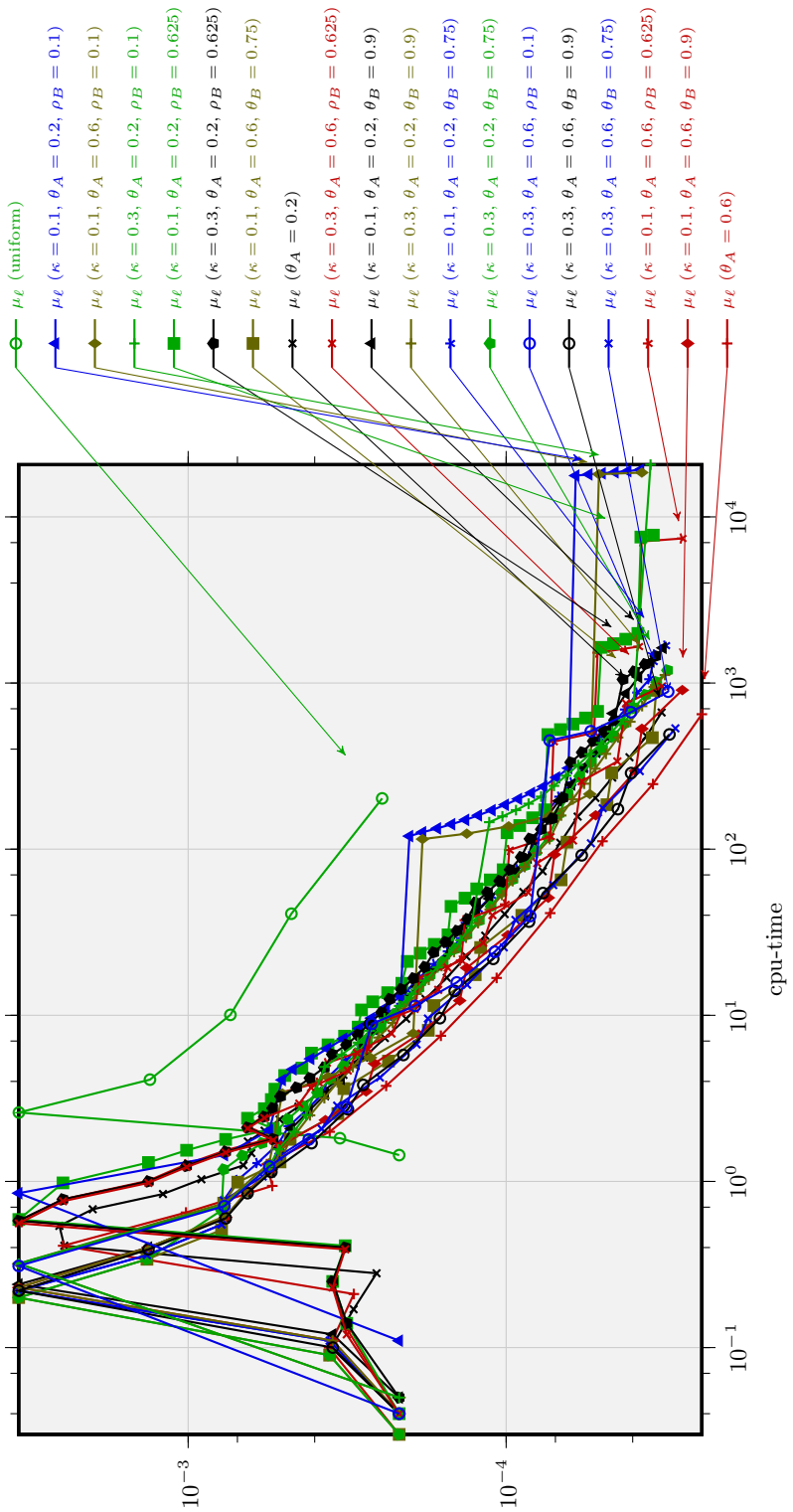

Figure 7.46: μ_ℓ versus overall processing time for the Stokes problem of Section 7.5, $\epsilon = 2^{-6}$.

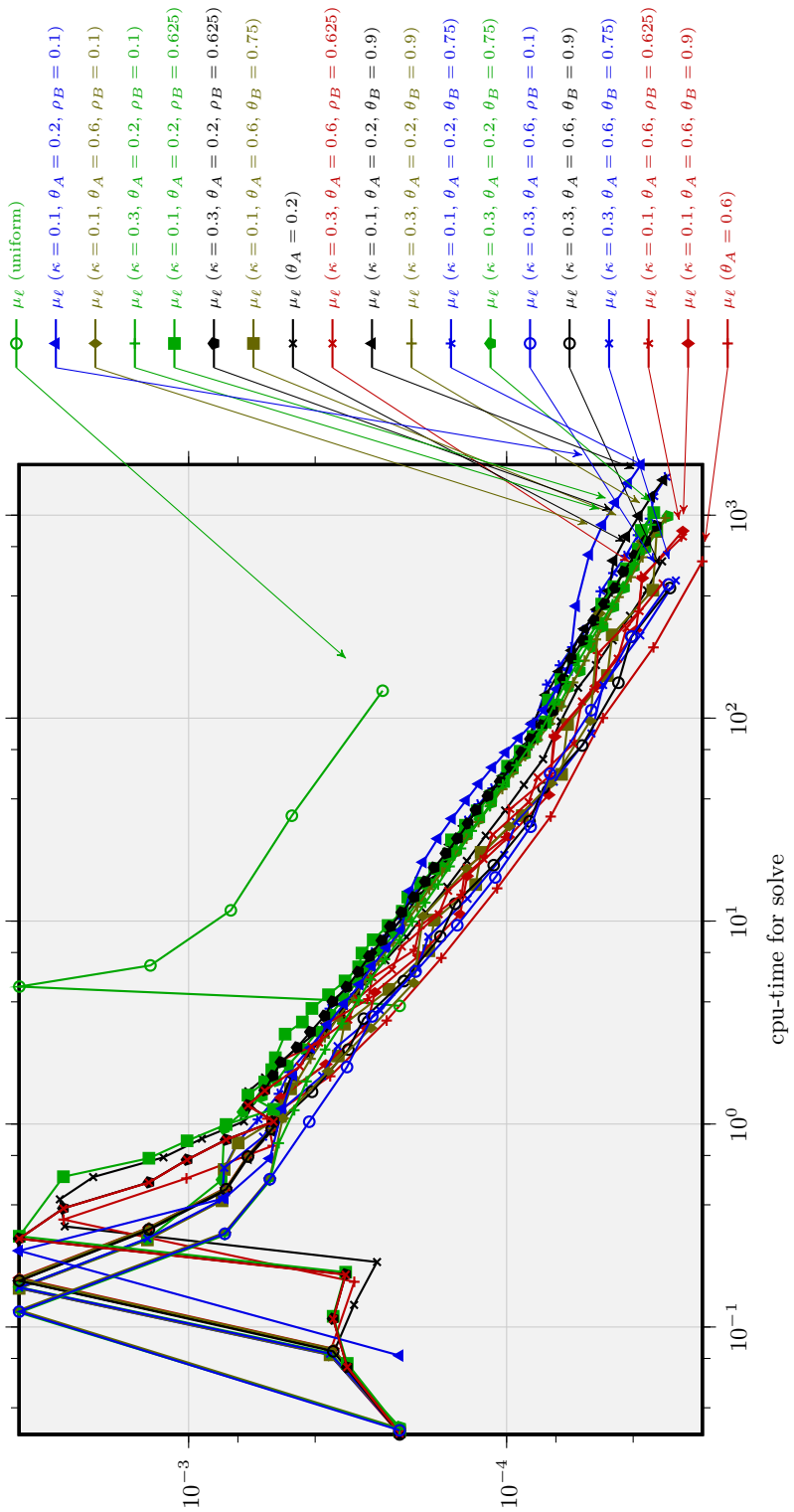

Figure 7.47: μ_ℓ versus cumulative processing time of SOLVE for the Stokes problem of Section 7.5, $\epsilon = 2^{-6}$.

eight refinements. The convergence plots for the adaptive schemes are close together and have the same optimal convergence rate of 1/2. Compared to $\epsilon = 2^{-6}$, the pre-asymptotic range is considerably wider.

Computational costs

As for $\epsilon = 2^{-6}$, the lowest computational costs are observed for C-AFEM with $\theta_A = 0.6$. At an early state, there are parameter sets for S-AFEM-AA that cause μ_ℓ to decrease faster (e.g., $\rho_B = 0.625$); see Figures 7.50 and 7.51. The advantage of S-AFEM-AA is apparent in Figure 7.52. The decrease of μ_ℓ as a function of the number of levels shows that S-AFEM-AA (with parameters $\kappa = 0.1$ or $\kappa = 0.3$, $\theta_A = 0.6$ and $\rho_B = 0.01$ or $\rho_B = 0.1$) performs better than C-AFEM or S-AFEM-DM. Again, C-AFEM with $\theta_A = 0.6$ catches up later, while S-AFEM-DM is not competitive (the best values are achieved with $\theta_B = 0.9$).

Progress of separate marking algorithms

To conclude this section, the use of Cases (A) and (B) for S-AFEM algorithms is compared in Figures 7.53 and 7.54. It is obvious that S-AFEM-AA performs exceptionally well in reducing the number of levels in the pre-asymptotic regime.

7.6 Concluding remarks

The numerical experiments of this chapter demonstrate the overall superiority of adaptive over uniform mesh refinement. Optimal convergence rates are observed for all benchmark problems for the adaptive algorithms for nonconforming FEM. Uniformly refined meshes have poorer convergence compared to adaptive meshes: The Poisson problem of Section 7.1 on the unit square exhibits the optimal convergence rate with a larger multiplicative constant. The benchmark of Section 7.2 on the L-shaped domain for all three model problems and uniform mesh refinements shows – as expected – a worse convergence rate. Nonconforming AFEMs have optimal convergence rates for all problems. The locking phenomenon is observed for conforming FEM and linear elasticity. It leads to large pre-asymptotic regimes. For the Stokes equations and the piecewise constant right-hand side function $f \in L^2(\Omega)$, convergence of uniform meshes is not obvious until $\texttt{ndof} \leqslant 10^{-5}$ for $\varepsilon = 2^{-10}$ and both μ_ℓ and η_ℓ.

The analysis of quasi-optimality of algorithm S-AFEM-AA is subject to this thesis. The advantage is that it can reduce the number of levels in the pre-asymptotic range. The benchmark problems of Section 7.2 simulate a simple microstructure with a piecewise constant right-hand side function $f \in L^2(\Omega)$ and a compact support of edge length $\epsilon = 2^{-n}$. The experiments of this benchmark suggest that highly complex microstructure problems pose a considerable challenge to adaptive algorithms. S-AFEM-AA is designed to resolve $f \in L^2(\Omega)$ in a small number of levels, while for C-AFEM and S-AFEM-DM the refinement of the triangulations in one level is restricted by the Dörfler marking. That is why S-AFEM-AA potentially requires less iterations of the adaptive scheme and therefore also reduces computing time. In particular, the step Solve contributes excessively to the overall costs (especially for nonlinear problems and more complicated FEMs). The feasibility of adaptive algorithms hence depends on their ability to resolve $f \in L^2(\Omega)$ sufficiently.

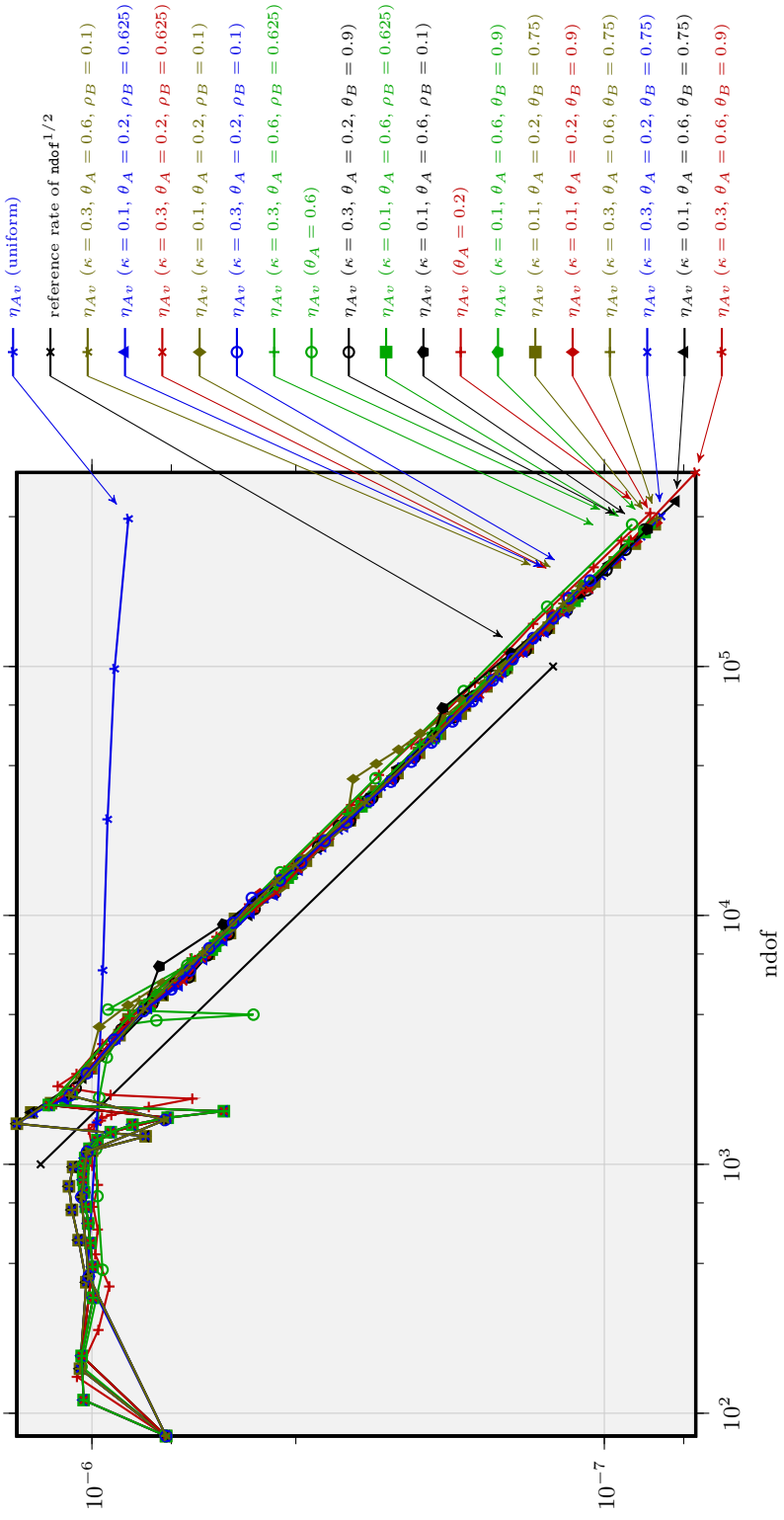

Figure 7.48: η_{Av} versus **ndof** for the Stokes problem of Section 7.5, $\epsilon = 2^{-10}$.

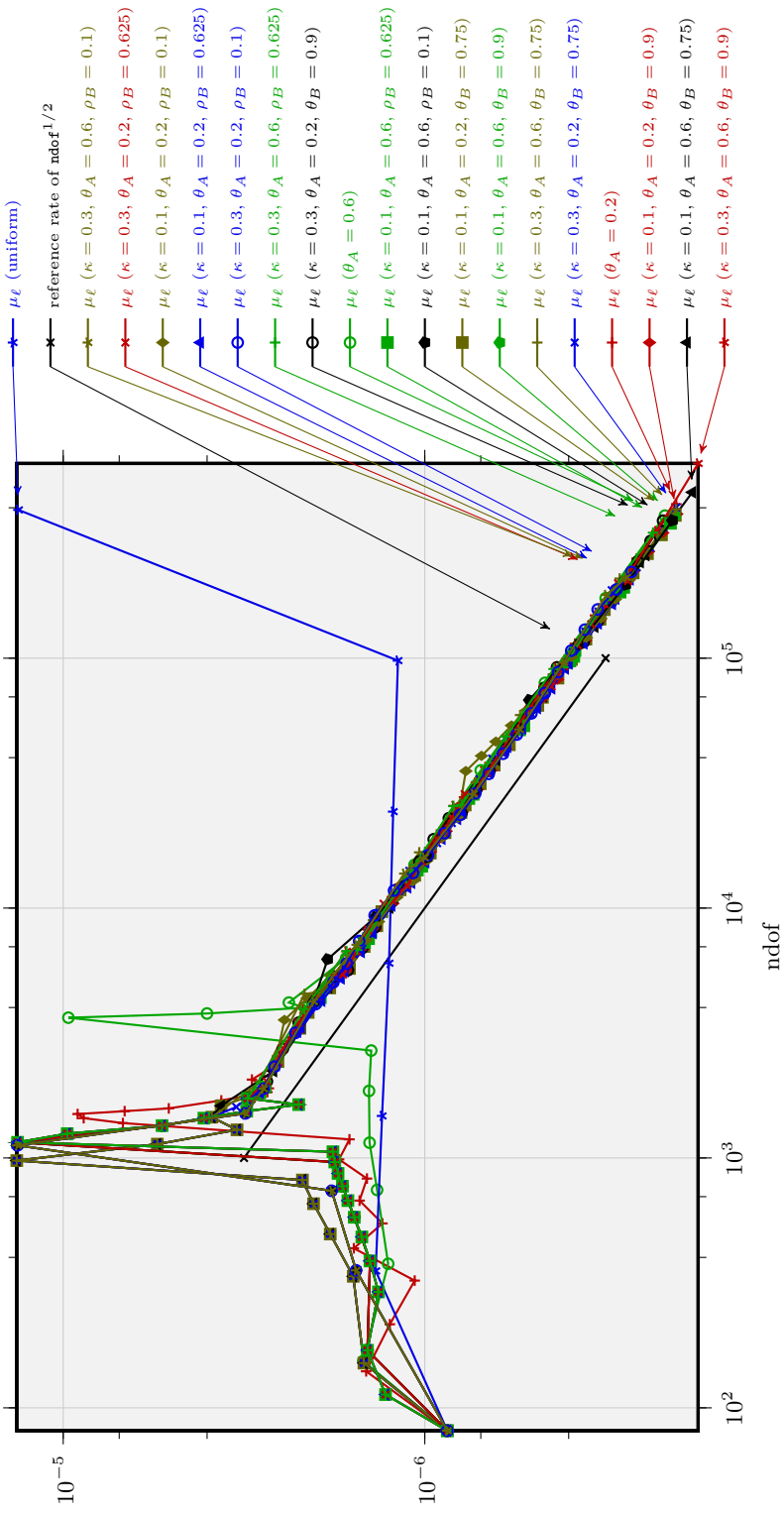

Figure 7.49: μ_ℓ versus **ndof** for the Stokes problem of Section 7.5, $\epsilon = 2^{-10}$.

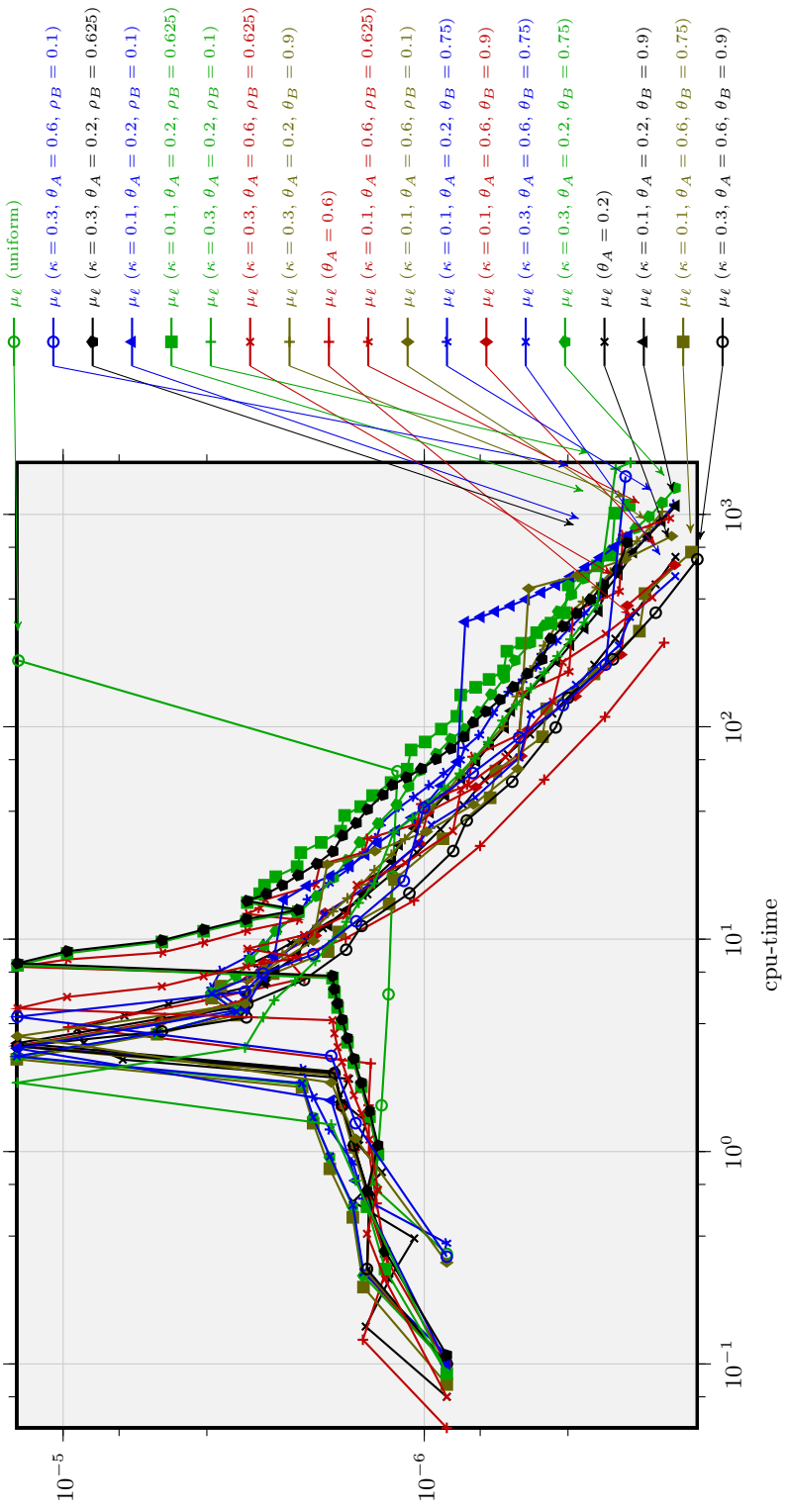

Figure 7.50: μ_ℓ versus overall processing time for the Stokes problem of Section 7.5, $\epsilon = 2^{-10}$.

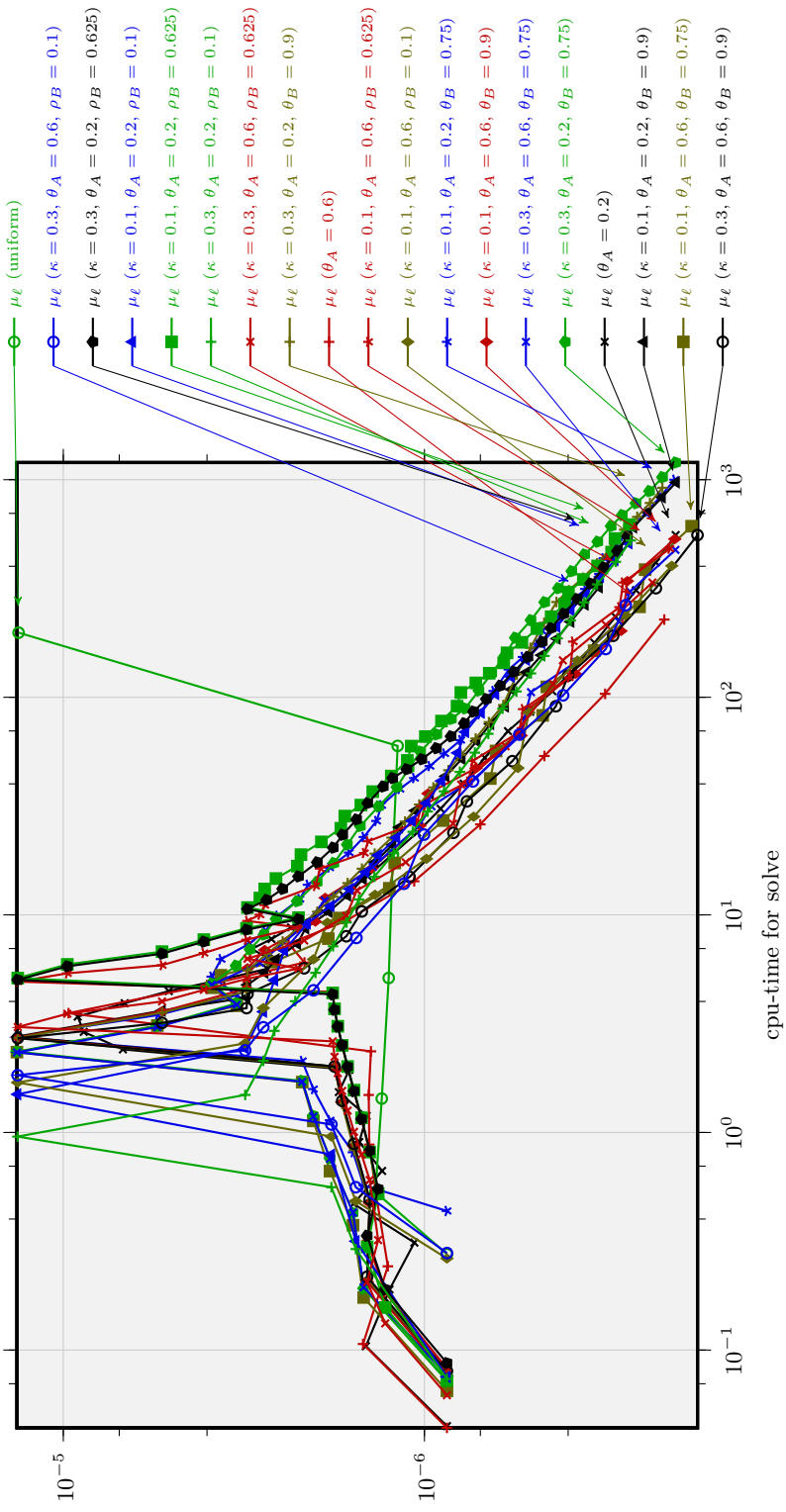

Figure 7.51: μ_ℓ versus cumulative processing time for SOLVE for the Stokes problem of Section 7.5, $\epsilon = 2^{-10}$.

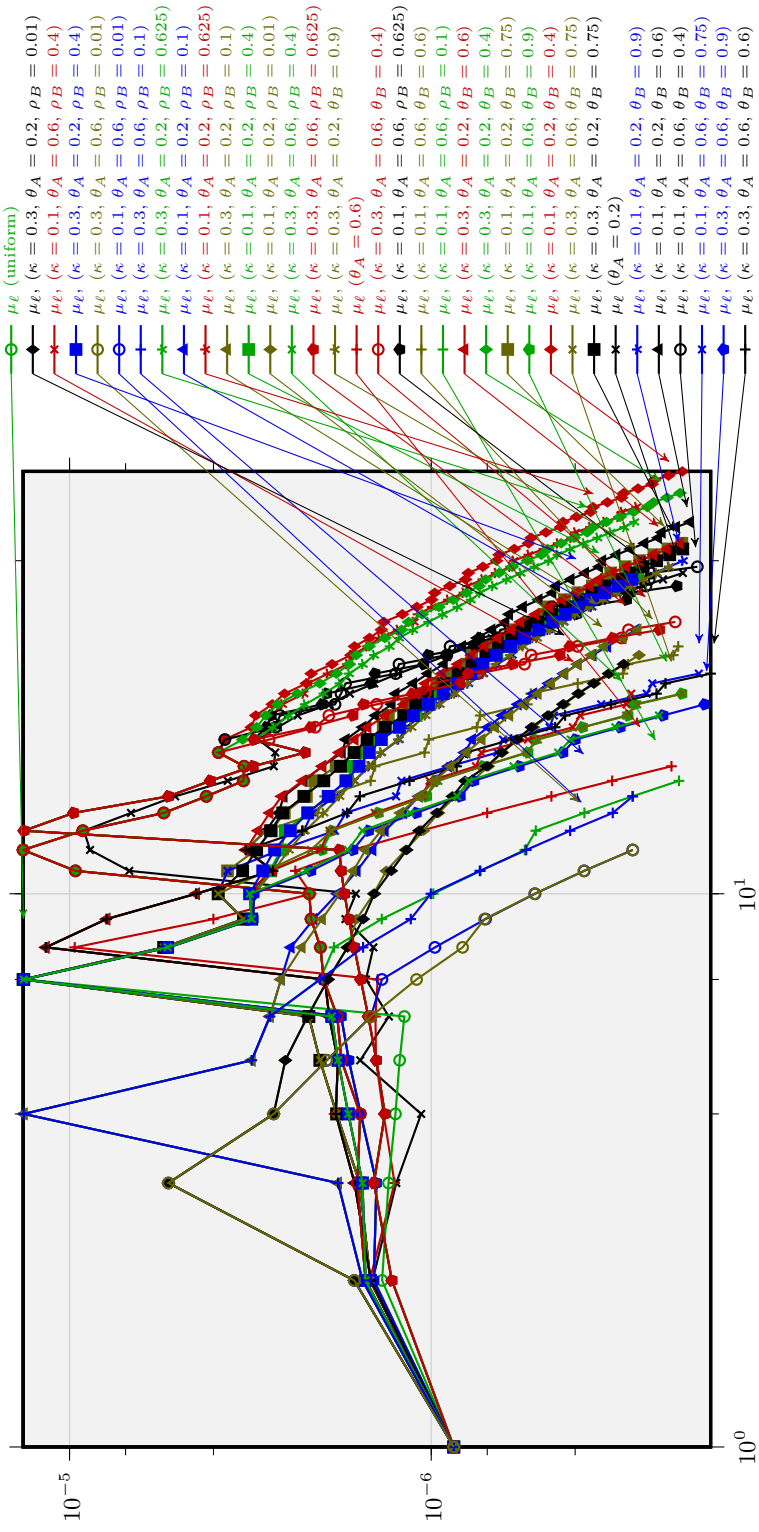

Figure 7.52: μ_ℓ versus number of levels for the Stokes problem of Section 7.5, $\epsilon = 2^{-10}$.

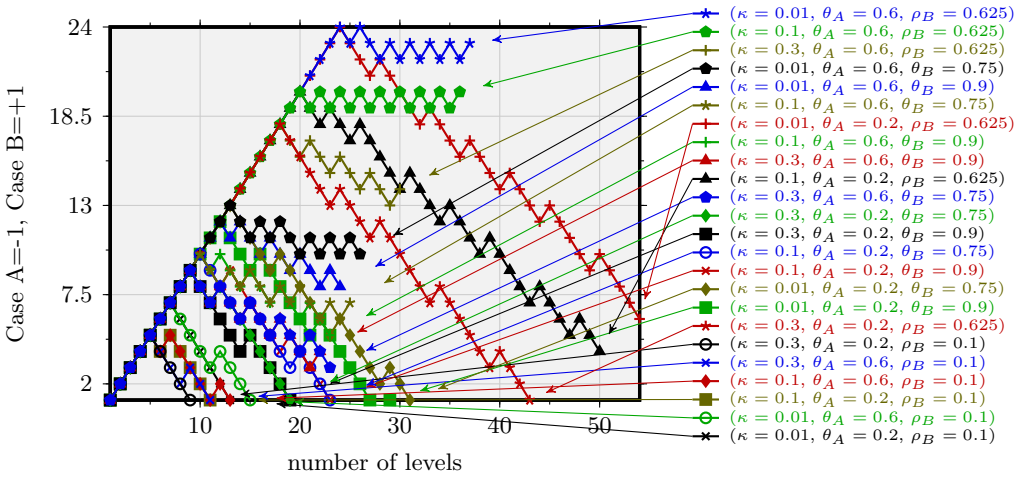

Figure 7.53: Use of Cases (A) and (B) in S-AFEM as a function of the number of levels for the Stokes problem of Section 7.5, $\epsilon = 2^{-10}$.

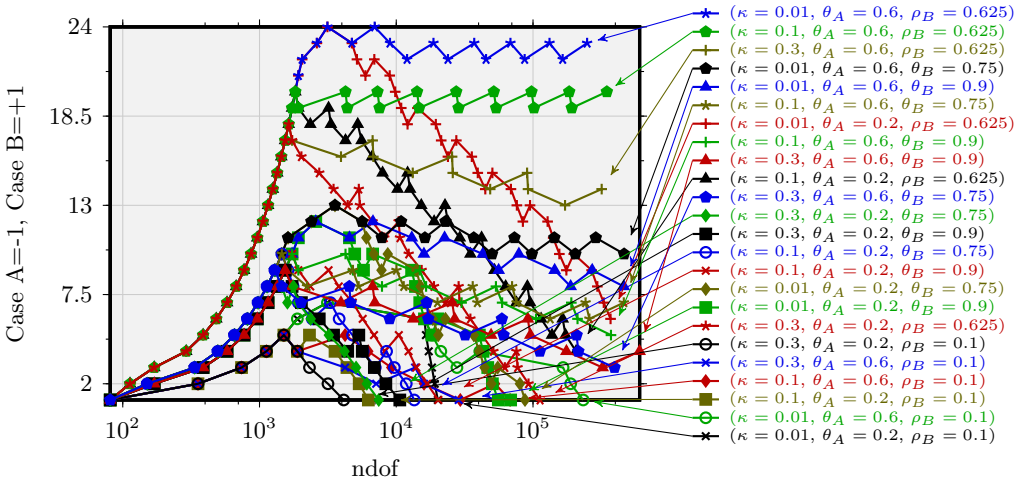

Figure 7.54: Use of Cases (A) and (B) in S-AFEM as a function of `ndof` for the Stokes problem of Section 7.5, $\epsilon = 2^{-10}$.

Appendix A

AFEM implementation

A.1 Introduction

The numerical experiments presented in Chapter 7 of this thesis were realised using the MATLAB software based on the AFEM package [CN09]. The experiments for this thesis were carried out on a cluster with eight CPUs per node (Intel®Xeon®CPU E5-4650L 0 @ 2.60 GHz, with openSUSE 12.2). The implemented code requires MATLAB (at least Version 8.1.0.604, R2013a) and the code package AFEM [CN09], which provides a general framework for adaptive finite element methods.

This appendix gives a short overview of the implemented software, which is provided under the terms of the GNU General Public Licence as published by the Free Software Foundation, either version 3 of the licence or any later version (at your discretion).

The following is a list of the `m` files required for the numerical experiments presented in this chapter. Thus, the different adaptive finite element algorithms based on separate and collective marking can be tested for the three examples. The list also includes two files with license information.

```
GNUGPLv3.txt
LICENSE.txt
afemcycle.m
afemplot-wb/afemLoadLevel.m
afemplot-wb/afemPlot1.m
afemplot-wb/afemPlot1Tables.m
afemplot-wb/afemPlot2.m
afemplot-wb/afemPlot3.m
afemplot-wb/afemPlotCore.m
afemplot-wb/defaultArgIn.m
common/P0AveragingP1.m
common/P0TangentJump.m
common/computeArea4e.m
common/computeArea4n.m
common/computeE4n.m
common/computeE4s.m
common/computeLength4s.m
common/computeMid4e.m
common/computeMid4s.m
common/computeN4s.m
common/computeNormal4e.m
common/computeNzNodes.m
common/computePhiF4CR.m
common/computePhiF4P1.m
common/computeS4e.m
common/computeS4n.m
common/computeTangent4e.m
common/computeTangent4s.m
common/loadGeometry.m
computeProblems.m
estimate/estimateCRCREtaElements.m
estimate/estimateCRCREtaTJumpSides.m
estimate/estimateCRCRStokesEtaTJumpSides.m
estimate/estimateCREtaSidesColl.m
estimate/estimateCREtaTJumpSides.m
estimate/estimateNCStokesEtaElements.m
estimate/estimateP1P1EtaElements.m
estimate/estimateSigmaAveragingP1.m
geometries/Lshape/Lshape.m
geometries/Lshape/Lshape_c4n.dat
geometries/Lshape/Lshape_n4e.dat
geometries/Lshape/Lshape_n4sDb.dat
geometries/Lshape/Lshape_n4sNb.dat
geometries/Square/Square.m
geometries/Square/Square_c4n.dat
geometries/Square/Square_n4e.dat
geometries/Square/Square_n4sDb.dat
geometries/Square/Square_n4sNb.dat
integrate/L2Norm.m
integrate/error4eCREnergy.m
integrate/error4eCRL2.m
integrate/error4eStokesCRStress.m
integrate/integrate.m
integrate/oscillations.m
integrate/volumeTerm.m
mark/approx.m
mark/markBulk.m
meshPlots.m
par_acrfem.m
plotting_results.m
postproc.m
problems/becker_mao_new.m
problems/linElast_f1centLsh.m
problems/poisson_f1centLsh.m
problems/poisson_f1centSqu.m
problems/poisson_lshape_exact.m
problems/stokes_f1centLsh.m
refine/closure.m
```

```
refine/completion.m
refine/overlay.m
refine/refineBi3GB.m
refine/refineBi3GB_irregular.m
refine/refineUniformRed.m
saveLvl.m
solve/solveCRCRLinElast.m
solve/solveCRCRStokes.m
solve/solveCRPoisson.m
solve/solveP1P1LinElast.m
```

The functionality and use of the MATLAB implementation is introduced in the following sections. The data structure is adopted from the finite element implementations introduced in [CN09, ACF99]. For each MATLAB function the prototype at least is given. See the output of the MATLAB `help` function for further details on usage.

The MATLAB software is attached to this thesis: as a CD for the hardcopy or as a zip archive for the pdf-file.

A.2 Controlling the computation

The function `computeProblems` controls the (parallel) computation of numerical experiments. Before running this `m` file, the user can modify it to select the problem to be solved, the adaptive algorithm and parameters that control the AFEM loop. To solve a new problem, this function has to be modified (i.e., parameter settings and solvers have to be selected) and a file containing the problem's description (see Appendix A.10 for examples) has to be included. `computeProblems` is started at the MATLAB prompt. `computeProblems` has neither input nor output parameters.

Listing A.1: Selection of problems and parameter sets.

```
function computeProblems
```

`computeProblems` calls the function `par_acrfem` for the selected set of problems and parameters. `par_acrfem` does the pre-processing, including assembling of file names and handling parameters. `afemcycle`, which realises the algorithms C-AFEM, S-AFEM-AA and S-AFEM-DM, is called and finally `postproc` performs several post-processing computations.

Listing A.2: Managing multiple (parallel) processes of AFEM loops for the given problems and parameter sets.

```
function par_acrfem(problem, sepMark, regular, fast, loadlevel,...
    savelevel, kappa, thetaA, tsa4B, thetaB, rhoB, minNrDoF,...
    para1, para2, para3)
```

A.3 Afem loop

The AFEM loop is realised in `afemcycle`. Depending on the input parameters, `afemcycle` realises one of the Algorithms 3.1, 3.3 and 3.4. The input parameters for `afemcycle` are explained in Table A.1.

Listing A.3: The AFEM loop.

```
function  afemcycle(sepMark, tsa4B, ...
    problemDef, rhsterm, solver, minNrDoF, minEta,...
    kappa, thetaA, facB, rhsDegree, estDegree, ...
    errDegree, regular, fast, saveName, loadlevel,...
    savelevel,E,nu,width)
```

`sepMark`	`true`: separate marking; `false`: collective marking, i.e., C-AFEM
`tsa4B`	`true`: S-AFEM-AA; `false` S-AFEM-DM (if `sepMark` == `false`; the value of `tsa4B` is irrelevant)
`problemDef`	name of the `m` file that specifies the class of the problem to be solved
`rhsterm`	`oscillations` or `volumeTerm`
`solver`	`solveCRPoisson`, `solveCRCRlinElast` or `solveCRCRStokes`
`minNrDoF`	halting criterion for the adaptive scheme for the number of degrees of freedom
`minEta`	halting criterion for the adaptive scheme for $(\|h_\ell f\|^2_{L^2(\Omega)}+\eta_\ell^2)$ if `sepMark` or μ_ℓ otherwise
`kappa`	parameter κ for the adaptive algorithms based on separate marking; it controls whether Case (A) or (B) applies
`thetaA`	bulk parameter for Case (A) for S-AFEM-AA and S-AFEM-DM or the bulk parameter θ_A in C-AFEM
`facB`	parameter to control the refinement in Case (B) (if `sepMark`): θ_B for S-AFEM-DM or ρ_B in S-AFEM-AA
`rhsDegree`	degree of accuracy for the quadrature formula of the numerical integration of the rhsterm
`estDegree`	degree of accuracy for the quadrature formula of the numerical integration of the rhsterm of the refinement indicator η_ℓ or μ_ℓ
`errDegree`	degree of accuracy for the quadrature formula of the numerical integration when calculating the error
`regular`, `fast`	if both parameters are set to `false`, in S-AFEM-AA algorithm AA is realised as described in [BDdV04] (besides the introduction of some threshold parameter as explained in Appendix A.9 below); other values are used for testing, only. If `regular` == `true`, then in each run of the loop of AA the triangulation is regularised using CLOSURE.
`saveName`	if `savelevel` == `true`, then at each level the current state of the adaptive algorithm (including the current numerical solution) is saved to a `mat` file named `saveName`
`loadlevel`	if `loadlevel` == `true`, the algorithm tries to load an already computed level of the adaptive scheme
`savelevel`	if `savelevel` == `true`, the state of the adaptive scheme is saved at each level
`E, nu`	parameters for linear elasticity problems
`width`	parameter for `poisson_f1centSqu`, `poisson_f1centLsh` and `linElast_f1centLsh`; assigns the width of the domain, where the right-hand side f does not vanish

Table A.1: Input parameters for `afemcycle`.

A.4 Solve

The step Solve is realised using problem-dependent functions shown below. Some of the functions are in the software package AFEM [CN09]. Some of the `m` files that are used to solve the problems (in particular for linear elasticity) are not yet part of [CN09]. Several students and colleages contributed to the code used in this thesis.

Listing A.4: `m` files in the directory solve.

```
function [u, nDoFs, A, b, sigma4e, div4e] = solveCRCRLinElast(...
    f, g, u4Db, c4n, n4e, n4sDb, n4sNb, lambda, mu, problem)

function [u, p, A, b, nrDofs, gradU4e] = solveCRCRStokes(f, g, ...
    u4Db, c4n, n4e, n4sDb, n4sNb, problem)

function [x,nrDof,A,b] = solveCRPoisson(f, g, ...
    u4Db, c4n, n4e, n4sDb, n4sNb, problem)

function [u, nDoFs, A, b, sigma4e, div4e] = solveP1P1LinElast(...
    f, g, u4Db, c4n, n4e, n4sDb, n4sNb, lambda, mu, problem)
```

A.5 Estimate

The following is a list of the refinement indicators based on residual-based error estimators for the three types of adaptive algorithms used in this thesis, namely c-afem, s-afem-aa and s-afem-dm. The function `volumeTerm` is contained in the directory `integrate`, although this function is applied in step Estimate to compute the volume Term for s-afem.

Listing A.5: `m` files in the directory estimate.

```
function [eta4s, n4s] = estimateCREtaTJumpSides(u4Db, x, c4n, ...
    n4e, n4sDb, n4sNb)

function [eta4s, n4s] = estimateCREtaSidesColl(f, g, u4Db, ...
        x, c4n, n4e, n4sDb, n4sNb, degree, problem)

% Refinement indicators for linear elasticity
function eta4e = estimateCRCREtaElements(f, Du4Db1, ...
    Du4Db2, g, u, c4n, n4e, n4sDb, n4sNb, mu, ...
    lambda, Sigma4e, gradsU)

function [eta4s, n4s] = estimateCRCREtaTJumpSides(u4Db1, ...
    u4Db2, u, c4n, n4e, n4sDb, n4sNb)

function eta4e = estimateP1P1EtaElements(f, g, u, c4n, n4e,...
    n4sDb, n4sNb, mu, lambda, Sigma4e)

% Refinement indicators for the Stokes equations
function [eta4s, n4s] = estimateCRCRStokesEtaTJumpSides(...
    Du4Db1, Du4Db2, c4n, n4e, n4sDb, u, gradU4e)

function [eta4e] = estimateNCStokesEtaElements(c4n, n4e, ...
    n4sDb, f, Du4Db1, Du4Db2, u, gradU4e)

% Averaging estimator
function eta4e = estimateSigmaAveragingP1(c4n, n4e, sigma4e)
```

A.6 Integrate

Several `m` files realise the numerical integration of a function on a given mesh to compute the volume term, the L^2-norm or some exact error. These functions are collected in the directory `integrate`.

Listing A.6: `m` files in the directory integrate.

```
% General function for integration on a triangulation
function val = integrate(c4n, n4p, integrand, degree, ...
   OPTsize4parts)

% L2 Norm
function [L2norm4Omega, L2norm4p] = L2Norm(c4n, n4e, f, degree)

% Exact errors
function val = error4eCREnergy(c4n, n4e, gradExact, uApprox)

function error4e = error4eCRL2(c4n, n4e, uExact, uApprox)

function error4e = error4eStokesCRStress(c4n, n4e, ...
   component, stressExact, uApprox, pApprox, gradUApprox)
```

The function `volumeTerm` has an important role in the ESTIMATE step of S-AFEM.

Listing A.7: Computation of $\|h_\ell f\|_{L^2(\Omega)}$

```
function [vol4e] = volumeTerm(c4n,n4e,f,degree,problem)
```

A.7 Mark

The function `markBulk` has been slightly modified: $\theta_A = 1$ enforces uniform refinement, which is not the case in [CN09].

Listing A.8: Dörfler's marking.

```
function n4sMarked = markBulk(n4p, eta4p, OPTtheta)
%% markBulk - Mark given parts using the bulk criterion.
%   n4sMarked = markBulk(n4p, eta4p, OPTtheta) marks the parts with the
%       largest estimated errors. The aggregate error of the marked parts
%       is OPTtheta times the overall error. By default, OPTtheta is set
%       to 0.5. n4p contains the nodes for the parts: 2 entries per row
%       for sides, 3 entries per row for elements.
%       The output is a list of marked sides given by their end nodes.
```

```
dimParts = size(n4p,2);
if theta >=1
    % uniform refinement
    % Mark all parts
    I = 1: size(n4p,1);
else
    % adaptive refinement
    % Bulk criterion
    [eta4p,ind] = sort(eta4p,'descend');
    % avoid round-off errors between sum and cumsum (esp. if theta=1)
    cumsumEta4p = cumsum(eta4p);
    J = find(cumsumEta4p >= theta*cumsumEta4p(end),1,'first');
    I = ind(1:J);
end
%% Mark sides
if dimParts == 2 % Sides were given. Mark 'em all.
```

```
      n4sMarked = n4p(I,:);
elseif dimParts == 3 % Elements were given. Mark all sides of these.
      allSidesMarked = [n4p(I,[1 2]);n4p(I,[2 3]);n4p(I,[3 1])];
      % Eliminate duplicates.
      [b, ind]  = unique(sort(allSidesMarked,2), 'rows');
      n4sMarked = allSidesMarked(sort(ind),:);
end
end
```

A.8 NVB refinement: Case (A) and Case (B)

Some of the functions that realise the mesh refinement for Cases (A) and (B) are in the AFEM software package:

Listing A.9: `m` files in the directory refine.

```
function n4sRefine = closure(n4e, n4sMarked)

function [c4nNew,n4eNew,n4sDbNew,n4sNbNew] = ...
   refineBi3GB(c4n,n4e,n4sDb,n4sNb,n4sMarked)

function [c4nNew, n4eNew, n4sDbNew, n4sNbNew] = ...
   refineUniformRed(c4n, n4e, n4sDb, n4sNb)
```

The Matlab function `refineBi3GB_irregular.m` realises NVB refinement with or without completion applied to the set of marked edges or elements (depending on the input parameter `regular`). The implementation is adopted from the standard refinement routines in the AFEM software package [CN09] through the addition of the error functionals e and $\tilde{e}$ for proper refinements for use in algorithm AA in `approx.m`.

Listing A.10: NVB refinement.

```
function [c4nNew, n4eNew, n4sDbNew, n4sNbNew, err4eNew] = ...
                refineBi3GB_irregular(c4n, n4e, n4sDb, ...
                n4sNb, n4sMarked, err4e, rhsf, regular)

%% refineBi3GB_approx
%               - Refine using the Bisec3-Green-Blue-strategy
%                 furthermore calculate err4eNew based on rhsf
%                 used in approx based on err4e.
%                       For details on data structures
%                       (cf. refineBi3GB.m).
%  However, do not use closure or completion if not regular. Thus, the
%  output triangulation will probably has hanging nodes.
%
% Input: c4n, n4e, n4sDb, n4sNb
%                       - triangulation
%        n4sMarked      - set of marked sides to be refined
%        err4e = [rhsf4e, etilde4e]
%                       - error functional and error functional
%                         etilde from Tresholding second algorithm
%                         of the input triangulation
%        rhsf           - function handle of the error
%                         functional for TSA
%       regular         - true: run closure after each marking step
%                       - false : do not run closure simultaneaously
%                              i.e., after each marking loop

% Output: c4nNew, n4eNew, n4sDbNew, n4sNbNew
%                       - new triangulation
%         err4eNew = [rhsf4eNew, etilde4eNew]
%                       - error functional and error functional
%                         etilde from Tresholding second algorithm
```

```
%                          of the output triangulation
```

```
42  %% Initialisation
    nrNodes = size(c4n,1);
    nrElems = size(n4e,1);
45  %%  Avoid Closure Algorithm ?
    if (regular)
       n4sRefine = closure(n4e,n4sMarked);
    else
       n4sRefine = n4sMarked;
50  end

    %% Compute newNodes4n to find new nodes faster.
    newNodes4s = sparse(n4sRefine(:,1),n4sRefine(:,2),...
                        (1:size(n4sRefine,1))'+ nrNodes, ...
55                          nrNodes, nrNodes);
    if (regular)
        newNodes4s = newNodes4s + newNodes4s';
    end

60  %% Compute coordinates of new nodes.
    mid4sRefine = (c4n(n4sRefine(:,1),:)+c4n(n4sRefine(:,2),:))/2;
    c4nNew = [c4n;mid4sRefine];

    %% bisec3 refinement
65  % Count elements in new triangulation. For each newNode, one
    % new elements will be created.
    if (regular)
       nrNewElems = nrElems+2*size(n4sRefine,1)-size(n4sDb,1)...
                           -size(n4sNb,1);
70  else
       nrNewElems = nrElems+nnz(newNodes4s);
    end
    n4eNew = zeros(nrNewElems,3);
    err4eNew = zeros(nrNewElems,2);
75  % index to keep track of the current element number in n4eNew
    ind = 0;
    for curElem = 1 : nrElems
        curNodes = n4e(curElem,:);
        curErr = err4e(curElem,:);
80      curNewNodes = [newNodes4s(curNodes(1),curNodes(2));
                       newNodes4s(curNodes(2),curNodes(3));
                       newNodes4s(curNodes(3),curNodes(1));
                      ];
        nrNewNodes4curElem = nnz(curNewNodes);
85      if nrNewNodes4curElem == 0 % no refinement
            n4eNew(ind+1,:) = curNodes;
            err4eNew(ind+1,:) = curErr;
            ind = ind+1;
        elseif nrNewNodes4curElem == 1 % green refinement
90          n4eNew(ind+1:ind+2,:) = ...
                [ curNodes(3)    curNodes(1) curNewNodes(1);
                  curNodes(2)    curNodes(3) curNewNodes(1);
                ];
            % Compute rhsf_term
95          rhs4e = rhsf(c4nNew, n4eNew(ind+1:ind+2,:));
            % Compute etilde
            if sum(curErr)<=0
               err4eNew(ind+1:ind+2,:) = [rhs4e zeros(2,1)];
            else
100            err4eNew(ind+1:ind+2,:) = [rhs4e ...
               sum(rhs4e)/sum(curErr)*curErr(2)*ones(2,1)];
            end
            ind = ind+2;
        elseif nrNewNodes4curElem == 2
105         if curNewNodes(2) > 0 % blue right
                curn4eNew = ...
```

A.9 Approximation algorithm in Case (B): Algorithm 3.17, completion and overlay

`approx.m` is a slightly modified version of Approx algorithm of [BDdV04], in that a threshold `rhsf_factor` is introduced in the Mark step of that algorithm. Originally only the elements T with $\tilde{e}(T) = \tilde{e}_{\max} := \max_{T\in\mathcal{T}} \tilde{e}(T)$ were marked for refinement. In the modified version, all elements $T \in \mathcal{T}$ that satisfy $\tilde{e}(T) \geqslant (1 - \texttt{rhsf\_factor})\tilde{e}_{\max}$ are marked. See line 82 of `approx.m` in Listing A.11. In the computations, `rhs_factor=1e-6` has been used. As in the original, this step is repeated until $\tilde{e}(\mathcal{T}) \leqslant \mathrm{Tol}$ is satisfied.

Listing A.11: Approx (tsa plus completion).

```
function [c4n, n4e, n4sDb, n4sNb, err4e,c4n_nc, n4e_nc, ...
                n4sDb_nc, n4sNb_nc, err4e_nc] = ...
                approx(rhsf, c4n_nc, ...
                n4e_nc, n4sDb_nc, n4sNb_nc, err4e_nc, ...
                c4n_initial, n4e_initial, n4sDb_initial,...
                n4sNb_initial, err4e_initial, ...
                threshold)

%% approx   - generates an optimal triangulation wrt.
%              the reduction of rhsf, s.t.
%              sum(err4e(:,1)) <= threshold.
%           - this algorithm marks elements as in approx
%            (cf. BBdV); completion is applied after tsa has
%            finished.
% INPUT
%      rhsf - error function that has to be reduced
%               (e.g. osc(f,T) or vol(f,T))
%  c4n_nc, n4e_nc, n4sDb_nc, n4sNb_nc
%           - last output of approx but without running completion
%             (if Case B has been applied at least once before)
%             otherwise initial triangulation
%  err4e_nc - matrix of error functional for the _nc
%             triangulation
%             size(err4e_nc)=[size(n4e_nc,1),2]
%             err4e_nc(:,1)= error functional for elements
%              err4e_nc(:,2)= tilde e, weighted error functional as
%              defined by Binev, Dahmen and deVore
%  c4n_initial, n4e_initial, n4sDb_initial, n4sNb_initial
%           - initial triangulation
%  err4e_initial
%           - matrix of error functional of the _initial
%              triangulation
%  intDegree
%           - degree for integrating when computing the
%               error functional
%  threshold - tolerated threshold for the error functional
%
%   OUTPUT
%     c4n_nc, n4e_nc, n4sDb_nc, n4sNb_nc
%           - refined triangulation (no completion,
%             not regular) with sum(err4e(:,1)) <= threshold
%           - for later use, if TSA needs to be started again
%      c4n, n4e, n4sDb, n4sNb
%           - refined triangulation (after completion,
%             regular) with sum(err4e(:,1)) <= threshold
%      err4e - matrix of the error functional
```

```
while (loop)
      %% MARK elements with largest e tilde
          maxerr4e=max(err4e_nc(:,2));
          I = err4e_nc(:,2) >= (1-rhsf_factor)*maxerr4e;
      % choose the reference edge
      n4sMarked = n4e_nc(I,1:2);
```

```
85
        % markMaximum marks all edges of the triangles with maxError
        %n4sMarkedb = markMaximum(n4e_nc, err4e_nc(:,2), 1.0);

        %% REFINE those elements and compute [rhsf, etilde]
90      [c4n_nc,n4e_nc,n4sDb_nc,n4sNb_nc, err4e_nc] = ...
            refineBi3GB_irregular(c4n_nc, n4e_nc, n4sDb_nc, ...
            n4sNb_nc, n4sMarked, err4e_nc, rhsf, false);
        errT = sum(err4e_nc(:,1));

95      status = min((errT_old-errT)/(errT_old - threshold)*100,100);
        fprintf(1,'\b\b\b\b\b\b\b\b\b\b\b\b\b\b\b\b\b\b\b\b\b\b\b\b\b\b');
        fprintf(1,'\b\b\b\b\b\b\b\b %6.2f%%, ||rhs f||^2: %9.3e', ...
            status, errT);

100     %% BREAK if rhsf(f,T) satisfies threshold
        if errT<=threshold, loop=false; end;
    end
    fprintf(1,'\n');
    %% Completion of the triangulation to generate a regular one
105 [c4n, n4e, n4sDb, n4sNb, err4e]=completion(c4n_nc,...
        c4n_initial, n4e_initial, n4sDb_initial, ...
        n4sNb_initial, err4e_initial,rhsf);
end
```

Listing A.12: Compute a regular triangulation by completion.

```
1  function [c4n,n4e,n4sDb,n4sNb,err4e]=completion(c4n_nc,...
2      c4n, n4e, n4sDb,n4sNb,err4e,rhsf)
   %% completion - generate a regular triangulation
   %               by means of completion algorithm
   %               needed for the real tsa + completion algorithm
   %
7  %% Input
   % c4n_nc,n4e_nc,n4sDb_nc,n4sNb_nc
   %               - triangulation with possible hanging nodes
   % c4n, n4e, n4sDb, n4sNB
   %               - last regular triangulation
12 % err4e,rhsf    - input to compute e and etilde of tsa
   %
   %% Output
   % c4n,n4e,n4sDb,n4sNb - regular triangulation after completion
   % err4e              - refinement indicator for tsa (e, etilde)
```

```
25 % compute all midpoints the last regular triangulation triangulation
   n4s = computeN4s(n4e);
   mid4s = computeMid4s(c4n, n4s);
   % index = numbers the midpoints, that belong to the _nc triangulation
   % (i.e. these edges will be refined)
30
   % Mark
   c4n_new = unique(c4n_nc,'rows');
   c4n_new = setdiff(c4n_new, c4n, 'rows');
   [~, index, indexc4n] = intersect(mid4s, c4n_new, 'rows');
35 fprintf(1,'     completion: nr Nodes in irregular mesh: %6.0f \n',...
       size(unique(c4n_nc, 'rows'), 1));
   fprintf(1,'     nr Nodes: %9.0f; nr of marked edges: %7.0f',...
       size(c4n, 1),size(index, 1));
   while ~isempty(index)&&~isempty(c4n_new)
40
       % REFINE
       [c4n, n4e, n4sDb, n4sNb, err4e] = refineBi3GB_irregular(c4n, n4e,...
            n4sDb, n4sNb, n4s(index, :), err4e, rhsf, true);
       c4n_new = setdiff(c4n_new, c4n_new(indexc4n, :), 'rows');
45     %MARK
       n4s = computeN4s(n4e);
       mid4s = computeMid4s(c4n, n4s);
       % Update the Output on the screen
       [~,index,indexc4n] = intersect(mid4s,c4n_new,'rows');
```

```
50      fprintf(1,'\b\b\b\b\b\b\b\b\b\b\b\b\b\b\b\b\b\b\b\b\b\b\b\b\b\b');
        fprintf(1,'\b\b\b\b\b\b\b\b\b\b\b\b\b\b\b\b\b\b\b\b\b\b\b\b\b\b');
        fprintf(1,'\b');
        fprintf(1,'nr Nodes: %9.0f; nr of marked edges: %7.0f\n',...
            size(c4n, 1), size(index, 1));
55  end
```

Listing A.13: Compute the overlay of two regular triangulations.

```
 1  function [c4n, n4e, n4sDb, n4sNb] = overlay(c4n, n4e, n4sDb, ...
                                                  n4sNb,c4n2,c4n3)

    %% overlay - Computes the overlay (coarsest common refinement)
 5  %            of two triangulations T2 and T3 refined by NVB
    %            from a coarse triangulation T0
    % INPUT
    %     c4n, n4e, n4sDb, n4sNb
    %                 - initial (regular) triangulation T0
10  %       c4n2      - (regular) triangulation T2 refined from T0
    %       c4n3      - (regular)triangulation T3 refined from T0
    %
    % OUTPUT
    %     c4n, n4e, n4sDb, n4sNb
15  %                 - overlay triangulation of T2 and T3
```

```
24  % matrix of coordinates of all nodes that will belong
25  % to the overlay triangulation
    c = unique([c4n2;c4n3],'rows');

    %% MARK
    % compute n4s and all midpoints in T0;
30  n4s = computeN4s(n4e);
    mid4s = computeMid4s(c4n,n4s);

    % index = numbers the midpoints of edges in T0,
    %         that belong to the overlay
35  %         (i.e. these edges will be refined)
    [dummy{2},index] = intersect(mid4s,c,'rows');

    % output
    fprintf(1,'\n compute overlay:');
40
    % Loop:
    % as long as there are coordinates in c that match a midpoint
    while ~isempty(index)

45      % output points, that indicate further computing
        fprintf(1,'.');

        % REFINE the edges, whose midpoints belong to the overlay
        [c4n, n4e, n4sDb, n4sNb] = refineBi3GB(c4n, n4e, n4sDb, ...
50                                    n4sNb,n4s(index,:));
        %compute n4s and all midpoints
        n4s = computeN4s(n4e);
        mid4s = computeMid4s(c4n,n4s);
        % MARK : the intersection of c and the midpoints defines
55      %           the set of to be refined edges
        [dummy{2},index] = intersect(mid4s,c,'rows');
    end
    fprintf(1,'\n');
```

A.10 Problems

The problems solved in this thesis are in `m` files, which contain the problem description via a class definition. The following is a list of these `m` files:

Listing A.14: `classdef` files in the directory problems

```
% Poisson problem
classdef becker_mao_new         % Section 7.1
classdef poisson_lshape_exact   % Introduction
classdef poisson_f1centLsh      % Section 7.3

% pure displacement in linear elasticity
classdef linElast_f1centLsh     % Section 7.4

% the Stokes problem
classdef stokes_f1centLsh       % Section 7.5
```

To give a hint on the structure of these `classdef` files, `poisson_f1centLsh` is shown in the following listing.

Listing A.15: Poisson problem of Section 7.3 for the benchmark of Section 7.2.

```
classdef poisson_f1centLsh
% Problem - benchmark for Poisson of section 7.3
%               of the PhD thesis of Hella Rabus

%    Copyright (C) 2013  Hella Rabus
%
%    You should have received LICENSE.txt along with this file
%    that gives further information an the license.
%    See the GNU General Public License for more details.

    properties
        width;
        widthSqu;
        origin = [0.5 0.5];
        probstring = 'poisson_f1centLsh';
    end
    methods
        function obj = poisson_f1centLsh(input)
            obj.width = input;
            obj.widthSqu = input^2;
            obj.origin = [0.5 0.5];
            obj.probstring = 'poisson_f1centLsh';
        end
        %% RHS
        function val = f(this,x)
            n = size(x,1);
            y = x(:,1);
            z = x(:,2);

            p1 = this.origin;
            val = zeros(n,1);
            fp1 =max(abs(y-p1(1)),abs(z-p1(2)));
            I = fp1<this.width;
            val (I) = 1;
        end
    end
    methods (Static)

        function domain = geometry
            domain = 'Lshape';
        end

        function val = exact
            val = false;
        end
        %% problem input data

        %% exact solution
        function exactu = exactSolU(x)
            error('no exact solution');
```

```
            end

            function exactp = exactSolP(x)
                error('no exact solution');
            end


            %% Boundary data
            function val = u4Db(x)
                val = zeros(size(x,1),1);
            end

            function val = g(x)
                val = zeros(size(x,1),1);
            end

        end
    end
```

A.11 Functions generating the data structure

Most of the functions in the directory `common` are taken from [CN09] and do not needed to be changed. Some of the functions are implemented from scratch, i.e., `computeNzNodes`, `computePhiF4CR` and `computePhiF4P1`. These provide an exact and fast computation of the right-hand side for the solve functions for the benchmark setting of Section 7.2 and the three examples.

Listing A.16: Compute nodes in the support of f.

```
function [nzNodes1, nzNodes2] = computeNzNodes(problem,c4n)

%% computeNzNodes (compute nonzero nodes): returns to arrays
% nzNodes1, nzNodes2 for a given problem
% with a RHS f, that vanishes on the domain, but not
% in the neighbourhood with edge length (problem.width) of a
% single point problem.origin
%
% Input:  problem   classdef of the problem
%         c4n       c4n for the current triangulation
%
% Output: nzNodes1, nzNodes2 correspond to the index of c4n with
%         nzNodes1  max(problem.origin,nzNodes1)<problem.width
%         nzNodes2  max(problem.origin,nzNodes1)<=problem.width

%    Copyright (C) 2013  Hella Rabus
%
%    You should have received LICENSE.txt along with this file
%    that gives further information an the license.
%    See the GNU General Public License for more details.

% Initialisation
        origin = problem.origin;
        widthSqu = problem.widthSqu;

% Compute the nodes in c4n, where f does not vanish
% i.e., that belong to the neighourhood fo problem.origin
%       with edge length problem.width
        nzNodes1 = find(max(abs(c4n(:,1)-problem.origin(1)),...
            abs(c4n(:,2)-problem.origin(2)))<problem.width);
        nzNodes2 = find(max(abs(c4n(:,1)-problem.origin(1)),...
            abs(c4n(:,2)-problem.origin(2)))<=problem.width);
```

Listing A.17: Compute the exact value for the integral of $\psi \cdot f$ on an element.

```
function [phi4mid,area4intersection] = computePhiF4CR(...
    c4n, n4e, problem, elem, iN4e)

%% computes phi*f for the CR basis function of some Element elem
% this can be used in the solve methods (such as in solveCRPoisson,
% solveCRCRlinElast or solveCRCRStokes for the benchmark of
% Hella Rabus' PhD thesis. There, the RHS function f has a small
% support in a rectangular neighbourhood of problem.origin of
% edge length problem.width

% Input c4n,n4e - the triangulation
%       elem    - the current element in n4e
%       problem - the problem for which phi*f shall be computed
%       i4N     - an array of indizes subseteq [1 2 3],
%                 the prescribes the nodes of elem, for which the
%                 following holds
%                 max(prolem.origin,nzNodes1)<problem.width
% Output
%    phi4mid           - 3 times 1 array: (CRBasisFunktion * f) (mid)
%    area4intersection - the area of the intersection between elem
%                        and the domain, where f does not vanish

%    Copyright (C) 2013  Hella Rabus
%
%    You should have received LICENSE.txt along with this file
%    that gives further information an the license.
%    See the GNU General Public License for more details.

% Initialisation
tangents4elem = computeTangent4e(c4n,n4e(elem,:));
c4nzNode = c4n(n4e(elem,iN4e),:);
p1 = c4n(n4e(elem,1),:);
p2 = c4n(n4e(elem,2),:);
p3 = c4n(n4e(elem,3),:);

width = problem.width;
widthSqu = problem.widthSqu;

% first node (45 degree angle) belongs to that area
if iN4e == 1
    % compute the coordinates for the intersection of elem and supp(f)
    c4n4intersection = [c4nzNode; ...
        c4nzNode + sqrt(2)*width*tangents4elem(1,:);...
        c4nzNode - width*tangents4elem(3,:)];
    area4intersection = widthSqu/2;
    mid4intersection = computeMid4e(c4n4intersection,[1 2 3]);
    % compute the value of phi_i at the midpoint of the intersection
    phi4mid=[ -1+2*norm(p1-mid4intersection,2)/ ...
        norm(p1-(p2+p3)/2,2); ...
        -1+2*norm(p2-mid4intersection,2)/ ...
        norm(p2-(p1+p3)/2,2); ...
        -1+2*norm(p3-mid4intersection,2)/ ...
        norm(p3-(p2+p1)/2,2)];

% second node (45 degree angle) belongs to that area
elseif iN4e == 2
    % compute the coordinates for the intersection of elem and supp(f)
    c4n4intersection = [...
        c4nzNode - sqrt(2)*width*tangents4elem(1,:);...
        c4nzNode; ...
        c4nzNode+width*tangents4elem(2,:)];
    area4intersection = widthSqu/2;
    mid4intersection = computeMid4e(c4n4intersection,[1 2 3]);
    % compute the value of phi_i at the midpoint of the intersection
    phi4mid=[ -1+2*norm(p1-mid4intersection,2)/ ...
        norm(p1-(p2+p3)/2,2); ...
        -1+2*norm(p2-mid4intersection,2)/ ...
        norm(p2-(p1+p3)/2,2); ...
        -1+2*norm(p3-mid4intersection,2)/ ...
```

```
            norm(p3-(p2+p1)/2,2)];

    % third node (90 degree angle) belongs to that area
73  elseif iN4e == 3
        % compute the coordinates for the intersection of elem and supp(f)
        c4n4intersection = [...
            c4nzNode + width*tangents4elem(3,:); ...
            c4nzNode - width*tangents4elem(2,:);...
78          c4nzNode;
            c4nzNode-ones(1,2)*width];
        % split area into two triangles
        n4e4intersection = [1 2 3; 2 1 4];
        mid4intersection = computeMid4e(c4n4intersection,n4e4intersection);
83      % compute the value of phi_i at the midpoint of each triangle
        % of the intersection
        phi4mid1=[ -1+2*norm(p1-mid4intersection(1,:),2)/ ...
            norm(p1-(p2+p3)/2,2); ...
            -1+2*norm(p2-mid4intersection(1,:),2)/ ...
88          norm(p2-(p1+p3)/2,2); ...
            -1+2*norm(p3-mid4intersection(1,:),2)/ ...
            norm(p3-(p2+p1)/2,2)];
        phi4mid2=[ -1+2*norm(p1-mid4intersection(2,:),2)/ ...
            norm(p1-(p2+p3)/2,2); ...
93          -1+2*norm(p2-mid4intersection(2,:),2)/ ...
            norm(p2-(p1+p3)/2,2); ...
            -1+2*norm(p3-mid4intersection(2,:),2)/ ...
            norm(p3-(p2+p1)/2,2)];
        area4intersection = widthSqu/2;
98      phi4mid = phi4mid1+phi4mid2;
    end
    end
```

Listing A.18: Compute the exact value for the integral of $\phi \cdot f$ on an element.

```
function [phi4mid,area4intersection] = computePhiF4P1(...
    c4n, n4e, problem, elem, iN4e)
```

Listing A.19: `m` files in the directory common

```
function area4e = computeArea4e(c4n,n4e)
function area4n = computeArea4n(c4n,n4e)

function e4n = computeE4n(n4e)
function e4s = computeE4s(n4e)

function length4s = computeLength4s(c4n,n4s)
function mid4e = computeMid4e(c4n, n4e)
function mid4s = computeMid4s(c4n, n4s)
function n4s = computeN4s(n4e)

function normal4e = computeNormal4e(c4n,n4e)

function s4e = computeS4e(n4e)
function s4n = computeS4n(n4e)
function tangent4e = computeTangent4e(c4n,n4e)
function tangent4s = computeTangent4s(c4n,n4s)
function [c4n n4e n4sDb n4sNb] = loadGeometry(name, ...
    OPTRefinementLevel)

function val = P0AveragingP1(c4n,n4e,sigma4e)
function jump4s = P0TangentJump(c4n,n4e,n4sDb,n4sNb,sigma4e,u4Db)
```

A.12 Post-processing

Several functions perform post-processing. They compute or plot special data, which is saved to `tex` or `mat` files. The following list includes functions for mesh-plotting and solution plots (`meshPlots`), and the steering function for the generation of convergence graphs (`plotting_results`) using `afemplot-wb`, which was adopted and slightly modified from Wolfgang Boiger's thesis [Boi13]. `afemplot-wb` uses a default style for uniformly formatting various plots for visualisation.

The function `postproc` performs post-processing (i.e., computing exact errors and additional error estimators) after AFEM has finished for some level.

```
function meshPlots
function plotting_results
function postproc(dirName, fname)
```

A.13 Plotting

The colourful plots in this thesis for the convergence history, adaptive meshes and the corresponding discrete solutions, as well as plots for computational costs and the visualisation of the development of separate marking algorithms are based of Wolfgang Boiger's `afemplot` routines; see [Boi13]. These methods generate tikz files (for use with the LaTeX package tikz) to produce convergence graphs, and 2D and 3D plots and can be found in the directory `afemplot-wb`.

```
function varargout = afemLoadLevel(filePrefix,level,varargin)

function afemPlot1(varargin)

function afemPlot1Tables(tablefilename, dirprefix, xString, ...
   yString, maxy, slopeweight, varargin)

function afemPlot2(c4n, n4e, u4e, output, color, lines, ...
   axes,tics, view, colorbox)

function afemPlot3(c4n, n4e, u4n4e, u4e, output, color, ...
   lines, axes, tics, view)

function afemPlotCore(type, output, color, axes, tics, view, ...
   varargin)

function defaultArgIn(name,def)

function saveLvl(filePrefix, lvl, varargin)
```

The function `afemPlot1Tables` has been modified to fit personal requirements.

The function `saveLvl` saves specific data to a `mat` file. It is possible to use this function to add more data to the `mat`-file later. This function is adapted from a function in [Boi13].

Appendix B

Primary publications of the author

This appendix lists the publications by this thesis' author that are essential in the analysis presented. For the hardcopy version of this thesis, all papers are printed as originally published and so the notation is not completely consistent with the notation used in this thesis. The pdf-file contains the full references instead and for each publication a link to the respective journal's website, where it is available for download.

The first paper (Appendix B.1, [CR11]) was written with Carsten Carstensen. It analyses the convergence behaviour of an adaptive algorithm based on separate marking. The Poisson model problem is solved with the lowest-order Raviart–Thomas FEM. The algorithms analysed in the current thesis follow the same idea. As stressed in this thesis, κ of Lemma 5.2 needs to be bounded from above and below. That is why β and D can be chosen independently of κ. Optimal convergence is guaranteed for all κ with $\kappa \in (\kappa_1, \kappa_2)$. With respect to the aforementioned observation, this thesis concretises Lemma 5.2 and Theorem 5.8 in [CR11] of Appendix B.1.

Unlike the first publication, the remaining three publications contain the convergence analysis of the sequence of FEM solutions using the nonconforming Crouzeix–Raviart FEM for the three model problems, i.e., the Poisson problem (Appendix B.2, [Rab10]), the pure displacement problem in linear elasticity (Appendix B.3, [CR12]) and the Stokes equations (Appendix B.4, [CPR13]), for an adaptive algorithm based on collective marking. These three publications contain proofs of important properties for the sequence of Crouzeix–Raviart solutions and the corresponding triangulations. They are a prerequisite for the analysis in this thesis, which proves quasi-optimality for adaptive algorithms based on separate marking, namely S-AFEM-AA, for the three examples.

B.1 An optimal adaptive mixed finite element method.

[CR11] C. Carstensen and H. Rabus. An optimal adaptive mixed finite element method. *Math. Comp.*, 80(274):649–667, 2011.
http://www.ams.org/journals/mcom/2011-80-274/S0025-5718-2010-02397-X/home.html.

B.2 A natural adaptive nonconforming FEM of quasi-optimal complexity.

[Rab10] H. Rabus. A natural adaptive nonconforming FEM of quasi-optimal complexity. *Comput. Methods Appl. Math.*, 10(3):315–325, 2010.
http://www.degruyter.com/view/j/cmam.2010.10.issue-3/cmam-2010-0018/cmam-2010-0018.xml?format=INT.

B.3 The adaptive nonconforming FEM for the pure displacement problem in linear elasticity is optimal and robust.

[CR12] C. Carstensen and H. Rabus. The adaptive nonconforming FEM for the pure displacement problem in linear elasticity is optimal and robust. *SIAM J. Numer. Anal.*, 50(3):1264–1283, 2012.
http://epubs.siam.org/doi/abs/10.1137/110824139.

B.4 Optimal adaptive nonconforming FEM for the Stokes problem.

[CPR13] C. Carstensen, D. Peterseim, and H. Rabus. Optimal adaptive nonconforming FEM for the Stokes problem. *Numerische Mathematik*, 123(2):291–308, 2013.
http://link.springer.com/article/10.1007%2Fs00211-012-0490-8.

Bibliography

[ACF99] J. Alberty, C. Carstensen, and S. A. Funken. Remarks around 50 lines of Matlab: short finite element implementation. *Numer. Algorithms*, 20(2–3):117–137, 1999.

[AF89] D. N. Arnold and R. S. Falk. A uniformly accurate finite element method for the Reissner-mindlin plate. *SIAM J. Numer. Anal.*, 26:1276–1290, 1989.

[Alo96] A. Alonso. Error estimators for a mixed method. *Numer. Math.*, 74:385–395, 1996.

[ANS01] T. Apel, S. Nicaise, and J. Schöberl. A non-conforming finite element method with anisotropic mesh grading for the Stokes problem in domains with edges. *IMA J. Numer. Anal.*, 21(4):843–856, 2001.

[AO00] M. Ainsworth and J. T. Oden. *A Posteriori Error Estimation in Finite Element Analysis*. Wiley, New York, 2000.

[BBF08] D. Boffi, F. Brezzi, and M. Fortin. Finite elements for the Stokes problem. In D. Boffi, F. Brezzi, L. F. Demkowicz, R. G. Durán, R. S. Falk, and M. Fortin, editors, *Mixed finite elements, compatibility conditions, and applications*, volume 1939 of *Lecture Notes in Mathematics*, pages x+235. Springer-Verlag, Berlin, 2008. Lectures given at the C.I.M.E. Summer School held in Cetraro, June 26–July 1, 2006, Edited by Boffi and Lucia Gastaldi.

[BC04] S. C. Brenner and C. Carstensen. Finite element methods. In E. Stein, R. de Borst, and T. J. R. Hughes, editors, *Encyclopedia of Computational Mechanics*, chapter 4. John Wiley and Sons, 2004.

[BC05] C. Bahriawati and C. Carstensen. Three MATLAB implementations of the lowest-order Raviart-Thomas MFEM with a posteriori error control. *Comput. Methods Appl. Math.*, 5(4):333–361, 2005.

[BCJ02] S. Bartels, C. Carstensen, and S. Jansche. A posteriori error estimates for nonconforming finite element methods. *Numer. Math.*, 92(2):233–256, 2002.

[BDdV04] P. Binev, W. Dahmen, and R. de Vore. Adaptive finite element methods with convergence rates. *Numer. Math.*, 97:219–268, 2004.

[BdV04] P. Binev and R. de Vore. Fast computation in adaptive tree approximation. *Numer. Math.*, 97:193–217, 2004.

[BF91] F. Brezzi and M. Fortin. *Mixed and Hybrid Finite Element Methods*. Springer-Verlag, New-York, 1991.

[BM08] R. Becker and S. Mao. An optimally convergent adaptive mixed finite element method. *Numer. Math.*, 111:35–54, 2008.

[BM11] R. Becker and S. Mao. Quasi-optimality of adaptive nonconforming finite element methods for the Stokes equations. *SIAM J. Numer. Anal.*, 49(3):970–991, 2011.

[BMN02] E. Bänsch, P. Morin, and R. H. Nochetto. An adaptive Uzawa FEM for the

Stokes problem: convergence without the inf-sup condition. *SIAM J. Numer. Anal.*, 40(4):1207–1229, 2002.

[BMS10] R. Becker, S. Mao, and Z. Shi. A convergent nonconforming adaptive finite element method with quasi-optimal complexity. *SIAM J. Numer. Anal.*, 47(6):4639–4659, 2010.

[Boi13] W. Boiger. *Stabilised Finite Element Approximation for Degenerate Convex Minimisation Problems*. PhD thesis, Humboldt-Universität zu Berlin, 2013.

[Bra01] D. Braess. *Finite Elements: Theory, Fast Solvers, and Applications in Solid Mechanics*. Cambridge University Press, 2001.

[BS01] I. Babuška and T. Strouboulis. *The Finite Element Method and its Reliability*. Oxford University Press, 2001.

[BS08] S. C. Brenner and L. R. Scott. *The Mathematical Theory of Finite Element Methods*, volume 15 of *Texts in Applied Mathematics*. Springer-Verlag, New York, Berlin, Heidelberg, third edition, 2008.

[Car97] C. Carstensen. A posteriori error estimate for the mixed finite element method. *Math. Comp.*, 66:465–476, 1997.

[Car01] C. Carstensen. Numerical analysis of microstructure. In J. P. Coleman J. F. Blowey and A. W. Craig, editors, *Theory and numerics of differential equations (Durham, 2000)*, Universitext, pages 59–126, Berlin, 2001. Springer-Verlag.

[Car04] C. Carstensen. An adaptive mesh-refining algorithm allowing for an H^1-stable L^2-projection onto Courant finite element spaces. *Constr. Approx.*, 20(4):549–564, 2004.

[Car05] C. Carstensen. A unifying theory of a posteriori finite element error control. *Numer. Math.*, 100(4):617–637, 2005.

[Car08] C. Carstensen. Three remarks on the convergence of adaptive finite element methods. Preprint, Humboldt-Universität zu Berlin, 2008.

[Car09a] C. Carstensen. Convergence of adaptive finite element methods in computational mechanics. *Appl. Numer. Math.*, 59:2119–2130, 2009.

[Car09b] C. Carstensen. Yonsei lectures at the WCU department computational science and engineering on finite element method. 2009.

[CB02] C. Carstensen and S. Bartels. Each averaging technique yields reliable a posteriori error control in FEM on unstructured grids. Part I: Low order conforming, nonconforming, and mixed FEM. *Math. Comp.*, 71(239):945–969, 2002.

[CBJ02] C. Carstensen, S. Bartels, and S. Jansche. A posteriori error estimates for nonconforming finite element methods. *Numer. Math.*, 92(2):233–256, 2002.

[CD98] C. Carstensen and G. Dolzmann. A posteriori error estimates for mixed FEM in elasticity. *Numer. Math.*, 81:187–209, 1998.

[CF01] C. Carstensen and S. A. Funken. Averaging technique for FE — a posteriori error control in elasticity. Part II: λ-independent estimates. *Comput. Methods Appl. Mech. Engrg.*, 190:4663–4675, 2001.

[CGR12] C. Carstensen, D. Günther, and H. Rabus. Mixed finite element method for a

degenerate convex variational problem from topology optimization. *SIAM J. Numer. Anal.*, 50(2):522–543, 2012. Previously published: Mixed finite element method for a degenerate convex variational problem from topology optimization (2012) Humboldt-Universität zu Berlin, Preprint 12-03.

[CH06a] C. Carstensen and R. H. W. Hoppe. Convergence analysis of an adaptive nonconforming finite element method. *Numer. Math.*, 103(2):251–266, 2006.

[CH06b] C. Carstensen and R. H. W. Hoppe. Error reduction and convergence for an adaptive mixed finite element method. *Math. Comp.*, 75(255):1033–1042, 2006.

[CH07] C. Carstensen and J. Hu. A unifying theory of a posteriori error control for nonconforming finite element methods. *J. Numer. Math.*, 107(3):473–502, 2007.

[Chi00] M. Chipot. *Elements of Nonlinear Analysis.* Birkhäuser Advanced Texts. Birkhäuser Verlag, Basel - Boston - Berlin, 2000.

[CHX09] L. Chen, M. Holst, and J. Xu. Convergence and optimality of adaptive mixed finite element methods. *Math. Comp.*, 78(265):35–53, 2009.

[Cia78] P. G. Ciarlet. *The Finite Element Method for Elliptic Problems.* North-Holland, Amsterdam, 1978.

[CKNS08] J. M. Cascon, C. Kreuzer, R. H. Nochetto, and K. G. Siebert. Quasi-optimal convergence rate for an adaptive finite element method. *SIAM J. Numer. Anal.*, 46(5):2524–2550, 2008.

[Clé75] P. Clément. Approximations by finite element functions using local regularization. *Sér. Rouge Anal.*, 2:77–84, 1975.

[CM02] C. Carstensen and S. Müller. Local stress regularity in scalar non-convex variational problems. *SIAM J. Math. Anal.*, 34:495–509, 2002.

[CN09] C. Carstensen and Numerical Analysis Group, HU Berlin. AFEM. unpublished MATLAB software package, 2009.

[COV06] C. Carstensen, A. Orlando, and J. Valdman. A convergent adaptive finite element method for the primal problem of elastoplasticity. *International Journal for Numerical Methods in Engineering*, 67:1851–1887, 2006.

[CP] C. Carstensen and E.-J. Park. Convergence of adaptive FEM in the $H(\mathrm{div})-$norm. in preparation.

[CP97] C. Carstensen and P. Plecháč. Numerical solution of the scalar double-well problem allowing microstructure. *Math. Comp.*, 66(219):997–1026, 1997.

[CP01] C. Carstensen and A. Prohl. Numerical analysis of relaxed micromagnetics by penalised finite elements. *Numer. Math.*, 90(1):65–99, 2001.

[CPR13] C. Carstensen, D. Peterseim, and H. Rabus. Optimal adaptive nonconforming FEM for the Stokes problem. *Numerische Mathematik*, 123(2):291–308, 2013.

[CPS11] C. Carstensen, D. Peterseim, and M. Schedensack. Comparison results of three first-order finite element methods for the Poisson model problem. *Preprint 831, DFG Research Center Matheon Berlin*, 2011.

[CR73] M. Crouzeix and P.-A. Raviart. Conforming and nonconforming finite element methods for solving the stationary Stokes equations. I. *Rev. Française Automat. Informat. Recherche Opérationnelle Sér. Rouge*, 7(R-3):33–75, 1973.

[CR08] C. Carstensen and H. Rabus. New adaptive mixed finite element method

(AMFEM). *PAMM - Proc. Appl. Math. Mech.*, 8:10049 – 10052, 2008.

[CR11] C. Carstensen and H. Rabus. An optimal adaptive mixed finite element method. *Math. Comp.*, 80(274):649–667, 2011. Previously published: An optimal adaptive mixed finite element method (2009) Matheon Preprint No.569 04/2009.

[CR12] C. Carstensen and H. Rabus. The adaptive nonconforming FEM for the pure displacement problem in linear elasticity is optimal and robust. *SIAM J. Numer. Anal.*, 50(3):1264–1283, 2012.

[DDP95] E. Dari, R. Durán, and C. Padra. Error estimators for nonconforming finite element approximations of the Stokes problem. *Math. Comp.*, 64(211):1017–1033, 1995.

[Dör96] W. Dörfler. A convergent adaptive algorithm for Poisson's equation. *SIAM J. Numer. Anal.*, 33(3):1106–1124, 1996.

[DS11] A. Demlow and R. Stevenson. Convergence and optimality of an adaptive FEM for controlling L2 errors. *Numer. Math.*, 117:185//218, 2011.

[EEHJ95] K. Eriksson, D. Estep, P. Hansbo, and C. Johnson. *Computational Differential Equations*. Cambridge University Press, Cambridge, 1995.

[Fre90] D. A. French. On the convergence of finite-element approximations of a relaxed variational problem. *SIAM J. Numer. Anal.*, 27(2):419–436, 1990.

[Glo80] R. Glowinski. *Numerical methods for non-linear variational problems*. Springer Verlag, 1980.

[GLT81] R. Glowinski, J.-L. Lions, and R. Trémolières. *Numerical analysis of variational inequalities*, volume 8 of *Studies in mathematics and its applications*. North-Holland Publishing Company, 1981.

[GR86] V. Girault and P.-A. Raviart. *Finite Element Methods for Navier-Stokes Equations*, volume 5 of *Springer Series in Computational Mathematics*. Springer-Verlag, Berlin, Heidelberg, New York, 1986.

[Gud10] T. Gudi. A new error analysis for discontinuous finite element methods for linear elliptic problems. *Math. Comp.*, 79(272):2169–2189, 2010.

[Hac98] W. Hackbusch. From classical numerical mathematics to scientific computing. *Doc. Math. J. DMV, extra volume, ICM, Berlin*, 1:235–254, 1998.

[Han05] W. Han. *A posteriori error analysis via duality theory : with applications in modeling and numerical approximations*. Sciences Engineering Library. Springer, 2005.

[Han10] P. Hansbo. A discontinuous finite element method for elasto-plasticity. *Int. J. Numer. Methods Biomed. Eng.*, 26(6):780–789, 2010.

[HL01] P. Hansbo and M. G. Larson. Discontinuous Galerkin and the Crouzeix-Raviart element: Application to elasticity. Technical Report 2000-09, Chalmers Finite Element Center, Chalmers University of Technology, Göteborg Sweden, 2001.

[HSX09] J. Hu, Z. Shi, and J. Xu. Convergence and optimality of adaptive nonconforming methods for high-order differential equations. *Research Report 19*, 2009. School of Mathematical Sciences and Institute of Mathematics, Peking University, available at www.math.pku.edu.cn:8000/var/preprint/7280.pdf.

[HSX12] J. Hu, Z. Shi, and J. Xu. Convergence and optimality of the adaptive morley element method. *Numerische Mathematik*, pages 1–22, 2012. 10.1007/s00211-012-0445-0.

[HX08] J. Hu and J. Xu. Convergence of adaptive conforming and nonconforming finite element methods for the perturbed Stokes equation. Technical Report 7297, Institute of Mathematics, Peking University, 2008. Available as preprint at `http://www.math.pku.edu.cn:8000/var/preprint/7297.pdf`.

[HX11] J. Hu and J. Xu. Convergence and optimality of the adaptive nonconforming linear finite element methods for the Stokes equation. *Research Report*, 2011. School of Mathematical Sciences and Institute of Mathematics, Peking University.

[Kaw85] B. Kawhol. *Rearrangements and Convexity of Level Sets in PDE*, volume 1150/1985 of *Lecture Notes in Mathematics*. Springer Berlin/Heidelberg, 1985.

[KPP12] M. Karkulik, D. Pavlicek, and D. Praetorius. On 2D newest vertex bisection: Optimality of mesh-closure and H^1-stability of L_2-projection. ASC report 10/2012, Institute for Analysis and Scientific Computing, Vienna University of Technology, 2012.

[KS95] R. Kouhia and R. Stenberg. A linear nonconforming finite element method for nearly incompressible elasticity and Stokes flow. *Comput. Methods Appl. Mech. Engrg.*, 124:195–212, 1995.

[LW] R. Luce and B. I. Wohlmuth. A local a posteriori error estimator based on equilibrated fluxes. *SIAM J. Numer. Anal.*, 42(4):1394–1414.

[Mar85] L. D. Marini. An inexpensive method for the evaluation of the solution of the lowest order Raviart–Thomas mixed method. *SIAM J. Numer. Anal.*, 22:493–496, 1985.

[MNS02] P. Morin, R. H. Nochetto, and K. G. Siebert. Convergence of adaptive finite element methods. *SIAM Rev.*, 44(4):631–658, 2002.

[MSV08] P. Morin, K. G. Siebert, and A. Veeser. A basic convergence result for conforming adaptive finite elements. *Math. Models Methods Appl. Sci.*, 18(5):707–737, 2008.

[MZS10] S. Mao, X. Zhao, and Z. Shi. Convergence of a standard adaptive nonconforming finite element method with optimal complexity. *Appl. Numer. Math.*, 60:673–688, July 2010.

[NR04] P. Neittaanmäki and S. Repin. *Reliable methods of computer simulation: Error control and a posteriori estimates*. Elsevier, Amsterdam, 2004.

[OP08] C. Ortner and D. Praetorius. On the convergence of adaptive non-conforming finite element methods. Technical Report 25, Institute for Analysis and Scientifc Computing, Vienna University of Technology, TU Wien, 2008.

[Pro01] A. Prohl. *Computational Micromagnetism*. Teubner Stuttgart/Leipzig/Wiesbaden, 2001.

[PW60] L. E. Payne and H. F. Weinberger. An optimal Poincaré inequality for convex domains. *Arch. Rat. Mech. Anal.*, 5:286–292, 1960.

[Rab10] H. Rabus. A natural adaptive nonconforming FEM of quasi-optimal complexity.

Comput. Methods Appl. Math., 10(3):315–325, 2010.

[RB01] R. Rannacher and R. Becker. An optimal control approach to error estimation and mesh adaptation in finite element methods. *Acta Numerica*, 10:1–102, 2001.

[RC12] H. Rabus and C. Carstensen. Optimal mesh refinement strategies. In *Advanced Computational Engineering*, number 09/2012 in Oberwolfach Reports, pages 72–74. Mathematisches Forschungsinstitut Oberwolfach (MFO), 2012.

[Rep08] S. Repin. *A Posteriori Estimates for Partial Differential Equations*. Number 4 in Radon Series on Computational and Applied Mathematics. de Gryuter, 2008.

[Ste07] R. Stevenson. Optimality of a standard adaptive finite element method. *Foundations of Computational Mathematics*, 7(2):245–269, 2007.

[Ste08] R. Stevenson. The completion of locally refined simplicial partitions created by bisection. *Mathematics of Computation*, 77(261):227–241, 2008.

[SZ90] L. R. Scott and S. Zhang. Finite element interpolation of nonsmooth functions satisfying boundary conditions. *Mathematics of Computation*, 54(190):483–493, 1990.

[Ver96] R. Verfürth. *A Review of A Posteriori Estimation and Adaptive Mesh-Refinement Techniques*. Advances in Numerical Mathematics. Wiley-Teubner, 1996.

[Ver99] R. Verfürth. Error estimates for some quasi-interpolation operators. *M2AN Math. Model. Numer. Anal.*, 33(4):695–713, 1999.

List of Figures

List of Tables

List of Algorithms

Selbstständigkeitserklärung

Ich erkläre, dass ich die vorliegende Arbeit selbstständig und nur unter Verwendung der angegebenen Literatur und Hilfsmittel angefertigt habe.

Berlin, den 29. Nov. 2013 Hella Andrea Rabus